PREPARATION AND DEVELOPMENT OF NEW BIOACTIVE RESORBABLE POLYMERIC SYSTEMS LOADED WITH BEMIPARIN FOR DRUG DELIVERY AND TISSUE ENGINEERING

TESIS DOCTORAL

FELISA REYES ORTEGA

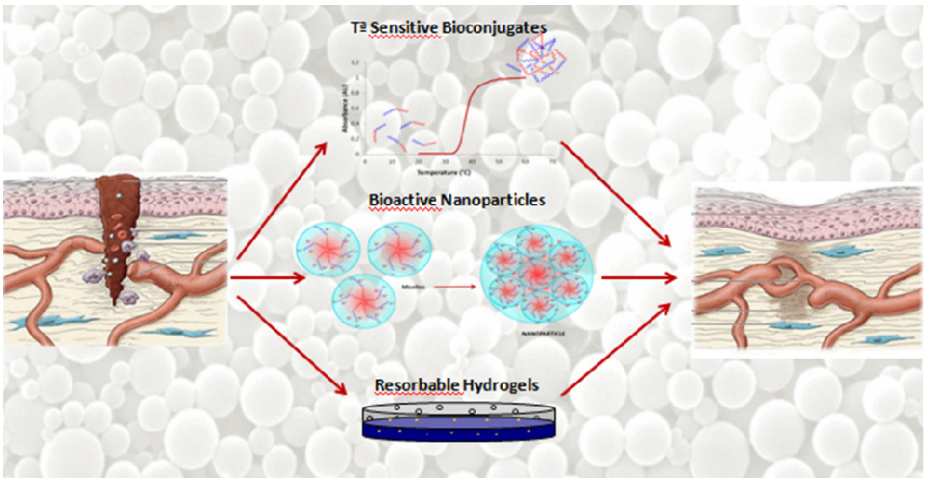

DIRECTORES

JULIO SAN ROMÁN DEL BARRIO

GEMA RODRÍGUEZ CRESPO

Mª ROSA AGUILAR DE ARMAS

GOBIERNO DE ESPAÑA MINISTERIO DE ECONOMÍA Y COMPETITIVIDAD

CSIC

ICTP

UAM UNIVERSIDAD AUTÓNOMA DE MADRID

Index

1. Introducción General y Objetivos

1. General Introduction and Aims of this Thesis

Introducción General y Objetivos

CAPÍTULO 1.

1.1. OBJETIVOS

La aplicación de sistemas poliméricos bioactivos constituye hoy día una de las herramientas más eficaces a la hora de desarrollar nuevos sistemas bioactivos vectorizados, sistemas de dosificación controlada de medicamentos y sistemas de cicatrización y regeneración tisular[1].

Los glicosaminoglicanos (GAGs) son unos excelentes candidatos para la formulación de nuevos sistemas poliméricos bioactivos debido a su origen natural, alta biocompatibilidad y funcionalidad, además de formar parte de la matriz extracelular (MEC), brindando una integridad estructural y permitiendo la migración celular. Los glicosaminoglicanos son estructuras basadas en glúcidos de cadenas largas, no ramificadas de heteropolisacáridos, compuestas generalmente por una unidad repetitiva de disacárido con la fórmula general (azúcar ácido-amino azúcar)$_n$. Estos glicosaminoglicanos juegan un papel importante en la activación y recuperación de tejidos como el tejido nervioso, tejido epidérmico, tejido endotelial, cartílago o tejido óseo y forman parte de los tejidos conectivos animales, destacando su importantísimo papel en la componente amorfa fundamental de la matriz extracelular (MEC)[2]. Como modelos más representativos de estos sistemas podemos citar heparina, sulfato de condroitina, heparan sulfato o ácido hialurónico. Todos ellos intervienen en la integridad estructural y/o remodelación de diversos tejidos. En concreto, la heparina juega un papel modulador de la actividad de factores de crecimiento dependientes de heparina, tales como el factor de crecimiento de fibroblastos (FGF) o la mayoría de las isoformas del factor de crecimiento del endotelio vascular (VEGF)[3]. Además, la heparina presenta propiedades anticoagulantes, evitando la formación de coágulos y la extensión de los coágulos existentes en la sangre a partir de la unión a la enzima inhibidora de la antitrombina III (AT). Esta unión inactiva la trombina y otras proteasas implicadas en la coagulación sanguínea X_a, y por ello la heparina constituye hoy día uno de los medicamentos más relevantes para el tratamiento y prevención de procesos

trombóticos y reestenóticos, siendo fundamental para evitar la trombosis en alteraciones vasculares asociadas a accidentes traumatológicos, o a situaciones de inmovilidad prolongada de pacientes, con problemas de retorno vascular[4]. La heparina se administra por vía parenteral, ya que se degrada cuando se toma por vía oral. Puede ser inyectada por vía intravenosa o subcutánea. Las inyecciones intramusculares se evitan debido a la posibilidad de formar hematomas o hemorragias de evolución poco previsible.

Sin embargo, la heparina presenta numerosas desventajas, tales como una baja biodisponibilidad (15-29%) y una corta vida media (60 s - 1.5 h), por lo que se debe administrar con frecuencia o en infusión continua. Esto provoca efectos secundarios graves, como el riesgo de hemorragias o la trombocitopenia inducida, causada por una reacción inmunológica que provoca la degradación de las plaquetas. Sin embargo, estos efectos secundarios se pueden solucionar con el uso de heparinas de bajo peso molecular (HBPM), que presentan mayor vida media permitiendo reducir la administración de este anticoagulante a una dosis al día, y además al presentar un peso molecular más bajo evita la trombocitopenia y disminuye el riesgo de hemorragia. Por otro lado, el aumento de estabilidad o vida media de la heparina se puede conseguir con el uso de nuevas formulaciones poliméricas, que permiten mantener la actividad farmacológica de dicho fármaco, alargando la vida media dentro del organismo y actuando además como sistema de vectorización de este medicamento. De esta forma, la formulación heparina-polímero constituye un excelente sistema para su aplicación en recubrimientos bioactivos, sistemas inyectables y sistemas de acción muy localizada en un punto del organismo donde son necesarios, evitando la dispersión del medicamento a través del flujo sanguíneo.

Este trabajo de tesis doctoral se centra en la preparación de sistemas poliméricos portadores de heparina, en concreto de bemiparina, una heparina de bajo peso molecular de nombre comercial HIBOR®, comercializada y donada por Laboratorios Rovi, para su posible utilización en procesos de regeneración tisular.

Los resultados de este trabajo se pueden agrupar en distintas líneas de preparación y aplicación que corresponderán con los distintos capítulos de la memoria:

- Por un lado, se prepararon nanopartículas reabsorbibles
- cargadas con bemiparina por el método de emulsión múltiple, utilizando como sistemas poliméricos nuevos copolímeros de bloque en base a poli(metacrilato de metilo) PMMA y poli(2-[metacriloiloxi etil] trimetilamonio) (PMAETMA), sintetizados por polimerización radical controlada por adición, fragmentación y transferencia reversible (RAFT). Estos copolímeros de bloque se inspiraron en el copolímero comercial Eudragit RS PO® (copolímero al azar de metacrilato de metilo, acrilato de etilo y metacrilato de *N,N*-dimetilaminoetilo). La naturaleza catiónica del Eudragit RS PO® le permite formar complejos reversibles con heparina, además ha sido ampliamente utilizado en la formulación de biomateriales, como sistema de liberación controlada de fármacos[5], recubrimento de materiales[6], etc., debido a que permite una liberación de principios activos controlada en el tiempo, permite la modulación de dicha liberación dentro de los límites terapéuticos establecidos, reduciendo el número de dosis a administrar, y suministra una protección de los fármacos a lo largo del tracto intestinal.[7] Los resultados de liberación y actividad biológica de estos sistemas se han comparado no sólo con nanopartículas basadas en Eudragit RS PO sino con nanopartículas basadas en un copolímero comercial, biocompatible y biodegradable de ácido láctico y glicólico, PLGA (Resomer® RG 504 H), utilizado en numerosos dispositivos biomédicos.
- Paralelamente, y en este mismo sentido, se han desarrollado complejos polielectrolíticos de quitosano-bemiparina para ser utilizados como sistemas nanoparticulados para su utilización en dispositivos biomédicos, en la liberación de fármacos y en administración de agentes bioactivos. Estos complejos polielectrolíticos se pueden aplicar como películas, esponjas, polvo, micro y nanopartículas, etc., en regeneración tisular, ingeniería de tejidos o terapia anticancerígena.
- Por otro lado, se ha llevado a cabo la preparación de fármacos poliméricos, mediante el anclaje químico covalente de bemiparina a cadenas poliméricas

hidrofílicas sensibles al pH y a la temperatura, de forma que podrían ser inyectados en el organismo.

- Además, se han preparado formulaciones de sistemas hidrofílicos basados en hidrogeles de gelatina e hialuronato sódico, entrecruzados con distintos agentes químicos y físicos, originando una red tridimensional con capacidad de incorporar distintos agentes bioactivos que posteriormente se liberarán en función de su grado de hinchamiento en distintos medios acuosos. Este sistema ha servido de soporte para la liberación del péptido *N*-terminal de 20 aminoácidos de la proadrenomedulina[8] (PAMP).

- Con el mismo fin de soporte de sistemas bioactivos, se ha llevado a cabo la síntesis de un poliuretano segmentado biodegradable, bioabsorbible y biocompatible en base al diisocianato de L-lisina y policaprolactona-diol que ha sido cargado con las partículas de bemiparina y se ha utilizado junto con el hidrogel anteriormente mencionado para formar un sistema bicapa que permite la liberación y dosificación de ambos componentes bioactivos (PAMP y bemiparina). Con este sistema, utilizado para el recubrimiento de heridas y úlceras, se ha conseguido que la dosificación sea secuencial y controlada, permitiendo así la revascularización y cicatrización de pacientes con heridas comprometidas, como por ejemplo, pacientes con problemas de diabetes y/o reducido riego sanguíneo.

Los sistemas poliméricos descritos en esta tesis han sido caracterizados de forma exhaustiva mediante técnicas analíticas avanzadas, tales como técnicas espectroscópicas de infrarrojo con transformada de Fourier (FTIR), Resonancia Magnética Nuclear (RMN) de protón y de carbono 13, espectroscopía UV-visible, espectroscopía de fluorescencia. Además se emplearon diferentes técnicas de visualización de las muestras como microscopía óptica, microscopía electrónica de barrido ambiental (ESEM), microscopía de fuerza atómica (AFM). En el análisis térmico se empleó termogravimetría y calorimetría diferencial de barrido. También se determinó el comportamiento reológico de los geles. Diferentes técnicas cromatográficas se emplearon en la determinación de las concentraciones de diversos analitos como la cromatografía de líquidos de alta resolución (HPLC), y en la determinación del peso molecular de los polímero sintetizados la cromatografía de

exclusión por tamaños (SEC). Además, se han llevado a cabo estudios de citotoxicidad y actividad biológica, tanto a nivel celular "*in vitro*", como "*in vivo*" en animales de experimentación, gracias a la colaboración de otros grupos de investigación.

Para conseguir los objetivos citados se han empleado las siguientes metodologías:

1. La preparación de las nanopartículas se realizó utilizando dos métodos diferentes, por un lado la emulsión múltiple de los componentes a partir de las respectivas disoluciones en disolventes adecuados, y por otro lado el método de formación de complejos polielectrolíticos. Con ello se han conseguido nanopartículas de tamaño alrededor de los 100 nm, que han sido dispersados de forma homogénea en hidrogeles de gelatina/hialuronato sódico. Para la preparación de estos sistemas nanoparticulados se han utilizado copolímeros de bloque anfifílicos formados por poli(metacrilato de metilo) (PMMA) y poli([2-metacriloiloxi etil] trimetil amonio) (PMAETMA) sintetizados por polimerización radical controlada por adición, fragmentación y transferencia reversible (RAFT)[9]. Estos sistemas anfifílicos dan lugar a un balance hidrófobo/hidrófilo que permiten la formación de estructuras multimicelares, que forman sistemas nanoparticulados.

2. Sistemas poliméricos en los que el principio activo está enlazado covalentemente o mediante complejos a la matriz acrílica soporte. Estos sistemas se prepararon a partir de la funcionalización de la heparina de bajo peso molecular con propargil amina, utilizando una novedosa vía de esterificación a través de activación con cloruro de 4-(4,6-dimetoxi-1,3,5-triazin-2-il)-4-metilmorfolinio (DMTMM), que ha demostrado resultar más efectiva que la activación convencional con carbodiimidas. Este derivado de heparina puede unirse por química "click" a polímeros portadores de grupos funcionales sensibles al pH y a la temperatura, con peso molecular y estructura controlada preparados por polimerización radical controlada. Estos sistemas bioconjugados proporcionan una sensibilidad específica a cambios de temperatura o/y de pH, de tal forma que se contraen a temperatura fisiológica, facilitando su inyección directa, con una buena adhesión en la zona de inyección, y pueden ser utilizados para la activación a nivel local de procesos de regeneración tisular. Para la preparación de los bioconjugados poliméricos, se han

preparado polímeros metacrílicos funcionalizados de peso molecular y polidispersidad controlados, mediante la técnica de polimerización controlada por transferencia de átomo (ATRP). Paralelamente se ha llevado a cabo la funcionalización de la bemiparina con grupos alquinos, que permitieron la formación de bioconjugados polímero-bemiparina mediante química click. El carácter hidrofílico proporcionado por la bemiparina en estos sistemas bioconjugados está controlado por la composición de sistemas copoliméricos. Además la introducción del componente polimérico (poli(dimetilaminoetil metacrilato) (PDMAEMA) o el copolímero formado por el éter metílico de monometacrilato de dietilenglicol y el metacrilato de polietilenglicol (P(MEO_2MA-co-$OEOMA_{300}$)) proporciona una sensibilidad a la temperatura, que resulta muy interesante a la hora de establecer interacciones entre el "fármaco polimérico" y el tejido receptor.

3. En la última parte de este trabajo se describe un apósito constituido por dos capas bio-funcionalizadas capaces de mejorar la cicatrización de heridas y úlceras, especialmente en los casos en que este proceso está comprometido, como sucede en pacientes diabéticos con reducido riego sanguíneo y personas de edad avanzada. Para ello, se han preparado materiales compuestos poliméricos biodegradables y reabsorbibles capaces de actuar como soporte y de liberar controladamente los componentes activos. Este apósito bicapa está formado por: una capa interna constituida por el hidrogel de gelatina/hialuronato sódico impregnada con el péptido *N*-terminal de 20 aminoácidos de proadrenomedulina (PAMP), y una capa externa formada por el poliuretano segmentado cargado con nanopartículas de bemiparina encapsulada en un polímero o un copolímero biocompatibles.

Los hidrogeles formados por ácido hialurónico-gelatina tienen la ventaja de proporcionar un ambiente húmedo idóneo para la migración y proliferación celular. La gelatina presenta en su estructura química residuos de lisina o glutamina que presentan grupos amino libre que pueden actuar como puntos de entrecruzamiento y permite así obtener un gel mucho más estable. Por su parte, el hialuronato sódico presenta la propiedad de retener grandes cantidades de agua y adoptar una conformación extendida en disolución, aportando buenas propiedades de

hidratación al hidrogel. El entrecruzamiento permite a su vez obtener un hidrogel con buena estabilidad mecánica y térmica[10].

Los poliuretanos segmentados son copolímeros de bloque que están constituidos por dos tipos de segmentos: blandos y rígidos[11]. Los segmentos rígidos incluyen las conexiones de un diisocianato (alifático o aromático) y una diamina o un diol de bajo peso molecular, estos últimos se denominan extendedores de cadena. La combinación de ambos tipos de segmentos forman un copolímero del tipo $(AB)_{m.}$ Existe cierto grado de inmiscibilidad entre los segmentos rígidos y los blandos del poliuretano segmentado, esto significa que aunque los poliuretanos son isotrópicos, microscópicamente no son estructuralmente homogéneos. Existe un cierto grado de mezclado entre estos dos tipos de segmentos, aunque la separación de fases de los dos segmentos ocurre, produciendo una estructura consistente en micro dominios de segmentos rígidos dispersos en una matriz de segmentos blandos. Esta estructura con micro dominios exhibida por los poliuretanos es la responsable de sus excelentes propiedades mecánicas, así como también contribuye a su biocompatibilidad[12].

El uso de nanopartículas como sistemas portadores de fármacos ha sido muy utilizado en las últimas décadas, por ser un sistema eficiente de encapsulación, liberación de fármacos y de fácil administración como sistema inyectable en pacientes. El uso de polímeros biodegradables derivados de los ácidos láctico y glicólico, conocidos como PLGA y sus derivados está muy extendido por ser un material ejemplar por sus propiedades biodegradables, biocompatibles y poder encapsular eficientemente una gran variedad de moléculas[13,14] (proteínas, péptidos, genes, vacunas, antígenos, factores de crecimientos, etc.). Las matrices en base a EUDRAGIT[15,6] son bastante atractivas en la empresa farmacéutica debido a su alta estabilidad química, buena compactabilidad y disponibilidad de una gran variabilidad de productos en el mercado que presentan distintas propiedades químicas. Numerosos trabajos se han publicado de nanopartículas preparadas con PLGA y EUDRAGIT para encapsular heparina, con objeto de mejorar la estabilidad de dicho fármaco en el organismo[16].

Cada capa que compone el apósito tiene una función determinada:

- Por un lado, la función del hidrogel es proporcionar el ambiente húmedo para facilitar la migración y proliferación celular, ofreciendo un equilibrio de hidratación mantenida en el tiempo necesario para conseguir una óptima cicatrización de las lesiones. Este hidrogel se degrada y reabsorbe a lo largo del tiempo, por lo que no es necesario su posterior retirada. Además, está impregnado con el péptido PAMP, el cual tiene propiedades proangiogénicas, antimicrobianas y reepitelizantes, lo que le hace idóneo para esta aplicación. La adecuada dosificación de PAMP a lo largo del tiempo, estimula la revascularización de la herida en las capas más externas de la piel, estimulando la formación de vasos sanguíneos en la parte más superficial de la dermis. La administración de PAMP incorporado en la matriz de gelatina/hialuronato sódico mejora la actividad del péptido en el proceso de cicatrización ya que, si se administra directamente sobre la herida, migra a las capas más profundas de la piel y ejerce su actividad en la dermis, donde no es tan necesario.
- Por otro lado, la base de poliuretano, aísla y protege el hidrogel del exterior, es biodegradable y permite la liberación controlada de la bemiparina. Esta capa es de naturaleza hidrófoba y degradación lenta, y libera partículas a base de bemiparina que mejoran la actividad del apósito debido al efecto modulador de este fármaco sobre la actividad de los factores de crecimiento proangiogénicos (*e.g.* FGF y VEGF).

En esta tesis doctoral se ha desarrollado un modelo de apósito experimental que ha dado lugar a una solicitud de patente (P201231750), que está basado en la liberación controlada de dos componentes bioactivos: PAMP y bemiparina, que se aplica directamente en la zona a recuperar. Este sistema descrito en el capítulo 5 de esta tesis, además de mejorar la cicatrización, tiene la ventaja de que al aplicar ambas moléculas bioactivas de forma secuencial y local se evitan los efectos adversos que pueden originar su administración sistémica.

1.2. INTRODUCCIÓN

La heparina es una mezcla compleja de polisacáridos lineales sulfatados, que pertenecen a la familia de los glicosaminoglicanos. Las cadenas polisacarídicas están formadas por enlaces glucosídicos 1-4 de ácido urónico (α-L-idurónico ácido [I] o ácido β-D-glucurónico [G]) y α-D-glucosamina. La heparina posee numerosas actividades biológicas importantes, asociadas con su interacción con una amplia gama de proteínas, entre las que destaca principalmente como agente anticoagulante y como un regulador de la actividad complementaria en la enfermedad inflamatoria. Además, las heparinas regulan la actividad de factores de crecimiento, tales como FGF y VEGF, lo que resulta interesante para la modulación de la angiogénesis y el desarrollo tisular (Figura 1).

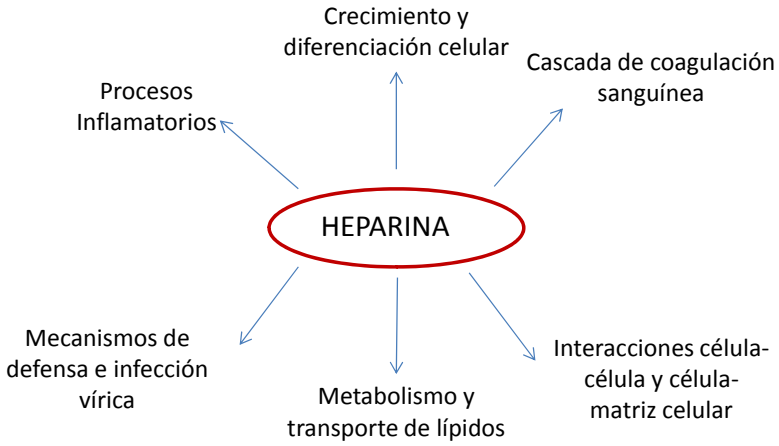

Figura 1. Procesos fisiológicos en los que está involucrada la heparina.

1.2.1. ESTRUCTURA QUÍMICA DE HEPARINA

La estructura química de la heparina está formada por un polímero lineal que consiste en unidades repetitivas de ácido urónico ligado a residuos de glucosamina. Los residuos de ácido urónico son en un 90% de ácido L-idurónico y un 10% de ácido

D-glucorónico. La heparina tiene por tanto, la densidad de carga negativa más alta que cualquier macromolécula biológica conocida, (2.7 unidades de carga negativas por disacárido). Esta alta densidad de carga es el resultado de su alto contenido de grupos sulfónicos cargados negativamente y grupos carboxilos (Figura 2).

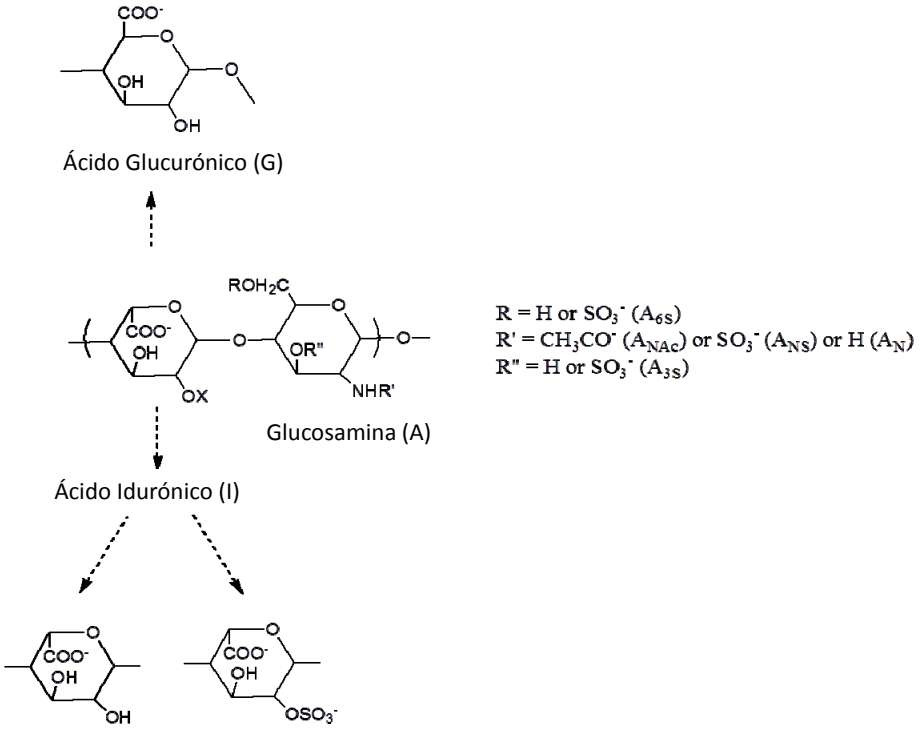

Figura 2. Estructura química de la secuencia disacárida mayoritaria de la heparina.

La estructura más común que ocurre en la heparina es el disacárido trisulfatado (Figura 3), sin embargo, existe una serie de variaciones estructurales de este disacárido, lo que conlleva a una alta microheterogeneidad que dificulta en gran medida su determinación estructural exacta. El grupo amino del residuo de glucosamina puede estar sustituido con un grupo acetilo, un grupo sulfónico, o no estar sustituido. Las posiciones 3- y 6- de los residuos de glucosamina pueden estar o no sustituidos con un grupo O-sulfónico. El ácido urónico, que puede ser o bien L-

idurónico o ácido D-glucurónico, también puede contener un grupo O-sulfónico en la posición 2 del anillo.

Las heparinas no fraccionadas tiene un intervalo de pesos moleculares de 5-40 kDa, con un peso molecular medio de aproximadamente 15 kDa y una carga negativa promedio de aproximadamente -75 eV. Esta variabilidad estructural hace que la heparina sea una molécula extremadamente difícil de caracterizar. La complejidad estructural de la heparina se puede considerar en varios niveles. La heparina es un polisacárido lineal no ramificado, altamente sulfatado que existe principalmente como una estructura helicoidal (Figura 3). A diferencia de las proteínas, la heparina no muestra ninguna estructura terciaria en particular. La especificidad de sus interacciones con la gran variedad de proteínas biológicamente importantes depende de las orientaciones en el espacio de sus grupos sulfónicos y carboxilos. Además, la flexibilidad conformacional del ácido L-idurónico que forma parte de la estructura química de la heparina se cree que es también responsable de la amplia gama de interacciones de proteínas específicas.

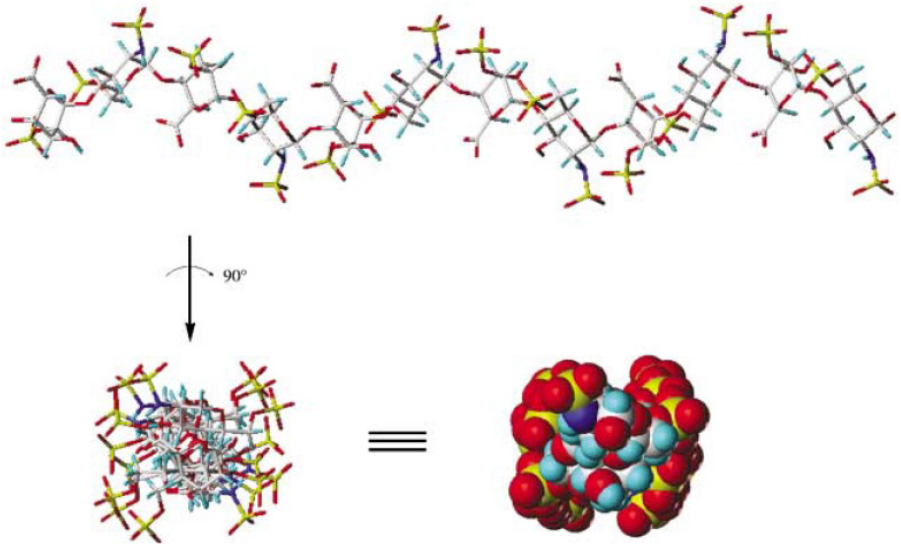

Figura 3. Conformación helicoidal de la secuencia dodecasacárida de la heparina con la secuencia disacárida más repetida en su estructura (mostrada anteriormente en la figura 2). Átomos de azufre (amarillos), átomos de oxígeno (rojos), átomos de nitrógeno (azules) y átomos de hidrógeno (azules oscuros). *Angew. Chem. Int. Ed. 2002, 41, 390-412*.

1.2.2. HEPARINAS DE BAJO PESO MOLECULAR

La eficacia del tratamiento con heparina en la prevención de la trombosis postoperatoria quedó establecida por Crafoord[17] y sigue en vigor utilizándose en clínica médica hasta nuestros días. Sin embargo, el uso de heparinas no fraccionadas (HNF) conlleva varios efectos secundarios indeseables, tales como complicaciones hemorrágicas o trombocitopenia inducida por heparina (HIT). Estas complicaciones, junto con una mejor comprensión de la cascada de la coagulación, y el fraccionamiento de la heparina condujeron al desarrollo de las heparinas de bajo peso molecular (HBPM) que presentan mejores propiedades químicas y biológicas. La HBPM tiene una actividad farmacológica más predecible, presentan una actividad constante, y mejoran la biodisponibilidad y el índice terapéutico en el organismo.[18] Las HNF presentan una alta polidispersidad, mientras que las HBPM, tales como bemiparina (HIBOR ®) se obtienen por despolimerización química (β-eliminación) de las HNF, obteniéndose pesos moleculares de menos de 6 kDa. Las HBPMs contienen una composición de disacárido definido que permite reducir los efectos secundarios de las HNF, incluyendo los problemas de la coagulación y sangrado. Las heparinas (tanto las HNF como las HBPM) se administran por vía sistémica, debido a la falta de absorción cuando se administra por vía oral y su inestabilidad a pH ácido. Adicionalmente tiene una vida media corta "*in vivo*". Las líneas de investigación de los últimos años se ha enfocado al uso de las propiedades biológicas y químicas de las heparinas para desarrollar métodos de administración más eficaces, disminuyendo los efectos secundarios asociados con las inyecciones repetidas de HP, la trombocitopenia inducida por HNF, la osteoporosis y la alopecia. De esta forma, las HBPMs han ido desplazado a las HNFs como agentes anticoagulantes en clínica. Bemiparina (HIBOR ®) es una HBPM de segunda generación. Entre sus características destaca una vida media larga (5,3 h) y una relación de actividad anti-FX_a/anti-FII_a[19] más alta (08:01) que cualquiera de las HBPMs de segunda generación. Esta bemiparina es la HBPM que se ha utilizado para desarrollar todo el trabajo de esta tesis doctoral y se caracteriza por obtenerse a partir de la despolimerización química

de la heparina no fraccionada por β-eliminación, dando lugar a una HBPM con un peso molecular de 3,6 kDa.

Para facilitar la difusión de fármacos, evadir la degradación proteolítica, prolongar el tiempo de retención intestinal, y en última instancia, para mejorar la biodisponibilidad oral de las heparinas, los hidrogeles (HG) y los sistemas de partículas se han desarrollado recientemente[20,18, 21]. Además, la conjugación química de la heparina con un polímero o su incorporación en una matriz polimérica se han desarrollado potencialmente en los últimos años para la fabricación de recubrimientos biocompatibles, sistemas de inyección subcutánea, fabricación de fibras de heparina por técnicas de electrohilado, preparación de micro y nanopartículas cargadas con heparina, etc., con un enfoque no sólo como anticoagulante, sino también como participante importante en la señalización del metabolismo de distintos factores de crecimiento, como el factor de crecimiento de fibroblastos (FGF). Las proteínas de la familia de FGF son probablemente las proteínas más extensamente estudiadas que forman complejos de unión con la heparina. Estudios estructurales y experimentales han demostrado que la presencia de los grupos 6-O-sulfónicos dentro de heparina no determinan la unión heparina-FGF-2, sin embargo sí son necesarios para que dicha unión tenga lugar entre el FGF-1 y la heparina. Estas diferencias sugieren una especificidad de la interacción de varios miembros de la misma familia de factores de crecimiento. Mientras que la interacción entre las proteínas y la heparina es principalmente iónica y basada en la presencia y el posicionamiento apropiado de los grupos sulfónicos y carboxilos, esto puede no ser siempre el caso. Por ejemplo, se ha observado que en la interacción entre el inhibidor de la proteasa leucocitaria secretora (SLPI) y heparina, se requieren menores de secuencias de oligosacáridos sulfatados de heparina para obtener una interacción específica de alta afinidad, lo que sugiere la importancia de las interacciones de enlace de hidrógeno a través de los grupos hidroxilo presentes en heparina.

1.2.3. FORMACIÓN DE COMPLEJOS FGF-HEPARINA

Los factores de crecimiento de fibroblastos (FGF) son miembros de una gran familia de proteínas que están implicadas en los procesos de desarrollo y fisiológicos, incluyendo la proliferación celular, la diferenciación, la morfogénesis y la angiogénesis. Los FGF son proteínas que presentan una alta afinidad de unión a heparina. En vertebrados tienen una región de núcleo interno de 28 aminoácidos invariantes y seis aminoácidos que varían, y presentan en peso molecular de 17-34 kDa. El factor de crecimiento de fibroblastos ácido (FGF-1) y el factor de crecimiento de fibroblastos básico (FGF-2) fueron los primeros miembros de la familia en ser descubiertos, y la termodinámica y cinética de su interacción con la heparina han sido ampliamente estudiados. Estos factores de crecimiento ejercen sus efectos biológicos mediante la unión a diferentes receptores de superficie celular específicos, llamados receptores del factor de crecimiento de fibroblastos (FGFR). Los FGFR son receptores de tirosina quinasa transmembrana expresados en múltiples variantes: FGFR-1, FGFR-2, FGFR-3 y FGFR-4, con diferentes afinidades de unión. Los FGFR también son proteínas de unión a heparina, por lo tanto, los tres compuestos de FGF, FGFR, y heparina deben interactuar simultáneamente para iniciar la transducción de señales. En cada complejo FGF-FGFR-heparina, la heparina puede interaccionar por distintos sitios de unión, pudiendo obtenerse una unión 1:1:1 o 2:2:1 (Figura 4)[18].

FGF-2-FGFR1:heparina 2:2:2 | FGF-1-FGFR2:heparina 2:2:1

Figura 4. Estructuras de los complejos FGF-FGFR-heparina. Se muestran el FGFR (Amarillo), el FGF (verde) y la heparina con todos sus átomos definidos: azufre (Amarillo), oxígeno (rojo), nitrógeno (azul) e hidrogenos (blancos). *Angew. Chem. Int. Ed. 2002, 41, 390-412.*

1.3. SISTEMAS DE LIBERACIÓN CONTROLADA DE FÁRMACOS

En los últimos años, el desarrollo científico-experimental en el sector farmacéutico ha facilitado el diseño y producción de formulaciones farmacéuticas de liberación controlada, que ha permitido mejorar el perfil terapéutico de numerosos medicamentos cuya eficacia y seguridad habían sido previamente establecidas en ensayos clínicos controlados y, posteriormente, contrastados en la práctica clínica[22]. Ello ha sido posible gracias a la introducción de nuevos materiales, especialmente los polímeros biocompatibles, al mejor conocimiento de las características farmacocinéticas y farmacodinámicas de los medicamentos, así como su aplicación a la optimización de la respuesta y al progreso experimentado por las operaciones industriales necesarias para la fabricación de estas formulaciones.

Los sistemas poliméricos de liberación controlada son matrices en las que se integran fármacos y que pueden presentar actividad en su forma original y/o actuar como soporte y dosificador de sustancias farmacológicamente activas. Los polímeros

empleados con este fin pueden ser biodegradables o no, en función de su capacidad de ser degradados o no en el medio biológico.

La principal ventaja del desarrollo y aplicación de sistemas de liberación controlada de fármacos se encuentra en la relación dosis/actividad de un medicamento, sin tener que recurrir a la invasión generalizada del organismo humano[23] y en la optimización de la vectorización de la acción de dicho medicamento hacia los tejidos, células o incluso compartimentos subcelulares apropiados, así como el ajuste de los perfiles de liberación al ritmo circadiano, además de cubrir otras necesidades como:

1. Conseguir una liberación lenta de medicamentos hidrosolubles.
2. Mejorar la biodisponibilidad de medicamentos poco solubles en agua.
3. Desarrollar transportadores o soportes realmente eliminables.
4. Optimizar la biodistribución de medicamentos de metabolismo rápido o fácilmente excretables.
5. Controlar la liberación de medicamentos altamente tóxicos.

La aplicación de sistemas poliméricos proporciona una clara optimización de las formas de dosificación para conseguir una respuesta terapéutica adecuada en el punto requerido, con los mínimos efectos adversos.

La mayor parte de los compuestos farmacológicos administrados por vía oral, intravenosa o intramuscularmente, son rápidamente absorbidos por la mucosa intestinal o por los tejidos en los que se aplica la inyección, hasta que son transferidos al flujo sanguíneo que finalmente lo distribuye a todo el organismo. Este es el caso de las heparinas, cuya administración actual en clínica (intravenosa o intramuscular) origina un máximo de liberación del fármaco inicial que puede llegar a sobrepasar la concentración mínima tóxica (CMT) y posteriormente disminuye con el tiempo quedando por debajo de la concentración mínima efectiva (CME), (curvas A y B, Figura 5). Con un sistema de liberación controlada (curva C) lo que se pretende es que la dosificación de dicho fármaco sea estable en el tiempo, de forma que se permita prolongar el efecto de este fármaco sin tener que aumentar la dosis. Por

tanto la liberación controlada de fármacos permite disminuir la toxicidad derivada de la sobredosificación y además constituyen una alternativa más cómoda para el paciente ya que se disminuye la toma de dosis.

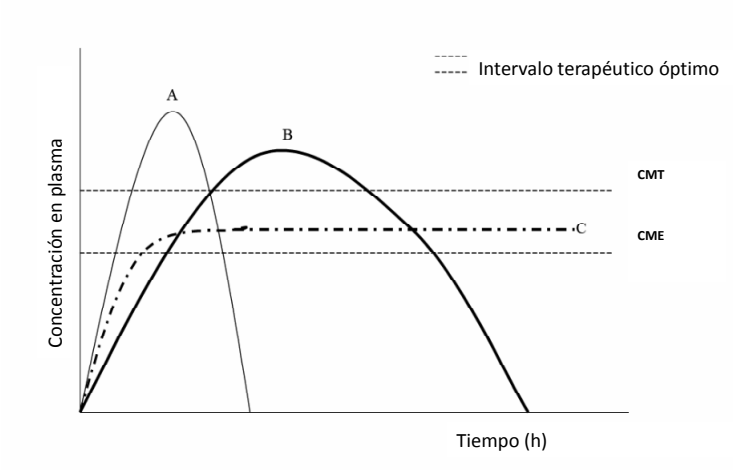

Figura 5. Variación de la concentración plasmática de fármaco cuando se administran fármacos convencionales o sistemas de liberación controlada, siendo el peso molecular de A mayor que el de B.

En las últimas décadas se han llevado a cabo grandes avances dentro del campo de la tecnología farmacéutica, desarrollando en este sentido sistemas nanoparticulados, hidrogeles biodegradables y bioabsorbibles, bioconjugados poliméricos, polímeros "inteligentes" etc., que permiten mejorar la biodisponibilidad y bioactividad de fármacos hidrosolubles, que siendo administrados directamente presentan una vida corta de actividad en el organismo.

1.3.1. DESARROLLO DE SISTEMAS PARA LIBERACIÓN CONTROLADA

A la hora de desarrollar sistemas de liberación controlada, tenemos que tener en cuenta la estructura y estabilidad química del fármaco, así como el mecanismo de liberación que se pretende conseguir. Existen muchos tipos de mecanismos de liberación de fármaco, destacando entre éstos los siguientes:

1.3.1.1 Sistemas controlados por difusión

En estos sistemas el agente bioactivo se libera gracias a un fenómeno de difusión a través del polímero, existiendo restricciones de transferencia de masa en la interfase polímero/líquido.

El coeficiente de difusión del agente bioactivo a través del polímero depende de la estructura, morfología y concentración del soluto. La matriz polimérica tiene que ser capaz de liberar fármacos a velocidad constante durante un tiempo determinado. La migración del fármaco al medio acuoso desde un sistema de esta naturaleza implica un proceso de absorción de agua o fluido biológico, y otro simultáneo de liberación del fármaco mediante un mecanismo de difusión, controlado por el hinchamiento que sufre el material polimérico.

1.3.1.2 Sistemas controlados por hinchamiento

Son sistemas en los que el compuesto activo se encuentra disuelto o disperso en un soporte de polímero hidrófilo, entrecruzado o no, el cual se hincha sin disolverse cuando se pone en contacto con un medio acuoso. Estos sistemas polímeros se denominan hidrogeles y son capaces de conseguir una velocidad de liberación constante. El grado de hinchamiento depende del balance hidrófilo/hidrófobo de la matriz polimérica y del grado de entrecruzamiento.

La migración del fármaco al medio acuoso implica un proceso de absorción de agua y otro simultáneo de deserción del compuesto bioactivo por un mecanismo de difusión controlado por el hinchamiento que sufre el polímero. Cuando el agua penetra en la matriz hidrófila, el polímero, que presenta inicialmente un estado vítreo, se hincha y su temperatura de transición vítrea puede alcanzar valores inferiores a la temperatura del medio que la rodea pasando con ello a un estado tipo elastomérico. En estas condiciones, el soluto difunde desde las regiones hinchadas al medio externo y la liberación de éste está controlada por la velocidad y posición de la interfase vítrea/elástica.

1.3.1.3 Sistemas controlados por vía química

Son sistemas en los que el fármaco se une a la cadena polimérica mediante un enlace covalente. Para que esta unión se produzca, el sistema polimérico debe tener grupos funcionales que puedan ser degradados en medios fisiológicos. La liberación del principio activo se produce mediante una reacción química, a través de un enlace débil que puede romperse por hidrólisis o enzimáticamente.

Los conjugados polímero-fármaco están constituidos por unidades de cadena con grupos funcionales a los que pueda unirse covalentemente el fármaco (Figura 6). Esta unión debe ofrecer una resistencia química adecuada, capaz de mantener estable al compuesto farmacológicamente activo hasta el momento de su actuación. Hay varios conjugados polímero-fármaco en fase clínica, son los considerados polímeros terapéuticos[24].

Los conjugados de polímero-fármaco se han explorado como uno de los nuevos enfoques en la quimioterapia del cáncer[25,26]. Los fármacos pueden ser conjugados al polímero empleando varias uniones degradables, además los diferentes ligandos pueden ser unidos a la columna polimérica para una localización específica del fármaco, como en el caso de la Doxorubicina, Paclitaxel, Campotecina o Platinato, que se conjugan a polímeros de *N*-(2-hidroxipropil) metacrilamida (HPMA), poliglutamato y polietilenglicol, estos polímeros conjugados tienen como ventaja aumentar la solubilidad y/o aumentar el tiempo de vida útil y biodisponibilidad de los principios activos, reduciendo la dosis requerida y la toxicidad asociada a éstos[27].

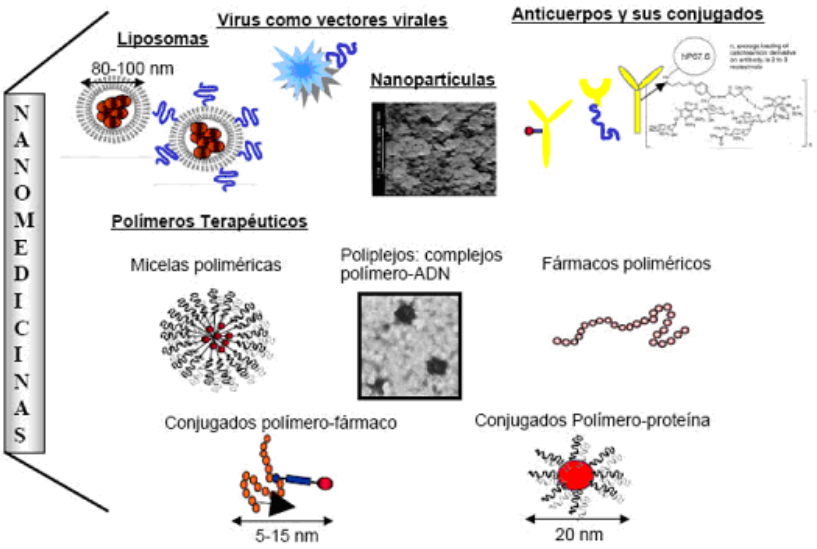

Figura 6. Representación de los tipos de nanomedicinas desarrollados, entre ellas los polímeros terapéuticos. Advanced Drug Delivery Reviews. Volume 65, Issue 1, January 2013, Pages 60–70.

1.3.1.4 Sistemas controlados bioerosión

Los sistemas bioerosionables son aquellos en los que la liberación del fármaco está controlada por la velocidad de degradación del polímero. El compuesto activo se encuentra disperso en un material polimérico, el cual se va erosionando con el tiempo, permitiendo así la liberación del fármaco. Tenemos dos tipos de bioerosión:

- Bioerosión en volumen: la absorción de agua se sigue mediante un proceso de erosión que ocurre en todo el volumen del sistema polimérico sólido. En función de la velocidad de penetración del agua en la matriz polimérica, ésta será más o menos soluble en agua.
- Erosión superficial: la velocidad a la cual el agua penetra en el sistema polimérico es más lenta que la velocidad de transformación del polímero en un

material soluble en agua y, por lo tanto, esta última se ve limitada por la cara superficial del sistema sólido.

Los principales factores que afectan al proceso de erosión son:

1. La estabilidad química de las cadenas de polímero.
2. La hidrofobia de la matriz polimérica.
3. La morfología del polímero.
4. El peso molecular inicial del polímero.
5. El grado de hinchamiento de la matriz polimérica cargada de fármaco.
6. El proceso de fabricación.
7. La presencia de catalizadores, aditivos o plastificantes.
8. La geometría del sistema.

1.3.2. POLÍMEROS INTELIGENTES

En estos sistemas la liberación del fármaco se lleva a cabo mediante la respuesta a un estímulo como puede ser un cambio de temperatura, de pH, de concentración del fármaco, efecto del campo eléctrico o magnético, efecto de la luz, etc. Como respuesta a dicho estímulo externo se produce un cambio en la conformación pasando de un estado colapsado (no existe liberación) a un estado expandido (donde se produce la liberación del fármaco).

Los sistemas de liberación de fármacos más estudiados son los sensibles a temperatura y al pH[28]. Los sistemas sensibles a la temperatura presentan una estrategia que se basa en el hecho de que, en presencia de agentes patógenos o pirógenos, la temperatura corporal normal (37 °C) se altera. Por tanto, se emplean en tratamientos de patologías acompañadas de fiebre. Este tipo de sistemas también se han estudiado para tratamientos de determinados tumores con hipertermia local, de manera que se combina un aumento en la temperatura con la liberación local de fármacos anticancerígenos.

Los sistemas sensibles al pH aprovechan los cambios de pH en determinadas áreas del organismo como el tracto intestinal. Han sido estudiados para el desarrollo de cubiertas entéricas de medicamentos, así como para sistemas de liberación dirigida en tratamientos con antitumorales.

Uno de los polímero más estudiados para el desarrollo de sistemas inteligentes es el poli(metacrilato de 2,2-dimetil amino etilo), que tiene la característica de ser sensible al pH y a la temperatura, propiedades que le hacen bastante interesante para su aplicación en biomedicina. Este polímero se ha utilizado para formar bioconjugados polímero-fármaco unidos covalentemente, que posteriormente han permitido la liberación del mismo de forma controlada a partir de un proceso de hidrólisis o enzimático.

1.3.3. SISTEMAS PARTICULADOS

Existen diversos tipos de partículas poliméricas empleadas en la administración de medicamentos. En función de su tamaño podemos clasificarlas en micropartículas y nanopartículas.

Las micropartículas son partículas poliméricas cuyo tamaño oscila entre 1 y 250 µm. Las nanopartículas son partículas poliméricas de tamaño inferior a 1 µm. Debido a que las micropartículas son de tamaño superior a las nanopartículas, éstas tienen mejor comportamiento para la liberación sostenida aunque por un problema también de tamaño puede que resulten menos confortables para el paciente. Las propiedades requeridas para los polímeros destinados al diseño de micropartículas y nanopartículas son: biodegradación, bioadhesión y biocompatibilidad.

Se pueden emplear diversos métodos para la preparación de micro y nanopartículas[29], de todos ellos podemos destacar los métodos de evaporación del disolvente[30], separación de fase orgánica, polimerización interfacial, polimerización en emulsión y secado por spray. Son numerosos los factores a tener en cuenta para el desarrollo de este tipo de sistemas, entre ellos podemos destacar el tipo de material, la cantidad de fármaco a incorporar, la estabilidad y farmacocinética del mismo, toxicidad del sistema de liberación, etcétera. Por ello es importante un

cuidadoso diseño del procedimiento de preparación. Además, la cesión de fármaco se ve afectada por el estado físico del fármaco en el sistema, el tipo de matriz, las proporciones de fármaco y matriz, el grado y la naturaleza del entrecruzamiento, la interacción entre fármaco y matriz, y el medio de liberación.

La liberación del fármaco tiene lugar a través de varias rutas: erosión de la superficie, total desintegración, difusión y combinación de todas. Las propiedades fisicoquímicas requeridas para el diseño de un sistema particulado están gobernadas por el tipo de fármaco y la aplicación in vivo para la que se van a emplear[31]:

- Tamaño de partícula: la ruta de administración determinará el tamaño requerido para las microesferas.
- Área superficial/porosidad: las matrices de porosidad variable facilitan la modulación de la liberación del fármaco. La degradación del polímero también se controla alterando la porosidad de dicha matriz.
- Contenido de fármaco/liberación del fármaco: depende de la dosis que se trate de alcanzar, la velocidad de dosificación del fármaco, y de la cantidad de fármaco que es capaz de aceptar la ruta de administración para la que ha sido diseñado.
- Tiempos de biodegradación: viene gobernado por la ruta de administración y la frecuencia de las dosis.

Las aplicaciones de micro y nanopartículas en el campo de la farmacología están enfocadas en dos áreas diferentes pero complementarias: sistemas de liberación controlada y vectorización.

Para la aplicación de **liberación controlada**, la gran ventaja es que al tener un tamaño tan pequeño, pueden ser inyectados con una jeringa convencional, no necesitando una intervención quirúrgica. Además es más fácil que una partícula de tamaño nanométrico se introduzca en la célula antes que el fármaco libre. Estos sistemas son también interesantes para el transporte de fármacos que no pueden administrarse por vía oral por sí solos, como los anticancerígenos, inmunosupresores, vitaminas, antibióticos, etc.

En cuanto a la **vectorización**, lo que se pretende es que la distribución del compuesto activo se dirija selectivamente al tejido afectado o a un área local. Esto es muy importante sobre todo para aquellos compuestos de alta toxicidad o para los de

bajo índice terapéutico. Con la vectorización se reduce el número de dosis necesarias, evitando efectos tóxicos sistémicos y aumenta y aumentando la concentración en el lugar deseado.

1.4. INGENIERÍA TISULAR: CICATRIZACIÓN DE HERIDAS

A pesar del cuidado de los cirujanos y de los avances recientes en el campo de la curación de las heridas, el tratamiento sin conocimiento de las heridas, en especial las postquirúrgicas, sigue siendo una causa significativa de costos, morbilidad y mortalidad en la sociedad. El conocimiento de los mecanismos complejos de la curación de la herida ha permitido el desarrollo de nuevas y eficaces modalidades de tratamiento, incluyendo a los diferentes apósitos sintéticos, los láseres, las matrices extracelulares y las células madre. Para entender cómo pueden corregirse las condiciones de curación anormal de la herida, y cómo optimizar la cicatrización normal, es importante primero conocer la estructura de la piel, su fisiología y los principios básicos de la curación de este tipo de lesiones.

La curación de la herida cutánea es un proceso complejo, que requiere la coordinación de muchos tipos de células para alcanzar la reparación apropiada del tejido. Se han identificado cuatro procesos traslapados principales en este fenómeno: hemostasia, inflamación, formación del tejido de granulación y reepitelialización, y la remodelación final del tejido[32]. En ello participan la dermis, la epidermis, el endotelio de los vasos sanguíneos y los canales linfáticos, que junto con las células del sistema inmune, los neutrófilos, macrófagos, linfocitos T y B, T citotóxicos, T reguladores y las células asesinas naturales (NK), etc., de forma coordinada montan un proceso controlado, en donde hay lisis de la zona dañada, para que se vuelvan a sintetizar los componentes de matriz que le den la resistencia y la arquitectura, lo más semejante posible a lo que tenían originalmente esos tejidos.

Los neutrófilos y los macrófagos regulan las fases inflamatoria y fibroproliferativa tempranas de la curación de la herida no patológica. Estas células

son un componente significativo de la inflamación temprana de la herida y regulan la producción local de un subconjunto clave de citocinas, las quimiocinas, que junto con otros factores de crecimiento como el factor de crecimiento transformante beta 1 (TGF-β1), el derivado de las plaquetas (PDGF) y el del tejido conjuntivo (CTGF), entre otros, promueven el depósito de matriz extracelular, y en gran proporción el del colágeno. No obstante, cuando están ausentes, particularmente los neutrófilos, el cierre inicial de la herida se acelera marcadamente y ello se debe al control de la inflamación.

Después del reclutamiento en el lecho de la herida, los monocitos se diferencian en macrófagos, los cuales desempeñan un papel central en todas las etapas de la curación de la herida y orquestan el proceso. Su fenotipo funcional es dependiente del microambiente de la herida, que cambia durante la curación. Durante la fase inflamatoria temprana y corta, los macrófagos ejercen funciones pro-inflamatorias, como presentación de antígenos, fagocitosis y producción de citocinas y de otros factores pro-inflamatorios que facilitan el proceso curativo de la herida. Durante la fase proliferativa, los macrófagos estimulan la proliferación de las células mesenquimáticas como los fibroblastos y miofibroblastos, las endoteliales y epiteliales (queratinocitos epidérmicos) de manera directa e indirecta. Especialmente los fibroblastos, los queratinocitos y las células endoteliales son estimulados por los macrófagos durante esta fase, para inducir y completar la formación de matriz extracelular, particular en cada caso. Luego, los macrófagos pueden participar en el recambio de la composición de la matriz extracelular, durante la angiogénesis y en la fase de remodelación, por la liberación de enzimas específicas que degradan a la matriz extracelular, las metaloproteinasas (MMPs) y estimulando la síntesis de moléculas de la matriz extracelular.

Otros procesos que afectan la restauración son la infección, la presencia de cuerpos extraños o patologías concomitantes en el individuo que sufrió la herida, el entorpecimiento del cierre de la herida, como sucede en las úlceras crónicas no cicatrizadas, las hernias recurrentes, y la dehiscencia de la herida. Mantener la herida limpia y húmeda, reducir al mínimo el trauma y la infección son los puntos

clave para una buena reparación de la herida. Además, se deben minimizar los medicamentos que inhiben los procesos de curación de la herida, suministrar una nutrición adecuada, protección UV y paliar el dolor.

Las estrategias terapéuticas para el manejo de la cicatriz hipertrófica y queloide, así como para las lesiones ulcerosas o incluso para favorecer y promover una cicatrización normal con mayor calidad, son enormes. La herida debe mantenerse en un ambiente húmedo, pero no mojado. Tampoco debe ser seco, porque las células no viven en ausencia de agua. Se pueden aplicar esponjas o apósitos para el manejo de los fluidos, que los absorben o permiten que se evaporen, o los retienen y bloquean, con lo que se mantiene la humedad en torno a la herida, las mejores características para cicatrizar, y se evita que se macere el tejido.

Los apósitos absorbentes sencillos, por ejemplo, espumas y textiles de algodón, viscosa o poliéster, mantienen el líquido en los espacios de su estructura, a modo de esponja, sin evitar la infección. Estos apósitos permiten que se evapore la humedad desde su superficie, con tasas de transmisión de vapor húmedo (TTVH) bajas, lo que puede provocar maceración a partir del líquido que se mantiene bajo el apósito, o TTVH muy altas, que son útiles para tratar el exudado cuando se prefiere un volumen mínimo. Los apósitos interactivos, por ejemplo hidrocoloides, alginatos y fibras de carboximetilcelulosa (CMC), captan el líquido para formar un gel y pueden reducir el desplazamiento lateral del líquido y el riesgo de maceración alrededor de la herida, tienen más probabilidades de mantenerse intactos durante su uso, lo cual es útil cuando se aplica compresión. Los apósitos con sistemas antimicrobianos inespecíficos, como la plata y el yodo, o específicos, como los asociados a antibióticos y antimicóticos, como la gentamicina, favorecen el control de la infección y de la colonización microbiana.

La cicatrización y la terapéutica varían de acuerdo con:

- el estadio de la lesión;
- la colonización, contaminación o infección de la herida;

- la edad del paciente;
- la localización de la herida, por ejemplo, no es lo mismo si se aplica la terapia de presión negativa a un recién nacido que a un paciente adulto, o a uno anciano, donde debido a la fragilidad de sus capilares podría generarse una hemorragia por el exceso de succión;
- la presencia de patologías concomitantes.

La mayoría de las lesiones cicatrizan de manera favorable, con fibrosis mínima suficiente y la restauración del daño sin dejar una secuela importante. El estudio de la cicatrización fetal ha llevado a un mayor conocimiento de los mecanismos de la fisiología de la reparación, y cómo acelerar y mejorar los procesos de cicatrización, principalmente en pacientes postoperados, quemados y con lesiones por traumatismos, para lograr el resultado esperado o el control de la inflamación, lo cual permite no solo pensar en la humedad y en la infección sino también en el acomodo de las proteínas y los componentes no proteicos de la matriz extracelular, para que sea reticular y más parecido a una piel normal, y no paralelo a la epidermis, dejando una secuela cicatrizal.

Las técnicas de cicatrización convencionales como la sutura, cauterización o el empleo de grapas presentan varias desventajas como el dolor y la necesidad de tenerlas que retirar tras la regeneración del tejido. Sin embargo, el uso de otros materiales sanitarios como son los apósitos tiene la ventaja de no ser dolorosos para el paciente, se adhiere a la piel fácilmente, su utilización es fácil y simple y no necesita ser retirado[33]. Para que el apósito cumpla esta serie de ventajas debe de ser biodegradable, biocompatible (va a estar en contacto directo con la herida por lo que no puede presentar toxicidad), bioabsorbible y presentar una cierta estabilidad (buenas propiedades mecánicas) para que pueda ser efectivo en el proceso de cicatrización de la herida.

Algunas enfermedades provocan que la cicatrización de las heridas sea más lenta y difícil de lo normal. Es el caso de los pacientes diabéticos, que no sólo presentan una cicatrización alterada en heridas agudas, sino que además son más

sensibles a padecer heridas crónicas, como lesiones ulcerosas en los miembros inferiores.

En este trabajo se han seleccionado compuestos como el péptido *N*-terminal de 20 aminoácidos de la proadrenomedulina (PAMP)[34], que tiene propiedades angiogénicas, re-epitalizantes y antimicrobianas; y la bemiparina[35] previamente descrita y que puede actuar como modulador trombótico y/o reestenótico y además de ser capaz de formar complejos activos con factores de crecimiento (FGF y VEGF entre otros), incrementando la actividad biológica de dichos factores, como se ha descrito en el apartado anterior de este capítulo. Estos compuestos han sido incorporados en un apósito bicapa biodegradable, bioabsorbible y biocompatible, formado por un hidrogel entrecruzado de gelatina e hialuronato sódico y por un poliuretano segmentado, que han permitido la liberación secuencial y modulada de ambos componentes bioactivos, favoreciendo el proceso de cicatrización de heridas en la piel.

1.5. BIBLIOGRAFÍA

1. Francis Suh, J. K.; Matthew, H. W. T., Application of chitosan-based polysaccharide biomaterials in cartilage tissue engineering: a review. *Biomaterials* **2000,** *21* (24), 2589-2598.
2. (a) Friedrich, M. V. K.; Göhring, W.; Mörgelin, M.; Brancaccio, A.; David, G.; Timpl, R., Structural basis of glycosaminoglycan modification and of heterotypic interactions of perlecan domain V. *Journal of Molecular Biology* **1999,** *294* (1), 259-270; (b) Giacoletto, K. S.; Rumbarger, T.; Schwartz, B. D., Chapter 8 Glycosaminoglycan Modifications of Membrane Proteins. In *Methods in Cell Biology*, Alan, M. T., Ed. Academic Press: 1989; Vol. Volume 32, pp 207-230; (c) Reubsaet, F. A. G.; Langeveld, J. P. M.; Veerkamp, J. H., Glycosaminoglycan content of glomerular and tubular basement membranes of various mammalian species. *Biochimica et Biophysica Acta (BBA) - General Subjects* **1985,** *838* (1), 144-150.
3. (a) Ho, Y.-C.; Mi, F.-L.; Sung, H.-W.; Kuo, P.-L., Heparin-functionalized chitosan–alginate scaffolds for controlled release of growth factor. *International Journal of Pharmaceutics* **2009,** *376* (1–2), 69-75; (b) Iwamoto, R.; Mekada, E., Heparin-binding EGF-like growth factor: a juxtacrine growth factor. *Cytokine & Growth Factor Reviews* **2000,** *11* (4), 335-344; (c) Sakiyama-Elbert, S. E.; Hubbell, J. A., Controlled release of nerve growth factor from a heparin-containing fibrin-based cell ingrowth matrix. *Journal of Controlled Release* **2000,** *69* (1), 149-158.
4. Capila, I.; Linhardt, R. J., Heparin–Protein Interactions. *Angewandte Chemie International Edition* **2002,** *41* (3), 390-412.
5. Streubel, A.; Siepmann, J.; Bodmeier, R., Multiple unit gastroretentive drug delivery systems: A new preparation method for low density microparticles. *Journal of Microencapsulation* **2003,** *20* (3), 329-347.
6. Moustafine, R. I.; Zaharov, I. M.; Kemenova, V. A., Physicochemical characterization and drug release properties of Eudragit® E PO/Eudragit® L 100-55 interpolyelectrolyte complexes. *European Journal of Pharmaceutics and Biopharmaceutics* **2006,** *63* (1), 26-36.
7. Ibrić, S.; Jovanović, M.; Djurić, Z.; Parojčić, J.; Solomun, L., The application of generalized regression neural network in the modeling and optimization of aspirin extended release tablets with Eudragit® RS PO as matrix substance. *Journal of Controlled Release* **2002,** *82* (2–3), 213-222.

8. Martínez, A.; Zudaire, E.; Portal-Núñez, S.; Guédez, L.; Libutti, S. K.; Stetler-Stevenson, W. G.; Cuttitta, F., Proadrenomedullin NH2-Terminal 20 Peptide Is a Potent Angiogenic Factor, and Its Inhibition Results in Reduction of Tumor Growth. *Cancer Research* **2004,** *64* (18), 6489-6494.
9. York, A. W.; Kirkland, S. E.; McCormick, C. L., Advances in the synthesis of amphiphilic block copolymers via RAFT polymerization: Stimuli-responsive drug and gene delivery. *Advanced Drug Delivery Reviews* **2008,** *60* (9), 1018-1036.
10. Nickerson, M. T.; Farnworth, R.; Wagar, E.; Hodge, S. M.; Rousseau, D.; Paulson, A. T., Some physical and microstructural properties of genipin-crosslinked gelatin–maltodextrin hydrogels. *International Journal of Biological Macromolecules* **2006,** *38* (1), 40-44.
11. Cervantes-Uc, J. M.; Espinosa, J. I. M.; Cauich-RodrÃ-guez, J. V.; Ã vila-Ortega, A.; VÃ¡zquez-Torres, H.; Marcos-FernÃ¡ndez, A.; San RomÃ¡n, J., TGA/FTIR studies of segmented aliphatic polyurethanes and their nanocomposites prepared with commercial montmorillonites. *Polymer Degradation and Stability* **2009,** *94* (10), 1666-1677.
12. (a) Chiu, L. L. Y.; Chu, Z.; Radisic, M., 2.07 - Tissue Engineering. In *Comprehensive Nanoscience and Technology*, Editors-in-Chief: David, L. A.; Gregory, D. S.; Gary, P. W., Eds. Academic Press: Amsterdam, 2011; pp 175-211; (b) Guan, J.; Fujimoto, K. L.; Sacks, M. S.; Wagner, W. R., Preparation and characterization of highly porous, biodegradable polyurethane scaffolds for soft tissue applications. *Biomaterials* **2005,** *26* (18), 3961-3971.
13. Acharya, S.; Sahoo, S. K., PLGA nanoparticles containing various anticancer agents and tumour delivery by EPR effect. *Advanced Drug Delivery Reviews* **2011,** *63* (3), 170-183.
14. Zhang, H.; Cui, W.; Bei, J.; Wang, S., Preparation of poly(lactide-co-glycolide-co-caprolactone) nanoparticles and their degradation behaviour in aqueous solution. *Polymer Degradation and Stability* **2006,** *91* (9), 1929-1936.
15. Dillen, K.; Vandervoort, J.; Van den Mooter, G.; Ludwig, A., Evaluation of ciprofloxacin-loaded Eudragit® RS100 or RL100/PLGA nanoparticles. *International Journal of Pharmaceutics* **2006,** *314* (1), 72-82.
16. Hoffart, V.; Lamprecht, A.; Maincent, P.; Lecompte, T.; Vigneron, C.; Ubrich, N., Oral bioavailability of a low molecular weight heparin using a polymeric delivery system. *Journal of Controlled Release* **2006,** *113* (1), 38-42.
17. Crafoord C, J. E., Heparin as a prophylactic against thrombosis. *Journal of the American Medical Association* **1941,** *116* (26), 2831-2835.
18. (a) Gutowska, A.; Bae, Y. H.; Feijen, J.; Kim, S. W., Heparin release from thermosensitive hydrogels. *Journal of Controlled Release* **1992,** *22* (2), 95-104; (b) Nie, T.; Baldwin, A.; Yamaguchi, N.; Kiick, K. L., Production of heparin-functionalized hydrogels for the development of responsive and controlled growth factor delivery systems. *Journal of Controlled Release* **2007,** *122* (3), 287-296.
19. Javot, L.; Lecompte, T.; Rabiskova, M.; Maincent, P., Encapsulation of low molecular weight heparins: Influence on the anti-Xa/anti-IIa ratio. *Journal of Controlled Release* **2009,** *139* (1), 8-14.
20. (a) Chung, Y.-I.; Tae, G.; Hong Yuk, S., A facile method to prepare heparin-functionalized nanoparticles for controlled release of growth factors. *Biomaterials* **2006,** *27* (12), 2621-2626; (b) Eidi, H.; Joubert, O.; Attik, G.; Duval, R. E.; Bottin, M. C.; Hamouia, A.; Maincent, P.; Rihn, B. H., Cytotoxicity assessment of heparin nanoparticles in NR8383 macrophages. *International Journal of Pharmaceutics* **2010,** *396* (1-2), 156-165.
21. Kemp, M. M.; Linhardt, R. J., Heparin-based nanoparticles. *Wiley Interdisciplinary Reviews: Nanomedicine and Nanobiotechnology* **2010,** *2* (1), 77-87.
22. Dumitriu, S., *Polymeric Biomaterials*. Dekker: Jassy, Romania, 1994.
23. SanRoman, J., Sistemas macromoleculares biocompatibles: una nueva concepción de aplicaciones farmacológicas. *Revista de Plásticos Modernos* **1989,** *396*, 888-900.
24. Pasut, G.; Veronese, F. M., Polymer–drug conjugation, recent achievements and general strategies. *Progress in Polymer Science* **2007,** *32* (8–9), 933-961.
25. Lee, D. Y.; Kim, S. K.; Kim, Y. S.; Son, D. H.; Nam, J. H.; Kim, I. S.; Park, R. W.; Kim, S. Y.; Byun, Y., Suppression of angiogenesis and tumor growth by orally active deoxycholic acid-heparin conjugate. *Journal of Controlled Release* **2007,** *118*, 310-317.
26. Lee, G. Y.; Kim, S. K.; Byun, Y., Glucosylated heparin derivatives as non-toxic anti-cancer drugs. *Journal of Controlled Release* **2007,** *123*, 46-55.
27. Rojas Cortés, M. G.; Vallejo Díaz, B. M.; Perilla, J. E., Los biopolímeros como materiales para el desarrollo de productos en aplicaciones farmacéuticas y de uso biomédico. *Ingeniería e Investigación* **2008,** *28*, 57-71.
28. González, N. Nuevos Sistemas Poliméricos Sensibles a pH y Temperatura. Aplicaciones Biomédicas. Universidad Complutense de Madrid, Madrid, 2006.

29. Bilati, U.; Allemann, E.; Doelker, E., Development of a nanoprecipitation method intended for the entrapment of hydrophilic drugs into nanoparticles. *European Journal of Pharmaceutical Sciences* **2005,** *24*, 65-75.
30. Picos;, D. R.; Carril;, M. G.; Mena, D. F., Métodos de obtención de microesferas biodegradables. *Revista Cubana de Farmacia* **2001,** *35* (2).
31. Stolnik, S.; Garnett, M. C.; Illum, L.; Davis, S. S.; Govender, T., PLGA nanoparticles prepared by nanoprecipitation: drug loading and release studies of a water soluble drug. *Journal of Controlled Release* **1999,** *57*, 171-185.
32. Peter J. van Winterswijk, M., Erik Nout, MD, Tissue Engineering and Wound Healing: An Overview of the Past, Present, and Future. *Wounds* **2007,** *19* (10), 277-284.
33. (a) Chen, S.-H.; Tsao, C.-T.; Chang, C.-H.; Lai, Y.-T.; Wu, M.-F.; Chuang, C.-N.; Chou, H.-C.; Wang, C.-K.; Hsieh, K.-H., Assessment of reinforced poly(ethylene glycol) chitosan hydrogels as dressings in a mouse skin wound defect model. *Materials Science and Engineering: C* (0); (b) Corkhill, P. H.; Hamilton, C. J.; Tighe, B. J., Synthetic hydrogels VI. Hydrogel composites as wound dressings and implant materials. *Biomaterials* **1989,** *10* (1), 3-10.
34. Fu, Y.; Létourneau, M.; Nguyen, Q. T.; Chatenet, D.; Dupuis, J.; Fournier, A., Characterization of the adrenomedullin receptor acting as the target of a new radiopharmaceutical biomolecule for lung imaging. *European Journal of Pharmacology* **2009,** *617* (1–3), 118-123.
35. Martínez-González J, V. L., Rodríguez C., Bemiparin: a second generation low-molecular weight heparin for treatment and prophylaxis of venous thromboembolism. *Expert Rev Cardiovasc Ther* **2008,** *6*, 793-802.
36. Whitelock, J.; Melrose, J., Heparan sulfate proteoglycans in healthy and diseased systems. *Wiley Interdisciplinary Reviews: Systems Biology and Medicine* **2011,** *3* (6), 739-751.
37. Pike, D. B.; Cai, S.; Pomraning, K. R.; Firpo, M. A.; Fisher, R. J.; Shu, X. Z.; Prestwich, G. D.; Peattie, R. A., Heparin-regulated release of growth factors in vitro and angiogenic response in vivo to implanted hyaluronan hydrogels containing VEGF and bFGF. *Biomaterials* **2006,** *27* (30), 5242-5251.
38. Depasse, F.; González de Suso, M. J.; Lagoutte, I.; Fontcuberta, J.; Borrell, M.; Samama, M. M., Comparative study of the pharmacokinetic profiles of two LMWH - bemiparin (3500 IU, anti-Xa) and tinzaparin (4500 IU, anti-Xa) - administered subcutaneously to healthy male volunteers. *Thrombosis Research* **2003,** *109* (2-3), 109-117.
39. Kemp, M. M.; Linhardt, R. J., Heparin-based nanoparticles. *Wiley Interdiscip. Rev.-Nanomed. Nanobiotechnol.* **2010,** *2* (1), 77-87.
40. Norrby, K., Low-molecular-weight heparins and angiogenesis. *APMIS* **2006,** *114* (2), 79-102.
41. Martínez-González, J.; Vila, L.; Rodríguez, C., Bemiparin: second-generation, low-molecular-weight heparin for treatment and prophylaxis of venous thromboembolism. *Expert Review of Cardiovascular Therapy* **2008,** *6* (6), 793-802.
42. Duncan, R.; Gac-Breton, S.; Keane, R.; Musila, R.; Sat, Y. N.; Satchi, R.; Searle, F., Polymer–drug conjugates, PDEPT and PELT: basic principles for design and transfer from the laboratory to clinic. *Journal of Controlled Release* **2001,** *74* (1–3), 135-146.
43. Kohane, D. S., Microparticles and nanoparticles for drug delivery. *Biotechnology and Bioengineering* **2007,** *96* (2), 203-209.
44. Stages of Healing. *Curad. 4* **2013**.
45. Pinto Reis, C.; Neufeld, R. J.; Ribeiro, A. J.; Veiga, F., Nanoencapsulation I. Methods for preparation of drug-loaded polymeric nanoparticles. *Nanomedicine: Nanotechnology, Biology and Medicine* **2006,** *2* (1), 8-21.
46. (a) Glaessl, B.; Siepmann, F.; Tucker, I.; Rades, T.; Siepmann, J., Deeper insight into the drug release mechanisms in Eudragit RL-based delivery systems. *International Journal of Pharmaceutics* **2010,** *389* (1–2), 139-146; (b) Karthikeyan, K.; Guhathakarta, S.; Rajaram, R.; Korrapati, P. S., Electrospun zein/eudragit nanofibers based dual drug delivery system for the simultaneous delivery of aceclofenac and pantoprazole. *International Journal of Pharmaceutics* **2012,** *438* (1–2), 117-122; (c) Yoo, J.-W.; Giri, N.; Lee, C. H., pH-sensitive Eudragit nanoparticles for mucosal drug delivery. *International Journal of Pharmaceutics* **2011,** *403* (1–2), 262-267.
47. Gosain, A.; DiPietro, L. A., Aging and Wound Healing. *World J. Surg.* **2004,** *28* (3), 321-326.
48. Mathieu, D.; Linke, J.-C.; Wattel, F., Non-Healing Wounds. In *Handbook on Hyperbaric Medicine*, Mathieu, D., Ed. Springer Netherlands: 2006; pp 401-428.
49. Broughton G 2nd, J. J., Attinger CE., The basic science of wound healing. *Plast Reconstr Surg.* **2006,** *117* (7 Suppl), 12S-34S.
50. Meszaros, A. J.; Reichner, J. S.; Albina, J. E., Macrophage-Induced Neutrophil Apoptosis. *The Journal of Immunology* **2000,** *165* (1), 435-441.

51. Campos, A. C.; Groth, A. K.; Branco, A. B., Assessment and nutritional aspects of wound healing. *Current Opinion in Clinical Nutrition & Metabolic Care* **2008,** *11* (3), 281-288 10.1097/MCO.0b013e3282fbd35a.
52. Keylock, K. T.; Vieira, V. J.; Wallig, M. A.; DiPietro, L. A.; Schrementi, M.; Woods, J. A., Exercise accelerates cutaneous wound healing and decreases wound inflammation in aged mice. *American Journal of Physiology - Regulatory, Integrative and Comparative Physiology* **2008,** *294* (1), R179-R184.
53. Swift, M. E.; Burns, A. L.; Gray, K. L.; DiPietro, L. A., Age-Related Alterations in the Inflammatory Response to Dermal Injury. **2001,** *117* (5), 1027-1035.
54. Tandara, A. A.; Mustoe, T. A., Oxygen in Wound Healing—More than a Nutrient. *World J. Surg.* **2004,** *28* (3), 294-300.
55. Woo, K.; Ayello, E. A.; Sibbald, R. G., The Edge Effect: Current Therapeutic Options to Advance the Wound Edge. *Advances in Skin & Wound Care* **2007,** *20* (2), 99-117.

General Introduction and Aims of this thesis

CHAPTER 1

1.1. AIMS

Nowadays, the application of bioactive polymer systems constitutes one of the most powerful tools in the approach of tissue regenerative processes in the application of vectorized bioactive systems, in drug delivery systems body, and in healing and tissue engineering. Glycosaminoglycans are long chain carbohydrate structures, usually composed of a repeating disaccharide unit with the following general formula (acid sugar - amino sugar)$_n$. These glycosaminoglycans play an important role in the activation and recovery of tissues such as nerve tissue, epidermal tissue, endothelial tissue, cartilage or bone tissue and part of the animal connective tissue, emphasizing their important role in the extracellular matrix (ECM). Some of the most important examples of these systems are heparin (or low molecular weight heparins), chondroitin sulphate, heparan sulphate or hyaluronic acid. They all play a role in the reconstitution of tissues, especially when systems are associated with proteins as fibroblast growth factors, FGF, or vascular endothelial growth factors, VEGF. Particularly, heparin and low molecular weight heparin are some of the most important drugs for the treatment and prevention of thrombotic and restenotic processes today. These drugs are essential in preventing thrombosis in vascular disorders associated with trauma accidents or with patients who suffer from prolonged immobility situations or vascular problems.

This doctoral thesis is based on the preparation of polymeric systems loaded with heparin, in particular low molecular weight heparin (bemiparin, donated by Rovi Laboratories), to be applied as bioactive and resorbable systems, and the development of polymeric bioconjugates that protect and stabilize the bemiparin, for its use in tissue regeneration processes.

The results of this work can be grouped into different lines of development and application:

• Firstly, the preparation of resorbable nanoparticles loaded with low molecular weight heparin, by multiple emulsion technique using well defined polymer systems, such as block copolymers based on poly (methyl methacrylate)

(PMMA) and poly (2 - [methacryloyloxy ethyl] trimethylammonium) (PMAETMA) synthesized by radical polymerization controlled by Reversible Addition-Fragmentation Transfer (RAFT) processes. These block copolymers have been prepared following the chemical structure model of Eudragit (copolymers of methyl methacrylate with methacrylate, *N, N*-dimethyl aminoethyl methacrylate), which is able to form reversible complexes with heparin. The release of bemiparin and the biological activity of these systems were compared with the commercial biocompatible and biodegradable copolymer of poly(lactic acid) and poly(glycolic acid), PLGA, which is commonly used in numerous biomedical devices.

• In parallel, chitosan-bemiparin polyelectrolyte complexes have been developed to be used as nanoparticle carriers for biomedical devices in drug delivery and as bioactive agents. These polyelectrolyte complexes can be applied as films, sponges, dust, micro and nanoparticles, etc., on tissue engineering or anticancer therapy.

• Additionally, polymer drugs were prepared by the covalent attachment of the bemiparin to hydrophilic polymer chains sensitive to pH and temperature. Consequently, these systems can be applied by direct injection into the body. Polymeric drugs have the advantages of maintaining good pharmacological activity, as well as cting as vectoring systems supporting specific drugs. Therefore, they are excellent components for the application of bioactive coatings, injection systems, and systems with a targeted action in the body, i.e. application of the site of interest, where they are needed, there-by avoiding the dispersion of the drug throughout the bloodstream.

• Furthermore, hydrogel formulations were prepared based on hydrophilic gelatin and sodium hyaluronate polymers, cross-linked with different chemical and physical agents, resulting in a three dimensional network with the ability to incorporate different bioactive agents, subsequently released according to their degree of swelling in aqueous media of differing pH. This system served as a support for different bioactive molecules, including the *N*-terminal peptide of 20 amino acids from proadrenomedulin (PAMP) and the free and encapsulated bemiparin.

• For the same purpose, the synthesis of bioactive films formed by biodegradable segmented polyurethane was carried out, based on the L-lysine

diisocyanate and the polycaprolactone-diol. This film was joined with the previously mentioned hydrogel to form a bilayer system that allows for the sequential release and dosage modulation of both bioactive components (PAMP and bemiparin). This system was used for covering wounds and ulcers in ear rabbits and a sequential dosage release of both bioactive compounds has been achieved (PAMP and heparin), allowing revascularization and wound healing. This proposes system could be a promising device to improve and accelerate the healing process in compromised wound patients, i.e. patients with diabetes problems or with reduced blood flow.

The polymeric systems described in this thesis have been extensively characterized by advanced analytical techniques, such as FTIR, proton and carbon-13 NMR, UV-visible, and fluorescence spectroscopies, optical microscopy, and environmental scanning electron microscopy (ESEM), atomic force microscopy (AFM), thermal analysis (thermogravimetry (TGA), differential scanning calorimetry (DSC)), rheological behavior, gas chromatography (GC), high performance liquid chromatography (HPLC), and size exclusion chromatography (SEC). Moreover, there have been studies of cytotoxicity and biological activity, both *in vitro* and *in vivo* (in experimental animals), in collaboration with other research partners.
To achieve the above objectives, the following methodologies were used:

1. Nanoparticles were prepared using two types of methodologies, the first one was the multiple emulsion technique, where the polymer and the bemiparin were dissolved in the corresponding solvents and an emulsion was formed to obtain the nanoparticle suspension; and the second one was the polyelectrolyte complex formation technique, where both polymer and bemiparin are dissolved in the same solvent and one of them was added dropwise over the other resulting in nanoparticle suspension. With both techniques nanoparticles with a mean diameter of approximation 100 nm were fielded. These nanoparticle systems were dispersed homogeneously and deposited in a polyurethane or hydrogel carrier for their application in tissue engineering. In order to prepare these nanoparticle systems, amphiphilic block copolymers were prepared consisting of poly (methyl methacrylate) (PMMA) and poly ([2-metacriloiloxy ethyl] trimethyl ammonium chloride) (PMAETMA) synthesized by RAFT. These block copolymers have

amphiphilic properties due to a hydrophobic / hydrophilic balance, which allows for the formation of micellar structures, thus causing the formation of self-assembled nanoparticle systems.

2. Bioconjugate systems in which the bioactive bemiparin was covalently linked to the polymer matrix were prepared through “click coupling reaction” using Cu(I) catalyzed azide-alkyne [3 + 2] dipolar cycloaddition. Previously, the alkyne functionalization of bemiparin with propargyl amine was carried out using a novel esterification activation way using the 4-(4,6-Dimethoxy-1,3,5-triazin-2-yl)-4-methylmorpholinium chloride (DMTMM), which was proven to be more effective than conventional activation with carbodiimides. This bemiparin derivative was chemically bonded by "click chemistry", becoming sensitive to pH and temperature polymers bearing functional azide groups, with controlled molecular weight distributions prepared by atom transfer controlled radical polymerization (ATRP). These systems provide bioconjugates with specific sensitivity to temperature and pH changes, due to the fact that they contract at physiological temperature, which facilitates direct injection, with good adhesion at the site of injection and can be used for locally activating the tissue regeneration processes. The hydrophilic character of these bioconjugates was controlled by the composition of the copolymer systems, introducing the polymer component (PDMAEMA or P(MEO_2MA-co-$OEOMA_{300}$)), which can be modulate to get a specific critical transition temperature, which is very interesting to establish interactions between the "polymeric-drug" and the host tissue.

3. In the final part of this work a bilayer wound dressing was described consisting of two bio-functionalized layers that are able to improve the healing of wounds and ulcers, especially in cases where the process is difficult, as in diabetic people, patients with a reduced blood flow and seniors. For this purpose, biodegradable polymeric materials capable of acting as scaffolds that allow for the controlled release of the bioactive components were prepared. This bilayer dressing is composed of two layers loaded with different bioactive compounds: the inner layer formed by the gelatin / sodium hyaluronate hydrogel was impregnated with

the *N*-terminal peptide of 20 amino acids of proadrenomedullin (PAMP) and the outer layer formed by the segmented polyurethane loaded with bemiparin nanoparticles encapsulated in a biodegradable polymer or copolymer.

The hydrogels formed by hyaluronate-gelatin have the advantage of providing an ideal moist environment for cell migration and proliferation, due to its hydrophilic properties. Gelatin has glutamine and lysine residues in its chemical structure, which support free amino groups which may act as crosslinking points and allows for the formation of a stable gel. The other hydrogel component, the sodium hyaluronate, possesses the property of water retention, and can adopt an extended conformation in solution, there-by providing good moisturizing properties to the hydrogel. Crosslinking of both components allows for the formation of a hydrogel with good mechanical and thermal stability.

Segmented polyurethanes (SPU) are block copolymers which consist of two types of chain segments: hard and soft. The hard segments include connections of a diisocyanate (aromatic or aliphatic) and a diamine or a low molecular weight diol, this one is called chain extender. The combination of both types of segments form a copolymer with the general formula $(AB)_m$. There is some degree of immiscibility between hard and soft segments in the SPU, this means that although the polyurethanes are isotropic, microscopically they are not structurally homogeneous. A certain degree of mixing exists between these two segments, although phase separation of both segments occurs, producing a structure consisting of micro hard segment domains dispersed in a soft segments matrix. This micro domains structure exhibited by polyurethanes is responsible for its excellent mechanical properties and also contributes to its biocompatibility.

Each layer of the bilayer dressing formed with the hydrogel and the SPU has a specific function:

- On the one hand, the hydrogel function is to provide a moist environment to facilitate cell migration and proliferation, providing moisture balance maintained in the time required for an optimal wound healing process. This hydrogel is degraded and absorbed over time, so no subsequent removal is necessary.
- On the other hand, the SPU function is the isolation and protection of the rest of the system. It should be biodegradable allowing for the bemiparin to

be released, achieving a symbiotic effect when both bioactive compounds (PAMP and bemiparin) are released sequentially. This layer is hydrophobic and therefore, slow time degrade, stimulating revascularization of damaged tissue and protecting the wound against infectious agents. With this appropriate sequential dosage over time, the prepared PAMP material acts on the outermost layers of the skin, promoting the formation of blood vessels in the superficial dermis; instead of migrating to the deeper layers of the skin and stimulating angiogenesis in the dermis where it was not necessary, as happens when the peptide is applied directly to the wound.

1.2. INTRODUCTION

Heparin, a sulphated polysaccharide belonging to the family of glycosaminoglycans, is a linear polymer consisting of alternating 1,4-linked uronic acid (*α*-L-iduronic acid [I] or *β*-D-glucuronic acid [G]) and *α*-D-glucosamine (A) residues[4] with important biological activities, associated with its interaction with a diverse range of proteins.[36] It is mainly used as an anticoagulant agent and as a regulator of the complementary activity in inflammatory diseases. Furthermore, heparins regulate the activity of heparin-dependent growth factors, such as FGF and VEGF, resulting in the modulation of angiogenesis and even tumor development.[37] Heparin is widely used as an anticoagulant drug based on its ability to accelerate the rate at which antithrombin inhibits serine proteases in the blood coagulation cascade. It is ubiquitously distributed on the surfaces of animal cells and in the extracellular matrix. It also mediates various physiologic and pathophysiologic processes (Figure 1).

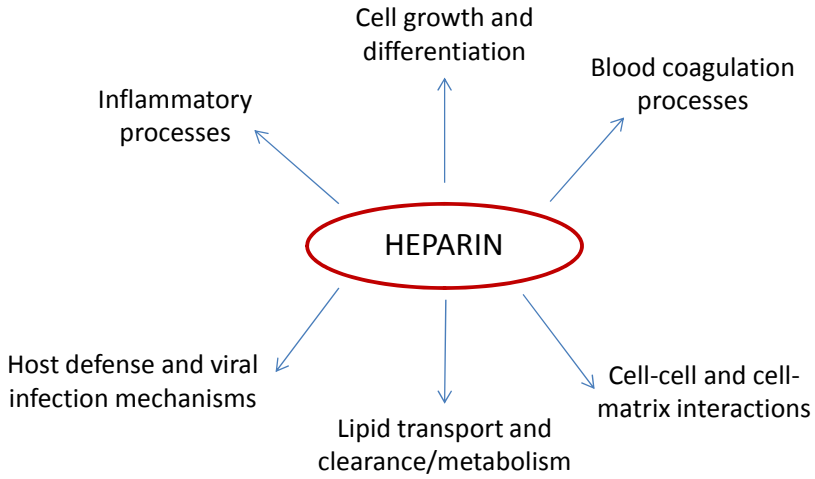

Figure 1. Processes in which heparin is involved.

1.2.1. CHEMICAL STRUCTURE OF HEPARIN

Heparin is a linear polymer consisting of repeating units of 1-4-linked pyranosyluronic acid and 2-amino-2-deoxyglucopyranose (glucosamine) residues. The uronic acid residues typically consist of 90% L-idopyranosyluronic acid (L-iduronic acid) and 10% D-glucopyranosyluronic acid (D- glucuronic acid) (Figure 2).

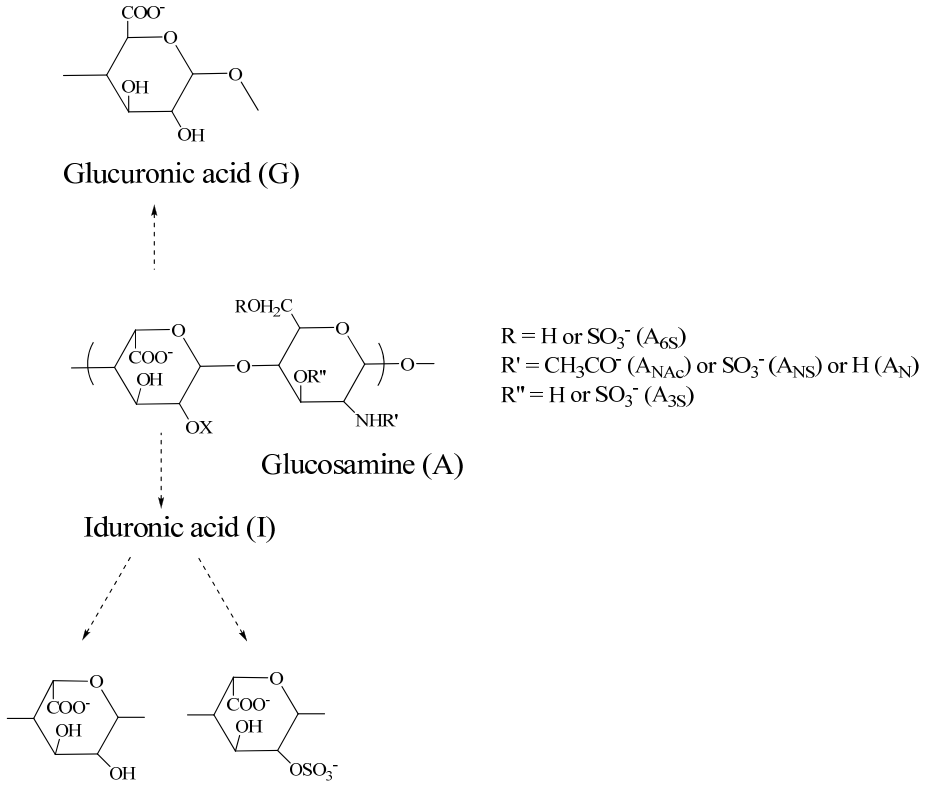

Figure 2. Chemical structure of the major sequence disaccharide unit of heparin.

Heparin has the highest negative charge density of any known biological macromolecule. This is as a result of its high content of negatively charged sulfonic and carboxyl groups. Indeed, the average heparin disaccharide contains 2.7 sulfonic groups. The most common structure occurring in heparin is the trisulphated disaccharide (Figure 3). However, a number of structural variations of this disaccharide exist, leading to the microheterogeneity of heparin. The amino group of the glucosamine residue may be substituted with an acetyl or sulfonic group or unsubstituted. The 3-and 6-positions of the glucosamine residues can either be substituted with an O-sulfonic group or unsubstituted. The uronic acid, which can either be L-iduronic or D-glucuronic acid, may also contain a 2-O-sulfo group. Glycosaminoglycan heparin has a molecular weight range of 5-40 kDa, with an average molecular weight of about 15 kDa and an average negative charge of

approximately -75 eV. The molecular weight distribution (M_w/M_n) of heparin corresponds to its polydispersity.

This structural variability makes heparin an extremely challenging molecule to characterize. The structural complexity of heparin can be considered at several levels. Heparin is a linear, unbranched, highly sulphated polysaccharide that exists primarily as a helical structure (Figure 3). Unlike proteins, heparin is not known to display or fold into any particular tertiary structure. The specificity of its interactions with a diverse range of biologically important proteins suggests that it displays its sulfo and carboxyl groups in defined patterns and orientations to promote specific protein interactions. The conformational flexibility of the L-iduronic acid residue within heparin is believed to be responsible for the wide range of specific protein interactions exhibited by this family of GAGs.

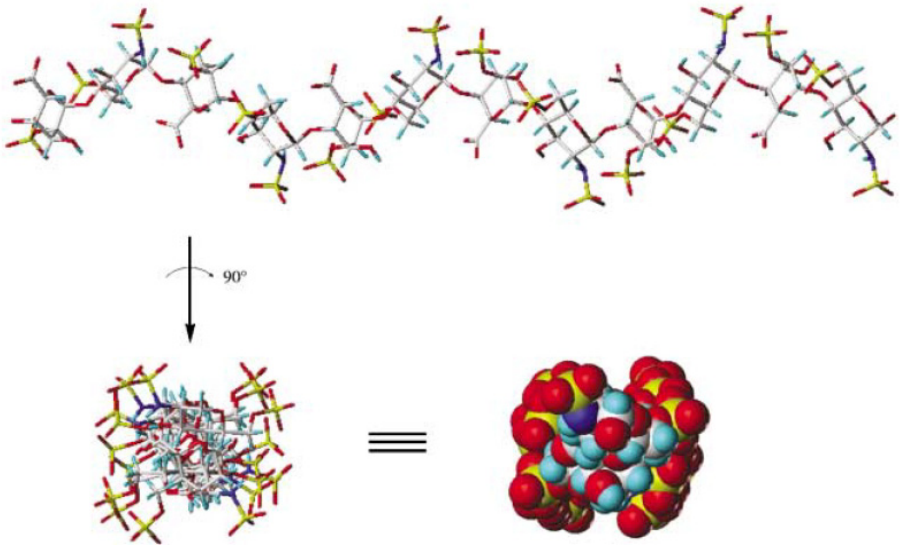

Figure 3. Helical conformation of a heparin dodecasaccharide sequence having the major disaccharide repeating structure shown in Figure 1 with sulfur atoms (yellow), oxygen atoms (red), nitrogen atoms (blue) and hydrogen atoms (cyan). *Angew. Chem. Int. Ed. 2002, 41, 390-412.*

1.2.2. LOW MOLECULAR WEIGHT HEPARIN

The effectiveness of heparin treatment in the prevention of postoperative thrombosis was quickly established through the work of Crafoord[17] and Best, and this medical practice continues to this day. However, using heparin also leads to undesirable side effects, such as bleeding complications or heparin-induced thrombocytopenia (HIT). These complications, an improved understanding of the coagulation cascade, and the fractionation of heparin has led to the development of low-molecular weight heparin (LMWH) fractions with better defined chemical and biological properties. These agents have more predictable pharmacological actions, sustained activity, improved bioavailability and a better therapeutic index.

Unfractionated heparin (UFH) is polydisperse while low molecular weight heparins (LMWH), such as Bemiparin (HIBOR®) are obtained by the chemical β-elimination depolymerization of UFH[38] with a molecular weight of less than 8 kDa. LMWHs contain a precisely defined disaccharide composition with a higher efficacy safety ratio due to the better defined anti-X_a / anti-II_a ratio that reduce heparin side effects, including problems of coagulation and bleeding. Heparin is administered systemically, due to the lack of absorption when administered orally and its instability at acidic pH. Additionally it has a short half-life *in vivo*. Past studies have been dedicated to using the biological and chemical properties of heparin to develop more efficient administration methods to decrease the side effects associated with repeated HP injections, such as HP-induced thrombocytopenia, osteoporosis, and alopecia. To facilitate drug permeation, evade proteolytic degradation and prolong the intestinal retention time, to ultimately improve the oral bioavailability of HP, hydrogels and particulate carrier systems have been recently developed[39].

Therefore, the use of LMWH allows for more predictable pharmacological actions, sustained activity and better biological properties,[40] therefore reducing the side effects. Thus, at the beginning of the new millennium, LMWH have displaced heparin as the major clinical anticoagulant. Bemiparin (HIBOR®), a second generation LMWH, was used in this thesis because it provides the longest half-life (5.3 h) and

the highest anti-FX_a/anti-FII_a activity ratio (8:1) of any second-generation LMWH. It was obtained by the chemical *β*-elimination depolymerization of UFH to give a LMWH with a molecular weight of 3.6 kDa[41].

1.2.3. FGF-HEPARIN COMPLEX FORMATION

Fibroblast growth factors (FGFs) are members of a large family of proteins that are involved in developmental and physiological processes including cell proliferation, differentiation, morphogenesis, and angiogenesis. FGFs are heparin-binding proteins that have a high affinity for cell surface heparan sulphate proteoglycans. Vertebrate FGFs have an internal core region of 28 highly conserved and six invariant amino acids and range in molecular weight from 17 to 34 kDa. Acidic fibroblast growth factor (FGF-1) and basic fibroblast growth factor (FGF-2) were the first members of the family to be discovered, and the thermodynamics and kinetics of their interaction with heparin have been extensively studied. High-resolution X-ray crystallographic data on these proteins in complexes with heparin oligosaccharides have been published. These growth factors exert their biological effects by binding to different, specific cell surface receptors called fibroblast growth factor receptors (FGFR-1-FGFR-4). The FGFRs are transmembrane tyrosine kinase receptors expressed as multiple splice variants with different affinities for the different FGFs. The FGFRs are also heparin-binding proteins. Thus, the three compounds FGF, FGFR, and heparan sulphate must interact simultaneously to initiate signal transduction. FGF-stimulated signal transduction is similar to other receptor-mediated pathways in that it involves the dimerization of the FGFRs. Cell membrane heparan sulphate binds multiple FGF molecules promoting FGFR dimerization and signal transduction. High-resolution X-ray crystal structures of complexes of FGF, FGFR, and a heparin oligosaccharide provide an insight into the stoichiometry and structural aspects of this physiologically relevant interaction.

In each FGF-FGFR 1:1 complex, heparin makes numerous contacts with both FGF-2 and FGFR-1 stabilizing FGF-FGFR binding(Figure 4). Heparin also makes

contacts with the FGFR-1 of the adjacent FGF-FGFR complex, thus seeming to promote FGFR dimerization.

FGF-2-FGFR1:heparin 2:2:2

FGF-1-FGFR2:heparin 2:2:1

Figure 4. Structures of the recently solved FGF-FGFR-heparin complexes. The FGFR is shown as a gold ribbon and the FGF as a green ribbon. The heparin oligosaccharides are shown as space-filling models with sulfur (yellow), oxygen (red) and nitrogen atoms (blue). The FGFR is shown as gold and the FGF as a green ribbon. The heparin oligosaccharides are shown as space-filling models with sulfur (yellow), oxygen (red) and nitrogen atoms (blue). *Angew. Chem. Int. Ed. 2002, 41, 390-412.*

Based on biochemical and crystallographic data, a model can be built in which heparin interacts through its nonreducing end with both FGF-2 and FGFR-1 resulting in the formation of a stable 1:1:1 complex of FGF, FGFR, and heparin. This complex can combine with another 1:1:1 complex through direct FGFR-FGFR contacts, secondary interactions between FGF-2 in one ternary complex and FGFR-1 in the adjacent ternary complex, and indirect heparin-mediated FGFR-FGFR contacts.

1.3. DRUG DELIVERY SYSTEMS (DDS)

In recent years, scientific and experimental development in the pharmaceutical sector has facilitated the design and production of drug delivery system formulations, which has improved the therapeutic profile of many drugs whose efficacy and safety had previously been established in clinical trials and subsequently applied to patients. This development has been possible thanks to the introduction of new materials, especially biocompatible polymers, thanks to a better knowledge of the drugs pharmaco-kinetics and pharmaco-dynamics, and thanks to the progress made by industrial companies necessary in the manufacturing of these formulations.

Polymeric matrices can be employed as a type of drug delivery systems in which a drug is embedded on it and this drug may present its original activity or act as a support and a disposal of pharmacologically active substances. The polymers used for this purpose may be biodegradable or not.

The main advantage of the development and application of polymeric drug delivery systems is in the controlled dosage of the activity of a drug during time, without resorting to widespread invasion of the organism, and the vectoring optimization of action of the drug into the human tissues, cells, or subcellular parts. In addition, other advantages of the use of drug delivery systems (DDS) are:

- ✓ The slow controlled release of water soluble drugs.
- ✓ Improving the bioavailability of poor water soluble drugs.
- ✓ Optimize biodistribution drug to be rapid or easily excreted.
- ✓ Controlling the release of highly toxic drugs.

The application of polymeric systems provides a clear optimization of drug dosage to achieve a therapeutic response in the extent desired with minimal adverse effects.

Most drugs administered orally, intravenously or intramuscularly, are rapidly absorbed by the intestinal mucosa or tissue in which it is injected until they are

transferred to the blood flow, which is ultimately distributed throughout the body. This is the case of heparin, whose current clinical administration (intravenously or intramuscularly) results in maximum initial release, which above the minimum toxic concentration that subsequently decreases with time, lowers the minimum effective concentration (curves A and B figure 5). A controlled release system (curve C) keeps the dosage of the drug stable over time, prolonging the effect of the drug without increasing the dosage. Therefore, drug delivery systems allow for the reduction of the toxicity associated with overdosage, and also provide a convenient alternative for the patient, as it reduces the dose administration such as repetitive injections.

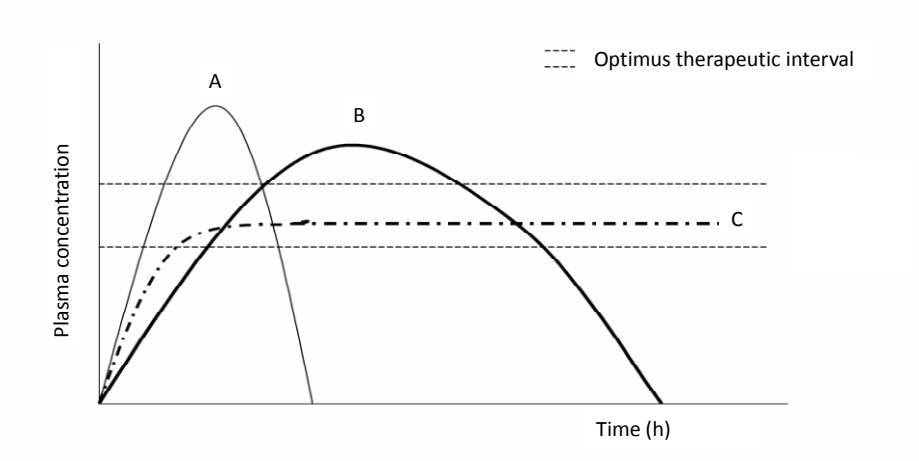

Figure 5. Variation of drug plasma concentration when it is administered in a conventional way (A and B) or with a drug delivery system systems (C). M_w(A) > M_w(B).

Research recent decades has been focused on the development of new nanoparticle systems, biodegradable hydrogels, and bioabsorbable polymer-drug bioconjugates to improve the drug bioavailability and bioactivity range into the body, therefore developing new pharmaceutical formulations.

1.3.1 DEVELOPMENT OF DRUG DELIVERY SYSTEMS

The preparation and development of a drug delivery system depends on the chemical structure and stability of the drug to be encapsulated or immersed into the polymeric matrix. It also depends of the release mechanism of the drug through the polymer chains. There are many kinds of drug release mechanisms, but the main ones include the following:

1.3.1.1 Diffusion controlled release systems

In these systems, the bioactive agent is released by a phenomenon of diffusion through the polymer, where some restrictions on the mass transfer at the polymer / liquid interface exits.

The diffusion coefficient of the bioactive agent through the polymer depends on the structure, morphology and solute concentration. The polymer matrix must be able to deliver drugs at a constant speed for a certain time. Drug migration to the aqueous medium involves a process of absorption of water or biological fluid, and a simultaneous process of drug release by a diffusion mechanism, controlled by the swelling of the polymeric material.

1.3.1.2 Swelling controlled release systems

These systems are characterized by having the active compound dissolved or dispersed in a hydrophilic polymer carrier. This polymer carrier swells without being dissolved when contacted with an aqueous environment. These kinds of systems are called hydrogels and are able to achieve a constant release rate. The degree of swelling depends on the hydrophilic / hydrophobic balance of the polymer matrix and the degree of crosslinking.

Drug migration to the aqueous medium is controlled by a water absorbing process and a simultaneous diffusion process which depend on the swelling degree of the polymeric matrix. When water penetrates into the hydrophilic matrix, the polymer chains, which are at glass state initially, swell and its glass transition temperature (T_g) decreases, moving to an elastomeric state. Under these conditions, the solute diffuses from the swollen region to the external environment and the release is controlled by the speed and conversion of the vitreous / elastic interface.

1.3.1.3 Chemically controlled release systems

The drug release is produced by a chemical reaction. This may be a hydrolytic or enzymatic attack to a weak, ionic, or protonated bond. The polymer-drug conjugates have to possess functional groups which can be attached by a covalent bond and can be hydrolysed in a physiological medium. The covalently bound drug can be released by hydrolysis or enzymatically. The polymer-drug bioconjugates are formed by chains with functional groups which can be covalently attached to the drug. This connection must provide adequate chemical resistance, keeping the pharmacologically activity until their use.

Vectorization systems are designed to achieve a local distribution of the active compound, directed only to the affected tissue or site interest (Figure 6). This is very important especially for highly toxic compounds or drugs with a low therapeutic index. With drug vectorization the number of doses needed is reduced, avoiding systemic toxicity and increasing the concentration in the desired location. Polymer-drug conjugates have been explored as one of the new approaches to vectorizated systems to be applied in anticancer therapies. The anticancer drug can be covalently attached to the polymer using different ligands to form biodegradable linkages, which allow the drug release into a specific location. Some of these anticancer drugs are the doxorubicin, paclitaxel, camptothecin or platinate, and some of the polymers used to form conjugates are *N*-(2-hydroxypropyl) methacrylamide (HPMA), polyglutamate and polyethylene, which have the

advantage of increasing the solubility and / or increase shelf life and bioavailability of the previous mentioned drugs, reducing the required dose and their toxicity[42].

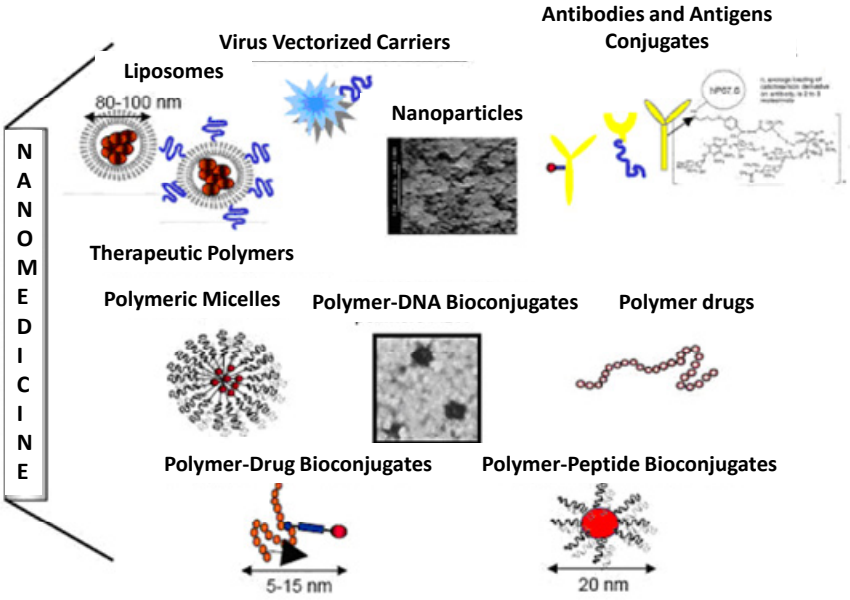

Figure 6. Scheme of different nanomedicine systems for drug delivery, anticancer therapeutics and vectorized systems. Advanced Drug Delivery Reviews. Volume 65, Issue 1, January 2013, Pages 60–70.

1.3.1.4 Bioerosion controlled release systems

In these systems, the drug release is controlled by the rate of polymer degradation. The active compound is dispersed in a polymeric material which is degraded over time, allowing for a controlled rated drug release. There are two types of bioerosion:

• Volume bioerosion: Water absorption promotes the erosion of the polymer in the whole system. Depending on the water penetration rate in the polymer matrix, it will be more or less soluble.

• Surface bioerosion: Water penetration speed in the polymer matrix is slower than the polymer degradation speed, and therefore, the release is limited by the surface of the system.

The main factors affecting the erosion process are:

1. The chemical stability of the polymer chains.
2. The hydrophobicity of the polymer matrix.
3. Polymer morphology.
4. The initial molecular weight of the polymer.
5. The degree of swelling of the drug-loaded polymer matrix.
6. The manufacturing process.
7. The presence of catalysts, additives or plasticizers.
8. The system geometry.

1.3.2 SMART POLYMERS

In these systems, the drug release mechanism is due to a stimulus response, such as a change in temperature, pH, concentration of the drug, electrical or magnetic field effect, light exposition, etc. In response to this external stimulus there is a change in the conformation of the polymer systems, which may cause a change from a collapsed state (no release) to an expanded state (where the drug release occurs). The smart polymer systems most used in biomedical applications are sensitive to pH or temperature polymers.

Temperature responsive polymers as the name suggest, respond to changes in the ambient temperature. Those most useful for biological applications generally possess a lower critical solution temperature (LCST) proximal to physiological

temperature, thus collapse at temperatures higher than this LCST or swell in lower temperatures.

In the body, temperature sensitive polymer system behavior is based on the alteration of the normal body temperature (37 °C) when pathogens or pyrogens are presented in the body, for example they can be used to detect the pathologies accompanied by fever. Recently, these systems have also been studied to act as anticancer therapies as they can change its structure, releasing the anticancer drug when there is a local hyperthermia due to the presence of certain tumors, therefore combining the increase in the temperature with the local delivery of anticancer drugs.

pH sensitive polymer systems can modify their structure due to the pH changes in certain areas of the body such as the intestinal tract. These systems have been studied to develop drug enteric coatings, as well as for targeted delivery systems in antitumor therapies.

One of the most studied polymers in the development of drug-conjugated polymer systems is the poly[(2-dimethyl amino)ethyl methacrylate], which shows double sensitive behavior. It is sensitive to pH and temperature, properties that make it very interesting for biomedical applications. Another interesting example is the temperature sensitive polymer formed by poly[(ethylene glycol) methyl ether methacrylate], whose lower critical solution temperature (LCST) can be modulated with the length of the ethylene glycol chains, thus it is possible to the LCST to close to physiological temperature (37 °C). Both polymers have been used in polymer-drug bioconjugates, through covalent bonding, which subsequently has allowed for the controlled release of drugs via enzymatic or hydrolytic processes.

1.3.3 PARTICLE SYSTEMS

Particle systems have been extensively studied in recent years to be used as drug delivery systems due to the advantages of their small sizes, which allows for the administration of the therapeutic agent via injection or directly application to the

focus area of interest[43]. Depending on their size, they can be classified into microparticles and nanoparticles.

Microparticles are polymeric particles with a sizes ranging from approximately 1 to 250 microns, while polymeric nanoparticles are particles of less than 1 micron. Since the microparticles are larger than the nanoparticles, they have better performance in terms of sustained release but they also present problems due to aggregation because of their bigger size and can be therefore less comfortable for the patient[44]. Three properties considered to be important for polymers to be used as microparticles or nanoparticles systems for biomedical applications are: biodegradation, biocompatibility, and bioadhesion.

Various methods can be employed for the preparation of micro-and nanoparticles[45], such as the solvent evaporation method, organic phase separation, interfacial polymerization, multiple emulsion technique, nanoprecipitation, and spray drying. There are many factors to consider for the development of nanoparticle systems, but the most important are kind of material, the amount of drug to be incorporated, particle stability, release pharmacokinetics, and toxicity. Furthermore, the drug transfer through the polymeric matrix is affected by:

i. The physical state of the drug.
ii. The matrix type.
iii. The drug/matrix proportion.
iv. The degree and nature of the crosslinking matrix.
v. The interaction between the drug, the matrix and medium release.

Drug release can take place through various routes: surface erosion, complete degradation of the matrix, diffusion, and a combination of these routes. The physicochemical properties and variables to take into account to prepare a nanoparticle system are:

• Particle size: the route of administration will determine the size required for the particles.

• Surface area/porosity: variable porosity makes the drug release modulation easier. Polymer degradation is also controlled by altering the porosity of the matrix.

• Drug encapsulated concentration/drug delivery: the release speed depends on the dose needed in the organism and the drug amount that the administration route for which it was designed, is able to accept.

• Biodegradation time: is governed by the administration route and the dosage frequency.

Applications of micro and nanoparticles in pharmacology companies are focused on two different but complementary areas: controlled drug delivery systems and vectorization systems.

Nanoparticles drug delivery systems show great advantages thanks to their small size, allowing for the injection of the drug with a conventional syringe, therefore avoiding invasive surgical intervention. They can be endocyted by cells. Therefore, the drug can be released inside the cell cytoplasm, and can be used as drug carriers for specific drugs which are not able to be administered orally, such as anticancer agents, immunosuppressants, vitamins, antibiotics, etc.

The uses of nanoparticles as drug carrier systems have been widely used in biomedical applications (described in the previous section). Nanoparticles are an efficient encapsulation drug delivery system since they make drug administration easier. The use of biodegradable copolymers derived from lactic and glycolic acids known as PLGA, and its derivatives are widely used as a material specimen due to their biodegradability, biocompatibility, and the abbility to efficiently encapsulate a variety of molecules[13] (proteins, peptides, genes , vaccines, antigens, growth factors, etc..). EUDRAGIT RS PO based matrices are quite attractive in the pharmaceutical field because of their high chemical stability, good compactness and the availability of a large variability of products in the market that have different chemical properties[46]. Several papers have been published describing nanoparticles prepared with PLGA and EUDRAGIT to encapsulate heparin, in order to improve the stability of the drug[6, 16].

1.4. TISSUE ENGINEERING: WOUND HEALING.

The wound-healing process consists of four highly integrated and overlapping phases: hemostasis, inflammation, proliferation, and tissue remodeling or resolution[47]. These phases and their biophysiological functions must occur in the proper sequence, at a specific time, and continue for a specific duration at an optimal intensity[48]. There are many factors that can affect wound healing which interfere with one or more phases in this process, thus causing improper or impaired tissue repair.

The events of each of the phases described must happen in a precise and regulated manner. Interruptions, aberrancies, or prolongation in the process can lead to delayed wound healing or a non-healing chronic wound.

In adult humans, optimal wound healing involves the following the events: (1) rapid hemostasis; (2) appropriate inflammation; (3) mesenchymal cell differentiation, proliferation, and migration to the wound site; (4) suitable angiogenesis; (5) prompt re-epithelialization (re-growth of epithelial tissue over the wound surface); and (6) proper synthesis, cross-linking, and alignment of collagen to provide strength to the healing tissue. The first phase of hemostasis begins immediately after wounding, with vascular constriction and fibrin clot formation. The clot and surrounding wound tissue release pro-inflammatory cytokines and growth factors such as transforming growth factor (TGF)-β, platelet-derived growth factor (PDGF), fibroblast growth factor (FGF), and epidermal growth factor (EGF). Once bleeding is controlled, inflammatory cells migrate into the wound (chemotaxis) and promote the inflammatory phase, which is characterized by the sequential infiltration of neutrophils, macrophages, and lymphocytes[49]. The critical function of neutrophils is the clearance of invading microbes and cellular debris in the wound area, although these cells also produce substances such as proteases and reactive oxygen species (ROS), which cause some additional bystander damage.

Macrophages play multiple roles in wound healing. In the early wound, macrophages release cytokines that promote the inflammatory response by recruiting and activating additional leukocytes. Macrophages are also responsible for

inducing and clearing apoptotic cells (including neutrophils), thus paving the way for the resolution of inflammation. As macrophages clear these apoptotic cells, they undergo a phenotypic transition to a reparative state that stimulates keratinocytes, fibroblasts, and angiogenesis to promote tissue regeneration[50]. In this way, macrophages promote the transition to the proliferative phase of healing.

The proliferative phase generally follows and overlaps with the inflammatory phase, and is characterized by epithelial proliferation and migration over the provisional matrix within the wound (re-epithelialization). In the reparative dermis, fibroblasts and endothelial cells are the most prominent cell types present and support capillary growth, collagen formation, and the formation of granulation tissue at the site of injury. Within the wound bed, fibroblasts produce collagen as well as glycosaminoglycans and proteoglycans, which are major components of the extracellular matrix (ECM). Following robust proliferation and ECM synthesis, wound healing enters the final remodeling phase, which can last for years. In this phase, regression of many of the newly formed capillaries occurs, so that vascular density of the wound returns to normal. One critical feature of the remodeling phase is ECM remodeling to an architecture that resembles that of the normal tissue. The wound also undergoes physical contraction throughout the entire wound-healing process, which is believed to be mediated by contractile fibroblasts (myofibroblasts) that appear in the wound[51].

The use of polymeric dressings intends to promote the epithelialization process against contraction. The healing process is faster in a moist environment and polymeric hydrogels are very good candidates to be used as swelling systems, by retaining an adequate amount moisture in the wound environment. Skin lesions caused by an insufficient vascular mechanism affect a large number of people and are very costly to the health system in society.

Conventional techniques such as suturing, scarring, burning, or the use of staples have several disadvantages such as pain or/and the need of removal after the tissue regeneration. However, the use of other materials such as polymeric dressings have the advantages of being painless for the patient, adhering easily to the skin, easy manipulation, simple performance and if they are biodegradable they

do not need to be removed. Polymer dressings use for biomedical applications must be biodegradable, biocompatible, bioabsorbable, and with a good chemical stability (good mechanical properties) in order to be effective in the wound healing process.

Some diseases, such as diabetes, ulcerative lesions in the lower limbs or circulatory problems, cause some difficulties in the wound healing process, making it slower and more difficult than normal. Two of these examples are following described:

The elderly population (people over 60 years of age) has an increased risk of impaired wound healing compared to the younger population generally. It is commonly recognized that, in healthy older adults, the effect of aging causes a temporal delay in wound healing, but not an actual impairment in terms of the quality of healing[52]. Delayed wound healing in the aged is associated with an altered inflammatory response, such as delayed T-cell infiltration into the wound area with alterations in chemokine production and reduced macrophage phagocytic capacity[53]. Diabetic individuals exhibit a documented impairment in the healing of acute wounds. Moreover, this population is prone to developing chronic non-healing diabetic foot ulcers, like venous stasis disease and pressure-related chronic non-healing wounds, which are always accompanied by hypoxia[54]. A situation of prolonged hypoxia, which may be derived from both insufficient perfusion and insufficient angiogenesis, is detrimental for wound healing. Hypoxia can amplify the early inflammatory response, thereby prolonging injury by increasing the levels of oxygen radicals[55].

To treat these kinds of patients, some compounds that are known to promote the healing of wounds and ulcers have been developed, such as the *N*-terminal of 20 amino acid peptide of proadrenomedulin (PAMP), which have been demonstrated to show angiogenic properties, promote the re-epithelialization, and have antimicrobial properties. Bemiparin, previously described in this chapter, can act as a thrombotic and / or restenotic modulator, and is able to form active complexes with growth factors (FGF and VEGF etc.), increasing the biological activity of these factors as described previously.

In this thesis, we have developed a biocompatible and bioabsorbable bilayer dressing based on the controlled release of two bioactive components, PAMP and bemiparin, which make the wound healing process easier and faster, and can be applied directly to the affected area. This system is described in Chapter 5 of this thesis, and has resulted in the application for a Spanish Patent (ES P201231750). The main advantage of this bioactive polymeric system is the improvement of the healing process in patients with diseases such as diabetes or circulatory problems, thanks to both the sequential release of bioactive molecules and the ability to apply the dressing locally thus avoiding the side effects associated with systemic administration.

1.5. REFERENCES

1. Francis Suh, J. K.; Matthew, H. W. T., Application of chitosan-based polysaccharide biomaterials in cartilage tissue engineering: a review. *Biomaterials* **2000,** *21* (24), 2589-2598.
2. (a) Friedrich, M. V. K.; Göhring, W.; Mörgelin, M.; Brancaccio, A.; David, G.; Timpl, R., Structural basis of glycosaminoglycan modification and of heterotypic interactions of perlecan domain V. *Journal of Molecular Biology* **1999,** *294* (1), 259-270; (b) Giacoletto, K. S.; Rumbarger, T.; Schwartz, B. D., Chapter 8 Glycosaminoglycan Modifications of Membrane Proteins. In *Methods in Cell Biology*, Alan, M. T., Ed. Academic Press: 1989; Vol. Volume 32, pp 207-230; (c) Reubsaet, F. A. G.; Langeveld, J. P. M.; Veerkamp, J. H., Glycosaminoglycan content of glomerular and tubular basement membranes of various mammalian species. *Biochimica et Biophysica Acta (BBA) - General Subjects* **1985,** *838* (1), 144-150.
3. (a) Ho, Y.-C.; Mi, F.-L.; Sung, H.-W.; Kuo, P.-L., Heparin-functionalized chitosan–alginate scaffolds for controlled release of growth factor. *International Journal of Pharmaceutics* **2009,** *376* (1–2), 69-75; (b) Iwamoto, R.; Mekada, E., Heparin-binding EGF-like growth factor: a juxtacrine growth factor. *Cytokine & Growth Factor Reviews* **2000,** *11* (4), 335-344; (c) Sakiyama-Elbert, S. E.; Hubbell, J. A., Controlled release of nerve growth factor from a heparin-containing fibrin-based cell ingrowth matrix. *Journal of Controlled Release* **2000,** *69* (1), 149-158.
4. Capila, I.; Linhardt, R. J., Heparin–Protein Interactions. *Angewandte Chemie International Edition* **2002,** *41* (3), 390-412.
5. Streubel, A.; Siepmann, J.; Bodmeier, R., Multiple unit gastroretentive drug delivery systems: A new preparation method for low density microparticles. *Journal of Microencapsulation* **2003,** *20* (3), 329-347.
6. Moustafine, R. I.; Zaharov, I. M.; Kemenova, V. A., Physicochemical characterization and drug release properties of Eudragit® E PO/Eudragit® L 100-55 interpolyelectrolyte complexes. *European Journal of Pharmaceutics and Biopharmaceutics* **2006,** *63* (1), 26-36.
7. Ibrić, S.; Jovanović, M.; Djurić, Z.; Parojčić, J.; Solomun, L., The application of generalized regression neural network in the modeling and optimization of aspirin extended release tablets with Eudragit® RS PO as matrix substance. *Journal of Controlled Release* **2002,** *82* (2–3), 213-222.
8. Martínez, A.; Zudaire, E.; Portal-Núñez, S.; Guédez, L.; Libutti, S. K.; Stetler-Stevenson, W. G.; Cuttitta, F., Proadrenomedullin NH2-Terminal 20 Peptide Is a Potent Angiogenic Factor, and Its Inhibition Results in Reduction of Tumor Growth. *Cancer Research* **2004,** *64* (18), 6489-6494.
9. York, A. W.; Kirkland, S. E.; McCormick, C. L., Advances in the synthesis of amphiphilic block copolymers via RAFT polymerization: Stimuli-responsive drug and gene delivery. *Advanced Drug Delivery Reviews* **2008,** *60* (9), 1018-1036.

10. Nickerson, M. T.; Farnworth, R.; Wagar, E.; Hodge, S. M.; Rousseau, D.; Paulson, A. T., Some physical and microstructural properties of genipin-crosslinked gelatin–maltodextrin hydrogels. *International Journal of Biological Macromolecules* **2006,** *38* (1), 40-44.
11. Cervantes-Uc, J. M.; Espinosa, J. I. M.; Cauich-RodrÃ-guez, J. V.; Ã vila-Ortega, A.; VÃ¡zquez-Torres, H.; Marcos-FernÃ¡ndez, A.; San RomÃ¡n, J., TGA/FTIR studies of segmented aliphatic polyurethanes and their nanocomposites prepared with commercial montmorillonites. *Polymer Degradation and Stability* **2009,** *94* (10), 1666-1677.
12. (a) Chiu, L. L. Y.; Chu, Z.; Radisic, M., 2.07 - Tissue Engineering. In *Comprehensive Nanoscience and Technology*, Editors-in-Chief: David, L. A.; Gregory, D. S.; Gary, P. W., Eds. Academic Press: Amsterdam, 2011; pp 175-211; (b) Guan, J.; Fujimoto, K. L.; Sacks, M. S.; Wagner, W. R., Preparation and characterization of highly porous, biodegradable polyurethane scaffolds for soft tissue applications. *Biomaterials* **2005,** *26* (18), 3961-3971.
13. Acharya, S.; Sahoo, S. K., PLGA nanoparticles containing various anticancer agents and tumour delivery by EPR effect. *Advanced Drug Delivery Reviews* **2011,** *63* (3), 170-183.
14. Zhang, H.; Cui, W.; Bei, J.; Wang, S., Preparation of poly(lactide-co-glycolide-co-caprolactone) nanoparticles and their degradation behaviour in aqueous solution. *Polymer Degradation and Stability* **2006,** *91* (9), 1929-1936.
15. Dillen, K.; Vandervoort, J.; Van den Mooter, G.; Ludwig, A., Evaluation of ciprofloxacin-loaded Eudragit® RS100 or RL100/PLGA nanoparticles. *International Journal of Pharmaceutics* **2006,** *314* (1), 72-82.
16. Hoffart, V.; Lamprecht, A.; Maincent, P.; Lecompte, T.; Vigneron, C.; Ubrich, N., Oral bioavailability of a low molecular weight heparin using a polymeric delivery system. *Journal of Controlled Release* **2006,** *113* (1), 38-42.
17. Crafoord C, J. E., Heparin as a prophylactic against thrombosis. *Journal of the American Medical Association* **1941,** *116* (26), 2831-2835.
18. (a) Gutowska, A.; Bae, Y. H.; Feijen, J.; Kim, S. W., Heparin release from thermosensitive hydrogels. *Journal of Controlled Release* **1992,** *22* (2), 95-104; (b) Nie, T.; Baldwin, A.; Yamaguchi, N.; Kiick, K. L., Production of heparin-functionalized hydrogels for the development of responsive and controlled growth factor delivery systems. *Journal of Controlled Release* **2007,** *122* (3), 287-296.
19. Javot, L.; Lecompte, T.; Rabiskova, M.; Maincent, P., Encapsulation of low molecular weight heparins: Influence on the anti-Xa/anti-IIa ratio. *Journal of Controlled Release* **2009,** *139* (1), 8-14.
20. (a) Chung, Y.-I.; Tae, G.; Hong Yuk, S., A facile method to prepare heparin-functionalized nanoparticles for controlled release of growth factors. *Biomaterials* **2006,** *27* (12), 2621-2626; (b) Eidi, H.; Joubert, O.; Attik, G.; Duval, R. E.; Bottin, M. C.; Hamouia, A.; Maincent, P.; Rihn, B. H., Cytotoxicity assessment of heparin nanoparticles in NR8383 macrophages. *International Journal of Pharmaceutics* **2010,** *396* (1-2), 156-165.
21. Kemp, M. M.; Linhardt, R. J., Heparin-based nanoparticles. *Wiley Interdisciplinary Reviews: Nanomedicine and Nanobiotechnology* **2010,** *2* (1), 77-87.
22. Dumitriu, S., *Polymeric Biomaterials*. Dekker: Jassy, Romania, 1994.
23. SanRoman, J., Sistemas macromoleculares biocompatibles: una nueva concepción de aplicaciones farmacológicas. *Revista de Plásticos Modernos* **1989,** *396*, 888-900.
24. Pasut, G.; Veronese, F. M., Polymer–drug conjugation, recent achievements and general strategies. *Progress in Polymer Science* **2007,** *32* (8–9), 933-961.
25. Lee, D. Y.; Kim, S. K.; Kim, Y. S.; Son, D. H.; Nam, J. H.; Kim, I. S.; Park, R. W.; Kim, S. Y.; Byun, Y., Suppression of angiogenesis and tumor growth by orally active deoxycholic acid-heparin conjugate. *Journal of Controlled Release* **2007,** *118*, 310-317.
26. Lee, G. Y.; Kim, S. K.; Byun, Y., Glucosylated heparin derivatives as non-toxic anti-cancer drugs. *Journal of Controlled Release* **2007,** *123*, 46-55.
27. Rojas Cortés, M. G.; Vallejo Díaz, B. M.; Perilla, J. E., Los biopolímeros como materiales para el desarrollo de productos en aplicaciones farmacéuticas y de uso biomédico. *Ingeniería e Investigación* **2008,** *28*, 57-71.
28. González, N. Nuevos Sistemas Poliméricos Sensibles a pH y Temperatura. Aplicaciones Biomédicas. Universidad Complutense de Madrid, Madrid, 2006.
29. Bilati, U.; Allemann, E.; Doelker, E., Development of a nanoprecipitation method intended for the entrapment of hydrophilic drugs into nanoparticles. *European Journal of Pharmaceutical Sciences* **2005,** *24*, 65-75.
30. Picos;, D. R.; Carril;, M. G.; Mena, D. F., Métodos de obtención de microesferas biodegradables. *Revista Cubana de Farmacia* **2001,** *35* (2).

31. Stolnik, S.; Garnett, M. C.; Illum, L.; Davis, S. S.; Govender, T., PLGA nanoparticles prepared by nanoprecipitation: drug loading and release studies of a water soluble drug. *Journal of Controlled Release* **1999,** *57*, 171-185.
32. Peter J. van Winterswijk, M., Erik Nout, MD, Tissue Engineering and Wound Healing: An Overview of the Past, Present, and Future. *Wounds* **2007,** *19* (10), 277-284.
33. (a) Chen, S.-H.; Tsao, C.-T.; Chang, C.-H.; Lai, Y.-T.; Wu, M.-F.; Chuang, C.-N.; Chou, H.-C.; Wang, C.-K.; Hsieh, K.-H., Assessment of reinforced poly(ethylene glycol) chitosan hydrogels as dressings in a mouse skin wound defect model. *Materials Science and Engineering: C* (0); (b) Corkhill, P. H.; Hamilton, C. J.; Tighe, B. J., Synthetic hydrogels VI. Hydrogel composites as wound dressings and implant materials. *Biomaterials* **1989,** *10* (1), 3-10.
34. Fu, Y.; Létourneau, M.; Nguyen, Q. T.; Chatenet, D.; Dupuis, J.; Fournier, A., Characterization of the adrenomedullin receptor acting as the target of a new radiopharmaceutical biomolecule for lung imaging. *European Journal of Pharmacology* **2009,** *617* (1–3), 118-123.
35. Martínez-González J, V. L., Rodríguez C., Bemiparin: a second generation low-molecular weight heparin for treatment and prophylaxis of venous thromboembolism. *Expert Rev Cardiovasc Ther* **2008,** *6*, 793-802.
36. Whitelock, J.; Melrose, J., Heparan sulfate proteoglycans in healthy and diseased systems. *Wiley Interdisciplinary Reviews: Systems Biology and Medicine* **2011,** *3* (6), 739-751.
37. Pike, D. B.; Cai, S.; Pomraning, K. R.; Firpo, M. A.; Fisher, R. J.; Shu, X. Z.; Prestwich, G. D.; Peattie, R. A., Heparin-regulated release of growth factors in vitro and angiogenic response in vivo to implanted hyaluronan hydrogels containing VEGF and bFGF. *Biomaterials* **2006,** *27* (30), 5242-5251.
38. Depasse, F.; González de Suso, M. J.; Lagoutte, I.; Fontcuberta, J.; Borrell, M.; Samama, M. M., Comparative study of the pharmacokinetic profiles of two LMWH - bemiparin (3500 IU, anti-Xa) and tinzaparin (4500 IU, anti-Xa) - administered subcutaneously to healthy male volunteers. *Thrombosis Research* **2003,** *109* (2-3), 109-117.
39. Kemp, M. M.; Linhardt, R. J., Heparin-based nanoparticles. *Wiley Interdiscip. Rev.-Nanomed. Nanobiotechnol.* **2010,** *2* (1), 77-87.
40. Norrby, K., Low-molecular-weight heparins and angiogenesis. *APMIS* **2006,** *114* (2), 79-102.
41. Martínez-González, J.; Vila, L.; Rodríguez, C., Bemiparin: second-generation, low-molecular-weight heparin for treatment and prophylaxis of venous thromboembolism. *Expert Review of Cardiovascular Therapy* **2008,** *6* (6), 793-802.
42. Duncan, R.; Gac-Breton, S.; Keane, R.; Musila, R.; Sat, Y. N.; Satchi, R.; Searle, F., Polymer–drug conjugates, PDEPT and PELT: basic principles for design and transfer from the laboratory to clinic. *Journal of Controlled Release* **2001,** *74* (1–3), 135-146.
43. Kohane, D. S., Microparticles and nanoparticles for drug delivery. *Biotechnology and Bioengineering* **2007,** *96* (2), 203-209.
44. Stages of Healing. *Curad. 4* **2013**.
45. Pinto Reis, C.; Neufeld, R. J.; Ribeiro, A. J.; Veiga, F., Nanoencapsulation I. Methods for preparation of drug-loaded polymeric nanoparticles. *Nanomedicine: Nanotechnology, Biology and Medicine* **2006,** *2* (1), 8-21.
46. (a) Glaessl, B.; Siepmann, F.; Tucker, I.; Rades, T.; Siepmann, J., Deeper insight into the drug release mechanisms in Eudragit RL-based delivery systems. *International Journal of Pharmaceutics* **2010,** *389* (1–2), 139-146; (b) Karthikeyan, K.; Guhathakarta, S.; Rajaram, R.; Korrapati, P. S., Electrospun zein/eudragit nanofibers based dual drug delivery system for the simultaneous delivery of aceclofenac and pantoprazole. *International Journal of Pharmaceutics* **2012,** *438* (1–2), 117-122; (c) Yoo, J.-W.; Giri, N.; Lee, C. H., pH-sensitive Eudragit nanoparticles for mucosal drug delivery. *International Journal of Pharmaceutics* **2011,** *403* (1–2), 262-267.
47. Gosain, A.; DiPietro, L. A., Aging and Wound Healing. *World J. Surg.* **2004,** *28* (3), 321-326.
48. Mathieu, D.; Linke, J.-C.; Wattel, F., Non-Healing Wounds. In *Handbook on Hyperbaric Medicine*, Mathieu, D., Ed. Springer Netherlands: 2006; pp 401-428.
49. Broughton G 2nd, J. J., Attinger CE., The basic science of wound healing. *Plast Reconstr Surg.* **2006,** *117* (7 Suppl), 12S-34S.
50. Meszaros, A. J.; Reichner, J. S.; Albina, J. E., Macrophage-Induced Neutrophil Apoptosis. *The Journal of Immunology* **2000,** *165* (1), 435-441.
51. Campos, A. C.; Groth, A. K.; Branco, A. B., Assessment and nutritional aspects of wound healing. *Current Opinion in Clinical Nutrition & Metabolic Care* **2008,** *11* (3), 281-288 10.1097/MCO.0b013e3282fbd35a.

52. Keylock, K. T.; Vieira, V. J.; Wallig, M. A.; DiPietro, L. A.; Schrementi, M.; Woods, J. A., Exercise accelerates cutaneous wound healing and decreases wound inflammation in aged mice. *American Journal of Physiology - Regulatory, Integrative and Comparative Physiology* **2008,** *294* (1), R179-R184.
53. Swift, M. E.; Burns, A. L.; Gray, K. L.; DiPietro, L. A., Age-Related Alterations in the Inflammatory Response to Dermal Injury. **2001,** *117* (5), 1027-1035.
54. Tandara, A. A.; Mustoe, T. A., Oxygen in Wound Healing—More than a Nutrient. *World J. Surg.* **2004,** *28* (3), 294-300.
55. Woo, K.; Ayello, E. A.; Sibbald, R. G., The Edge Effect: Current Therapeutic Options to Advance the Wound Edge. *Advances in Skin & Wound Care* **2007,** *20* (2), 99-117.

Synthesis and Characterization of Methacrylate-based polymers prepared by Controlled Radical Polymerization: ATRP AND RAFT

CHAPTER 2

2.1. INTRODUCTION

Free radical polymerization (RP) is one of the most widely employed polymerization techniques. This technique is applied to prepare latexes to be used in paints, high molecular weight poly (methyl methacrylate) for safety glasses, and foamed poly (styrene) to be applied in coffee cups. Some advantages of radical polymerization, with respect to other techniques, are the relative insensitivity to impurities, the moderate reaction temperatures and the versatiles multiple polymerization processes available, e.g., bulk, solution, precipitation or emulsion polymerization. Some disadvantages related to the mechanism of free radical polymerization are the poor control of the molecular weight and the molecular weight distribution, and the difficulty (or even impossibility) of preparing well-defined copolymers or polymers with a predetermined functionality. To overcome these disadvantages new technique was developed based on either reversible deactivation of polymer radicals or degenerative transfer process, called 'living' or controlled radical polymerization (CRP).

2.1.1. CONTROLLED RADICAL POLYMERIZATION

Controlled radical polymerization depends upon the existence of a dynamic equilibrium between propagating radicals and dormant species. Propagating radicals may either be reversibly trapped in a deactivation/activation process (Figure 9a) or they can be involved in a 'reversible transfer', degenerative exchange process (Figure 9b)[56]. Two main kinds of CRP are atom transfer radical polymerizations (ATRP) and reversible addition-fragmentation chain transfer polymerization (RAFT), which represent key strategies for the preparation of well defined polymers with narrow molecular weight distribution[57].

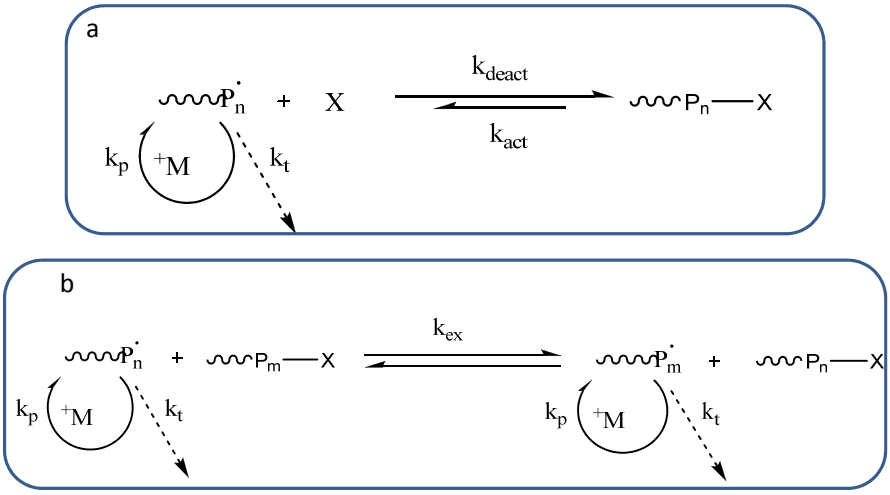

Figure 7. Scheme of the dynamic equilibriums possible in a CRP: a) radicals are reversibly trapped in a deactivation/activation process, b) radicals are involved in a reversible transfer, degenerative exchange process.

Fast exchange between the active and the dormant species is required for a good control over the molecular weight, polydispersity and chain architecture in all CRP systems. A growing species should ideally react only with a few monomer units (within a few milliseconds) before it is deactivated to the dormant state (where it remains for several seconds). The lifetime of a chain in its active state is comparable to the lifetime of a propagating chain in free RP. However, radicals spend more time in dormant state and therefore, there is lower chance of radical-radical termination and more opportunities to carry out chain-end functionalization or chain extension[58].

2.1.2. BENEFITS OF CRP VERSUS RP

CRP and free RP proceed via the same radical mechanism, exhibit similar chemo-, regio- and stereo-selectivities, and can polymerize a similar range of monomers. However RP processes present some limitations[59]:

- Little control over molar mass distribution, due to diffusion-controlled termination reactions between growing radicals.
- It is not possible to synthesize block copolymers or other chain topologies, since the typical life time of a propagating chain is very short, in the range of 1 second.
- There is no control over the polymer tacticity.

These disadvantages can be improved by CRP, since it provides a good control over the molecular weight and the molecular weight distribution, and the feasibility of preparing well-defined copolymers or polymers with a specific functionality.

As a summary, the main differences between CRP and RP mechanism are:

- The lifetime of growing chains is extended from 1 second in RP to more than 1 h in CRP through the participation of dormant species and intermittent reversible activation.
- Initiation is slow and free radical initiator is often left unconsumed at the end of a conventional RP. In most CRP systems, initiation is very fast and near instantaneous growth of all chains can be achieved, which ultimately enables control over chain architecture.
- Nearly all chains are dead in RP, whereas in CRP the proportion of dead chains is usually < 10%.
- Polymerization in CRP is often slower than in RP. However, the rates may be comparable in certain cases (e.g. when the targeted M_w in CRP is relatively low).
- A steady state radical concentration is established in RP with similar rates of initiation and termination, whereas CRP system is based on the persistent radical effect, where all chains are short at the early stages of the reaction and become progressively longer, causing the termination rate to significantly decrease with time. In RP processes, new chains are constantly generated by a

small amount of conventional initiator, and therefore termination is more likely throughout the reaction.

CRP also presents some disadvantages, such as the use of specific control agent, the limitation of getting high molecular weights, and the sensitivity to atmospheric oxygen.

2.1.3. ATRP POLYMERIZATION

Atom transfer radical polymerization (ATRP) is one of the most robust controlled/living radical polymerization (CRP) techniques, allowing the controlled polymerization of various vinyl and acrylic monomers under mild conditions.[60] This technology has been shown to also allow the production of a vast range of polymer morphologies, including systems with phase separation at the nano-scale.[61] Such morphologies are known to result in materials with unique mechanical properties, providing additional modes for regulating the release of therapeutic agents and for producing surfaces that are compatible with the *'in vivo'* environment.[62] An ATRP initiating system consists on an alkyl halide initiator and a transition metal catalyst in the lower oxidation state, being copper the most commonly studied metal.[60b, 63] Activators Generated by Electron Transfer (AGET) ATRP is a useful extension of the traditional ATRP process in that an oxidatively stable copper(II) ligand complex are added to the reaction and a fraction of the complex reduced to the active copper(I) species via the introduction of a reducing agent.[56,64]

The typical efficient ATRP catalyst consists of a transition metal species (Mtn) which can expand its coordination sphere and increase its oxidation number, a complexing ligand (L), and a counterion which can form a covalent or ionic bond with the metal center. The transition metal complex (Mt^n/L) is responsible for the homolytic cleavage of an alkyl halogen bond RX which generates the corresponding higher oxidation state metal halide complex Mt^{n+1}X/L (with a rate constant k_{act}) and an organic radical R* (Figure 8). This radical can then

propagates (k_p), terminates by either coupling or disproportionation (k_t), or be reversibly deactivated (k_{deact}) by $Mt^{n+1}X/L$ to form a halide-capped dormant species. Radical termination is diminished in ATRP as a result of the persistent radical effect and the ATRP equilibrium (KATRP = kact/kdeact) becomes strongly shifted towards the dormant species (rate constant of activation << rate constant of deactivation).

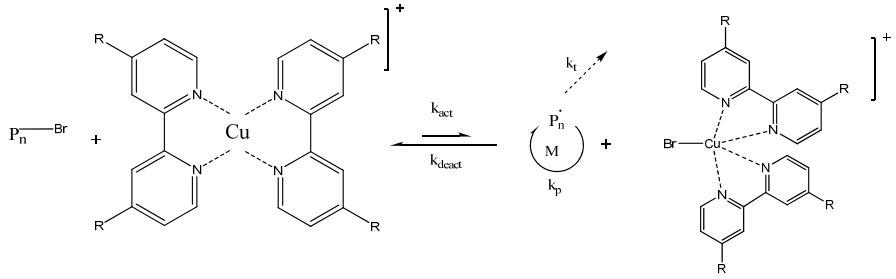

Figure 8. ATRP metal-ligand catalyst mechanism: the transition metal complex is responsible for the hemolytic cleavage of an alkyl halogen bond generating a higher oxidation state metal halide complex and an organic radical.

ATRP has been successfully mediated by a variety of metals[65-68], including those from groups 4 (Ti[66], Mo[67], Re, Fe[68], Ru[69], Os, Rh, Co[70], Ni[71], Pd[72], and Cu). Complexes of Cu have been found to be the most efficient catalysts in the ATRP of a broad range of monomers in diverse media[73].

K_{ATRP} can be expressed as a combination of four reversible reactions: oxidation of the metal complex, or electron transfer (K_{ET}), reduction of a halogen to a halide ion, or electron affinity (K_{EA}), alkyl halide bond homolysis (K_{BH}), and association of the halide ion to the metal complex, or 'halogenophilicity' (K_X) (Figure 9). These equilibrium constants, especially K_{EA} and K_X, are very solvent dependent[74]. The values of K_{EA} are expected to be relatively high in protic solvents as halide anions are stabilized by solvation in such media. K_X will likewise be affected with changes in solvent polarity. This has direct implications on the degree of control attainable in aqueous media as the majority of the halogen will be dissociated from the Cu deactivating species in water.

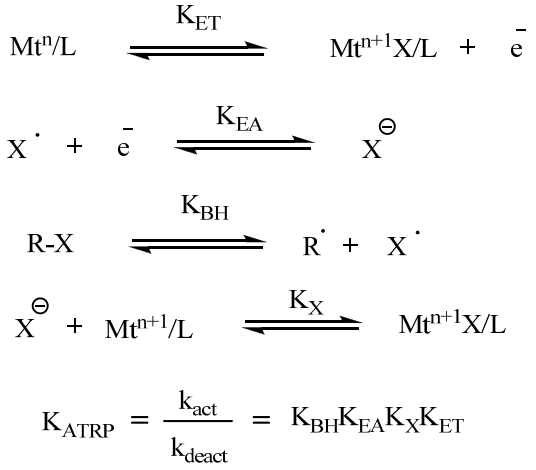

Figure 9. Sub-equilibria in K_{ATRP}.

Catalyst activity (in terms of K_{ATRP}) is also intrinsically dependent upon the redox potential of the complex. A linear correlation between K_{ATRP} and the redox potential ($E_{1/2}$) of the transition metal catalyst has been clearly demonstrates for a series of Cu^{I} complexes[75]. The $E_{1/2}$, which can be correlated with its catalytic activity in ATRP reactions, also depends upon the ratio of the stability constants of the complex in its two oxidation states. Most ligands affect the redox potential of Cu complexes through stabilization or destabilization of the Cu^{II} oxidation state. Therefore, if a ligand forms a very stable Cu^{II} complex, the corresponding Cu^{I} complex should be very reducing and catalytically active in ATRP.

Some studies have been carried out to determine the effect of ligand structure on the catalyst activation in ATRP process[76]. Several rules pertaining to catalyst activity were derived from these studies:

- Activity depends very strongly on the linking unit between the N atoms (C4<< C3< C2) and/or the coordination angle.
- The topology of the ligand (cyclic ≈ linear < branched) affects activity.
- Activity depends upon the nature of the N-ligand (aryl amine < aryl imine < alkyl imine < alkyl amine ≈ pyridine).

- Steric bulk around the metal center can affect the rate of activation/deactivation (e.g. the Me_6TREN complex is 1000 times more active than Et_6TREN).

The broad availability of initiators provides ATRP with a significant advantage over other CRP techniques. Most compounds with halogen atoms that are activated by α-carbonyl, phenyl, vinyl or cyano groups make efficient ATRP initiators. The reactivity of these initiators depends reciprocally on the alkyl halide bond dissociation energies[77]. Therefore it can be concluded that initiator activity depends on:

- The degree of initiator substitution (primary < secondary < tertiary).
- The leaving atom/group (for methyl 2-halopropionates: Cl < Br < I).
- The radical stabilizing groups (-Ph ≈ -C(O)OR << -CN).

Monomer unit can also have a strong effect on k_{act}. This realization is of particular relevance in copolymerization. In ATRP, the order of the equilibrium constants for a series of common monomers is acrylonitrile > methacrylates > styrene ≈ acrylates > acrylamides >> vinyl chloride > vinyl acetate. The efficient preparation of block copolymers requires this order to be obeyed when synthesizing each block to ensure near simultaneous growth from each macroinitiator (e.g. polyacrylonitrile should be chain extended with polyacrylate and not vice versa).

Activators Generated by Electron Transfer (AGET)

The limitation of normal initiation in ATRP is evident in the inability to produce clean block copolymers. In AGET ATRP, reducing agents that are unable to initiate new chains (rather than organic radicals) are used to reduce the higher oxidation state transtition metal complex[78](Figure 10). No homopolymers are produced during block copolymerization with this technique. Many reducing agents could theoretically be used. Also zero valent Cu could be used as a

reducing agent to react with Cu^{II} and enhance the rate of polymerization in ATRP[79]. The AGET principle was demonstrated using tin(II) 2-ethylhexanoate, ascorbic acid or triethylamine as the reducing agents, which reacted with the Cu^{II} complex to generate the Cu^{I} ATRP activator. This initiation technique has proven particularly useful in aqueous and miniemulsion systems[80].

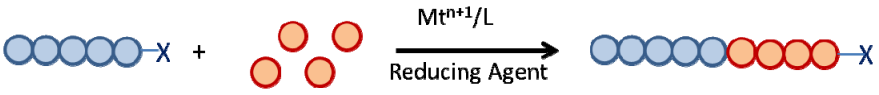

Figure 10. AGET-ATRP equilibrium scheme.

2.1.4. RAFT POLYMERIZATION

Reversible Addition-Fragmentation chain Transfer (RAFT) polymerization, a reversible deactivation radical polymerization (RDRP), is one of the most effective and versatile methods for providing living characteristic to radical polymerization allowing the synthesis of macromolecules with a strictly controlled chemical structure using mild reaction conditions[81,82]. This technique supposes an alternative approach for the formation of well-defined polymers by the use of a chain transfer agent in the form of a thiocarbonylthio compound (from here on referred to as a RAFT agent) to afford control over the generated molecular weight and polydispersity during a free-radical polymerization.

RAFT provides reversible deactivation of propagating radicals by degenerate chain transfer for which a general mechanism is shown in Figure 11. The chain transfer step has been termed degenerate because the process involves an exchange of functionality and the only distinction between the species on the two sides of the equilibrium is molar mass.

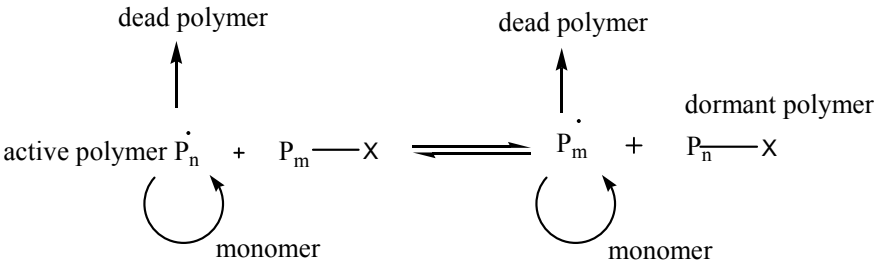

Figure 11. Scheme of polymerization with reversible deactivation by degenerate chain transfer.

Radical addition-fragmentation processes were firstly reported in the synthetic organic chemistry literature in the early 1970s[83]. Well-known examples include allyl transfer reactions with allyl sulfides and stannanes and deoxygenation process with xanthates. The use of (irreversible) addition-fragmentation chain transfer agents, such as vinyl ethers and allyl sulfides, to control molecular weight and end-group functionality of polymers was reported in the 1980s[84]. However, the direct use of addition-fragmentation chain transfer agents to provide living character to radical polymerization did not appear until the mid-1990s. The first RAFT agents (though that term was not used at the time) were macromonomers of general structure(Figure 12A), while the RAFT process making use of thiocarbonylthio compounds (Figure 12B) to control radical polymerization appeared in 1998. These compounds include dithioesters (Z = alkyl or aryl), trithiocarbonates (Z = SR'), xanthates (Z = OR') and dithiocarbamates (Z = NR'R'').

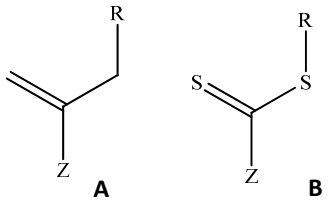

Figure 12. RAFT agent chemical structure.

RAFT polymerization comprises the addition-fragmentation equilibria shown in Figure 13 plus all the usual processes that make up radical polymerization, most notably initiation and termination. Note that in RAFT, radicals are neither formed nor destroyed. Thus, RAFT polymerization will not take place without an external supply of radicals. Therefore, apart from controlling the molar mass and molar mass distribution, the RAFT equilibrium have no direct influence on the rate of polymerization. It should also be noted that radical-radical termination is not directly suppressed by the RAFT process.

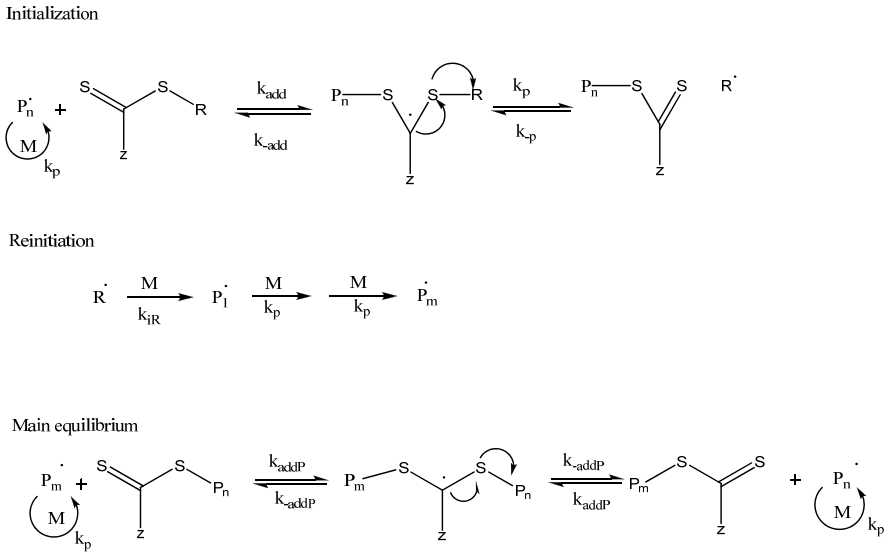

Figure 13. RAFT equilibria scheme.

Optimal control in RAFT polymerization requires choosing an appropriate RAFT agent for the monomer(s) to be polymerized and the reaction conditions. Monomers can be classified to two broad classes. The 'more activated' monomers (MAMs) are those where the double bond is conjugated to an aromatic ring (e.g., styrene (St), vinylpyridine), a carbonyl group (e.g., methyl methacrylate (MMA), methyl acrylate (MA), acrylamide (AM)), or a nitrile (e.g., acrylonitrile (AN)). The 'less activated' monomers (LAMs) are those where the

double bond is adjacent to saturated carbon (e.g., diallyldimethylammonium chloride), an oxygen, or nitrogen lone pair (e.g., vinyl acetate (VAc) or *N*-vinylpyrrolidone (NVP)) or the heteroatom of a heteroaromatic ring (e.g., *N*-vinylcarbazole (NVC)). The choice of the Z and R groups is dependent on the monomer to be polymerized.

The Z and R groups both play critical roles in determining the efficiency of the chain transfer and the likelihood of retardation or inhibition. When choosing a RAFT agent, R should be a good homolytic leaving group with respect to the propagating radical. The predicted degree of polymerization, assuming low initiation and low radical termination, is simply the ratio of [monomer consumed]:[RAFT agent consumed]. The Z group modifies both the rate of addition of propagating radicals (P_n^*) to the thiocarbonyl and the rate of fragmentation of the intermediate radicals.

The most typically used reactive RAFT agents are the dithio- and trithiocarbonates which have carbon or sulfur adjacent to the thiocarbonylthio group. RAFT agents with alone pair on nitrogen or oxygen adjacent to the thiocarbonyl, such as the O-alkyl xanthates, N,N-dialkyldithiocarbamates, and N-alkyl-N-aryldithiocarbamates, have dramatically lower reactivity toward radical addition[85]. General guideline for the selection of Z group is shown in Figure 14. Irrespective of the class of RAFT agent, the transfer constant is generally enhanced by the presence of electron-withdrawing groups on Z and by the capacity of Z to stabilize an adjacent radical center.

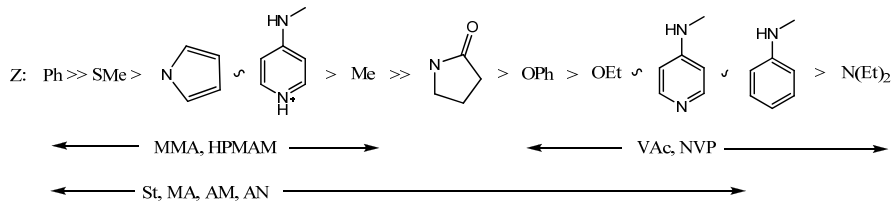

Figure 14. Guidelines for selection of the Z group of RAFT agents for various polymerizations. Addition rates decrease and fragmentation rates increase from left to right. HPMAM = *N*-(2-hydroxypropyl)methacrylamide.

Another important aspect to take into account about the Z group is the stability of the intermediate radicals formed. When Z is aryl, the intermediate is stabilized, and the rate of intermediate radical fragmentation is slower than when connecting atom of Z is a sp^3 carbon, oxygen, nitrogen or sulfur. In that sense, aromatic dithioesters hand to retardation. This is most apparent when higher RAFT agent concentrations are used (to give lower molecular weight polymers) and with faster propagating monomers (e.g., acrylates, vinyl esters). The Z group should also not cause any side reactions.

With xanthates (Z = OR') it is important for R' to be a poor homolytic leaving group. Otherwise, fragmentation with loss of R' will compete with the desired RAFT process. This requires R' to be primary alkyl or aryl. When Z is a strongly electron-withdrawing group, the thiocarbonyl group may undergo a direct reaction with monomers. Thus, RAFT agents having a alkylsulfonyl or phenylsulfonyl group (Z = $PhSO_2^-$) as the Z group, undergo direct reaction with (meth)acrylate monomers under polymerization conditions with consumption of the thiocarbonylthio group and ultimately leading to little control over the polymerization.

The other part of the RAFT agent, the R group must be a good homolytic leaving group with respect to P_n^* in order to get an optimal control of the polymerization. Radical stability is important in determining fragmentation rates. Experimental findings showed that the transfer coefficient, ϕ, increases in the order of primary < secondary < tertiary. The transfer ratio also increases with the introduction of substituents capable of delocalizing the radical center (Figure 15).

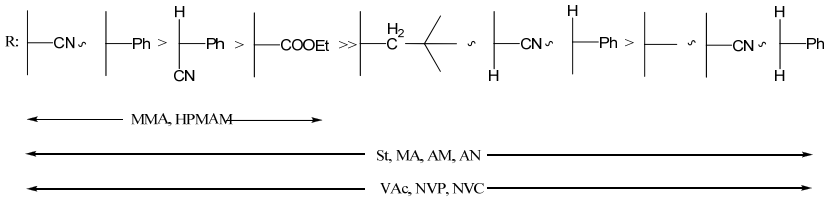

Figure 15. Guidelines for selection of the R group of RAFT agents for various polymerizations. Transfer coefficients decrease from left to right. Fragmentation rates also decrease from left to right.

All these considerations are very important in designing the synthesis of block copolymers by RAFT polymerization. In synthesizing a poly(MAM)-block-poly-(LAM), using switchable RAFT, the poly(MAM) block should be made first because poly(LAM) propagating radicals are relatively poor homolytic leaving groups, however, poly(MAM) propagating radicals are slow to reinitiate LAM polymerization.

2.2. AIMS OF THIS CHAPTER

In this chapter two kinds of polymeric carriers have been prepared: azide functionalized polymer sensitive to pH and temperature to be grafted to bemiparin in order to prepare new bioconjugates by click chemistry and amphiphilic block copolymers to be used as bemiparin nanoparticle carriers. Two different controlled radical polymerization (CRP) techniques have been used: Atom Transfer Radical Polymerization (ATRP) and Reversible Addition-Fragmentation Transfer (RAFT) polymerizations. Both of them allowed the production of well-controlled polymer systems with a low polydispersity and a controlled chemical structure.

Of the various CRP methods, ATRP and RAFT have proven to be the most effective methods for the synthesis of polymer-protein conjugates by the 'grafting from' or 'grafting to' approach. RAFT polymerization has been successfully used in the synthesis of homopolymers and block copolymers

conjugates as well as drug delivery systems (DDS)[9,86] due to its high versatility as can be carried out in the presence of many functional groups present on proteins and can also take place in aqueous medium.[81-82] AGET ATRP has been recently applied to the synthesis of polymer-protein conjugates by polymerization of PEGMA macromonomers from initiator-functionalized recombinant human growth hormone and trypsin[87]. A benefit of AGET ATRP is that the Cu(I) activator is formed *'in situ'* from an oxidatively stable Cu(II) complex. In these cases, the polymer proteins conjugates presented enhanced stability against denaturation and proteolysis, presumably due to the presence of the immobilized polymer. As these recent examples suggest, many of the challenges of ATRP bioconjugations can be addressed by proper selection of the polymerization conditions[88].

Thermoresponsive, water-soluble polymers exhibiting a Lower Critical Solution Temperature (LCST) have been increasingly investigated for nanotechnology and biotechnology applications. Recently, the predominance of PNIPAM[89] as the general example of a thermoresponsive polymer[90], was challenged by the discovery of random copolymers of 2-(2-methoxyethoxy)ethyl methacrylate (MEO_2MA) and oligo(ethylene glycol)methacrylate (OEO_xMA). This copolymer can be designed to exhibit a LCST in water, which can be finely tuned between 26 and 90 °C depending on OEOMA content[91]. In contrast to PNIPAM, the value for the LCST of the copolymers are almost independent of molar mass, concentration, and ionic strength[92]. In addition, since the addition of oligo(ethylene oxide) sequences to responsive polymers was shown to be non cytotoxic, these poly(ethylene glycol)-based copolymers are expected to be non-toxic and non-immunogenic[93].

Another polymer very interesting to be used as drug delivery system is the poly[2-(dimethylamino)ethyl methacrylate] (PDMAEMA), which is a water-soluble, temperature-sensitive and pH-sensitive polymer, due to the inherent amine protonation in physiological media[94,95,96].

In this chapter the synthesis of thermal and pH responsive homopolymer (PDMAEMA) and random copolymer ($POEO_xMA$) prepared by AGET-ATRP is fully described. The resulting azido- end functionalized polymer will then be attached to functionalized bemiparin (chapter 3). Moreover, synthetic block copolymers

based on poly(MMA-*b*-MAETMA) were prepared by RAFT polymerization are also described. The content on the cationic monomer was varied between 0.02 and 0.1 molar ratio in order to obtain well defined block copolymers with different lengths of the cationic segment (different charge densities). These block copolymer systems will be used as positively charged drug carriers of heparin (described in chapter 4). These synthetic block copolymers were inspired by the structure of Eudragit® RS PO (figure 19), which is a random copolymer based on methyl methacrylate (MMA), ethyl acrylate (EA) and trimethyl aminoethyl methacrylate (MAETMA), but with well defined microstructure and morphology. Variation of the amount of cationic charges, which will bind to bemiparin via electrostatic forces, will modulate the encapsulation efficiency and the release of bemiparin, thus altering the biological activity, as it will be described in chapter 4 of this thesis.

2.3. MATERIALS AND METHODS

2.3.1. MATERIALS

2-(Dimethylamino)ethyl methacrylate (DMAEMA) (Sigma-Aldrich, 98%), di(ethylene glycol) methyl ether methacrylate (MEO_2MA) (Sigma-Aldrich) and poly(ethylene glycol)methyl ether methacrylate ($OEOMA_{300}$) (Sigma-Aldrich, M_n = 300) were purified by passing the monomer through a column of basic aluminum oxide. Copper (II) bromide (Sigma-Aldrich, 99%) and tris[(2-pyridyl)methyl]amine (TPMA) (ATRP Solutions) were stored under vacuum and used without further purification. Tin 2-ethylhexanoate (Sn(II)EtHex) (Sigma-Aldrich, 95%), aluminum oxide basic (Sigma-Aldrich, >98%), toluene (Merck, analysis grade), tetrahydrofuran (THF) (Scharlau, analysis grade), *N,N*-dicyclohexylcarbodiimide (DCC) (Sigma-Aldrich, >99%), 4-(dimethylamino)pyridine (DMAP) (Sigma-Aldrich, 99%), and ethyl ether (SDS, 99.8%) were used as received.

Methyl methacrylate (MMA) (Acros Organics) and 2-(methacryloyloxy)ethyl]trimethylammonium (80% aqueous solution) (MAETMA) (Sigma-Aldrich) were purified by passing the monomer through a column of basic aluminium oxide. 2,2'-Azobisisobutyronitrile (AIBN, Merck) was recrystallized from methanol. 4, 4'-Azobis (4-cyanovaleric acid) (V501) (Sigma-Aldrich), ethyl acetate (Sigma-Aldrich, >99.5%), dimethyl disulfoxide (SCHARLAB, >98%) and HEPES minimum titration (Sigma-Aldrich, 99.5%) were used as received. Dithiobenzoic acid (BOC Science, 96%) was purified by recrystallization from benzene. Sodium methoxide solution (Sigma-Aldrich, 30%), elemental sulphur (Tianjin Haishengweibang Fine Chemical Co., Ltd.), anhydrous methanol (Sigma-Aldrich, 99%), and potassium ferricianide (III) (Sigma-Aldrich, >99%) were used as received. Brilliant Black BN dye (Sigma-aldrich, 60%) was diluted in distilled water (1:1000) before use.

2.3.2. METHODS

2.3.2.1. Synthesis of temperature and pH sensitive polymers by ATRP

The synthesis of the azido ATRP initiator (N_3-PEG_3-BPA) was carried out as previously reported.[97] Briefly, 2-(2-(2-azidoethoxy)ethoxy)ethanol (2.00 g, 11.4 mmol) was dissolved in 100 mL of dichloromethane. To this solution DCC (2.59 g, 14.9 mmol), and DMAP (0.139 g, 1.1 mmol) were added. 2-bromo-2-phenyl acetic acid was added dropwise and the reaction was stirred at room temperature under nitrogen for 16 hours. The reaction mixture was extracted with water (2x 50 mL), 0.1 N NaOH (2x 50 mL) and once with brine (50 mL). The organic layer was dried using sodium sulfate, filtered and evaporated under reduced atmosphere. N_3-PEG_3-OH:2-bromo-2-phenyl acetic acid:DCC:DMAP [1:1.3:1.1:0.1]. N_3-PEG_3-BPA initiator was used to obtain the azido-polymer by AGET-ATRP as it is shown in Figure 16.

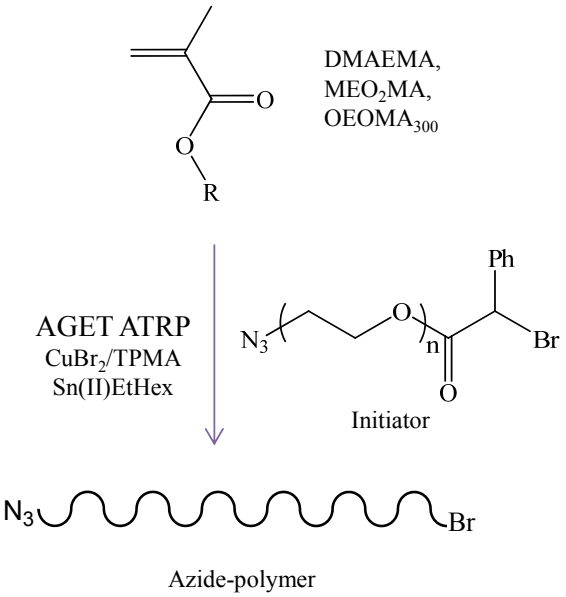

Figure 16. Azide-polymer synthesis scheme by ATRP-AGET polymerization.

2.3.2.1.1. Synthesis of N_3-PDMAEMA using AGET ATRP

N_3-PEG_3-BPA (207 mg, 0.56 mmol), $CuBr_2$ (11.2 mg, 0.05 mmol) TPMA (43.4 mg, 0.15 mmol) and DMAEMA (9.375 mL, 55.6 mmol) were dissolved in 9.4 mL of toluene in a 25 mL Schlenk flask. The flask was sealed and the solution was bubbled with nitrogen for 20 minutes. The reaction mixture was placed in an oil bath preheated to 40°C and 0.4 mL of a degassed Sn(II) EtHex solution (500 mg/mL) was injected into the flask to reduce the catalyst complex and start the polymerization. The reaction was stopped after one hour by opening the flask to air and adding of 10 mL of THF, before the solution was passed over a short column of basic alumina and the polymer isolated after precipitation into ethyl ether three times.

2.3.2.1.2. Synthesis of N_3-P(MEO_2MA-co-$OEOMA_{300}$) using AGET ATRP.

N_3-PEG_3-BPA (207 mg, 0.56 mmol), $CuBr_2$ (11.2 mg, 0.05 mmol) TPMA (43.4 mg, 0.15 mmol) $OEOMA_{300}$ (1.589 mL, 5.6 mmol) and MEO_2MA (7.561 mL 50.1 mmol) were dissolved in 9.4 mL of toluene in a 25 mL Schlenk flask. The flask was sealed and bubbled with nitrogen for 20 minutes. The reaction mixture was placed in an oil bath preheated to 40°C and 0.4 mL of a degassed Sn(II)EtHex solution (500 mg/mL) was injected into the reaction mixture to reduce the copper catalyst complex and start the polymerization. After one hour the reaction was stopped and 10 mL of THF was added to the flask. The solution was then passed through a short column of basic alumina before the polymer was precipitated by addition to ethyl ether three times.

2.3.2.2. Preparation of block copolymers by RAFT polymerization

The RAFT agent, 4-cyanopentanoic acid dithiobenzoate (CPADB), used to carry out the MMA polymerization was synthesized as reported by Y. Mitsukami et al [98]. Briefly, the dithiobenzoic acid (DTBA) was firstly prepared using sodium methoxide (30% solution in methanol, 45 g, 250 mmol), elemental sulphur (8.0 g, 250 mmol), anhydrous methanol (62.5 g) and benzyl chloride (15.75 g, 125 mmol). The reaction mixture was heated in an oil bath at 67 °C for 10 h. The mixture was cooled to 7 °C using an ice bath. The precipitated salt was removed by filtration and the solvent was removed under vacuum. The residue was dissolved in deionized water (125 mL). The crude sodium dithiobenzoate solution was acidified with 1.0 N HCl (125 mL) and extracted with diethyl ether (50 mL). Deionized water (75 mL) and 1.0 N NaOH (150 mL) were added, and sodium dithiobenzoate was transfered to the aqueous phase.

The sodium dithiobenzoate solution (87.5 mL) and potassium ferricianide (III) (8.23 g, 25 mmol) were mixed in deionized water (150 mL) under vigorous stirring. The red precipitate was filtered and washed with deionized water until the washings became colourless. The solid was filtered and dried under vacuum at room temperature overnight. The product, di(thiobenzoyl) disulphide, was recrystallized from ethanol.

Finally, the synthesis of 4-cyanopentanoic acid dithiobenzoate (CPADB) was carried out by dissolving 4,4'-azobis(4-cyanopentanoic acid) (2.92 g, 11.5 mmol) and di(thiobenzoyl)disulfide (2.13 g, 7 mmol) in 40 mL of distilled ethyl acetate. The reaction solution was heated at reflux for 18h. Afterwards, ethyl acetate was removed under vacuum. The crude product was isolated by column chromatography (silicagel 60 Å, 70-230 mesh) using ethyl acetate hexane (2:3) as eluent. Fractions that were red in colour were combined and dried over anhydrous sodium sulphate overnight. The solvent mixture was removed under vacuum, and the red oily residue placed in a freezer at -20 °C, whereupon it crystallized. The target compound was recrystallized with an acetate:hexane (2:3) mixture with a yield of 78%. The melting point obtained (98 °C, measured in a Perkin Elmer DSC7 apparatus from 20 to 180 °C at a constant rate of 10 °C/min) was in a good agreement with the value described in bibliography [99].

The PMMA macroRAFT agent (P1) was prepared by bulk radical polymerization, dissolving 1.64 mg AIBN (0.01 mmol) and 28 mg CPADB (0.1 mmol) in 10.6 mL of MMA (100 mmol). Five replicate samples were prepared and degassed by bubbling nitrogen N_2 (g) through the solution for 40 min. All samples were heated at 60 °C for 2, 4, 6, 21 and 24 h, respectively. The conversions were determined gravimetrically and by ^{1}H-NMR.

A series of block copolymers of different poly(MAETMA) sequence lengths were prepared using the same PMMA macroRAFT agent ($M_{w(GPC)}$ = 55000 g/mol, $M_w/M_{n(GPC)}$ = 1.24). These block copolymers were labelled as $PMMA_n$-*b*-$PMAETMA_m$ (Figure 17) where n and m are the number of the repeating unit of PMMA and PMAETMA blocks respectively, calculated from ^{1}H-NMR.

The block copolymers were prepared dissolving 6.2 mL of a PMMA stock solution 0.6 mM in DMSO (3.74 mmol) with 1.8 mL of an 4,4'-azobis(4-

cyanovaleric acid) (V501) stock solution 0.42 mM in DMSO solution (0.76 mmol) and different amount of MAETMA (80% aqueous solution) (374, 187 and 93.5 mmol respectively) in 34 mL DMSO. Samples were sealed, degassed by purging nitrogen for 30 min through the solution and heated in an oil bath (70 °C) for 6 h. The conversion was determined by ^{1}H-NMR using DMSO-d_6 as solvent. The block copolymers were purified by dialyzing for three days against water, using cellulose tubular membranes (Spectrum Laboratories, molecular weight cut-off: 3.5 kDa).

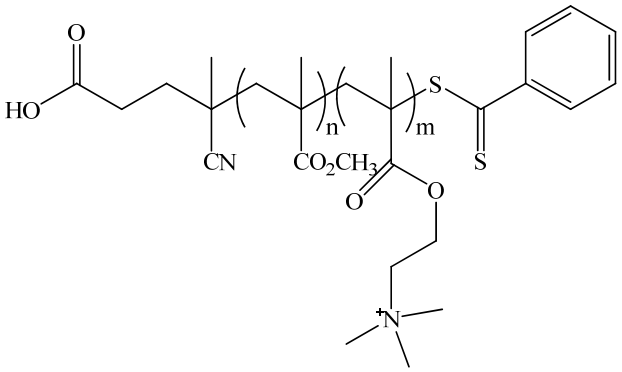

$PMMA_n$-*b*-$PMAETMA_m$

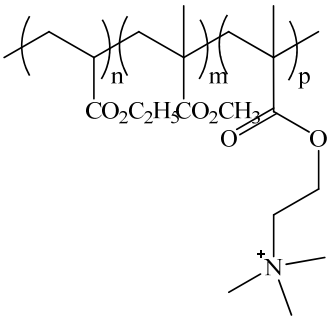

EUDRAGIT RS PO

Figure 17. Chemical structures of the amphiphilic block copolymers prepared by RAFT polymerization ($PMMA_n$-*b*-$PMAETMA_m$) and the commercial polymer, Eudragit® RS PO.

2.3.3. CHARACTERIZATION TECHNIQUES

2.3.3.1. NMR spectroscopy

^{1}H and ^{13}C NMR spectra were recorded on a Mercury 400BB spectrometer, operating at 400 and 133.3 MHz, respectively. The spectra were recorded by dissolving the corresponding sample (15 mg/mL for ^{1}H NMR and 100 mg/mL for ^{13}C NMR), in deuterated chloroform ($CDCl_3$), or deuterated dimethylsulfoxide (DMSO-d_6).

To determine the kinetic parameters of the reaction, PMMA-*b*-PMAETMA copolymerisation reactions were performed inside the NMR equipment. These experiments were carried out at 70 °C with a pulse sequence of 7 µs equivalent to a 90° tip angle, a 60 s delay time, a spinning rate of 7 Hz, and one acquisition (FID), nt = 1, for each datum.

2.3.3.2. FTIR spectroscopy

FTIR spectra of the isolated products were measured to characterize the azide-polymer. FTIR spectra were obtained in the Attenuated Total Reflection mode (ATR-FTIR) on a Perkin Elmer Spectrum One FT-IR spectrometer. Samples were analyzed at room temperature by 32 scans and with a resolution of 4 cm^{-1}.

2.3.3.3. SEC characterization

The evolution of number and weight average molecular weights with monomer conversion was determined by Size Exclusion Chromatography (SEC) in a Perkin-Elmer apparatus equipped with an isocratic pump serial 200 connected to a differential refractometric detector (serial 200a). Two Resipore columns (Varian) were conditioned at 70 °C and used to elute the samples (3 mg/mL

concentration) at 0.3 mL/min HPLC-grade *N,N'*-dimethylformamide (DMF) supplemented with 0.1% v/v LiBr. Calibration of SEC was carried out with monodisperse standard poly(methyl methacrylate) samples in the range of $2.9x10^3$ to $480x10^3$ g/mol (Varian) with sample injection volumes of 20 µL.

2.3.3.4. TGA analysis

Thermogravimetric Analysis (TGA) was performed on a TGA Q500 (TA Instruments), working from 30 to 600 °C at a heating rate of 10 °C/min, under 50 mL/min nitrogen flow.

2.3.3.5. LCST measurements

Lower Critical Solution Temperature (LCST) of N_3-P(MEO_2MA-co-$OEOMA_{300}$) and N_3-PDMAEMA was measured by UV spectroscopy, using a scanning temperature program to see the aggregation of the system when the LCST is reached. All the systems were analyzed at a concentration of 1 mg/mL aqueous solution. The temperature sweep was carried out from 20 °C to 90 °C at 1 °C/min and transmittance measured at 450 nm. LCST was defined as the temperature of the onset of aggregation measured by the transmittance/temperature diagram, during the heating ramp of the aqueous polymer solutions.

2.3.3.6. Dynamic light scattering (DLS): size distribution and zeta potential determination

Particle size distribution analysis was carried out by the determination of hydrodynamic diameter (D_h) and polydispersity index by dynamic light scattering in a Zetasizer NanoZS (Malvern Instruments, UK) equipped with a He-Ne laser

beam with wavelength of 633 nm and a scattering angle of 173°. The intensity of light scattered was used to calculate the mean hydrodynamic diameter (Z-average mean), based on the Stokes–Einstein equation, assuming that the particle is spherical. Samples were prepared at 0.01 mg/mL in three different solvents (H_2O, ethyl acetate and DMF) to study the solvent effect in the micelles formation. For each sample, the statistical average and standard deviation (SD) of data were calculated from at least five measurements at 25 ºC.

2.3.3.7. Morphology characterization of the amphiphilic block copolymer structure by SEM

The morphology of nanoparticles (NP) systems was determined using a Field Emission Scanning Electron Microscopy (SEM) equipped with a STEM detector (Hitachi S-8000). Suspensions of 0.1 mg/mL of the block copolymer system were prepared in water and placed onto glass discs. After casting drying, a drop of 1:1000 diluted solution of brilliant black was added onto the sample placed on a formvar/carbon TEM grid of 200 mesh (Science Services), to help to the contrast of colour of the shell and the core of the micelle formed.

2.3.3.8. Differential Scanning Calorimetry (DSC)

Glass transition temperatures (T_g) were measured by DSC with a Perkin Elmer DSC7 interfaced to a thermal analysis data system TAC 7/DX. The dried sample (10-15 mg) was placed in aluminium pans and heated from -20 to 180 °C at a constant rate of 10 °C/min. T_g was taken as the midpoint of the heat capacity transition.

2.4. RESULTS AND DISCUSSION

CRP methodology provides a procedure for preparation of clean homogeneous polymers with specific properties; such as controlled composition, molecular weight, and molecular weight distribution. It also allows the preparation of bioconjugates and drug delivery systems under mild conditions. In this chapter, two different well-defined copolymers systems have been prepared:

a. By one hand, ATRP produres have been used to synthesize azide-end functionalized polymer systems, which will be used to form bioconjugates with bemiparin (chapter 3). These polymers were N_3-P(MEO_2MA-co-$OEOMA_{300}$), which is a thermo-sensitive polymer, and the homopolymer N_3-PDMAEMA, which is sensitive to pH and temperature (dual stimulus responsive polymer).

b. On the other hand, RAFT polymerization has been used to prepare amphiphilic block copolymers to be used for the preparation of drug delivery nanoparticle systems, which are described in chapter 4.

2.4.1. SYNTHESIS OF α-N_3-FUNTIONALIZED POLYMERS BY ATRP

Atom transfer radical polymerization (ATRP) was used for the synthesis of well-defined polymer chains with well-controlled molecular weight, narrow molecular weight distribution and functional chain-ends.

2.4.1.1. Synthesis of N_3-PDMAEMA

ATRP of DMAEMA was performed under relatively mild conditions in a variety of organic solvents or in aqueous solution.[100] In this work the α-azido PDMAEMA was prepared in toluene at 40 °C in the presence of $CuBr_2$/TPMA as the precursor of the catalytic system, and using N_3-PEG_3-BPA as initiator (Figure

18). Sn(II)EtHex was added to the reaction to reduce the Cu(II) to Cu(I). This catalytic system allowed the application of very low concentration of copper as it simultaneously provides an excellent medium to avoid the oxidation of the in situ generated Cu(I).[56] The product was dialyzed against 1% v/v acetic acid for 3 days and isolated by freeze-drying.

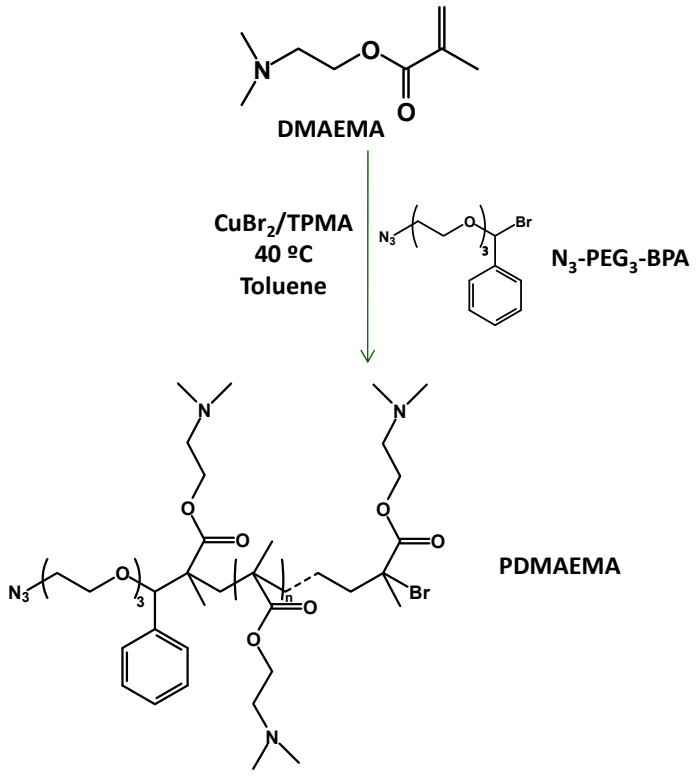

Figure 18. N_3-PDMAEMA synthesis reaction scheme.

SEC results showed the formation of polymers with monomodal molecular weight distributions and polydispersity indexes lower than 1.4 (Figure 19). The polymers displayed an increase of molecular weight with conversion while maintaining narrow molecular weight distributions, which indicates that the polymerization was carried out under controlled conditions.

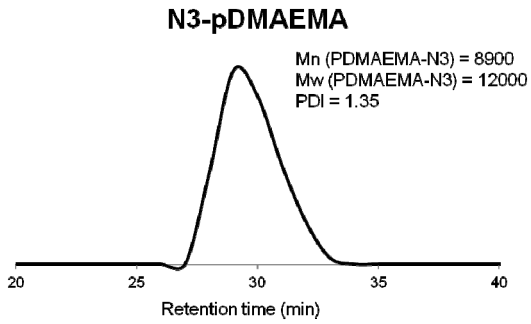

Figure 19. GPC trace of N_3-PDMAEMA measured in DMF GPC with PMMA standards.

Structural characterization of the N_3-PDMAEMA polymer confirmed the incorporation of fragments of the functionalized initiator at both polymer chain ends. ^{1}H NMR spectra (Figure 20) showed the signal from the initiator protons at 3.2 ppm and the characteristic signals of the polymer in particutar, the resonance signals from the α-methyl protons of the methacrylic group (CH_3COOR) in the range 0.8-1.2 ppm, the signal from methylene protons linked to azide function in the initiator (N_3-CH_2-) in the range 1.25-1.5 ppm, methylene protons of the main polymeric chain (CH_2 of DMAEMA) at 1.5-2.1 ppm, both methyl groups of DMAEMA [R-N-$(CH_3)_2$] at 2.2-2.4 ppm, methylene protons linked to tertiary amino group of DMAEMA (-CH_2-N-R_2) at 2.5-2.7 ppm, methylene groups of initiator linked to the ether function (CH_2-O-CH_2-) at 3.1-3.3 ppm, methylene protons of DMAEMA linked to the ether function (O-CH_2-R) at 3.9-4.2 ppm.

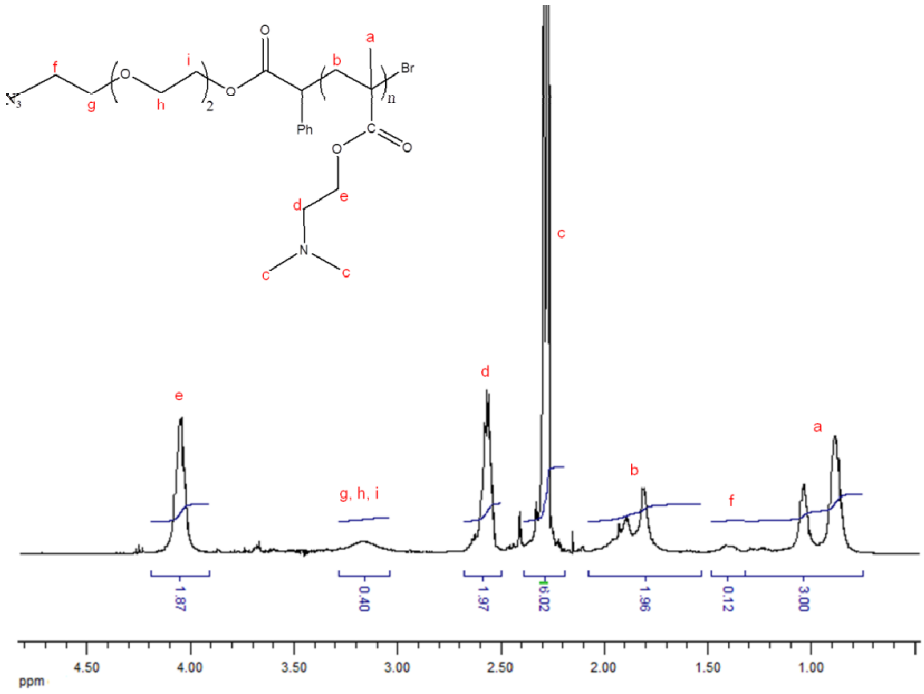

Figure 20. ^{1}H NMR 500 MHz spectrum of N_3-PDMAEMA in $CDCl_3$.

^{1}H NMR spectra was used to calculate the theorical molecular weight (M_{theo}) on the basis of the ratio of the methyl protons of the polymer at 0.8-1.2 ppm (3H) to the initiator protons at 3.2 ppm (10H). The M_{theo} obtained by this method was 81000 Da, which is in good agreement with the value obtained by SEC for the same polymer (M_n = 8900). Reaction yield of N_3-PDMAEMA was 91%.

FTIR analysis confirmed the functionalization of the polymer with azide groups, since it was shown an absorption band at 2194 cm^{-1} corresponding to the asymmetric stretching vibration of the azide group and the characteristic C=O stretching band of polyacrylates at 1728 cm^{-1} (Figure 21).

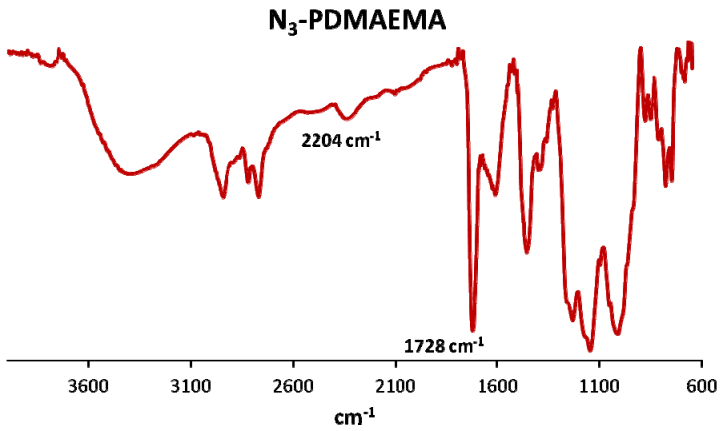

Figure 21. FTIR spectrum of N_3-PDMAEMA prepared by AGET-ATRP.

2.4.1.2. N_3-P(MEO_2MA-co-$OEOMA_{300}$) synthesis

A statistical copolymer of MEO_2MA with $OEOMA_{300}$ was prepared by ATRP with N_3-PEG_3-BPA initiator (Figure 22) targeting a copolymer that displayed a LCST closed to the physiological temperature (37 °C).

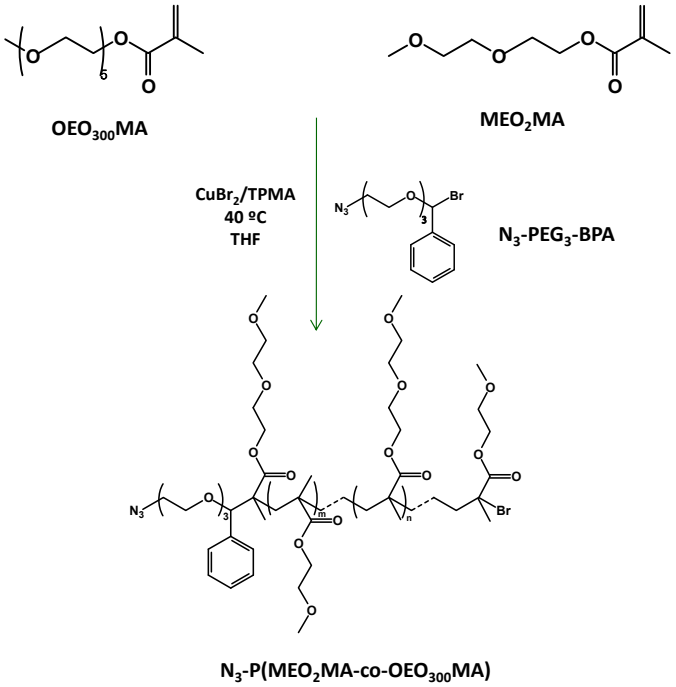

Figure 22. N_3-P(MEO_2MA-co-$OEOMA_{300}$) synthesis reaction scheme.

The copolymerization proceeded under controlled conditions leading to formation of a monodisperse copolymer with narrow molecular weight distribution (M_n = 9400, PDI = 1.20, PMMA standards in DMF) (Figure 23), with a reaction yield of 88%.

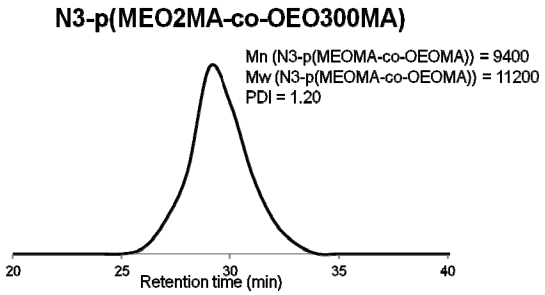

Figure 23. GPC trace of N_3-P(MEO_2MA-co-$OEOMA_{300}$) measured in DMF GPC with PMMA Standards.

^{1}H NMR structural characterization is shown in Figure 24. N_3-P(MEO_2MA-co-$OEOMA_{300}$) spectrum showed the characteristic signals of the final copolymer obtained: 0.8-1.2 ppm α-methyl protons of the methacrylic functions (CH_3COOR), 1.25-1.4 ppm methylene protons linked to azide function in the initiator (N_3-CH_2-), 1.6-2.1 ppm methylene protons of the main polymeric chain (CH_2 of both MEO_2MA and $OEO_{300}MA$), 3.2 ppm methyl protons of the methacrylic functions of the graft chain of both MEO_2MA and $OEO_{300}MA$ (CH_3-O-R), 3.2-3.8 ppm methylene groups of initiator linked to the ether function plus methylene groups of graft chain of both MEO_2MA and $OEO_{300}MA$ (CH_2-O-CH_2-), 3.9-4.1 ppm methylene protons of graft chains of MEO_2MA and $OEO_{300}MA$ linked to the ether function (O-CH_2-R). The number of monomer units was stimated to be 36 from the comparison between the phenyl-initiator protons (7.2 ppm) and the methyl group proton (0.9-1.2 ppm). The final composition of the copolymer was calculated considering the relative intensity of methylene signals at 3.7 ppm (d in Figure 24), by comparing the MEO_2MA methylene groups (3), and the methylene groups of the $OEOMA_{300}$ (9). This provides a final molar fraction of 0.75 MEO_2MA and 0.25 $OEOMA_{300}$ in the copolymer chains.

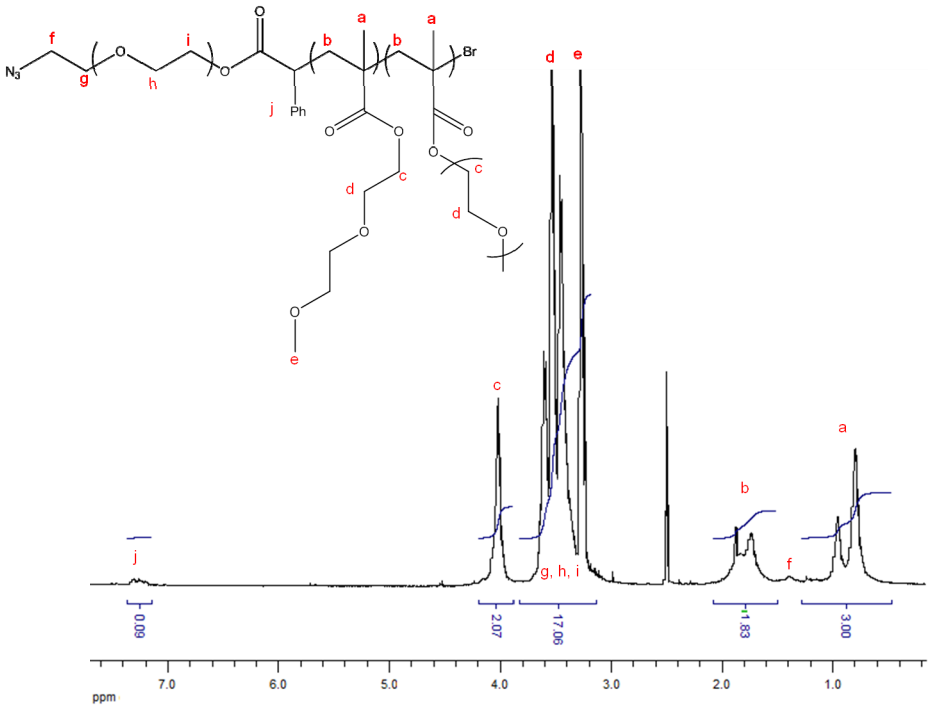

Figure 24. ^{1}H NMR 500 MHz spectrum of N_3-P(MEO_2MA-co-$OEOMA_{300}$) in d_6-DMSO.

FTIR analysis of the copolymers also confirmed the skilfulness of the ATRP process using the azido initiators (Figure 25). The absorption band at 2204 cm^{-1} observed corresponds to the asymmetric stretching vibration of the azide group and the absorption band at 1728 cm^{-1} corresponding to the C=O stretching vibration of polyacrylates.

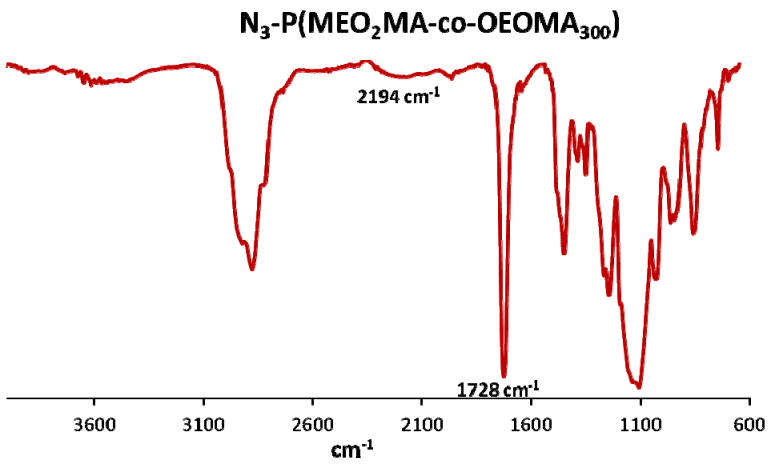

Figure 25. FTIR spectra of N_3-P(MEO_2MA-co-$OEOMA_{300}$) prepared by AGET-ATRP.

2.4.2. THERMAL PROPERTIES

The LCST of a copolymer is defined as the critical temperature at which polymer solution undergoes phase separation from one phase (isotropic state) to a two phase system (anisotropic state), one rich and one poor in polymer. Below the LCST, enthalpic interactions of the hydrogen bonding between the polymer and the water molecules is responsible for the polymer dissolution. When the temperature is raised above the LCST, entropy (hydrophobic interactions) dominates, leading to polymer aggregation/precipitation. The LCST of polymers in aqueous solutions can be modulated by incorporating hydrophilic or hydrophobic moieties into the copolymer backbones, therefore the incorporation of the hydrophilic bemiparin segment in the bioconjugate structure had a significant effect on the temperature-sensitive phase transition behavior.

In acidic media, a PDMAEMA-N_3 polymer is fully ionized and increasing the temperature has no significant effect on the swelling ratio up to pH 7 (pK_a = 7.6). However at pH 7.4, increasing the temperature caused a gradual decrease in the swelling ratio of the polymer and at above 43 °C the polymer precipitated. Increasing the pH decreases the degree of ionization of the amino groups along the polymer chain, leading to an increase of the hydrophobicity of the system,

which in turn decreased the phase transition temperature (LCST) from 43 °C to 35 °C. At lower pH (pH 3), the system remained soluble in all temperature ranges (Figure 26).

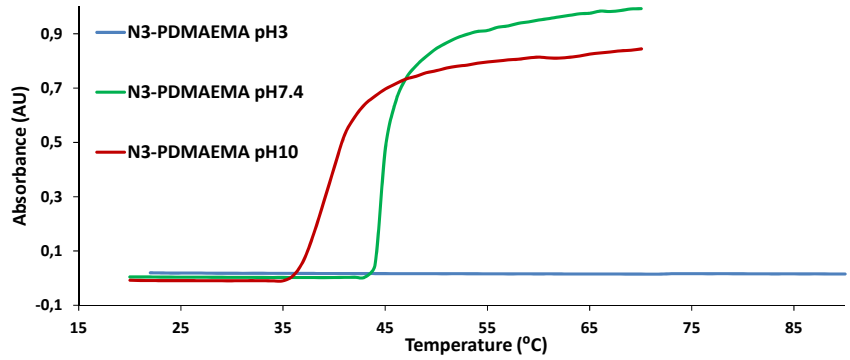

Figure 26. LCST behavior of N_3-PDMAEMA at different pH.

The LCST of the copolymers depends on composition and increase with increasing mole fraction of OEOMA in the polymer chain. The properties of PEG polymers in aqueous medium vary depending on the molecular structure of the monomer units; i.e. the nature of the polymerizable moiety, the length of the PEG side chain and end-group of the PEG chain. In fact, the balance between hydrophilic and hydrophobic moieties in the molecular structure of the polymers determines their solubility properties[91]. In the case of oligo(ethylene oxide) methyl ether methacrylates (MEO_2MA), the ether oxygen of PEG forms active H-bonds with water, whereas the non-polar carbon-carbon backbone leads to a competitive hydrophobic effect. Thus, polymers with very short PEG side-chains are either not water soluble or only weakly hydrophilic. On the other hand, polymers with longer PEG side chains, such as $OEOMA_{300}$, are soluble in water, even at higher temperatures. Random copolymers of MEO_2MA and $OEOMA_{300}$ exhibit LCST that can be precisely adjusted by varying the ratio of comonomers. Copolymerization of di(ethylene glycol) methyl ether methacrylate with poly(ethylene glycol) methyl ether methacrylate by ATRP was reported[91]. In this work, the comonomer composition was adjusted to obtain a LCST of 32-33° C,

which is close to the physiological temperature of 37°C. Changes in the pH of the medium did not appear affect the LCST of the P(MEO_2MA-co-$OEOMA_{300}$) system due to the absence of acidic or basic groups (Figure 27).

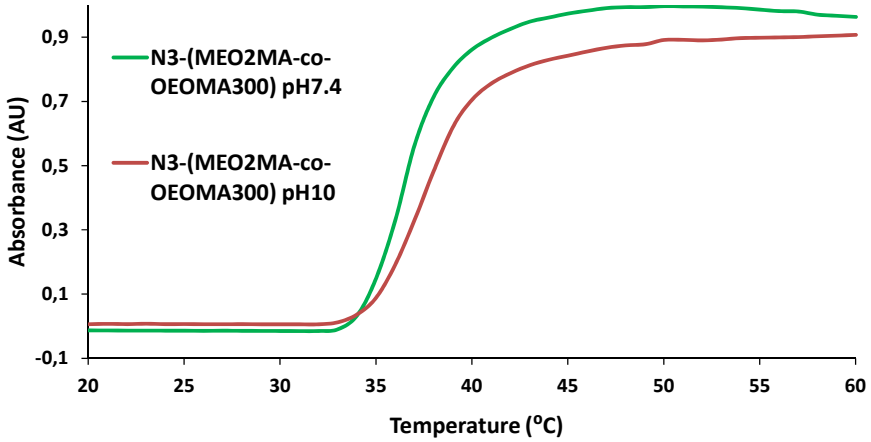

Figure 27. LCST behavior of N_3-P(MEO_2MA-co-$OEOMA_{300}$) at different pH.

2.4.3. SYNTHESIS OF BLOCK COPOLYMERS

RAFT polymerization is a versatile way to obtain block copolymers, especially considering the robustness of the process in the presence of many functional groups [82,101,102,103]. This work describes the synthesis of blockcopolymers with a chemical structure inspired by Eudragit® RS PO. The systems were based on PMMA segments and a second block obtained from trimethyl aminoethyl methacrylate (MAETMA).

2.4.3.1. *Synthesis of 4-cyanopentanoic acid dithiobenzoate (CPADB)*

The RAFT agent used for the copolymerization of PMMA and MAETMA was 4-cyanopentanoic acid dithiobenzoate (CPADB). The ^{1}H-NMR spectra of the CPADB is shown in Figure 28, where the resonance signals at 7.4 – 8.0 ppm corresponds to the aromatic protons designed as a, b, c, d and e in the chemical structure, the signals at 2.5 – 3.0 ppm represent the methylene protons (g,h) from the cyanopentanoic acid fragment and the signals at 2 ppm correspond to the protons from the methyl group in the same fragment (f).

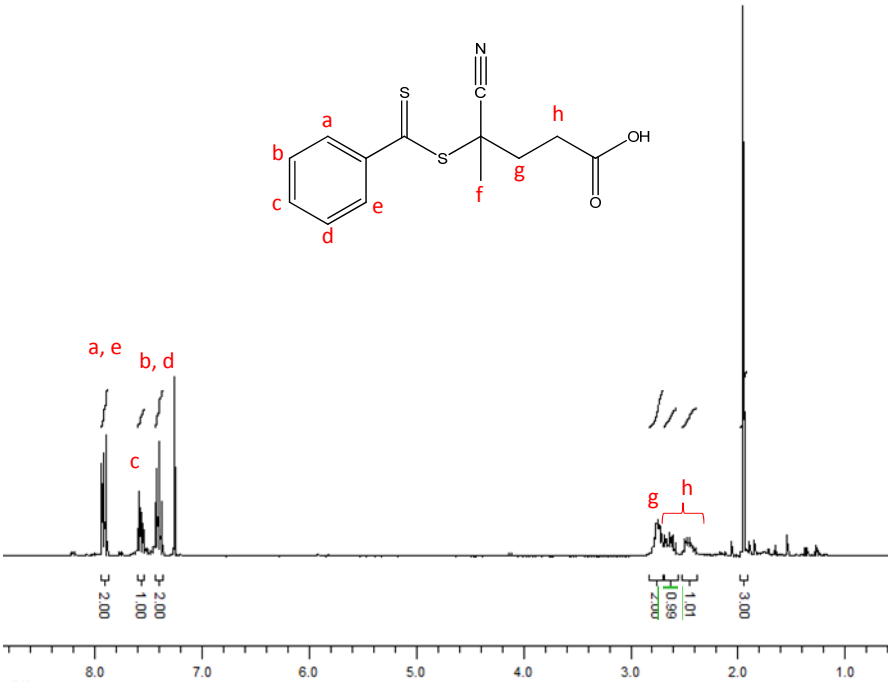

Figure 28. ^{1}H-NMR spectra of CPADB RAFT agent in $CDCl_3$.

2.4.3.2. *Synthesis of PMMA macroRAFT agent*

Controlled molecular weight PMMA was synthesized using CPADB as RAFT agent[99] (Figure 29). The theoretical molecular weight can then be calculated using M_n = [M]/[RAFT]•$M_{Monomer}$•c+M_{Raft} where [M] and [RAFT] are the initial concentrations of the monomer and the RAFT agent respectively, and c is the conversion.

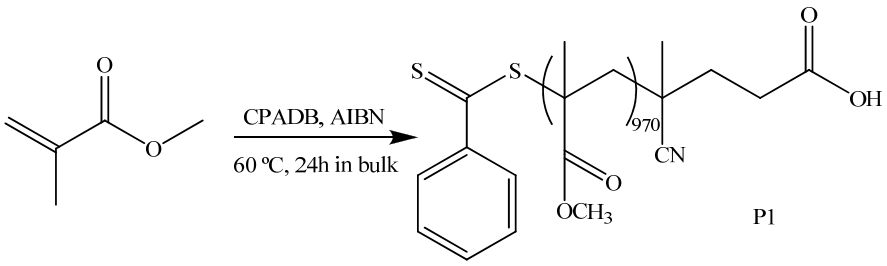

Figure 29. MMA polymerization scheme using CPADB RAFT agent to obtain the P1.

The conversion was increased linearly with time, which shows a good lingering characteristic of controlled radical polymerization (Figure 30). Conversion of MMA was calculated gravimetrically and corroborated by ^{1}H-NMR, obtaining the same value with both techniques. After 24h, a MMA conversion of 97% was obtained giving a final PMMA with a M_n = 55000, PDI = 1.24.

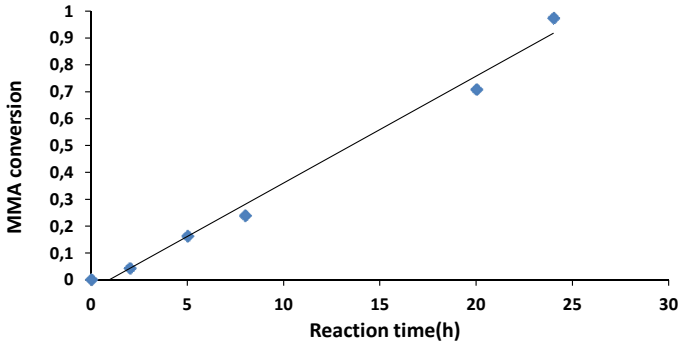

Figure 30. Kinetic plot of MMA macro-RAFT agent polymerization.

GPC elution curves (Figure 31A) clearly showed a peak shift to higher molecular weights with increasing polymerization time. The curves were all unimodal with no sign of coexisting low and high molecular weight species that may be yielded from uncontrolled polymerization.

The increase in M_n with conversion (Figure 31B) was linear and the resulting polydispersity was narrow (M_w/M_n = 1.24).

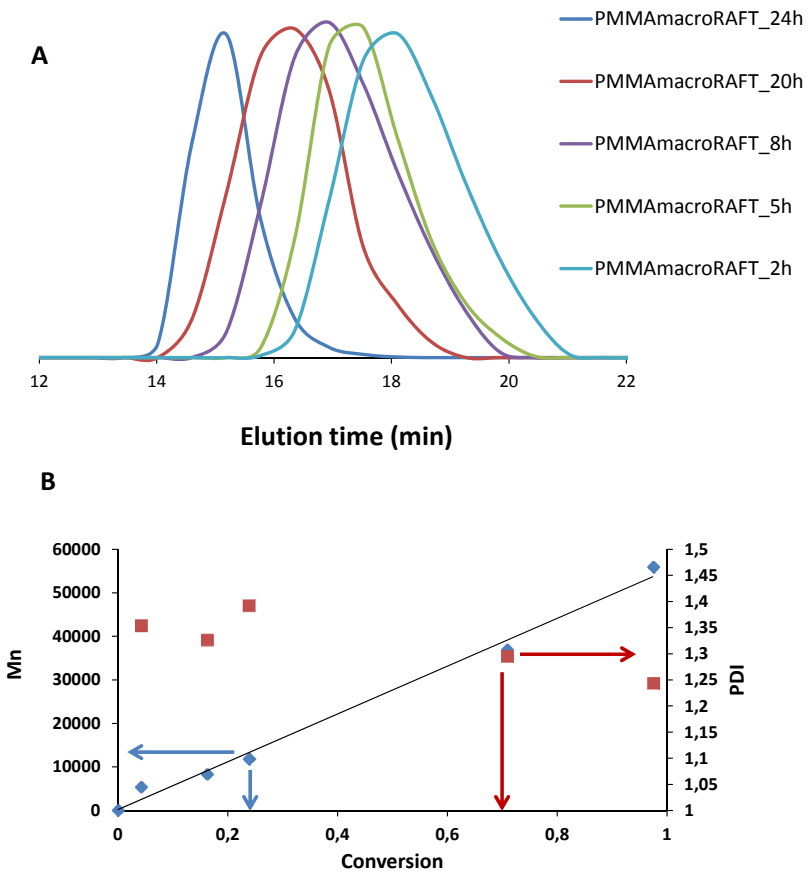

Figure 31. Molecular weight evolution of P1 agent with time and conversion.

^{1}H-NMR spectrum of PMMA without previous purification is shown in Figure 32 with the characteristic assignement of signals. Resonance signals that correspond to the protons from MMA residual monomer: δ ~ 5.6 – 6.1 ppm (CH_2) and δ ~ 3.75 ppm (OCH_3) are also indicated.

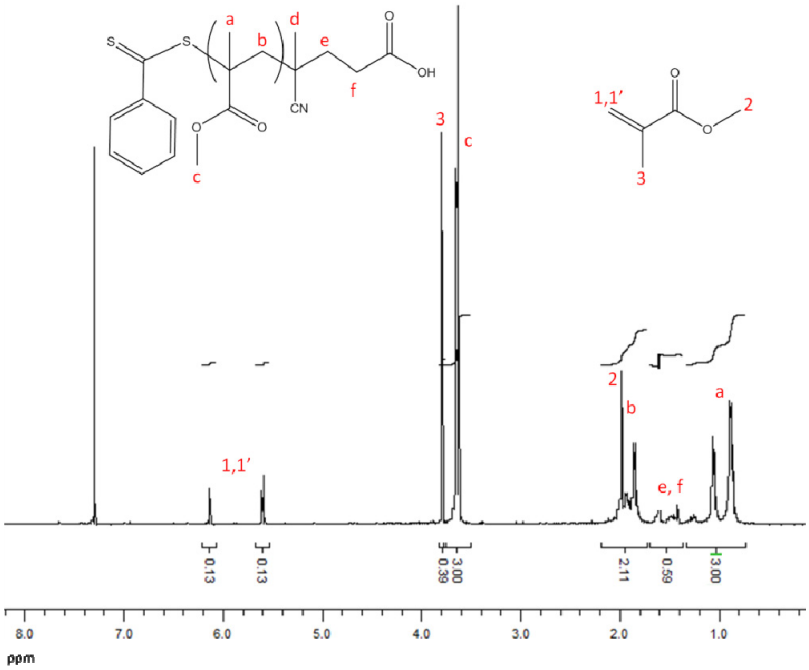

Figure 32. PMMA macroRAFT agent ^{1}H-NMR spectrum after 24h of bulk polymerisation in $CDCl_3$.

2.4.3.3. Synthesis of the block copolymers PMMA-b-PMAETMA

The polymerization of a second monomer, [2-(methacryloyloxy)ethyl] trimethylammonium, in the presence of poly(methylmethacrylate) macroRAFT agent leads to chain extension and therefore to the formation of amphiphilic block copolymers PMMA-*b*-PMAETMA (Figure 33), with a final reaction yield between (85-90)% in all of the block copolymer systems.

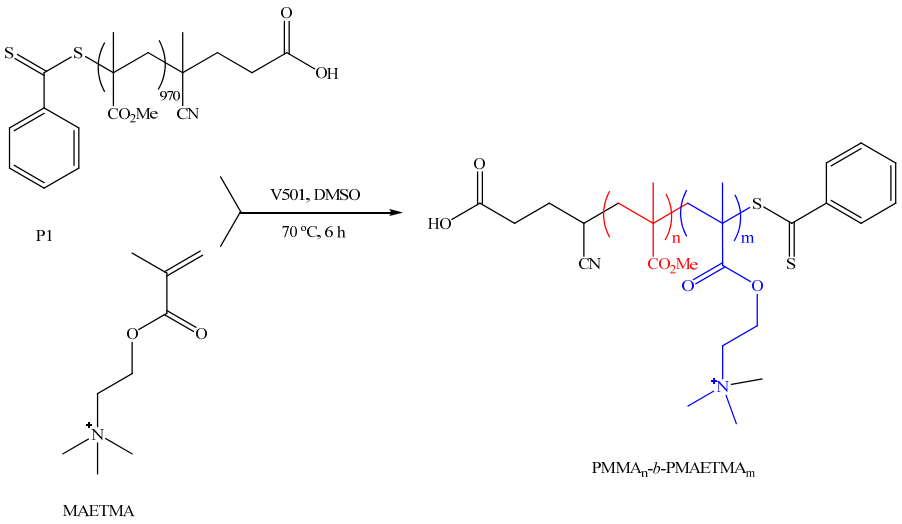

Figure 33. MAETMA polymerization scheme using P1-PMMA.

In an ideal RAFT polymerization, the molecular weight of the block copolymer and the ratio of both blocks can theoretically be predicted using the ratio of concentration of monomers, the thiocarbonylthio derivative concentration and the monomer conversion of the polymerization[104]. PMMA with M_w(GPC) of 55000 g mol^{-1} (PDI= 1.24) was initially prepared and was employed as macroRAFT agent in DMSO at 70 °C using three different ratios of MAETMA to thiocarbonylthiofunctionalities (100:1, 50:1 and 25:1). Aliquots were taken at two and six hours and the conversion was analysed by ^{1}H-NMR. For further confirmation of the formation of block copolymers, the polymers were purified using dialysis against water to remove unreacted MAETMA. The polymers obtained after a polymerization time of 6 hours were purified, freeze-dried and analysed by ^{1}H-NMR to determine the composition (Figure 34).

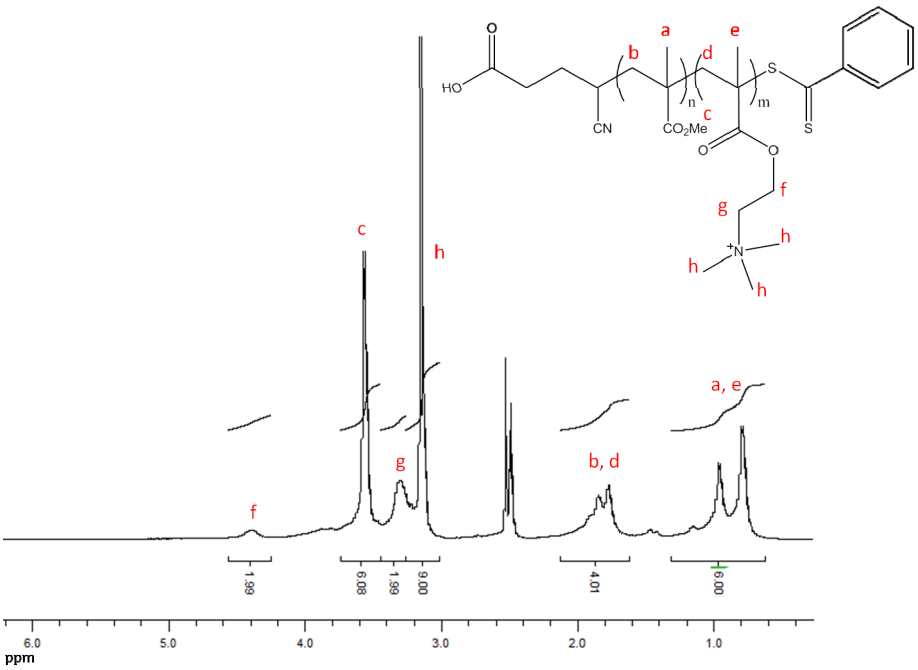

Figure 34. ^{1}H-NMR spectra of PMMA$_{970}$-*b*-PMAETMA$_{84}$ block copolymers in DMSO-d6.

2.4.4. Molecular weight characterization of PMMA-*b*-PMAETMA

A successful RAFT polymerization occurred so that all propagating species begin growth at the same time, which resulted in a narrow molecular weight distribution. The rate of polymerization increased with increasing monomer concentration (Figure 35). The linearity over time indicates that the concentration of propagating radicals was constant throughout the polymerization[105].

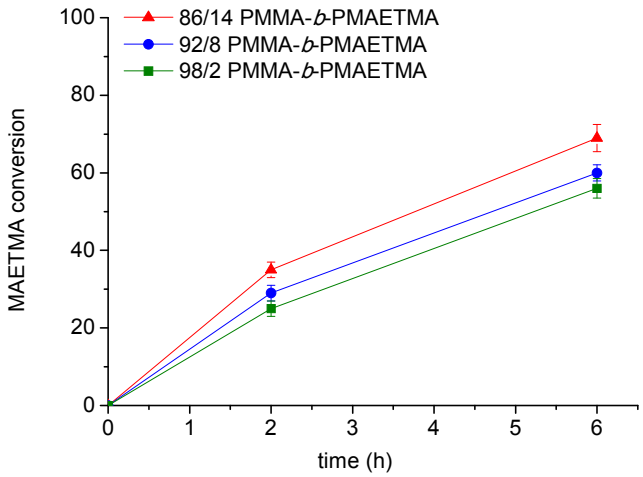

Figure 35. Time vs conversion of the polymerization of MAETMA in the presence of $PMMA_{970}$ macroRAFT agent using various ratios of [MAETMA] to [macroRAFT].

The molecular weight distribution of the resulting block copolymers increased linearly with conversion (Figure 36). This behavior defines a living polymerization in which all (or nearly all) propagating chains have the same lifetime, starting at essentially the same time and growing with negligible occurrence of chain-breaking reactions until high conversion of monomer is reached[106].

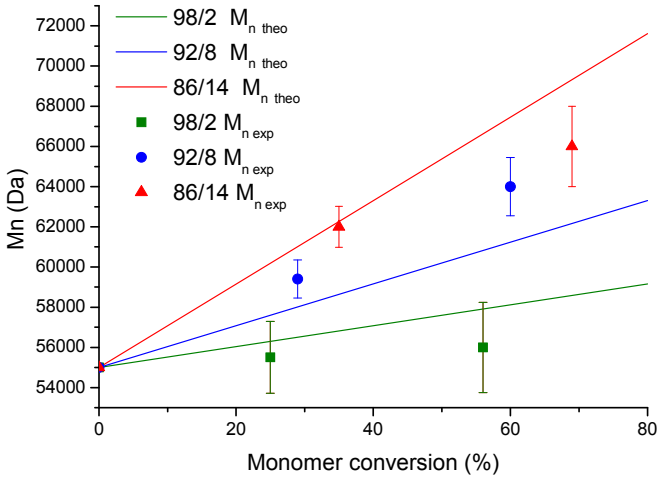

Figure 36. Molecular weight evolution of $PMMA_n$-*b*-$PMAETMA_m$ block copolymers with the conversion (symbols), theoretical M_n calculated using the formula [M]/[macroRAFT] x conversion x $M_{monomer}$ + $M_{macroRAFT}$ [107] (lines). Data presented as mean SD (n = 3).

The polydispersity index ranged between 1.40-1.45, which indicated a narrow molecular weight distribution of the resulting block copolymers. This suggests that the transfer of the radical to the macroRAFT agent was successful. Table 1 summarizes the characteristics of the AB diblock copolymers prepared, their targeted and measured molar compositions, M_n and polydispersity index.

Table 1. Block copolymer systems composition and mean molecular weight distribution measured by NMR and SEC respectively, for the polymerization of MAETMA in the presence of $PMMA_{970}$ macro RAFT agent in DMSO at 70 °C. F is defined as the molar composition percentage of each segment in the block copolymer system.

[MAETMA]:[PMMA macroRAFT]	% conversion after 6 h	$M_{n,theo}$	$M_{n,exp}$ (measured by SEC)	PDI	PMMA units (n)	PMAETMA units (m)	$F_{PMMA}/F_{PMAETMA}$ (calculated by NMR)*
[100]:[1]	67	69000	66000	1.40	970	158	6/14
[50]:[1]	60	61200	64000	1.41	970	84	92/8
[25]:[1]	56	57900	56000	1.45	970	20	98/2

*Units composition of the block copolymer systems were calculated by ^{1}H-NMR using the 0.3-1.2 ppm integration peak for PMMA+PMAETMA and 4.2-4.4 ppm integration peak for PMAETMA.

2.4.5. DLS characterization of PMMA-*b*-PMAETMA

Amphiphilic block copolymers are known to undergo self-organization into micelles[103], which would be suitable as drug carrier system. Light scattering studies not only confirm the formation of micellar aggregates but also reveal the hydrodynamic diameter (D_h) of them. Micelles formation on all block copolymers was promoted by dispersion in DMF and water. Since the particle size can be influenced by the concentration, all the samples were measured at a constant concentration of 3 mg/mL. All the block copolymers showed a tendency to form multimicellar aggregates depending of the solvent. DLS of the copolymer samples after a fine dispersion in water showed that the average size of aggregates in water increased with the increasing of the length of the PMAETMA block (Table 2). However, the average size indicates the relatively high tendency to the formation of multimicellar aggregates (Figure 37). When DMF is used as dispersion medium, the D_h is much smaller than in water, indicating that the block copolymer has a clear tendency to the formation of unimicellar system

(Figure 38). Block copolymers were soluble in ethyl acetate where micelle formation was absent.

Table 2. Hydrodynamic diameter (D_h) of the micelles measured by DLS using different solvents.

Sample	Composition	D_h (DMF) ± SD (nm)	D_h (H_2O) ± SD (nm)
86/14	$PMMA_{970}$-*b*-$PMAETMA_{158}$	14.01 ± 0.08	143 ± 18
92/8	$PMMA_{970}$-*b*-$PMAETMA_{84}$	16.54 ± 0.19	135 ± 27
98/2	$PMMA_{970}$-*b*-$PMAETMA_{20}$	18.22 ± 0.77	132 ± 12

The block copolymers PMMA-*b*-PMAETMA were soluble in ethyl acetate for any composition and concentration interval used in this work and when a diluted solution was added to water at high stirring, self-organised micelles dispersion were formed. The micelle nanoparticles have a core-shell organisation with the more hydrophobic MMA blocks in the core and the hydrophilic MAETMA sequences in the shell. According to the light scattering results, these micelles are not stable enough in water and tend to aggregate in multimicellar nanoparticles.

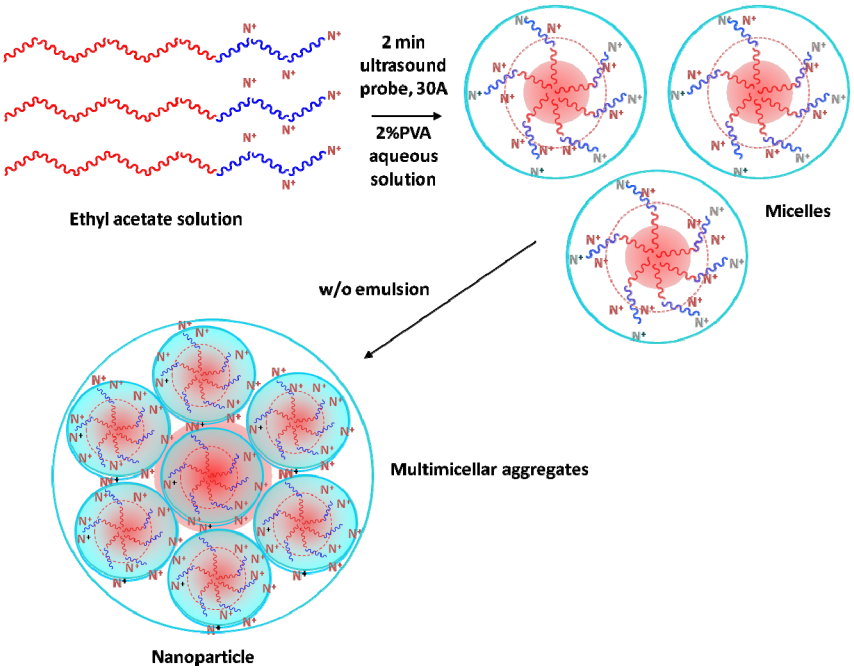

Figure 37. Micelles formation scheme in water emulsion.

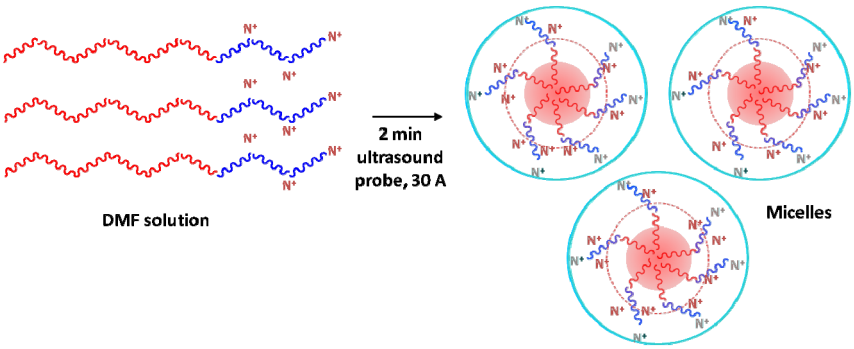

Figure 38. Micelles formation scheme in DMF solvent.

2.4.6. Size and morphology characterization of the amphiphilic block copolymer systems by Scanning Transmission Electronic Microscopy (STEM)

Field emission SEM equipped with STEM detection allowed the determination of amphiphilic supramolecular structure of the block copolymer systems forming micelles. A predominantly spherical morphology was observed in all the cases (Figure 39), showing a core-shell structure due to the amphiphilic nature of the block copolymers. The PMMA sequences, which constitute the hydrophobic part, are distributed forming the core of the micelle, surrounded by PMAETMA sequences, which form the hydrophilic part, and therefore are placed on the particle shell. This core-shell structure is characteristic of amphiphilic systems.

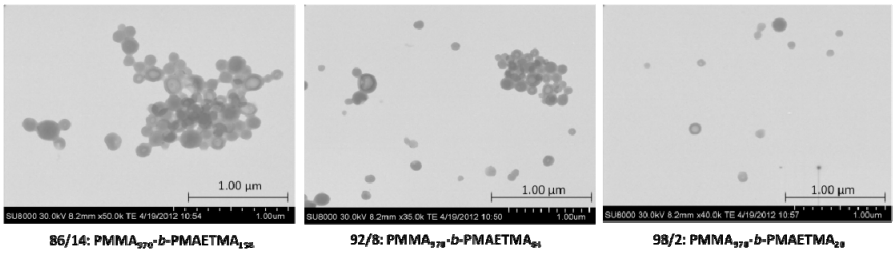

Figure 39. Images obtain in a Hitachi S800 Field Emission SEM instrument.

2.4.7. DSC measurements

PMMA-*b*-PMAETMA block copolymers showed a unique glass transition temperature (T_g) between 86 and 110 °C, depending on the composition. This transition can be attributed to the T_g of the MMA segment. The systems showed a decreasing of T_g value as the $F_{PMAETMA}$ was increased in the polymer (Table 3).

This feature can be due to the plastification effect of the MAETMA segments in the polymer system [108].

Table 3. T_g values of the NP systems measured by DSC under nitrogen atmosphere at 10 °C/min.

SAMPLE	T_{g1} (°C)	T_{g2} (°C)
86/14 $PMMA_{970}$-*b*-$PMAETMA_{158}$	-	86
92/8 $PMMA_{970}$-*b*-$PMAETMA_{84}$	-	93
98/2 $PMMA_{970}$-*b*-$PMAETMA_{20}$	-	110
Eudragit® RS PO	68	-

2.5. CONCLUSIONS

ATRP and RAFT polymerizations have been used to produce well-defined copolymers with different block-lengths and narrow molecular weight distributions. Both techniques allowed the formation of thermal and pH sensitive copolymers and amphiphilic block copolymers, which can be useful for the formation of bioactive systems to be used in drug delivery and tissue engineering.

The azido-containing polymer systems were prepared by controlled polymerization AGET-ATRP process from an oxidative stable catalyst complex. These azido functionalized methacrylic polymers can be used to form active bioconjugates by click chemistry conjugation (chapter 3)[109].

RAFT polymerisation was shown to be a suitable method to prepare amphiphilic block copolymers of PMMA-*b*-PMAETMA, which allowed control over the length and molecular weight of each sequences within the final block copolymer system. These amphiphilic block copolymers showed a micellar self-assembled nanoparticles structure with spherical morphology and a mean size between 130-150 nm, depending on the length of the PMAETMA sequences. The amphiphilic properties make them suitable to be used as drug carriers (chapter 4)[110].

2.6. REFERENCES

56. Braunecker, W. A.; Matyjaszewski, K., Controlled/living radical polymerization: Features, developments, and perspectives. *Progress in Polymer Science* **2007,** *32* (1), 93-146.
57. Sumerlin, B. S., Proteins as Initiators of Controlled Radical Polymerization: Grafting-from via ATRP and RAFT. *ACS Macro Letters* **2011,** *1* (1), 141-145.
58. Matyjaszewski, K., *Controlled/Living Radical Polymerization, from synthesis to materials*. American Chemical Society: Washington DC, 2006.
59. Greszta, D.; Mardare, D.; Matyjaszewski, K., "Living" radical polymerization. 1. Possibilities and limitations. *Macromolecules* **1994,** *27* (3), 638-644.
60. (a) Matyjaszewski, K., Atom Transfer Radical Polymerization: From Mechanisms to Applications. *Israel Journal of Chemistry* **2012,** *52* (3-4), 206-220; (b) Matyjaszewski, K., Atom Transfer Radical Polymerization (ATRP): Current Status and Future Perspectives. *Macromolecules (Washington, DC, U. S.)* **2012,** *45* (10), 4015-4039; (c) Tsarevsky, N. V.; Matyjaszewski, K., \"Green\" Atom Transfer Radical Polymerization: From Process Design to Preparation of Well-Defined Environmentally Friendly Polymeric Materials. *Chemical Reviews (Washington, DC, United States)* **2007,** *107* (6), 2270-2299; (d) Matyjaszewski, K.; Xia, J., Atom Transfer Radical Polymerization. *Chemical Reviews (Washington, D. C.)* **2001,** *101* (9), 2921-2990.
61. Jancar, J.; Douglas, J. F.; Starr, F. W.; Kumar, S. K.; Cassagnau, P.; Lesser, A. J.; Sternstein, S. S.; Buehler, M. J., Current issues in research on structure–property relationships in polymer nanocomposites. *Polymer* **2010,** *51* (15), 3321-3343.
62. Dan, L.; Hong, C., Regulation of Protein/Surface Interactions by Surface Chemical Modification and Topographic Design. In *Proteins at Interfaces III State of the Art*, American Chemical Society: 2012; Vol. 1120, pp 301-319.
63. di Lena, F.; Matyjaszewski, K., Transition metal catalysts for controlled radical polymerization. *Progress in Polymer Science* **2010,** *35* (8), 959-1021.
64. (a) Pintauer, T.; Matyjaszewski, K., Atom transfer radical addition and polymerization reactions catalyzed by ppm amounts of copper complexes. *Chemical Society Reviews* **2008,** *37* (6), 1087-1097; (b) Averick, S.; Simakova, A.; Park, S.; Konkolewicz, D.; Magenau, A. J. D.; Mehl, R. A.; Matyjaszewski, K., ATRP under Biologically Relevant Conditions: Grafting from a Protein. *ACS Macro Letters* **2012,** *1* (1), 6-10; (c) Konkolewicz, D.; Magenau, A. J. D.; Averick, S. E.; Simakova, A.; He, H.; Matyjaszewski, K., ICAR ATRP with ppm Cu Catalyst in Water. *Macromolecules (Washington, DC, U. S.)* **2012,** *45* (11), 4461-4468; (d) Simakova, A.; Averick, S. E.; Konkolewicz, D.; Matyjaszewski, K., Aqueous ARGET ATRP. *Macromolecules (Washington, DC, U. S.)* **2012,** *45* (16), 6371-6379.
65. di Lena, F.; Matyjaszewski, K., Transition metal catalysts for controlled radical polymerization. *Progress in Polymer Science* **2010,** *35* (8), 959-1021.
66. Barthélémy, B.; Devillers, S.; Minet, I.; Delhalle, J.; Mekhalif, Z., Induction heating for surface triggering styrene polymerization on titanium modified with ATRP initiator. *Journal of Colloid and Interface Science* **2011,** *354* (2), 873-879.
67. Poli, R., Stoffelbach, F., & Maria, S., New mechanistic insights into ATRP using molybdenum coordination compounds. *Polym Prep (Am Chem Soc, Div Polym Chem)* **2005,** *46*, 305-6.
68. Mukumoto, K.; Wang, Y.; Matyjaszewski, K., Iron-Based ICAR ATRP of Styrene with ppm Amounts of FeIIIBr3 and 1,1′-Azobis(cyclohexanecarbonitrile). *ACS Macro Letters* **2012,** *1* (5), 599-602.
69. He, D.; Noh, S. K.; Lyoo, W. S., In situ-generated Ru(III)-mediated ATRP from the polymeric Ru(III) complex in the absence of activator generation agents. *Journal of Polymer Science Part A: Polymer Chemistry* **2011,** *49* (21), 4594-4602.
70. KOUKI MATSUBARA, M. M., Cobalt(I)-Mediated Living Radical Polymerization of Methyl Methacrylate. *Journal of Polymer Science: Part A: Polymer Chemistry*
2006, *44*, 4222-4228.
71. Duquesne, E.; Habimana, J.; Degée, P.; Dubois, P., Nickel-Catalyzed Supported ATRP of Methyl Methacrylate Using Cross-Linked Polystyrene Triphenylphosphine as Ligand. *Macromolecules* **2005,** *38* (24), 9999-10006.
72. Albéniz, A. C.; Espinet, P.; López-Fernández, R., Polymerization of Acrylates by Neutral Palladium Complexes. Isolation of Complexes at the Initial Steps. *Organometallics* **2003,** *22* (21), 4206-4212.

73. Bortolamei, N.; Isse, A. A.; Di Marco, V. B.; Gennaro, A.; Matyjaszewski, K., Thermodynamic Properties of Copper Complexes Used as Catalysts in Atom Transfer Radical Polymerization. *Macromolecules* **2010,** *43* (22), 9257-9267.
74. Braunecker, W. A.; Tsarevsky, N. V.; Gennaro, A.; Matyjaszewski, K., Thermodynamic Components of the Atom Transfer Radical Polymerization Equilibrium: Quantifying Solvent Effects. *Macromolecules* **2009,** *42* (17), 6348-6360.
75. Kwak, R. N. Y.; Matyjaszewski, K., Dibromotrithiocarbonate Iniferter for Concurrent ATRP and RAFT Polymerization. Effect of Monomer, Catalyst, and Chain Transfer Agent Structure on the Polymerization Mechanism. *Macromolecules* **2008,** *41* (13), 4585-4596.
76. Tsarevsky, N. V.; Braunecker, W. A.; Tang, W.; Brooks, S. J.; Matyjaszewski, K.; Weisman, G. R.; Wong, E. H., Copper-based ATRP catalysts of very high activity derived from dimethyl cross-bridged cyclam. *Journal of Molecular Catalysis A: Chemical* **2006,** *257* (1–2), 132-140.
77. Tang, W.; Kwak, Y.; Braunecker, W.; Tsarevsky, N. V.; Coote, M. L.; Matyjaszewski, K., Understanding Atom Transfer Radical Polymerization: Effect of Ligand and Initiator Structures on the Equilibrium Constants. *Journal of the American Chemical Society* **2008,** *130* (32), 10702-10713.
78. (a) Choochottiros, C.; Park, E.; Chin, I.-J., Synthesis and characterization of polylactide–poly(methyl methacrylate) copolymer by combining of ROP and AGET ATRP. *Journal of Industrial and Engineering Chemistry* **2012,** *18* (3), 993-1000; (b) Sun, Y.; Liu, W., Synthesis and characterization of a new fluorinated macroinitiator and its diblock copolymer by AGET ATRP. *Journal of Fluorine Chemistry* **2011,** *132* (1), 9-14.
79. Magenau, A. J. D.; Kwak, Y.; Matyjaszewski, K., ATRP of Methacrylates Utilizing CuIIX2/L and Copper Wire. *Macromolecules* **2010,** *43* (23), 9682-9689.
80. Oh, J. K.; Perineau, F.; Charleux, B.; Matyjaszewski, K., AGET ATRP in water and inverse miniemulsion: A facile route for preparation of high-molecular-weight biocompatible brush-like polymers. *Journal of Polymer Science Part A: Polymer Chemistry* **2009,** *47* (7), 1771-1781.
81. Stenzel, M. H., RAFT polymerization: an avenue to functional polymeric micelles for drug delivery. *Chemical Communications* **2008,** (30), 3486-3503.
82. Barner-Kowollik, C.; Davis, T. P.; Heuts, J. P. A.; Stenzel, M. H.; Vana, P.; Whittaker, M., RAFTing down under: Tales of missing radicals, fancy architectures, and mysterious holes. *Journal of Polymer Science, Part A: Polymer Chemistry* **2003,** *41* (3), 365-375.
83. Beckwith, A. L. J., Radicals in organic synthesis: Formation of carbon—carbon bonds. Von B. Giese, Pergamon Press, Oxford 1986. XIII, 294 S., Paperback $ 25.00. — ISBN 0-08-032494-0. *Angewandte Chemie* **1987,** *99* (8), 824-825.
84. Mayadunne, R. T. A.; Rizzardo, E.; Chiefari, J.; Chong, Y. K.; Moad, G.; Thang, S. H., Living Radical Polymerization with Reversible Addition−Fragmentation Chain Transfer (RAFT Polymerization) Using Dithiocarbamates as Chain Transfer Agents. *Macromolecules* **1999,** *32* (21), 6977-6980.
85. Keddie, D. J.; Moad, G.; Rizzardo, E.; Thang, S. H., RAFT Agent Design and Synthesis. *Macromolecules* **2012,** *45* (13), 5321-5342.
86. Barner-Kowollik, C.; Buback, M.; Charleux, B.; Coote, M. L.; Drache, M.; Fukuda, T.; Goto, A.; Klumperman, B.; Lowe, A. B.; McLeary, J. B.; Moad, G.; Monteiro, M. J.; Sanderson, R. D.; Tonge, M. P.; Vana, P., Mechanism and kinetics of dithiobenzoate-mediated RAFT polymerization. I. The current situation. *Journal of Polymer Science Part A: Polymer Chemistry* **2006,** *44* (20), 5809-5831.
87. Lattuada, M.; Hatton, T. A., Functionalization of monodisperse magnetic nanoparticles. *Langmuir* **2007,** *23* (4), 2158-68.
88. Licciardi, M.; Tang, Y.; Billingham, N. C.; Armes, S. P.; Lewis, A. L., Synthesis of Novel Folic Acid-Functionalized Biocompatible Block Copolymers by Atom Transfer Radical Polymerization for Gene Delivery and Encapsulation of Hydrophobic Drugs. *Biomacromolecules* **2005,** *6* (2), 1085-1096.
89. Wei, K.; Su, L.; Chen, G.; Jiang, M., Does PNIPAM block really retard the micelle-to-vesicle transition of its copolymer? *Polymer* **2011,** *52* (16), 3647-3654.
90. Hongliang, K.; Xia, G.; Ruigang, L.; Yong, H., Synthesis and Properties of Cellulose Graft Copolymers with Well-Defined Architecture. In *Functional Materials from Renewable Sources*, American Chemical Society: 2012; Vol. 1107, pp 109-131.
91. Lutz, J.-F., Polymerization of oligo(ethylene glycol) (meth)acrylates: Toward new generations of smart biocompatible materials. *Journal of Polymer Science Part A: Polymer Chemistry* **2008,** *46* (11), 3459-3470.
92. Yamamoto, S.-I.; Pietrasik, J.; Matyjaszewski, K., The effect of structure on the thermoresponsive nature of well-defined poly(oligo(ethylene oxide) methacrylates) synthesized by ATRP. *Journal of Polymer Science Part A: Polymer Chemistry* **2008,** *46* (1), 194-202.

93. Dong, H.; Matyjaszewski, K., Thermally Responsive P(M(EO)2MA-co-OEOMA) Copolymers via AGET ATRP in Miniemulsion. *Macromolecules* **2010,** *43* (10), 4623-4628.
94. Cho, S. H.; Jhon, M. S.; Hong Yuk, S., Temperature-sensitive swelling behavior of polymer gel composed of poly (N,N-dimethylaminoethyl methacrylate) and its copolymers. *European Polymer Journal* **1999,** *35* (10), 1841-1845.
95. (a) Emileh, A.; Vasheghani-Farahani, E.; Imani, M., Swelling behavior, mechanical properties and network parameters of pH- and temperature-sensitive hydrogels of poly((2-dimethyl amino) ethyl methacrylate-co-butyl methacrylate). *European Polymer Journal* **2007,** *43* (5), 1986-1995; (b) Mespouille, L.; Coulembier, O.; Paneva, D.; Degée, P.; Rashkov, I.; Dubois, P., Synthesis of adaptative and amphiphilic polymer model conetworks by versatile combination of ATRP, ROP, and "Click chemistry". *Journal of Polymer Science Part A: Polymer Chemistry* **2008,** *46* (15), 4997-5013.
96. Agut, W.; Taton, D.; Lecommandoux, S., A Versatile Synthetic Approach to Polypeptide Based Rod−Coil Block Copolymers by Click Chemistry. *Macromolecules* **2007,** *40* (16), 5653-5661.
97. Averick, S. E.; Paredes, E.; Grahacharya, D.; Woodman, B. F.; Miyake-Stoner, S. J.; Mehl, R. A.; Matyjaszewski, K.; Das, S. R., A Protein–Polymer Hybrid Mediated By DNA. *Langmuir* **2012,** *28* (4), 1954-1958.
98. Mitsukami, Y.; Donovan, M. S.; Lowe, A. B.; McCormick, C. L., Water-Soluble Polymers. 81. Direct Synthesis of Hydrophilic Styrenic-Based Homopolymers and Block Copolymers in Aqueous Solution via RAFT. *Macromolecules* **2001,** *34* (7), 2248-2256.
99. Thang, S. H.; Chong, Y. K.; Mayadunne, R. T. A.; Moad, G.; Rizzardo, E., A novel synthesis of functional dithioesters, dithiocarbamates, xanthates and trithiocarbonates. *Tetrahedron Letters* **1999,** *40* (12), 2435-2438.
100. (a) Bertoldo, M.; Zampano, G.; Terra, F. L.; Villari, V.; Castelvetro, V., Amphiphilic Amylose-g-poly(meth)acrylate Copolymers through "Click" onto Grafting Method. *Biomacromolecules* **2010,** *12* (2), 388-398; (b) Jiang, X.; Lok, M. C.; Hennink, W. E., Degradable-Brushed pHEMA–pDMAEMA Synthesized via ATRP and Click Chemistry for Gene Delivery. *Bioconjugate Chemistry* **2007,** *18* (6), 2077-2084; (c) Zhang, X.; Matyjaszewski, K., Synthesis of Well-Defined Amphiphilic Block Copolymers with 2-(Dimethylamino)ethyl Methacrylate by Controlled Radical Polymerization. *Macromolecules* **1999,** *32* (6), 1763-1766; (d) Zhang, X.; Xia, J.; Matyjaszewski, K., Controlled/\"Living\" Radical Polymerization of 2-(Dimethylamino)ethyl Methacrylate. *Macromolecules* **1998,** *31* (15), 5167-5169.
101. Gregory, A.; Stenzel, M. H., Complex polymer architectures via RAFT polymerization: From fundamental process to extending the scope using click chemistry and nature's building blocks. *Progress in Polymer Science (Oxford)* **2012,** *37* (1), 38-105.
102. Lowe, A. B.; McCormick, C. L., Reversible addition-fragmentation chain transfer (RAFT) radical polymerization and the synthesis of water-soluble (co)polymers under homogeneous conditions in organic and aqueous media. *Progress in Polymer Science* **2007,** *32* (3), 283-351.
103. Yu, B.; Lowe, A. B.; Ishihara, K., RAFT Synthesis and Stimulus-Induced Self-Assembly in Water of Copolymers Based on the Biocompatible Monomer 2-(Methacryloyloxy)ethyl Phosphorylcholine. *Biomacromolecules* **2009,** *10* (4), 950-958.
104. Yusa, S.-i.; Fukuda, K.; Yamamoto, T.; Ishihara, K.; Morishima, Y., Synthesis of Well-Defined Amphiphilic Block Copolymers Having Phospholipid Polymer Sequences as a Novel Biocompatible Polymer Micelle Reagent. *Biomacromolecules* **2005,** *6* (2), 663-670.
105. Sun, X.; Luo, Y.; Wang, R.; Li, B.-G.; Liu, B.; Zhu, S., Programmed Synthesis of Copolymer with Controlled Chain Composition Distribution via Semibatch RAFT Copolymerization. *Macromolecules* **2007,** *40* (4), 849-859.
106. Drache, M.; Schmidt-Naake, G.; Buback, M.; Vana, P., Modeling RAFT polymerization kinetics via Monte Carlo methods: cumyl dithiobenzoate mediated methyl acrylate polymerization. *Polymer* **2005,** *46* (19), 8483-8493.
107. Stenzel, M. H.; Barner-Kowollik, C.; Davis, T. P.; Dalton, H. M., Amphiphilic Block Copolymers Based on Poly(2-acryloyloxyethyl phosphorylcholine) Prepared via RAFT Polymerisation as Biocompatible Nanocontainers. *Macromolecular Bioscience* **2004,** *4* (4), 445-453.
108. Garnier, S. b.; Laschewsky, A., Synthesis of New Amphiphilic Diblock Copolymers and Their Self-Assembly in Aqueous Solution. *Macromolecules* **2005,** *38* (18), 7580-7592.
109. Reyes-Ortega, F.; Parra-Ruiz, F. J.; Averick, S. E.; Rodriguez, G.; Aguilar, M. R.; Matyjaszewski, K.; San Roman, J., Smart heparin-based bioconjugates synthesized by a combination of ATRP and click chemistry. *Polymer Chemistry* **2013,** *4* (9), 2800-2814.
110. Reyes-Ortega, F.; Rodriguez, G.; Aguilar, M. R.; Lord, M.; Whitelock, J.; Stenzel, M. H.; San Roman, J., Encapsulation of low molecular weight heparin (bemiparin) into polymeric nanoparticles

obtained from cationic block copolymers: properties and cell activity. *Journal of Materials Chemistry B* **2013,** *1* (6), 850-860.

Synthesis and characterization of bemiparin-polymer bioconjugates prepared by click chemistry

CHAPTER 3

3.1 INTRODUCTION

Drug delivery investigation is focused on the synthesis of new compounds that improve biomolecules (polysaccharides, peptides, proteins, etc.) short plasma half-life, stability and reduce immune-geneticity within the body[111]. Specifically, bemiparin presents 5.3 h half-life and its conjugation with polymer systems can improve its stability in the body.

Polymer bioconjugates have been considered good candidates for achieving active targeting and controlled release of drugs due to enhanced biocompatibility, biodegradability and mucoadhesive properties[111,112]. Well defined bioconjugates can be synthesized using a 'grafting to' or 'grafting onto' approach, where a preformed polymer with a reactive end group is coupled to complementary functional groups along the backbone of a second polymer. The process of grafting polymer chains, to or onto surfaces can impart new properties to materials in a well defined manner[113].

Green-chemistry processes are characterized to be modular, wide in scope, give very high yields, generate only inoffensive byproducts that can be removed by non-chromatographic methods, and be stereospecific. Click reactions are coupling reactions that fulfill all these requirements. Moreover, they are tolerant for a wide range of functional groups, simple to perform and can be conducted to very high yield[114]. The required process characteristics include simple reactions conditions (ideally, the process should be insensitive to oxygen and water), readily available starting materials and reagents, the use of no solvent or a solvent that is benign (such as water) or easily removed, and simple product isolation. Purification, if required, must be by simple methods, such as crystallization or distillation, and the product must be stable under physiological conditions.

There are several well-known reactions that comply with the 'click chemistry' concept, including the hetero-Diels-Alder reaction, the thiol-ene

coupling, the Staudinger ligation, native chemical ligation, the amidation reaction between thio acids and sulfonyl azides (sulfo-click), and the most popular copper(I)-catalyzed alkyne-azide cycloaddition (CuAAC), which has been used for the systems described in this chapter. The broadly applied Cu(I)-catalyzed [3+2] Huisgen dipolar cycloaddition between azides and alkynes provides 1,2,3-triazole rings with 1,4 regioselectivity and quantitative transformation under mild conditions including *in vivo*[115], due to the orthogonal nature of the azide-alkyne reactive pair. Triazole moieties are also interesting conjugation entities as they are proven to be relatively stable to the metabolic degradation, and can participate in the hydrogen bonding, which enhances the biological importance of this specific click coupling reaction[116]. Therefore, this highly effective and selective 'click' reaction was used to overcome problems of low yield and poor selectivity frequently encountered in 'grafting to' reactions involving polysaccharides and synthetic hydrophobic polymers[117].

Additionally, the CuAAC can be performed in aqueous media with a high reaction rate and generally high resultant yields. Water is usually regarded as an ideal solvent in terms of its environmental impact and low cost. A benefit which is little appreciated but has enormous consequences is that most hydroxyl and amine groups will not interfere with click reactions performed in water. As a consequence, the incorporation and removal of protecting groups are avoided, which is probably the best single reason for adopting this style of synthesis. These benefits can be explained by several factors:

- The free energies of organic molecules are substantially greater when poorly solvated in water, and often impart increased reactivity.
- Nucleophile additions to epoxide and aziridine electrophiles are favored by solvents able to respond continuously to the demanding range of hydrogen-bonding situations that arise during these processes. In this respect, water is unique, and for the same reasons, it is the perfect medium for reversible carbonyl chemistry.

- The use of water offers the greatest average for differentiating the reactivities of competing 'hard' (non-polarizable) and 'soft' (polarizable) species.
- A highly favorable reaction of two solutes is usually much faster than a low driving force side-reaction of one of the solutes with solvent water.
- Water is a superb heat sink, due to its high heat capacity, and has a convenient boiling temperature; both are useful for large-scale processes.

Moreover, recent studies showed that the 1,2,3-triazole moiety, which is formed during the Cu(I)-catalyzed 1,3-diporal cycloaddition, is similar to the peptide-amide bond in terms of geometry. Therefore, the triazole moiety has been suggested as a mimic of a peptide amide bond and has been used for example as a dipeptide isostere in β-strands and α–helical coiled coils[118].

Taking this into account, the application of 'click chemistry' to polymer science has led to improvements in bioconjugation techniques[117b, c, 119]. Functional polymeric materials can be bioconjugated by 'click chemistry' to create bioactive conjugates, which can be used in biomedical applications including drug delivery, tissue engineering and medical imaging[120]. Creating bioconjugates by combining stimuli responsive polymers with proteins and polysaccharides can result in a synergistic combination of properties of the individual components and can additionally overcome their separate limitations. The protein or polysaccharide component can impart (bio)functional properties to the bioconjugate, whereas the polymer component can improve protein or polysaccharide stability, solubility and biocompatibility. The synthetic polymer can also introduce new properties to the bioconjugate such as stimuli responsiveness, self-assembly, phase separation behavior, and it can even modulate protein or polysaccharide activity[121].

3.2 AIMS OF THIS CHAPTER

The aim of this chapter was the synthesis and characterization of bemiparin-poly(2-dimethylaminoethyl methacrylate (PDMAEMA) and bemiparin-poly(dietilenglycol-*co*-oligo ethylene glycol methacrylate) [P(MEO_2MA-*co*-$OEOMA_{300}$)] bioconjugates by CuAAC. For these purpose, Bemiparin was functionalized with alkyne groups in order to use 'click chemistry' to obtain bemiparin bioconjugates with sensitivity to pH and temperature, as the synthetic scheme shows (Figure 40). In this sense, the carboxylic groups of bemiparin were modified with propargylamine to generate alkynyl side groups along polysaccharide backbone using dimethoxy-triazinyl-methylmorpholinium chloride (DMTMM). The product formed with DMTMM was compared with the product obtained using a carbodiimides reagent e.i. EDC[122,123]. This bemiparin derivative was combined by 'click coupling reaction' with azido-functionalized methacrylate polymers, PDMAEMA or P(MEO_2MA-*co*-$OEOMA_{300}$), which were synthesized and described in chapter 2, via AGET-ATRP.

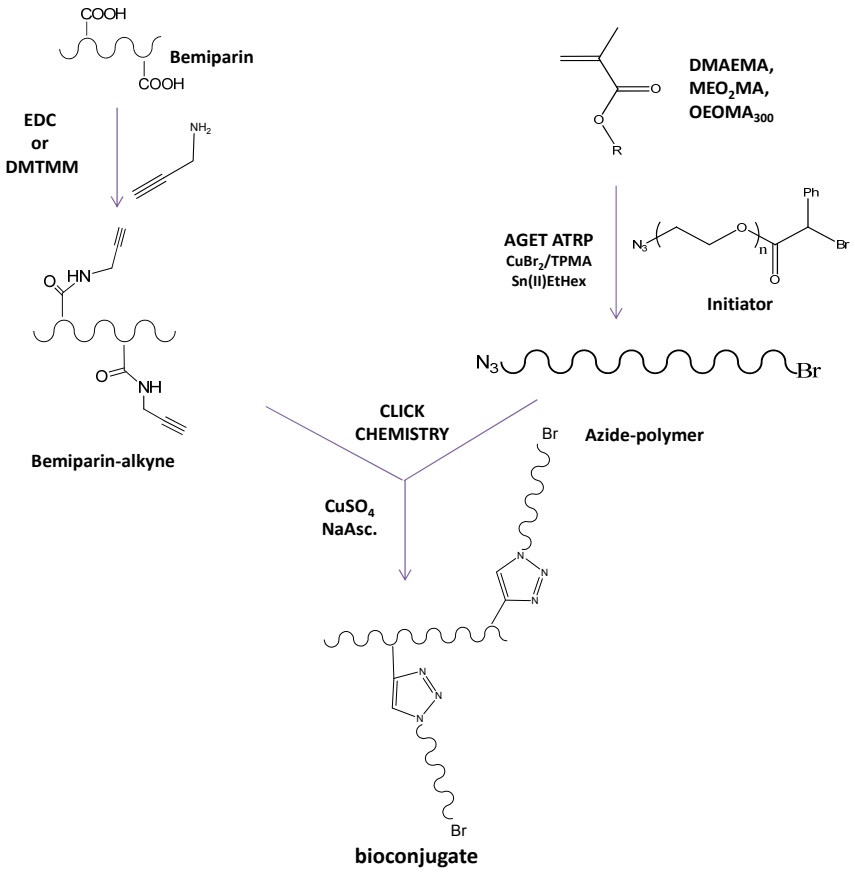

Figure 40. Bemiparin bioconjugate obtained by click chemistry with temperature sensitive polymers synthesized by AGET ATRP.

3.3 Materials and Methods

3.3.1 MATERIALS

Low Molecular Weight Heparin (LMWH), bemiparin (HIBOR®) (111,3 UI/mg, 3600 Da) was kindly donated by ROVI PHARMACEUTICALS LABORATORIES (Madrid, Spain). Propargylamine (Sigma-Aldrich, 98%), dimethoxy-triazinyl-methylmorpholinium chloride (DMTMM) (Sigma-Aldrich, 96%), 1-(3-dimethyl-aminopropyl)-3-ethylcarbodiimide hydrochloride (EDC)

(Acros Organics, 98%), *N*-hydroxysuccinimide (NHS) (Fluka, 98%), ascorbic acid (Fluka, >99%), Copper sulphate pentahydrate (Panreac), tin ethylhexanoate (Sn(II)EtHex) (Sigma-Aldrich, 95%), aluminum oxide basic (Sigma-Aldrich, >98%), toluene (Merck, analysis grade), Tetrahydrofuran (THF) (Scharlau, analysis grade) and ethyl ether (SDS, 99.8%) were used as received.

3.3.2 METHODS

3.3.2.1 Functionalization of Bemiparin with alkyne groups

Preparation of alkynyl-functionalized bemiparin was carried out by the modification of carboxylic groups of bemiparin with propargylamine using dimethoxy-triazinyl-methyl morpholinium chloride (DMTMM) or 1-ethyl-3-(3-dimethylaminopropyl)carbodiimide (EDC). For this purpose, bemiparin (100 mg, 0.02 mmol) was mixed with a 10 molar excess equivalents of propargylamine (11 mg, 0.2 mmol) and DMTMM (55.3 mg, 0.2 mmol) in 5 mL of distilled water. The reaction was kept under magnetic stirring at room temperature for 5 hours. The same reaction was carried out using EDC (38.3 mg, 0.2 mmol) and *N*-hydroxysuccinimide (NHS) (11.5 mg, 0.1 mmol) instead of DMTMM. Both products were purified by dialysis against water for 3 days, using a membrane with a M_w cut-off (MWCO) of3500 Da, changing the water twice a day and finally freeze-drying to get the bemiparin-alkyne.

3.3.2.2 Preparation of bioconjugates by click chemistry

The azido-end polymer (960 mg, 0.1 mmol) and the alkynyl-functionalized bemiparin (500 mg, 0.1 mmol), were dissolved in 15 mL distilled water. The catalyst system, $CuSO_4 .5H_2O$ (250 µL of a stock solution of 5 mg/mL, $5x10^{-3}$ mmol) and sodium ascorbate (352 µL, 0.01 mmol) were added and the mixture was degassed by purging with nitrogen for 2 hours. The reaction was maintained

under magnetic stirring for 24 hours at room temperature. The catalytic complex was removed by passing through a basic alumina column and purification of the product was carried out by dialysis (M_w Cut-off = 8000 Da) against water for 4 days and further freeze-drying. The solvent extract from dialysis process was used to analyse the M_w of non-conjugated bemiparin. Reaction yields were higher than 90% in both cases.

3.3.3 Characterization

Structural characterization of the polymers was carried out by ^{1}H and ^{13}C NMR and FTIR spectroscopies.

3.3.3.1 NMR spectroscopy

^{1}H, ^{13}C and Heteronuclear Multiple-Bond Correlation spectroscopy (HMBC) NMR analysis was performed using a Varian XL-500 spectrometer; spectra were recorded at room temperature from deuterium oxide solutions. Sample concentration was ~15 mg/mL for ^{1}H and ~100 mg/mL for ^{13}C and HMBC spectra. Spectra were analyzed with the MestreNova v 6.1 software.

3.3.3.2 FTIR spectroscopy

Fourier Transform Infrared spectra in Attenuated Total Reflection mode (ATR-FTIR) were recorded in a Spectrum One FT-IR spectrometer, Perkin Elmer. Polymer samples were analyzed without further treatment at room temperature by 32 scans, and with a resolution of 4 cm^{-1}.

3.3.3.3 Thermogravimetric Analysis

Thermogravimetric Analysis (TGA) was performed in a TGA Q500 (TA Instruments), working under 50 mL/min nitrogen flow, and at a heating rate of 10 °C/min, from 30 to 600 °C.

3.3.3.4 SEC characterization

Molecular weight distributions of bioconjugates were determined by Size Exclusion Chromatography (SEC) in a Perkin-Elmer apparatus equipped with an isocratic pump (Series 200) connected to a differential refractometric detector (Series 200a). Two Resipore columns (Varian) were conditioned at 70 °C and used to elute the samples (3 mg/mL concentration) at 0.3 mL/min in HPLC-grade *N,N'*-dimethylformamide (DMF) supplemented with 0.1% v/v LiBr. SEC calibration was carried out with monodisperse standard poly(methyl methacrylate) samples in the range of $2.9x10^3$ to $480x10^3$ g/mol obtained from Polymer Laboratories with sample injection volumes of 20 µL. Bemiparin and alkyne-bemiparin molecular weight distributions were measured by SEC, in a Shimadzu modular system comprising a DGU-20A3 solvent degasser, a LC-20AD pump, a CTO-20A column oven, a SIL-20A HT autosampler and a RID-10A refractive index detector and SPD-20A Shimadzu UV-VIS detector (flow rate: 1 mL/min, temperature 37 °C). The instrument was equipped with three columns (300mmx7.5mm, 8 µm): PL-aquagel-OH 30^{TM}, PL-aquagel-OH 40^{TM} and PL-aquagel-OH 50^{TM}, protected with a guard column (50mmx7.5mm, 8 µm) (Varian). The mobile phase used was milli-Q water adjusted to pH=3 with 0.2 M $NaNO_3$, 0.01 M $NaHPO_4$ and 1 M acetic acid aqueous solution. SEC calibration was performed with polysaccharide standards (Pullulan Polysaccharide, PL2090-0100 VARIAN) ranging from 1.8 x 10^2 to 708 x 10^3 g/mol.

3.3.3.5 *Thermal properties*

Lower Critical Solution Temperature (LCST) of all the systems N_3-P(MEO_2MA-co-$OEOMA_{300}$), Bemiparin-P(MEO_2MA-co-$OEOMA_{300}$), N_3-PDMAEMA and Bemiparin-PDMAEMA were measured by UV spectroscopy, using a scanning temperature program to detect the aggregation of the system when the LCST was reached. All the systems were analyzed at a concentration of 1 mg/mL aqueous solution at different pH (pH = 3, pH = 7.4 and pH = 10). Temperature sweep was carried out from 20 °C to 90 °C a rate of 1 °C/min and turbidity was evaluated at 450 nm. LCST was defined as the temperature of the onset of the transmittance/temperature diagram, during the heating ramp of the aqueous polymer solutions.

3.4 RESULTS AND DISCUSSION

New heparin-based bioconjugates were prepared by a combination of functionalization of bemiparin, preparation of homogeneous polymethacrylic chains by AGET ATRP, and 'grafting to' strategy by 'click' chemistry, according to figure 42. The methodology provides clean and mild conditions for the preparation of homogeneous polymer systems with controlled composition and molecular weight distribution of the polymeric compounds.

3.4.1 Preparation of bemiparin-alkyne derivative

Alkyne functionalization of bemiparin was carried out by the formation of amide bonds by the union of the carbonyl groups of carboxylic acid of bemiparin and the amine moieties of propargylamine. This amidation reaction usually needs an activator reagent that transforms the hydroxyl group into a good leaving

radical group prior to the reaction with the amine group. In this work, two different activators were used:

EDC, which is one of the most widely used activators for these kind of reactions, mainly due to its water solubility[124]. The amidation reaction has two steps: the first one involves the activation by EDC of the carboxylic acid groups, which forms an O-acyl isourea intermediate. The second step of the reaction is the nucleophilic attack by the amine to the activated carboxylic group, which leads to the formation of the amide bond.[125] The reaction is very delicate as it is strongly pH-dependent and the optimal pH for both steps is different. Indeed, carboxylic acid activation by EDC is better performed in an acidic environment, whereas amide formation is better produced at high pH, when the amine is deprotonated. At such a high pH, EDC is more rapidly hydrolyzed into the *N*-acyl urea by-product and no amidation occurs.

Although carbodiimides are widely used as activate coupling reagents, their synthetic byproducts can be difficult to remove and functionalization reactions are not always conducted in high yields. Indeed in the bemiparin functionalization with propargylamine, EDC residue was difficult to remove due to the formation of ammonium sulfate salts (Figure 41A) between the O-acyl urea byproducts and the sulfate groups of bemiparin[126]. The only way to eliminate the secondary products was washing at strong basic pH (pH = 10). This treatment resulted in some degradation of the polysaccharide[127]. Furthermore, the majority product obtained using EDC and NHS as activator reagents was the ionic salt, but none or very little amount of covalent linkage conjugate was obtained (Figure 41A and B).

To overcome these disadvantages of EDC, **DMTMM** was used as an alternative for the activation of hydroxyl groups of bemiparin in the amidation reaction. This is a triazine derivative which has the particular advantage of promoting amide synthesis in alcohols or aqueous media, without ester formation and with selectivity comparable to EDC or any other carbodiimides. Furthermore, the yields obtained with DMTMM are higher than yields obtained with carbodiimides based reagents[128].

Recently, DMTMM was described to facilitate an efficient one-step condensation of both small molecules and polymers[129]. Other favorable attributes of DMTMM are the easy removal of excess reagent and byproducts from the reaction, the compatibility with many solvents including water, alcohols, diethyl ether, ethyl acetate, and tetrahydrofuran, high reaction yields, and that it is relatively inexpensive. DMTMM can be adapted to a wide pH range, and in some cases, no rigorous pH control is necessary. It has been employed for the modification of a number of polymers including polysaccharides[130]. Herein, we report in Figure 41 the comparison of both activate agents (EDC versus DMTMM) to get alkynyl functionalized bemiparin.

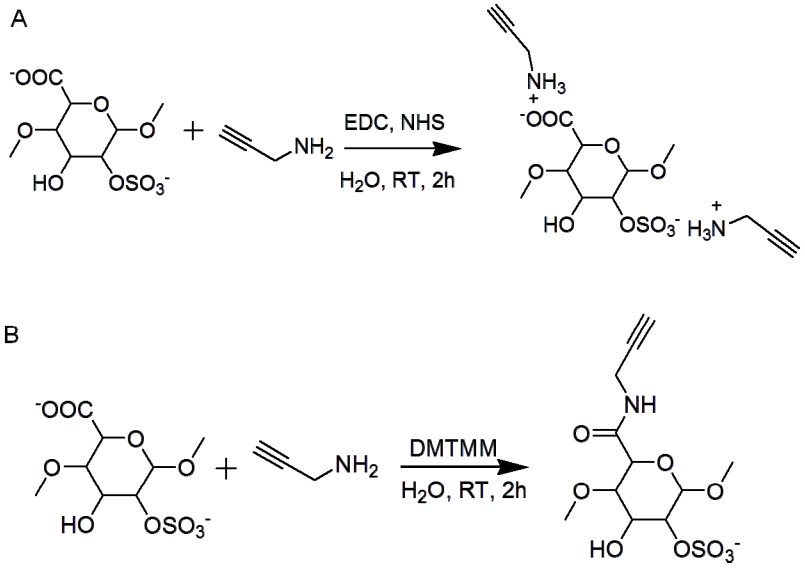

Figure 41. A) Ionic attachment of bemiparin with propargylamine using EDC+NHS. B) Covalent modification of bemiparin with propargylamine using DMTMM.

Figure 42 shows the 1H-NMR spectra of bemiparin before alkynyl functionalization. The content of sulphate amino groups of glucosamine (ANS) was calculated from the signal at 3.25 to 3.40 ppm because the anomeric resonance of ANS shows up as two peaks, the first at 6.10 ppm corresponding to

ANS linked to glucuronic acid (G) and the second at 5.58 ppm corresponding to ANS linked to iduronic acid (I) (Figure 2). The amount of acetate amino groups of glucosamine (A_{NAc}) was calculated by integration of the methyl signal of the *N*-acetyl group at 1.90 ppm and the sum of the integration signals of A_{NAc} + signal of sulphate groups of glucosamine in C-3 (A_{3S}) at 2.05 and 5.82 ppm respectively (Equation II).

Each bemiparin molecule (3600 Da) contains 10 disaccharide units, 2 of them are A_{NAc} (Equation III):

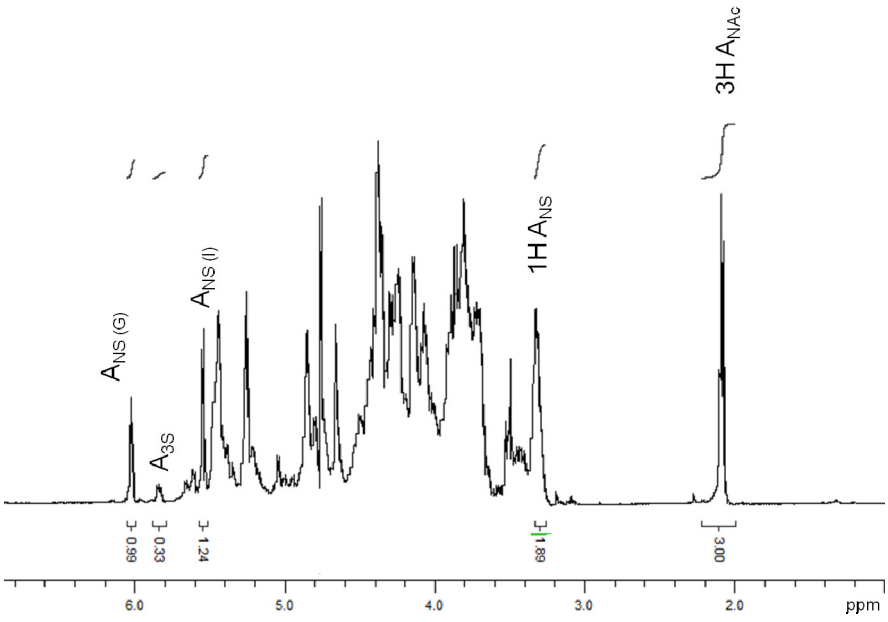

Figure 42. ^{1}H-NMR spectrum of bemiparin. The spectrum was recorded at 500 MHz on a Varian XL-500 spectrometer, at room temperature from D_2O solution.

Calculation of the percentage of substitution for glucosamine C_2 residue of bemiparin[131]:

$$A_{t} = \frac{A_{NAc}}{3} + A_{NS} \qquad \textbf{Equation I}$$

$$\%NAc = \frac{A_{NAc}/3}{A_t} \; x \; 100$$ **Equation II**

$$Nº\ NAc\ groups = \%NAc\ x\ disaccharide\ units\ per\ molecule$$ **Equation III**

$$Nº\ Carboxylic\ groups\ per\ bemiparin\ molecule = \frac{M_{w\ disaccharide}}{M_{w\ bemiparin}}$$ **Equation IV**

The bemiparin derivative was characterized by ^{1}H-NMR, ^{13}C-NMR, HMBC and FTIR. These techniques confirmed the effective functionalization of bemiparin. In the experimental conditions of this work the amidation of the carboxylic groups of bemiparin were selective when DMTMM was applied as activator. However, the application of EDC and NHS protocol gave the formation of ionic carboxylate and sulphate salts instead of the covalent product (Figure 41A). This was clearly demonstrated by FTIR and NMR spectroscopies reported in Figure 43 and Figure 44. FTIR spectrum (Figure 43) presented the stretching band at 2165 cm^{-1} that corresponds to the alkyne function in the conjugate bemiparin-alkyne. This band is not present in the dialyzed (pH 10) product prepared with EDC, which corresponds to the ionic sulphate ammonium salt as has been indicated in Figure 41

Figure 41A. It is clear from this figure that the modification of bemiparin with propargylamine activated by DMTMM gives a spectrum with a modification of the band at 2940 cm^{-1} which can be assigned to C-H aliphatic stretching vibration. Logically this band is the contribution of the components and the covalent product, but the change in the profile and the intensity makes clear the modification produced by the addition of the propargyl moiety to the heparin chains. It is interesting to highlight the bands at 1430 cm^{-1} and 1384 cm^{-1} (carboxylate carbonyl symmetric stretching) assigned to ionized carboxylate functions according to other works on carboxylate salt derivatives of heparin.[132,133] The ratio of the band at 1430 cm^{-1} respect to the 1640 cm^{-1} (carbonyl stretching in carboxylic acids and amides) decreased, and the band at 1384 cm^{-1} clearly disappear after the amidation of the carboxylic groups by

formation of an propargylamine, whereas the product of the reaction with EDC corresponds to the ionic salt as is shown in Figure 41A.

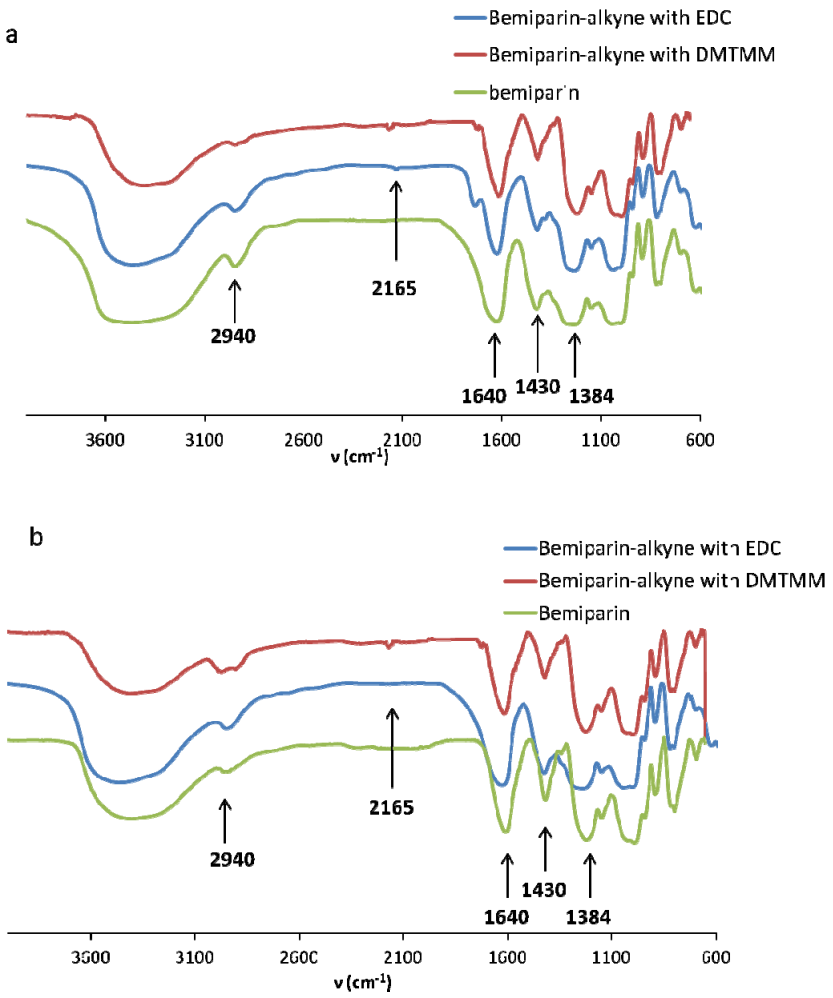

Figure 43. FTIR spectra of bemiparin (green), bemiparin-alkyne functionalized using EDC (blue) and bemiparin-alkyne functionalized using DMTMM (red), a) before pH 10 washing and b) after pH 10 washing.

^{1}H-NMR spectra confirmed ionic binding of propargylamine to bemiparin when EDC was used as the activator, and the covalent binding with DMTMM.

Figure 44 shows two peaks that may be assigned to the alkynyl proton (at 2.54 and 2.80 ppm)[100a, b]. When bemiparin was functionalized using EDC and NHS, it only one peak appeared at 2.80 ppm (Figure 44Ab). However when DMTMM was used as the activator the product of the reaction presents two different peaks, at 2.54 and 2.80 ppm. These peaks can be assigned to the covalent conjugate (amide), δ= 2.54 ppm, and the ionic salt, δ= 2.80 ppm (Figure 44Aa). When both products were dialyzed against pH 10 buffer for 48h, the peak at 2.80 ppm disappeared, meaning that the ionic interaction between propargylamine and bemiparin was broken (Figure 44B).

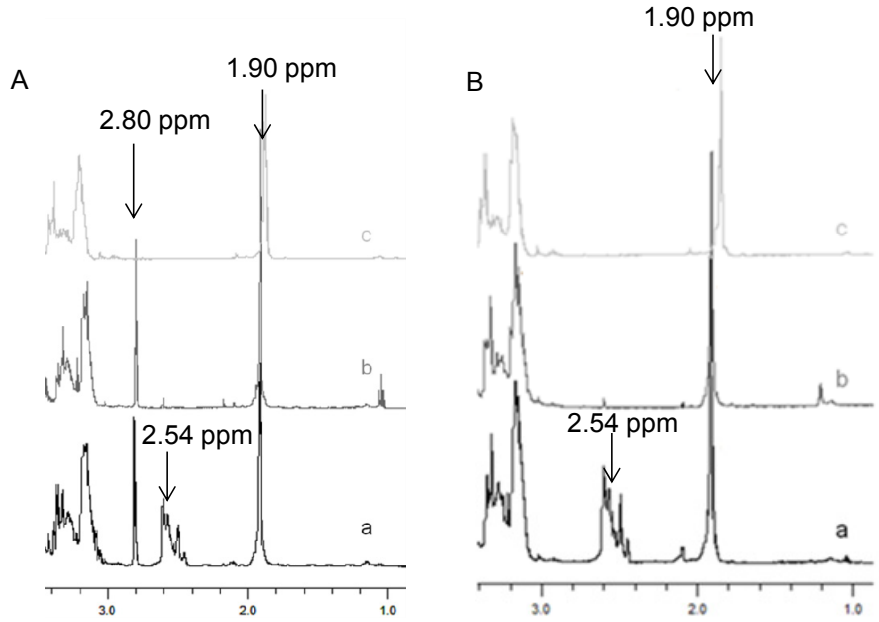

Figure 44. A) ^{1}H NMR spectra of bemiparin-alkyne funtionalizated using DMTMM (a), EDC and NHS (b) and bemiparin without any modification (c), in D_2O. B) ^{1}H NMR spectra of the same products after dialyzation against water at pH 10 for 48h.%Alkynyl functionalization was 55%, determined taking into account that acetamide sign belongs to bemiparin at 1.9 ppm.

According to the chemical structure of bemiparin, and applying the equations I to V, for each sequence of 10 disaccharide repeating units, there are on average 7 sulphate residues, 2 acetamide groups and 1 free amine function[131]. This allows for the determination of the propargyl functionalization degree by comparing the integrated intensities of the characteristic resonance signal of the acetamide group ($NHCOCH_3$, 1.90 ppm) and the signal of the alkyne group at 2.54 ppm of propargylamine Equation V and Equation VI), resulting in an alkyne functionalization degree $\%d_{alkyne}$ = 55 mol-% (Figure 45).

$$Nº\ alkyne\ groups = \frac{Nº\ N_{Ac\ groups}\ x\ A_{alkyne}}{A_{NAc}} \qquad \textbf{Equation V}$$

$$\%d_{alkyne} = \frac{Nº\ alkyne\ groups}{Nº\ carboxylic\ groups}\ x\ 100 \qquad \textbf{Equation VI}$$

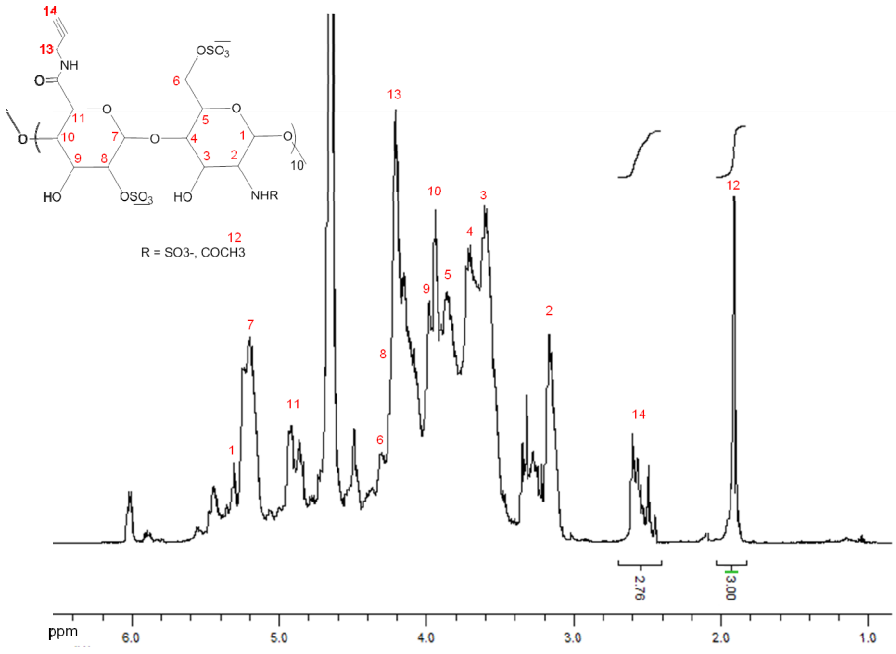

Figure 45. ^{1}H-NMR spectra of bemiparin-alkyne functionalized using DMTMM after dialysis for 48h against water.

The HBMC spectrum (Figure 46) of the alkyne-functionalized bemiparin prepared using DMTMM confirmed the presence of propargylamine covalently attached to bemiparin molecule. The appearance of a signal at 2.54 ppm, which can be assigned to an alkyne proton, can be correlated with the signals at 79.2 and 28.3 ppm belonging to methine and methylene carbons of propargylamine respectively. Furthermore, the signals from methylene protons of propargylamine signal at 3.93 ppm were correlated with the signals at 71.4, 79.2 and 164 ppm attributable to the methylene and methine carbons of propargylamine and the carboxylic carbon of bemiparin, respectively. This last correlation indicated that amidation had occurred. However, when EDC and NHS were used to prepare the alkyne-functionalized bemiparin, no correlation between the methylene protons of propargylamine and the carboxylic carbon of bemiparin was observed. The signal at 2.8 ppm disappeared from the ^{1}H NMR spectra of both products after dialysis against pH 10 buffer (pK_a of propargylamine = 9.8) for 48h, which also indicates that the signal at 2.8 ppm arises from the ionic attachment of propargylamine to bemiparin and, at a pH higher than 9.8 the amine of propargylamine is no longer protonated hence the ionic attachment disappeared.

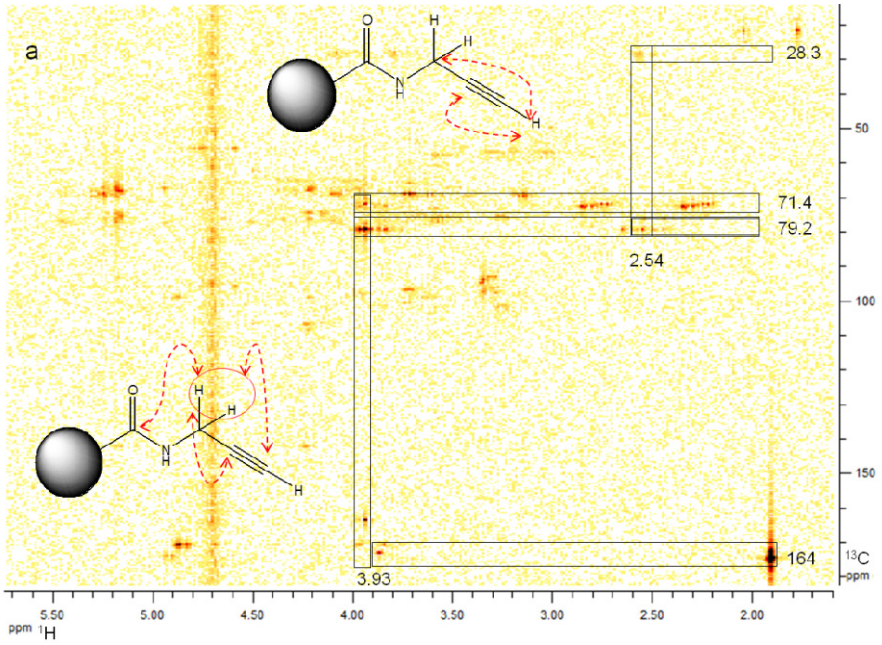

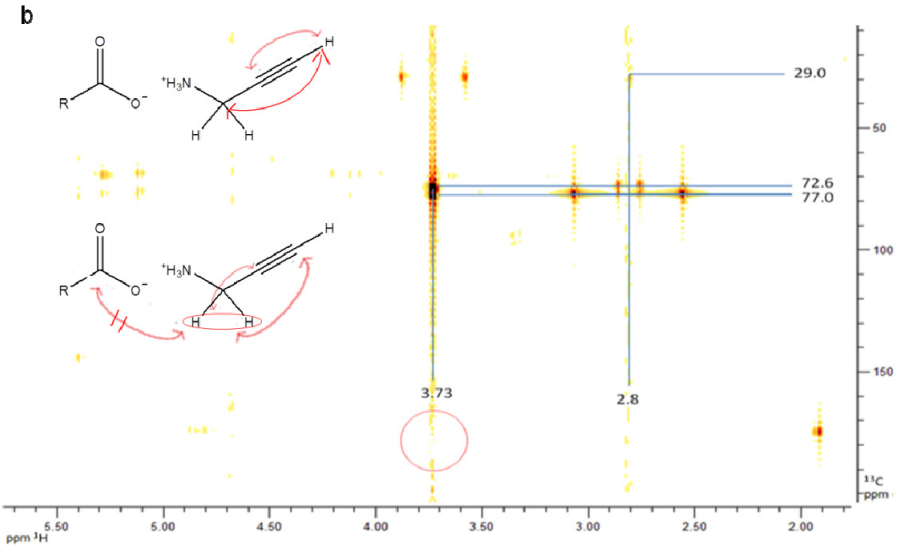

Figure 46. Two-dimensional ^{1}H-^{13}C correlation spectrum (HMBC) of bemiparin-alkyne functionalized using DMTMM (a) or EDC/NHS (b) in D_2O.

3.4.2 SEC characterization of bemiparin-alkyne

Molecular weight distributions of bemiparin and bemiparin-alkyne were obtained by SEC analysis to corroborate that no bemiparin degradation occured during the amidation reaction. Bemiparin-alkyne derivative slightly increased its molecular weight (Figure 47) due to the propargyl amine incorporation in its chemical structure, keeping the same polydispersity index as before being modified.

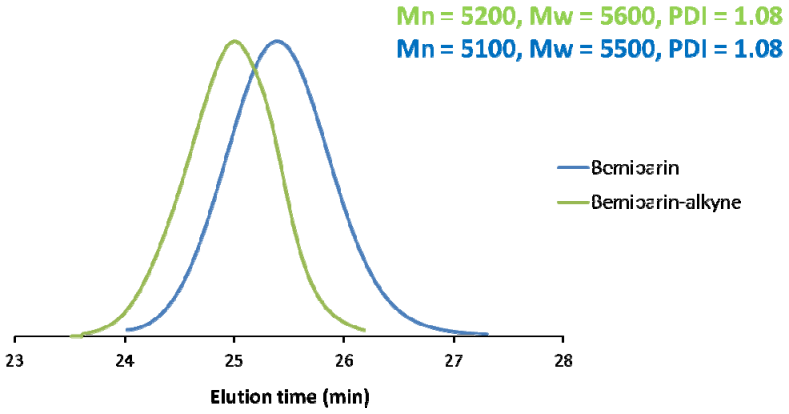

Figure 47. Molecular weight distribution of bemiparin and bemiparin-alkyne functionalized using DMTMM as activator.

3.4.3 Preparation of bemiparin-*g*-poly(meth)acrylate copolymers by click chemistry

The alkynyl-functionalized bemiparin was used for 'grafting to' reactions with N_3-end-functionalized polymers of PDMAEMA and P(MEO_2MA-*co*-$OEOMA_{300}$) by CuAAC. The reaction was carried out using an equimolar amount of azide polymer with respect to the alkynyl groups in homogeneous aqueous phase. The reaction was carried out at 25 °C for 24h, and the product was dialyzed against distilled water for 3 days and finally freeze-dried. ^{1}H-NMR and FTIR spectra of the isolated products were analyzed to corroborate the click reaction.

According to the FTIR spectrum, both the characteristic C=O stretching band of poly(methacrylates) at 1728 cm^{-1} and C=O stretching band of bemiparin at 1640 cm^{-1} are present. The complete disappearance of the N_3 stretching band at 2194 cm^{-1} for PDMAEMA and at 2204 cm^{-1} for P(MEO_2MA-*co*-$OEOMA_{300}$) and the alkynyl stretching band at 2165 cm^{-1} of the click product in the FTIR spectrum,

as well as the appearance of an ^{1}H-NMR resonance signal at 7.4 ppm (Figure 48 and Figure 49) assigned to the triazole ring proton, confirmed the formation of the bemiparin-*g*-PDMAEMA and bemiparin–*g*-P(MEO_2MA-*co*-$OEOMA_{300}$) copolymer by azide-alkyne cycloaddition.

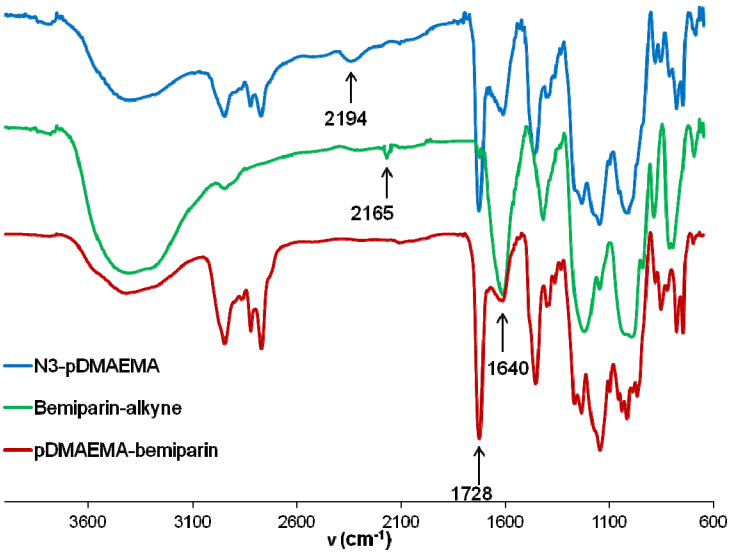

Figure 48. FTIR spectra of N_3-PDMAEMA (blue line), bemiparin-alkyne (green line) and click bioconjugate PDMAEMA-bemiparin (red line) .

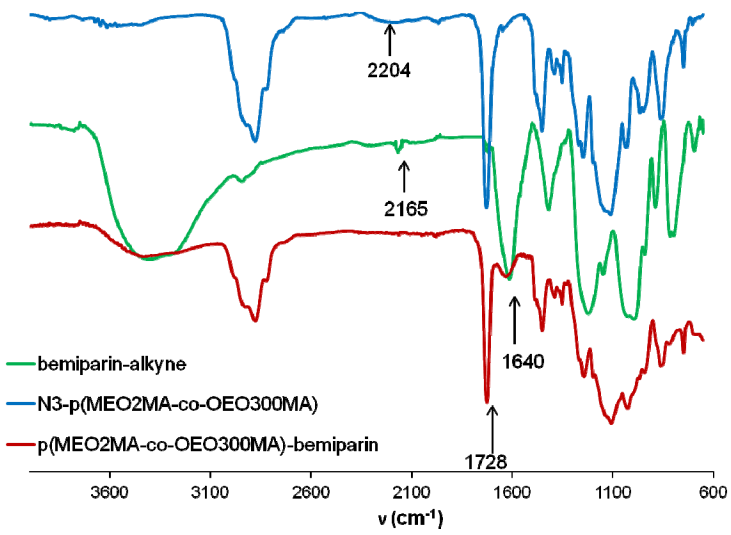

Figure 49. FTIR spectra of N_3-P(MEO_2MA-co-OEOMA$_{300}$) (blue line), bemiparin-alkyne (green line) and click bioconjugate P(MEO_2MA-coOEOMA$_{300}$)-bemiparin (red line) .

Figure 50 and Figure 51 show the ^{1}H-NMR spectra of both bioconjugates. Triazole peak was obtained in both cases, at 7.8 - 8.0 ppm for bemiparin-PDMAEMA and at 7.4 - 7.6 ppm for bemiparin-P(MEO_2MA-co-OEO_{300}MA).

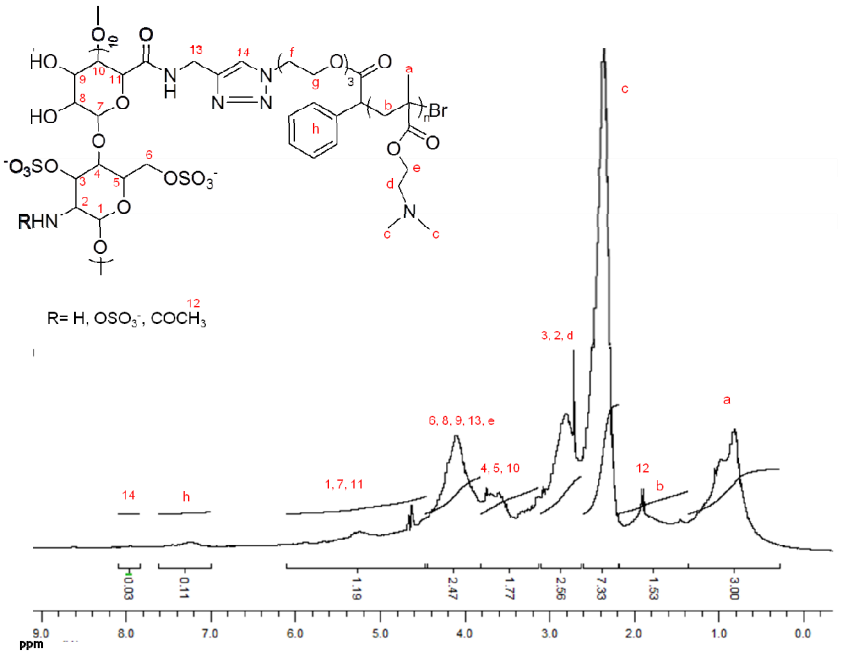

Figure 50. ^{1}H-NMR spectrum of PDMAEMA-bemiparin biocongujate in D_2O. Reaction yield was 97% for PDMAEMA-bemiparin biocongujate.

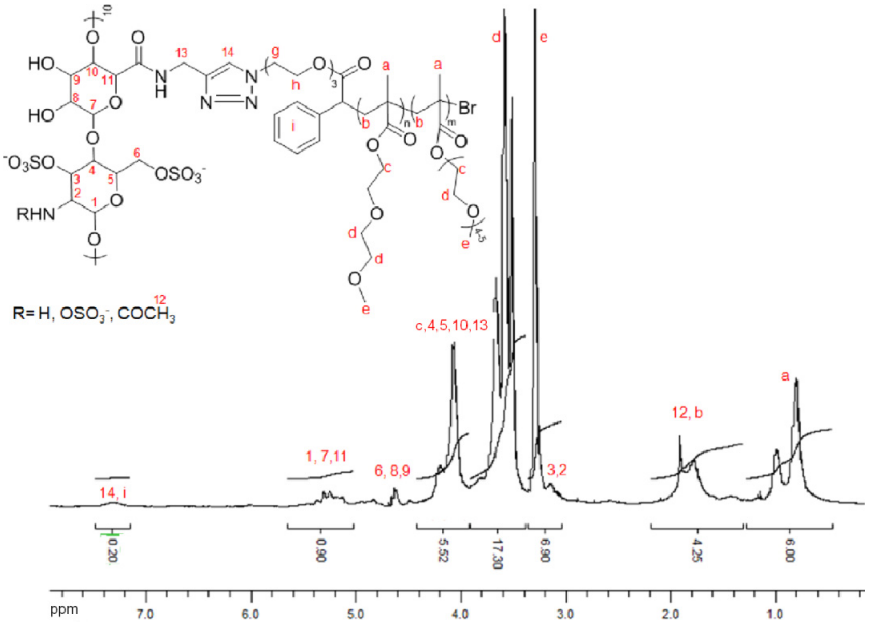

Figure 51. ^{1}H-NMR spectrum of P(MEO_2MA-*co*-$OEOMA_{300}$)-bemiparin biocongujate in D_2O. Reaction yield was 92% for P(MEO_2MA-*co*-$OEOMA_{300}$)-bemiparin biocongujate.

SEC characterization of diblock copolymers showed, monomodal traces and polydispersity index of less than 1.4. The bioconjugate prepared from bemiparin derivative and N_3-PDMAEMA showed a M_n = 11000 and a M_w = 15000 with a polydispersity of M_w/M_n = 1.36 (Figure 52). On the other hand, the click product of N_3-P(MEO_2MA-co-$OEO_{300}MA$) and bemiparin-alkyne showed a M_n = 10600 and a M_w = 14800 with a polydispersity of M_w/M_n = 1.39 (Figure 53). These values of molecular weight distributions were relative to poly(methyl methacrylates) standards used to calibrate the columns. An increase of the molecular weight was observed when bemiparin was incorporated into the polymer system, while maintaining the low polydispersity index.

In order to confirm that no polysaccharide degradation was produced in the click reaction conditions, the polysaccharide recovered from the solvent extracts was analyzed by SEC, showed a M_n = 5180 Da and a PDI = 1.09, practically the same as the unprocessed bemiparin-polymer conjugated, confirming that no polysaccharide degradation occured under the adopted click reaction conditions.

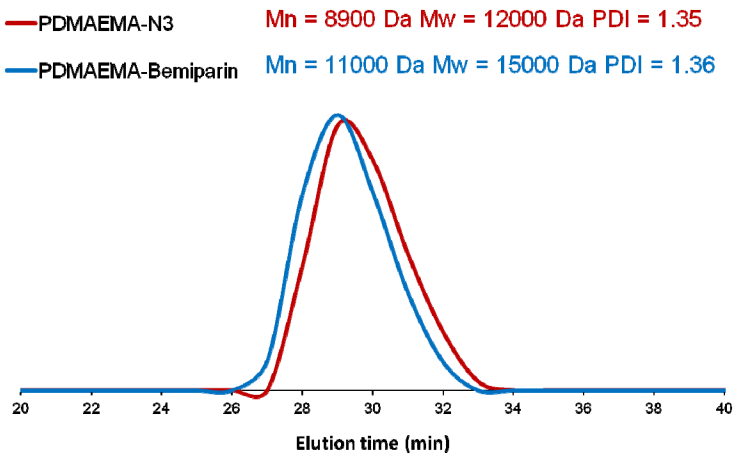

Figure 52. GPC trace of N_3-PDMAEMA (red curve) and the corresponding click bioconjugates pDMAEMA-bemiparin (blue curve) synthesized by a combination of AGET ATRP and click chemistry.

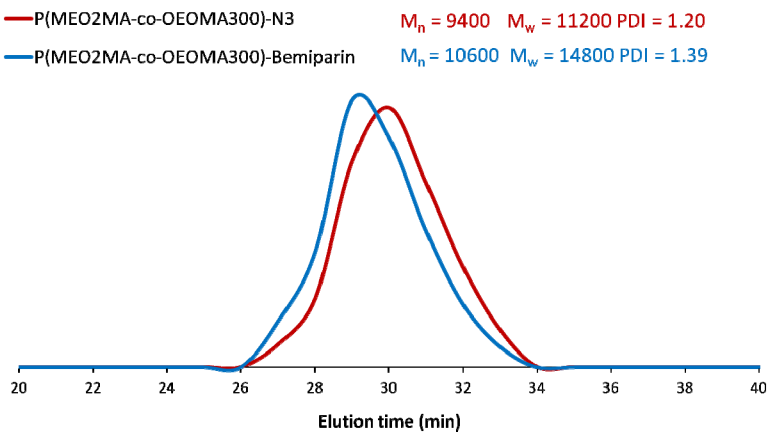

Figure 53. GPC trace of N_3-P(MEO_2MA-co-$OEOMA_{300}$) (red curve) and the corresponding click bioconjugated P(MEO_2MA-co-$OEOMA_{300}$)-bemiparin (blue curve) synthesized by a combination of AGET ATRP and click chemistry.

The weight loss curve recorded from the TGA analysis of the bemiparin graft copolymer systems showed two well-resolved degradation steps, thus allowing fot the quantitative evaluation of its composition, taking into account the total weight loss percentage and the residue left after thermal degradation. From TGA curves, the percentage of bemiparin-alkyne and N_3-end polymers were determined, considering the residue. The final molar composition was calculated taking into account the fractional weight percentages and the molecular weight (M_w) of the products (Table 4). The amount of bemiparin in the bioconjugates was found to be 23 wt% in the conjugation with PDMAEMA homopolymer (Figure 54) and 26 wt% in the P(MEO_2MA-*co*-$OEOMA_{300}$) bioconjugate (Figure 55), giving a molar composition of 1:1 for bemiparin-PDMAEMA system and 1:1 for bemiparin-P(MEO_2MA-*co*-$OEOMA_{300}$).

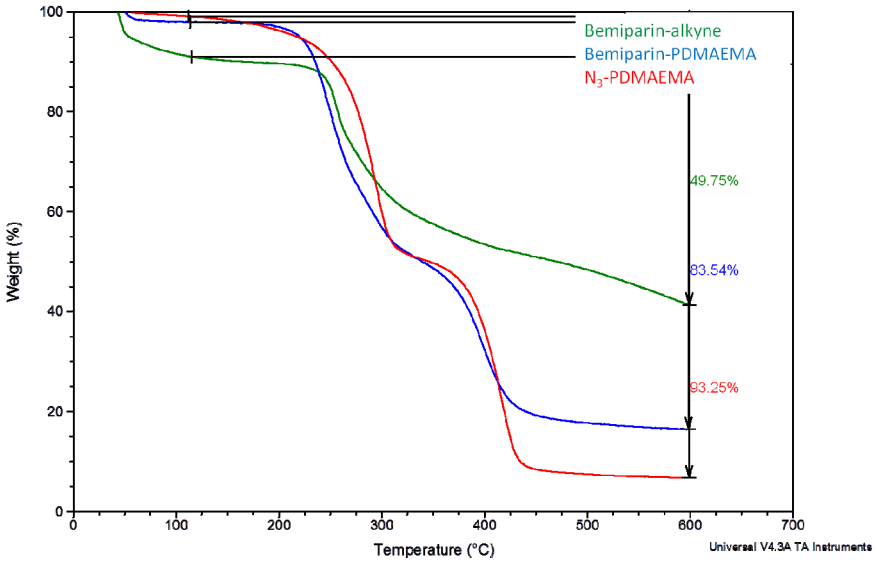

Figure 54. TGA degradation curves of bemiparin-alkyne (green curve), N_3-PDMAEMA (red curve) and click bioconjugate bemiparin-PDMAEMA (blue curve).

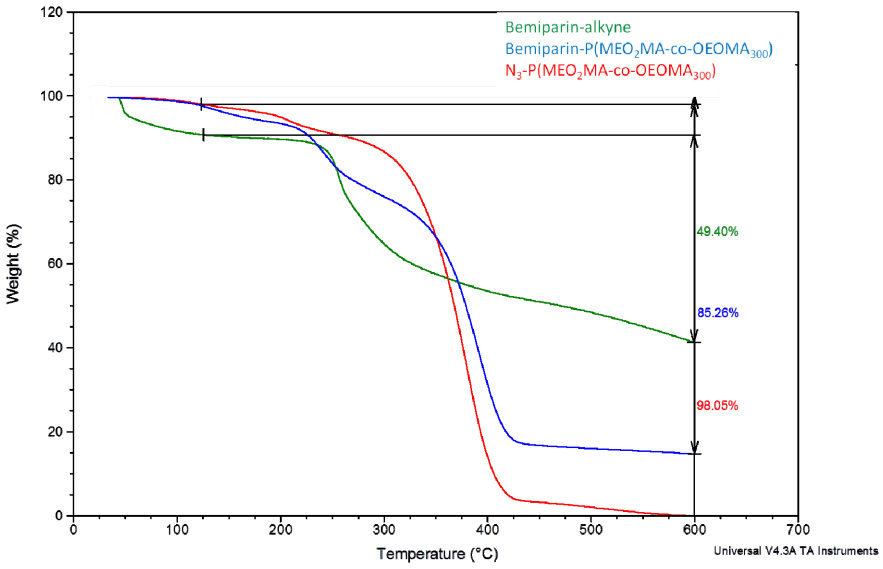

Figure 55. TGA degradation curves of bemiparin-alkyne (green curve), N_3-P(MEO_2MA-co-$OEOMA_{300}$) (red curve) and click bioconjugate bemiparin-PDMAEMA (blue curve).

Table 4. Residue weight percentages and percentages into the bioconjugate system of bemiparin and azide-polymer obtained from thermogravimetric curves.

	%wt bemiparin residue*	%wt polymer residue*	%wt bioconjugate residue*	%wt bemiparin bioconjugate **	%wt polymer bioconjugate **	Molar ratio (bemiparin:polymer) ***
N_3-PDMAEMA	50.56	6.76	16.48	23	77	1:1
N_3-P(MEO_2MA-co-$OEOMA_{300}$)	50.56	1.94	14.74	26	74	1:1

*Residue = 100 -% mass degradation (TGA curve).

**%wt bemiparin and%wt polymer in the bioconjugate were calculated using the following equation systems: 50.56x + 6.76y = 16.48 for PDMAEMA system and 50.56x + 1.94y = 14.74 for P(MEO_2MA-co-$OEOMA_{300}$) system.

***Molar ratio: ($M_{w\ bioconjugate}$ x$\%wt_{compound}$) / (100 x $M_{w\ compound}$).

3.4.4 Thermal Properties

The LCST of polymers in water solutions can be modulated by incorporating hydrophilic or hydrophobic moieties. Incorporation of the hydrophilic macromolecule (bemiparin) in the polymer structure has a significant effect on the temperature-sensitive phase transition behavior. In acidic media, PDMAEMA-N_3 polymer system is fully ionized and increasing the temperature has not significant effect on the swelling ratio (as it was described in chapter 2). At pH 7.4, increasing the temperature caused a gradual decrease in the swelling ratio of the polymer system and above 43 °C the system precipitated. Increase in the pH (pH 10) decreases the degree of ionization of the amino groups in the polymer chain, leading to an increase in the hydrophobicity of the system, which in turn decreases the phase transition temperature (LCST) from 43 °C to 35 °C. At a constant pH, the grafted bemiparin increases the hydrophilicity of the system,

resulting in a corresponding increase in the LCST from 35 °C to 44 °C at pH 10, and from 43 °C to 65 °C at pH 7.4 (Figure 56).

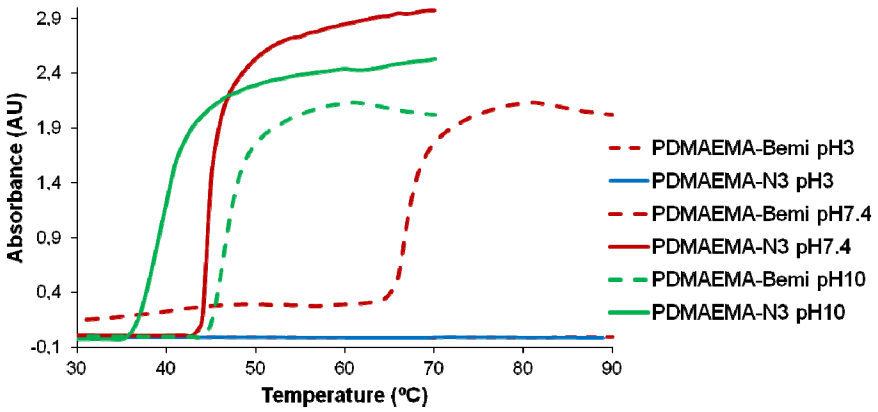

Figure 56. LCST of N_3-PDMAEMA and PDMAEMA-Bemiparin at different pH (3, 7.4 and 10) obtained by UV-visible spectroscopy at 450 nm (temperature sweep at 1 °C/min).

LCST did not change as a function of pH for P(MEO_2MA-co-$OEOMA_{300}$) due to the absence of acidic or basic groups (see chapter 2). The grafting of bemiparin increases the hydrophilicity of the system, which in turn increases the phase transition temperature from 32 °C to 41 °C at pH 7.4 and from 33 °C to 40 °C at pH 10 (Figure 57).

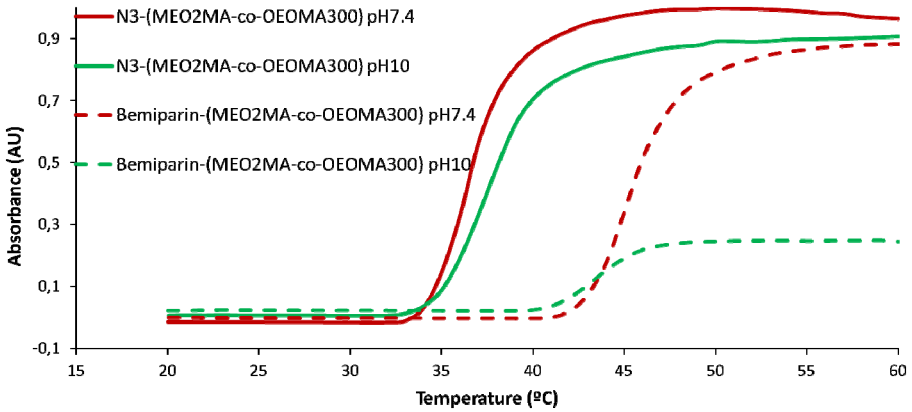

Figure 57. LCST of N_3-P(MEO_2MA-co-$OEOMA_{300}$) and P(MEO_2MA-co-$OEOMA_{300}$)-Bemiparin at different pH (7.4 and 10) obtained by UV-visible spectroscopy at 450 nm (temperature sweep at 1 °C/min).

3.5 CONCLUSIONS

Alkyne functionalized bemiparin was prepared by the amidation of carboxylic acid groups on the polysaccharide mediated with DMTMM. pH and temperature sensitive azido-containing polymers prepared by AGET-ATRP (described in chapter 2), were used to get well-defined hybrid polysaccharide structures prepared by 'grafting to' experiments using Cu(I) catalyzed azide-alkyne [3+2]-dipolar cycloaddition (Click) reactions, resulting in the formation of bemiparin bioconjugates with advanced functional properties. The coupling reactions proved to be quantitative, on the basis of size exclusion chromatography and NMR and FTIR spectroscopy analysis, yielding pure diblock copolymers composed of bemiparin and methacrylic polymers. The bioconjugates were both temperature and pH-sensitive water-soluble and polymeric building blocks. This simple reaction leads to the formation of hybrid double hydrophilic block copolymers that combine biocompatibility, water solubility and both pH and temperature sensitivity. The thermal properties of the bioconjugates were

studied in aqueous solution by UV-vis spectroscopy. The LCST values were directly related to the composition of the prepared bioconjugate systems.

3.6 REFERENCES

111. Zhang, X.-Q.; Xu, X.; Bertrand, N.; Pridgen, E.; Swami, A.; Farokhzad, O. C., Interactions of nanomaterials and biological systems: Implications to personalized nanomedicine. *Advanced Drug Delivery Reviews* **2012,** *64* (13), 1363-1384.

112. (a) Palmer, T. D.; Ashby, W. J.; Lewis, J. D.; Zijlstra, A., Targeting tumor cell motility to prevent metastasis. *Advanced Drug Delivery Reviews* **2011,** *63* (8), 568-581; (b) Dash, M.; Chiellini, F.; Ottenbrite, R. M.; Chiellini, E., Chitosan-A versatile semi-synthetic polymer in biomedical applications. *Progress in Polymer Science* **2011,** *36* (8), 981-1014; (c) Shapiro, Y. E., Structure and dynamics of hydrogels and organogels: An NMR spectroscopy approach. *Progress in Polymer Science* **2011,** *36* (9), 1184-1253; (d) Xu, F. J.; Yang, W. T., Polymer vectors via controlled/living radical polymerization for gene delivery. *Progress in Polymer Science* **2011,** *36* (9), 1099-1131; (e) Gomes, S.; Leonor, I. B.; Mano, J. F.; Reis, R. L.; Kaplan, D. L., Natural and genetically engineered proteins for tissue engineering. *Progress in Polymer Science* **2012,** *37* (1), 1-17; (f) Tian, H.; Tang, Z.; Zhuang, X.; Chen, X.; Jing, X., Biodegradable synthetic polymers: Preparation, functionalization and biomedical application. *Progress in Polymer Science* **2012,** *37* (2), 237-280; (g) Zhang, J.; Li, X.; Li, X., Stimuli-triggered structural engineering of synthetic and biological polymeric assemblies. *Progress in Polymer Science* **2012,** *37* (8), 1130-1176.

113. Siegwart, D. J.; Oh, J. K.; Matyjaszewski, K., ATRP in the design of functional materials for biomedical applications. *Progress in Polymer Science* **2012,** *37* (1), 18-37.

114. (a) Qin, A.; Lam, J. W. Y.; Tang, B. Z., Click Polymerization: Progresses, Challenges, and Opportunities. *Macromolecules* **2010,** *43* (21), 8693-8702; (b) Tsarevsky, N. V.; Bencherif, S. A.; Matyjaszewski, K., Graft Copolymers by a Combination of ATRP and Two Different Consecutive Click Reactions. *Macromolecules (Washington, DC, United States)* **2007,** *40* (13), 4439-4445; (c) Tsarevsky, N. V.; Sumerlin, B. S.; Matyjaszewski, K., Step-Growth \"Click\" Coupling of Telechelic Polymers Prepared by Atom Transfer Radical Polymerization. *Macromolecules* **2005,** *38* (9), 3558-3561; (d) Tsarevsky, N. V.; Bernaerts, K. V.; Dufour, B.; Du Prez, F. E.; Matyjaszewski, K., Well-Defined (Co)polymers with 5-Vinyltetrazole Units via Combination of Atom Transfer Radical (Co)polymerization of Acrylonitrile and \"Click Chemistry\"-Type Postpolymerization Modification. *Macromolecules* **2004,** *37* (25), 9308-9313.

115. Hasegawa, T.; Umeda, M.; Numata, M.; Li, C.; Bae, A.-H.; Fujisawa, T.; Haraguchi, S.; Sakurai, K.; Shinkai, S., 'Click chemistry' on polysaccharides: a convenient, general, and monitorable approach to develop (1-3)-β-d-glucans with various functional appendages. *Carbohydrate Research* **2006,** *341* (1), 35-40.

116. Elchinger, P.-H.; Faugeras, P.-A.; Boëns, B.; Brouillette, F.; Montplaisir, D.; Zerrouki, R.; Lucas, R., Polysaccharides: The “Click” Chemistry Impact. *Polymers* **2011,** *3* (4), 1607-1651.

117. (a) Binder, W. H.; Sachsenhofer, R., ‘Click’ Chemistry in Polymer and Material Science: An Update. *Macromolecular Rapid Communications* **2008,** *29* (12-13), 952-981; (b) Golas, P. L.; Tsarevsky, N. V.; Matyjaszewski, K., Structure-reactivity correlation in \"click\" chemistry: substituent effect on azide reactivity. *Macromolecular Rapid Communications* **2008,** *29* (12-13), 1167-1171; (c) Golas, P. L.; Matyjaszewski, K., Marrying click chemistry with polymerization: expanding the scope of polymeric materials. *Chemical Society Reviews* **2010,** *39* (4), 1338-1354.

118. (a) Angelo, N. G.; Arora, P. S., Nonpeptidic Foldamers from Amino Acids: Synthesis and Characterization of 1,3-Substituted Triazole Oligomers. *Journal of the American Chemical Society* **2005,** *127* (49), 17134-17135; (b) Tron, G. C.; Pirali, T.; Billington, R. A.; Canonico, P. L.; Sorba, G.; Genazzani, A. A., Click chemistry reactions in medicinal chemistry: Applications of the 1,3-dipolar cycloaddition between azides and alkynes. *Medicinal Research Reviews* **2008,** *28* (2), 278-308.

119. (a) Averick, S.; Paredes, E.; Li, W.; Matyjaszewski, K.; Das Subha, R., Direct DNA conjugation to star polymers for controlled reversible assemblies. *Bioconjugate chemistry* **2011,** *22* (10), 2030-7;

(b) Golas, P. L.; Matyjaszewski, K., Click chemistry and ATRP: a beneficial union for the preparation of functional materials. *QSAR & Combinatorial Science* **2007,** *26* (11-12), 1116-1134.
120. van Dijk, M.; Rijkers, D. T. S.; Liskamp, R. M. J.; van Nostrum, C. F.; Hennink, W. E., Synthesis and Applications of Biomedical and Pharmaceutical Polymers via Click Chemistry Methodologies. *Bioconjugate Chemistry* **2009,** *20* (11), 2001-2016.
121. Canalle, L. A.; Lowik, D. W. P. M.; van Hest, J. C. M., Polypeptide-polymer bioconjugates. *Chemical Society Reviews* **2010,** *39* (1), 329-353.
122. Ponedel'kina, I.; Odinokov, V.; Lukina, E.; Tyumkina, T.; Khalilov, L.; Dzhemilev, U., Chemical modification of heparin. *Russian Journal of Bioorganic Chemistry* **2006,** *32* (5), 472-477.
123. Pelet, J. M.; Putnam, D., An In-Depth Analysis of Polymer-Analogous Conjugation using DMTMM. *Bioconjugate Chemistry* **2011,** *22* (3), 329-337.
124. Maza, S.; Macchione, G.; Ojeda, R.; Lopez-Prados, J.; Angulo, J.; de Paz, J. L.; Nieto, P. M., Synthesis of amine-functionalized heparin oligosaccharides for the investigation of carbohydrate-protein interactions in microtiter plates. *Organic & Biomolecular Chemistry* **2012,** *10* (10), 2146-2163.
125. Schanté, C. E.; Zuber, G.; Herlin, C.; Vandamme, T. F., Chemical modifications of hyaluronic acid for the synthesis of derivatives for a broad range of biomedical applications. *Carbohydrate Polymers* **2011,** *85* (3), 469-489.
126. Li, A.-F.; Wang, J.-H.; Wang, F.; Jiang, Y.-B., Anion complexation and sensing using modified urea and thiourea-based receptors. *Chemical Society Reviews 39* (10), 3729-3745.
127. Goodall, K. T.; Chooi, C. C.; Gallus, A. S., Heparin stability: effects of diluent, heparin activity, container, and pH. *Journal of Clinical Pathology* **1980,** *33* (12), 1206-1211.
128. El-Faham, A.; Albericio, F., Novel Proton Acceptor Immonium-Type Coupling Reagents:â€‰ Application in Solution and Solid-Phase Peptide Synthesis. *Organic Letters* **2007,** *9* (22), 4475-4477.
129. (a) Kunishima, M.; Kawachi, C.; Hioki, K.; Terao, K.; Tani, S., ChemInform Abstract: Formation of Carboxamides by Direct Condensation of Carboxylic Acids and Amines in Alcohols Using a New Alcohol- and Water-Soluble Condensing Agent: DMT-MM. *ChemInform* **2001,** *32* (27), no-no; (b) Kunishima, M.; Kawachi, C.; Monta, J.; Terao, K.; Iwasaki, F.; Tani, S., 4-(4,6-dimethoxy-1,3,5-triazin-2-yl)-4-methyl-morpholinium chloride: an efficient condensing agent leading to the formation of amides and esters. *Tetrahedron* **1999,** *55* (46), 13159-13170.
130. Pelet, J. M.; Putnam, D., An In-Depth Analysis of Polymer-Analogous Conjugation using DMTMM. *Bioconjugate Chemistry 22* (3), 329-337.
131. Guerrini, M.; Bisio, A.; Torri, G., Combined Quantitative 1H and 13C Nuclear Magnetic Resonance Spectroscopy for Characterization of Heparin Preparations. *Semin Thromb Hemost* **2001,** *27* (05), 473-482.

Bemiparin loaded nanoparticle systems: preparation, characterization, properties and cell activity

CHAPTER 4

4.1 INTRODUCTION

Polymeric nanoscale drug delivery systems are attractive for the therapeutic delivery of drugs to target tissues.[134] Bemiparin, as previously described, is an ultra-LMWH with an average molecular weight of 3600 g/mol, that act in several biological functioning as an anticoagulant, and an interesting regulation role of growth factors activity, including fibroblast growth factors (FGFs) and vascular endothelial growth factors (VEGFs)[135]. Its pharmacological activity has been demonstrated in the treatment of many diseases such as asthma, allergic rhinitis, inflammatory bowel disease, vascular disorders[136,137,138] and it has recently been shown to exhibit antiangiogenic properties[139].

Nanoparticle drug delivery systems NP are nano carriers used to deliver drugs, including nanospheres, nanocapsules and nanoliposomes[140]. Compared with other forms of drug carriers, nanoparticle drug delivery systems have unique advantages: they can pass through the smallest capillary vessels because of their ultra-tiny volume and avoid rapid clearance by phagocytes so that their duration in blood stream is greatly prolonged, they can penetrate cells and tissue gap to arrive at target organs such as liver, spleen, lung, spinal cord, and lymph. In addition, they can also show controlled-release properties due to the biodegradability, pH and/or temperature sensibility of nanoparticle materials. Besides, they can improve the utility of drugs and reduce toxic side effects. Therefore, the incorporation of bemiparin in nanoparticulated systems is an attractive solution to improve its short half-life and improve its stability in biological media. Moreover, nanoparticles can be endocyted by cells[141]. NP allow bemiparin protection from degradation while the drug can be slowly released from the particles in an unaltered state[21]. Ubrich and co-workers showed previously that LMWH can be encapsulated into a range of NP based on either biodegradable poly-ε-caprolactone (PCL) and PLGA, or positively charged nonbiodegradable polymethacrylates, Eudragit® RS and RL microparticles[142]. A sequential w/o and o/w emulsifying technique was employed to generate these LMWH loaded microparticles either using the polymer alone or a blend of polymers

[142b]. The highest encapsulation efficiencies obtained in both studies were 39-47%. The LMWH release was limited to 20-30% when Eudragit® RS PO either alone or in combination with PCL or PLGA was used, possibly due to the strong ionic interactions between the drug and the polycationic polymer. These particles were then used for oral administration of LMWH-loaded NPs in rabbits. Each formulation increased the anti–factor X_a activity[142a]. These particles displayed high bioavailability of LMWH in vivo, probably by overcoming the slow absorption of the negatively charged LMWH[143].

The synthesis and characterization of bemiparin loaded NP is described in this chapter using commercial and synthetic polymers with very different chemical structure and properties. These polymers are detailed in Table 5.

Table 5. Polymer systems and their properties, used to prepare bemiparin loaded nanoparticles in this chapter.

Name	Ionic/non-ionic	Properties	Synthetic method
RESOMER RG 504H (PLGA)	Non-ionic	Equimolecular monomer composition, M_w = 40000 Da	Multiple emulsion
Chitosan	Cationic	pK_a = 6.5, DD= 83%, M_w = 150000-400000 Da	Polylectrolyte complexation
EUDRAGIT RS PO (poly(EA-co-MMA-co-MAETMA) (1:2:0.1)	Cationic	Random copolymer, M_w = 150000 Da	Multiple emulsion
Synthetic block copolymers RAFT (PMMA-*b*-PMAETMA)	Cationic	Well defined block copolymers	Multiple emulsion

A semisynthetic cantionic polymer, chitosan, and two commercial random copolymers, a biodegradable and non-charged polymer, poly(lactic-co-glycolic acid) (PLGA, RESOMER RG 504 H)[144] and a non-biodegradable and polycationic polymer, (Eudragit RS PO)[6], were applied to prepare nanoparticle loaded with bemiparin for the same purpose. Moreover, synthetic amphiphilic methacrylic block copolymers of well-defined microstructure, passively charged and low polydispersity, prepared by

Reversible Addition-Fragmentation chain-Transfer (RAFT) polymerization (described in chapter two), were also used in the preparation of bemiparin loaded NPs.

RESOMER RG 504 H is a biocompatible, neutral and biodegradable random copolymer of lactic and glycolic acids (PLGA) with equimolecular monomer composition obtained by ring-opening polymerization(Figure 58). It is a common choice in the formulation of nanoparticles due to its biological and biochemical properties[145,14,20a].

This is in contrast to Eudragit® RS PO, a non-biodegradable random polycationic synthetic polymer, widely used in the formulation of drug delivery systems and more specifically in nanoparticle formulations due to its mucoadhesive characteristics [15,16]. It is based on poly(ethyl acrylate-*co*-methyl methacrylate-*co*-trimethyl aminoethyl methacrylate) poly(EA-*co*-MMA-*co*-MAETMA) (1:2:0.1) and is insoluble at acidic and physiological pH, but swells at basic pH[146].

Block copolymers synthesized by RAFT (PMMA-*b*-PMAEMTA) were also used for the nanoencapsulation of bemiparin. The chemical structure of these systems was inspired by the structure of Eudragit® RS PO, based on methyl methacrylate (MMA) ethyl acrylate (EA) and trimethyl aminoethyl methacrylate (MAETMA), but with well defined microstructure and morphology.

Chitosan is a weak cationic polysaccharide composed essentially of β(1-4) linked glucosamine units together with some proportion of *N*-acetyl-glucosamine units (Figure 58). It is obtained by the extensive deacetylation of chitin, a polysaccharide commonly found in nature. Under mild acidic conditions, chitosan is positively charged, and therefore it is possible to form interpolyelectrolyte complexes with polyanionic drugs such as bemiparin, forming a stable polyelectrolyte complex, which allows for the sustained bemiparin release with time and enhanced bemiparin biological availability[147].

4.2 AIMS OF THIS CHAPTER

In this chapter, PLGA, Eudragit RS PO, Chitosan and PMMA-*b*-PMAEMTA polymer systems were used to prepare bioactive bemiparin loaded nanoparticle systems, which maintain biological bemiparin activity thus increasing the stability of this drug and attaining a controlled rate of release. Bemiparin release was studied in all of the polymeric NP systems, showing different behavior depending of the chemical structure of the polymer used to prepare the nanoparticles. For example, bemiparin-loaded PLGA NPs did not show any significant ionic interaction between this drug and the polymer, due to the absence of ionic functional groups in its structure, as a result the release of bemiparin was due to the bemiparin diffusion through PLGA chains. Eudragit RS PO and methacrylate block copolymer systems prepared by RAFT polymerization (PMMA-*b*-PMAETMA) presented quaternary ammonium groups in their structure, and therefore, ionic interactions (non pH dependent) between sulfonic and carboxylate groups of bemiparin and amino groups of those polymers determine the bemiparin release in these systems. Chitosan-bemiparin NPs are pH-dependent polymeric complexes due to the cationic nature of the chitosan amino group (pK_a = 6.5), which makes this polymer partially positively charged at pH< 6.5. Therefore, bemiparin in this NP system showed a pH-dependent release.

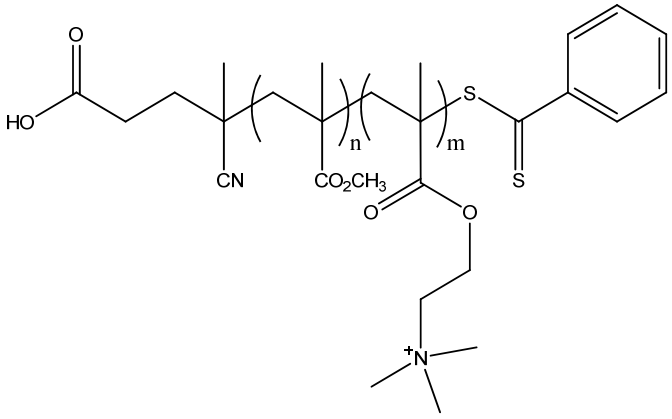

$PMMA_n$-*b*-$PMAETMA_m$

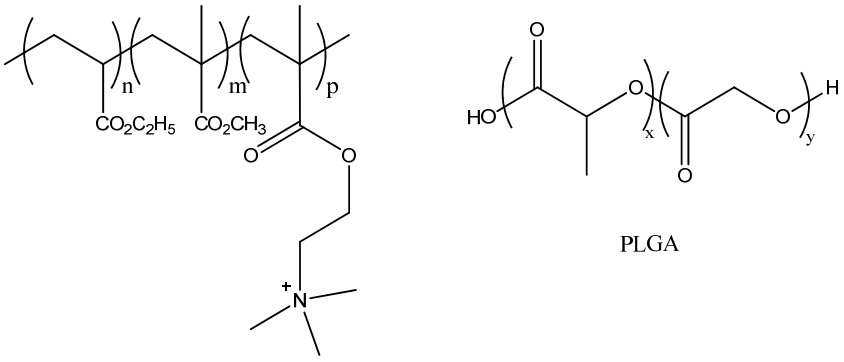

EUDRAGIT RS PO

PLGA

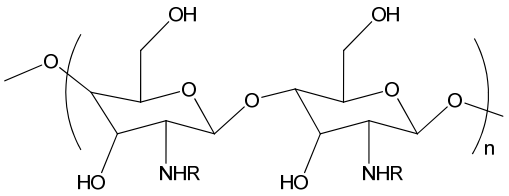

R= H or $COCH_3$

CHITOSAN

Figure 58. Chemical structures of the copolymer systems used for bemiparin encapsulation.

NPs were obtained by the multiple emulsion technique in the case of PLGA, Eudragit and the synthetic block copolymers NPs and the formation of polyelectrolyte complexes in the case of chitosan-based NPs.

The biological activity and the stability of the prepared bemiparin loaded nanoparticles, prepared either by the multiple emulsion technique or polyelectrolyte complexion, were analyzed. Heparin was shown to stabilize and protect growth factors, including different isoforms of fibroblast growth factor (FGF) and vascular endothelial growth factor (VEGF)[148], from degradation and at the same time increase the affinity of the complex to cell receptors[135a, 135c, d, 149]. In this work, the biological activity of bemiparin nanoparticles was evaluated using BaF32 cells expressing the FGF receptor 1, which interacts with FGF2. This *in vitro* model provides information about the bemiparin capacity to form the ternary system (bemiparin-FGF-FGFR-1c) that triggers proliferation in these cells[150,151].

4.3 Materials and methods

4.3.1 Materials

The Low Molecular Weight Heparin (LMWH) used was bemiparin (111,3 UI/mg, 5500 Da) and was kindly donated by ROVI PHARMACEUTICALS LABORATORIES (Madrid, Spain). Eudragit® RS PO (mean M_w 150000 Da) was purchased from Degussa (European Pharmacopoeia). PLGA 50:50 molar ratio (mean M_w 40000 Da) (RESOMER RG 504 H) was supplied by Boehringer Ingelheim Pharma GmbH & Co. Polyvinylalcohol used as surfactant (PVA, M_w 31000-50000 Da, 87-89% hydrolyzed) was purchased from Sigma. Chitosan chloride salt (M_w 150000-400000 g/mol, 83% deacetylation degree (DD)) was purchased from Novamatrix. Methyl methacrylate (MMA) (Acros Organics) and 2-(methacryloyloxy)ethyl]trimethylammonium (80% aqueous solution) (MAETMA) (Sigma-Aldrich) were purified by passing the monomer over a column with basic aluminium oxide. 2,2'-Azobisisobutyronitrile (AIBN, Merck) was recrystallized from methanol. 4, 4'-Azobis (4-cyanovaleric acid) (V501) (Sigma-Aldrich), ethyl acetate

(Sigma-Aldrich, >99.5%), acetic acid (Sigma-Aldrich, > 99.8%), dimethyl disulfoxide (SCHARLAB, >98%) and HEPES minimum (Sigma-Aldrich, 99.5% titration) were used as received.

4.3.2 *Cell culture reagents*

Recombinant human fibroblast growth factor-2 (FGF-2) (Invitrogen) was used without further purifications. Dye CellTiter 96® Aqueous One Solution Reagent ([3-(4,5-dimethylthiazol-2-yl)-5-(3-carboxymethoxyphenyl)-2-(4-sulfophenyl)-2H-tetrazolium, inner salt (MTS)) (Promega) was also used as received. BaF32 cells are an IL-3-dependent and Heparan sulphate proteoglycan deficient myeloid B cell line that has been stably transfected with FGF receptor 1c (FGFR-1c). BaF32 cells represent a model system developed to identify HP/Heparan sulphate structures that interact with FGFs and their receptors to form active ternary complexes [150-151]. RPMI 1640 powder culture medium (Sigma-Aldrich) was supplemented with 2 g/L sodium bicarbonate (Sigma-Aldrich, 99-100% purity, suitable for cell culture), 10% (v/v) fetal bovine serum (FBS) (Gibco®), a 1% (v/v) penicillin/streptomycin mixture (Gibco®), and the conditioned medium was stored at -20 °C until it was required.

4.3.3 Methods

4.3.3.1 Nanoparticle preparation

4.3.3.1.1 Nanoparticle preparation by Polyelectrolyte complex formation: chitosan-bemiparin NP

The nanoparticles were prepared by a complex coacervation method at room temperature. In brief, 1.5 mL of a 0.1% (w/v) chitosan solution in 1% (w/v) acetic acid (pH adjusted to 5) were added to an aqueous bemiparin solution (0.03% (w/v), 5 mL, pH 5) with constant stirring using an ultra-turrax homogeneizer (IKA T25) at 3400

rpm. The spontaneous formation of nanoparticles occurs upon incorporation, under gentle mechanical stirring at room temperature of the 1.5 mL chitosan solution. The nanoparticle dispersion solution was centrifugated at 12000 rpm for 1h at 20 °C. The supernatants were discarded and nanoparticles were re-suspended in 200 mL of purified water. Finally nanoparticles were isolated by freeze-drying, obtaining a white powder.

4.3.3.1.2 Nanoparticle preparation by Multiple emulsion method: PLGA or EUDRAGIT or PMMA-*b*-PMAETMA bemiparin-loaded NP.

The preparation of nanoparticles was carried out by the emulsion technique previously described [152] and modified as follows: 10 mL of the aqueous bemiparin solution (2% w/v) was first emulsified during the addition of 100 mL of each polymer solution in ethyl acetate (1% w/v). The resulting water-in-oil emulsion was subsequently mixed by sonication for 1 min with 2% PVA aqueous solution (400 mL), involving the inversion to an o/w emulsion. After evaporation of ethyl acetate under reduced pressure, the nanoparticles were isolated by centrifugation (12000 rpm for 20 min at 25 °C). After three cycles (washing with deionized water and then centrifugation) to remove the PVA, the supernatants from the previous centrifugation steps were pooled for free drug measurement and drug entrapment efficiency evaluation. After the final centrifugation, nanoparticles were resuspended in water as a colloidal suspension and freeze-dried.

4.3.4 Characterization techniques

4.3.4.1 Size distribution, zeta potential and morphology

The core-shell morphology of nanoparticles was analyzed by scanning electron microscopy (SEM) using a Philips XL 30 ESEM apparatus at an accelerating voltage of 15 keV. It is equipped with a field emission Hitachi SU800 apparatus. The samples were prepared by deposition of the corresponding nanoparticle suspension

(0.01 mg/mL) over small glass disks (14 mm diameter and 1 mm thickness), and the solvent (H_2O) was evaporated at room temperature during 24 h. All the samples were coated with chrome prior to examination by SEM. The evidence of bemiparin encapsulation and surface chemical characteristics were detected by Energy Dispersive X-ray analysis (EDAX). Zeta potential and particle size distribution were evaluated with a Zetasizer NanoZS (Malvern Instruments, UK) equipped with a He-Ne laser beam with wavelength of 633 nm and a scattering angle of 173°. The zeta potential measurements were performed in disposable folded capillary cells (DTS1060, Malvern Instruments) and particle-sized measurements were carried out in square polystyrene cuvettes (DTS0012, Malvern Instruments) with 0.01 mg/mL aqueous solutions at 25 °C.

The hydrodynamic diameter (D_h) of NPs and the polydispersity index were determined by dynamic light scattering (DLS). The intensity of light scattered was used to calculate the mean hydrodynamic diameter (Z-average mean), based on the Stokes–Einstein equation, assuming the particle to be spherical. The nanoparticle suspension (0.01 mg/mL) were prepared in 25 mM HEPES buffer. For each sample, the statistical average and standard deviation (SD) of data was calculated from at least five measurements.

Zeta potential analysis was carried out using laser doppler electrophoresis (LDE) with 20 runs per measurement. The zeta potentials were automatically calculated from the electrophoretic mobility, using Henry equation (Equation VII). When measurements are carried out in aqueous media, the Smoluchowski's approximation is generally applied, which assumes that Henry's function ($f(k_a)$) takes a value of 3/2[153].

$$\boldsymbol{U_E = 2 \bullet \varepsilon \bullet z \bullet \frac{f(k_a)}{3 \bullet \eta} \xrightarrow[f(ka)=3/2]{} z \approx U_E \bullet \frac{\eta}{\varepsilon}} \qquad \textbf{Equation VII}$$

Where U_E= electrophoretical mobility, z = zeta potential, ε =dielectric constant, η = viscosity, and f(ka) = Henry's function.

4.3.4.2 Thermogravimetrical analysis

Thermal stability of the particles was determined using a TGA Q500 (TA instruments) apparatus, in a temperature range of 30-600 °C, at a heating rate of 10 °C/min under a nitrogen atmosphere.

4.3.4.3 ATR-FTIR

ATR-FTIR spectra were recorded on a Perkin-Elmer-Spectrum One spectrophotometer, coupled to an attenuated total reflectance (ATR) device. Infrared (IR) spectra were obtained between 4000 and 400 cm^{-1} by 32 scans and with a scanning resolution of 4 cm^{-1}.

4.3.4.4 Size and morphology characterization of the NP systems by SEM and AFM

The morphology of NP systems was determined using Scanning Electron Microscopy (SEM) and Atom Force Microscopy (AFM). Both techniques allowed for the observation of the predominantly spherical morphology of all the NP systems. Evidence of the encapsulation of bemiparin was also provided by EDAX analysis and FTIR, where the sulfur band in the NP systems was observed. Non-loaded NP did not give a detectable signal of S in the corresponding EDAX. Logically, the contribution of the S signal is associated to the initiator linked at the end of the copolymer chains in PMMA-*b*-PMAETMA NP systems, but according to the high molecular weight, the contribution is very small.

4.3.4.5 Bemiparin encapsulation efficiency

Bemiparin encapsulation efficiency (EE) was determined by high performance liquid chromatography (HPLC) using a SHIMADZU SIL-20 equipment with UV-Vis detection at 242 nm. The mobile phase was 1% (w/v) acetic acid in milli-Q water and measurements were carried out at 37° C and 1 mL/min. The amount of non-entrapped drug recovered in the external aqueous phase after centrifugation was quantified using a calibration curve obtained from different solutions of known concentration, by the integration of the peak at 2.3 min ± 0.15 min. The percentage of EE was defined as Equation VIII:

$$\%\boldsymbol{EE} = \frac{[\boldsymbol{bemiparin}]_{\boldsymbol{0}} - [\boldsymbol{bemiparin}]_{\boldsymbol{i}}}{[\boldsymbol{bemiparin}]_{\boldsymbol{0}}}\ \boldsymbol{x}\ \mathbf{100} \qquad \textbf{Equation VIII}$$

Where $[bemiparin]_o$ is the total added bemiparin amount and $[bemiparin]_i$ is the non-encapsulated bemiparin amount.

4.3.4.6 Bemiparin content into Chitosan NPs

The compositional ratio of bemiparin in the NP was estimated by FTIR, using the absorption bands ratio A_{1521}/A_{1220} according to literature[154]. FTIR spectra were recorded in a Perkin-Elmer-Spectrum One spectrophotometer with a scanning resolution of 4 cm^{-1}. Samples were mixed with dried KBr and discs were prepared by compression under vacuum. The band at 1521 cm^{-1} is related to the amino group of chitosan and the band at 1220 cm^{-1} is related to the sulphate group of bemiparin. A previous calibration curve was obtained by physical mixing of chitosan and bemiparin at different ratios per triplicate.

4.3.4.7 Bemiparin release

Drug release from NP was evaluated in PBS (Phosphate Buffered Saline pH 7.4, 0.01 M, NaCl 0.15 mol/L). For this purpose, 10 mg of loaded bemiparin NP were suspended in 5 mL of PBS and incubated at 37 °C under gentle magnetic stirring. At various time intervals, 0.5 mL sample was withdrawn and replaced by 0.5 mL of fresh buffer. These aliquots of 0.5 mL were centrifuged at 12000 rpm for 15 min and the supernatants were analyzed by HPLC-UV at 242 nm (SHIMADZU SIL-20) for the quantification of Bemiparin released from the NPs. The pellet was then resuspended and placed in the original nanoparticles dispersion and fresh buffer was replaced. The mobile phase was 1% (w/v) acetic acid in milli-Q water and measurements were carried out at 37° C and 1 mL/min. A calibration curve of bemiparin was obtained previously from solutions of known concentration in the same medium, by measuring the integration of a peak at 2.3 min ± 0.15 min. To study the stability of nanoparticles at high pH, a parallel assay at pH 10 was carried out. Total release of bemiparin was confirmed by dissolution of the NPs in ethyl acetate and analysis of the bemiparin content by HPLC-UV.

4.3.4.8 BaF32 cell proliferation assay

The BaF32 cell proliferation assay was used to determine the activity of the bemiparin released from the polymer systems. The readout of this assay was cell proliferation which is indicated of the biological activity of free and encapsulated bemiparin by the formation of ternary complexes on the cell surface. BaF32 cells were maintained in RPMI 1640 medium containing 10% (v/v) FBS, 10% (v/v) WEHI-3BD conditioned medium, and a 1% (v/v) penicillin/streptomycin mixture. WEHI-3BD cells were maintained in RPMI 1640 medium supplemented with 2 g/L sodium bicarbonate, 10% (v/v) FBS, and a 1% (v/v) penicillin/streptomycin mixture, and the conditioned medium was collected three times per week and stored at -20 °C until it was required. For the mitogenic assays, the BaF32 cells were transferred into IL-3

depleted medium for 24 h prior to experimentation and seeded into 96-well plates at a density of $8x10^4$ cells/well in the presence of free bemiparin or encapsulated bemiparin at different concentrations and with and without FGF2 (0.03 nM). Cells in the presence of medium without any treatment were used as a negative control. Cells were incubated for 72 h in 5% CO_2 at 37 °C, and the number of viable cells was assessed using the MTS assay. The MTS reagent was added to the cell cultures 6 h prior to measurement of the absorbance at 490 nm. Cell proliferation was assayed by measuring the increase of absorbance, which corresponded to the cell number. To compare the difference between the free and encapsulated bemiparin, analysis of variance (ANOVA) of the results were carried out using $p<0.05$ of significance level.

4.4 RESULTS AND DISCUSSION

Bemiparin was incorporated into nanoparticulated systems by two different methods.

4.4.1 Polyelectrolyte complexation: bemiparin-chitosan NP

Chitosan/bemiparin nanoparticles were prepared by the complexation between chitosan and oppositely charged bemiparin leading to the formation of polyelectrolyte complexes[155]. An estimation of the positive to negative (+/-) charge ratios for the different formulations was made, based on the following assumptions:

Chitosan was considered to have one positive charge per de-acetylated monomer and, since it has a de-acetylation degree of 83%, a mean value of 0.8 positive charges per monomer was used. According to a reported method[156], an average monomeric molecular weight of 169 g/mol for this de-acetylation degree was obtained.

Bemiparin was assumed to be in the sodium salt form, which corresponds to a mass of 408 g/mol and 2.7 negative charges per disaccharide monomer unit[4]. The

mass of each compound in every formulation was then converted to moles of charge and the +/- charge mixing ratio was calculated.

Formulations with chitosan/bemiparin mass ratios around 1/1, which evidence a +/- charge mixing ratio below 1, resulted in opalescence. The observed opalescence for equimolar ratios is due to the presence of an excess of anionic charges, which neutralize chitosan positive charges and, thus, reduce or eliminate electrostatic repulsion, leading to the formation of a stable nanoparticle suspension. In fact, a 1:1 +/- charge stoichiometry does not mean that complete charge neutralization will occur, due to different charge spacings in the intervenient species and to steric constraints. FTIR studies determined the compositional mass ratio of the polyelectrolyte complexes, by the extrapolation of the value obtained by A_{1526}/A_{1220} for the nanoparticles after freeze-drying into the calibration curve. A bemiparin content of 45 ± 2 wt% and a 55 ± 2 wt% of chitosan was stimated. That means a +/- molar ratio of 0.87:1 and nanoparticles were obtain with a diameter size of around 99 ± 1 nm. When the +/- molar ratio is higher than 1 nanoparticle aggregation occurs and the nanoparticle suspension is not stable anymore. Measurements were carried out in triplicate.

4.4.2 Nanoparticle prepared by Multiple emulsion

Bemiparin-RESOMER (PLGA)

Bemiparin-Eudragit RS PO (poly(MMA-co-EA-co-MAETMA))

Bemiparin-RAFT block copolymers (PMMA-*b*-PMAETMA)

The systems prepared by multiple emulsion method were developed by a two step process as is shown in Figure 59. The first step was the preparation of bemiparin loaded micelles by adding a diluted solution of bemiparin in water to the solution of the block copolymer in ethyl acetate under vigorous stirring. This results in the formation of very small micelles with the hydrophilic ionized bemiparin in the core of the micelle, whereas in the outer part is more concentrated with

hydrophobic copolymer sequences. With this arrangement, the formation of bridges is easy by ionic interactions of the sulphate groups of bemiparin and the ammonium ions of the PMMA-b-PMAETMA block copolymer, with this characteristic distribution of microdomains. In a second step, this water in oil emulsion is added to a diluted solution of poly(vinyl alcohol) (PVA) in water, and in these conditions a phase inversion is produced in such a way that the more hydrophobic component (PMMA segments) are concentrated in the core, and the hydrophilic (bemiparin+PMAETMA sequences) are distributed in the shell phase. The consequence is the formation of nanoaggregates, which are stabilised by the complexation between the ionic sulphate groups of bemiparin and the ammonium ions of the copolymer entities. The PVA acts as an o/w emulsifying agent to avoid aggregation of nanoparticles.

The nanoparticle formation with PLGA and Eudragit polymers was carried out in a similar manner; however PLGA nanoparticles did not form core-shell micelles by phase inversion like the EUDRAGIT and PMMA-*b*-PMAETMA systems. In the case of PLGA, nanoparticles were formed by multiple emulsion instead.

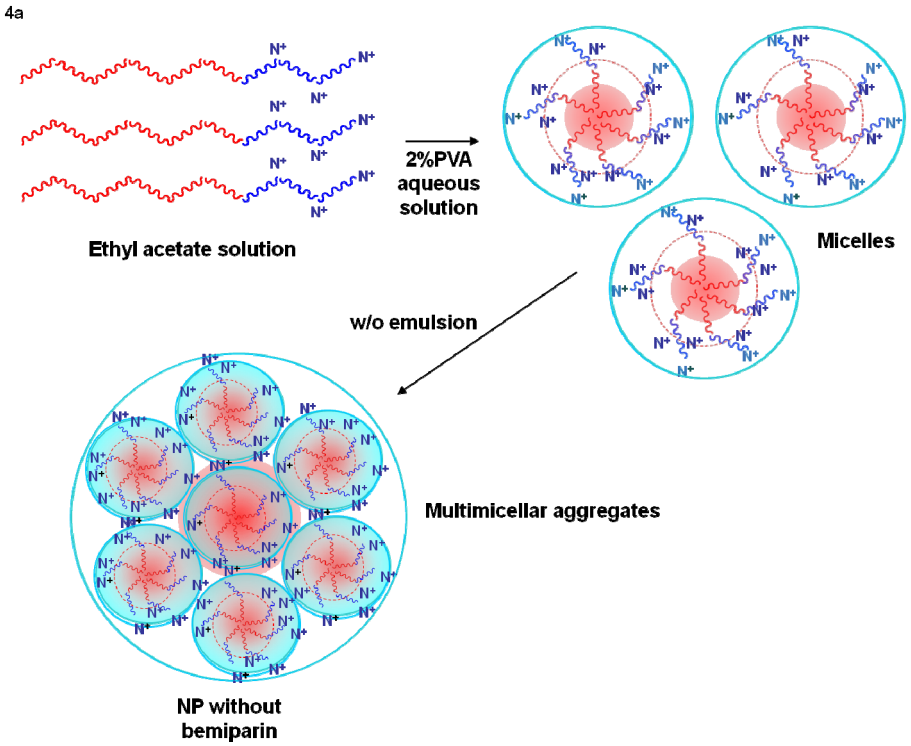

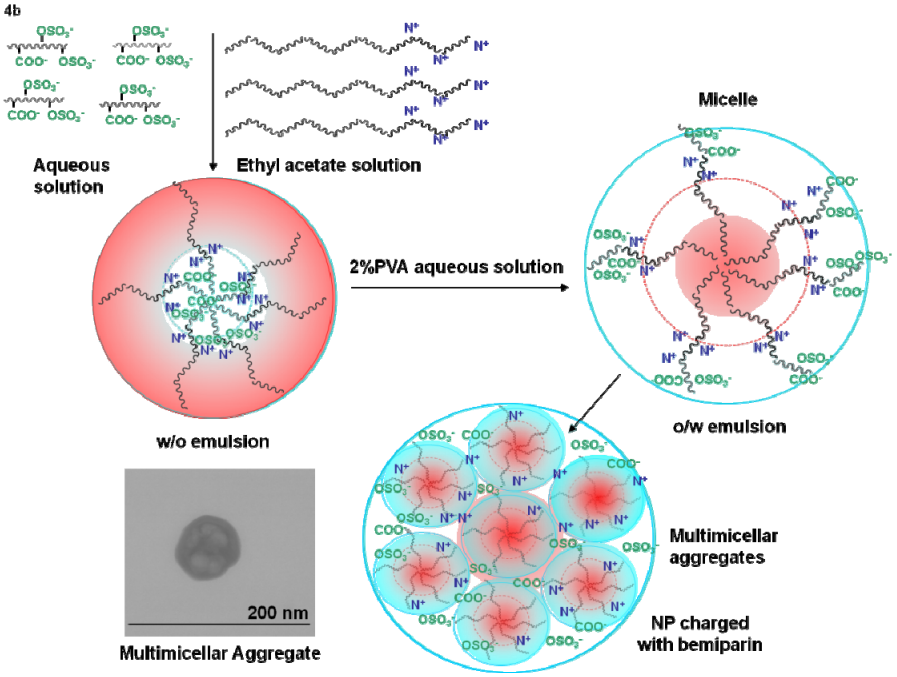

Figure 59. Nanoparticle formation scheme prepared by emulsion technique using the block copolymers obtained by RAFT polymerization, PLGA and Eudragit RS PO. 2a) Preparation of non-loaded polymeric nanoparticles, 2b) Preparation of loaded nanoparticles with bemiparin. TEM image of the NP system 86/14 PMMA-*b*-PMAETMA obtained with field emission Hitachi SU8000 apparatus is included.

4.4.3 FTIR characterization of NP systems

Bemiparin presents characteristic peaks at 807 cm^{-1} corresponding to the stretching vibration of C-O-S bonds, at 1240 cm^{-1} corresponding to the asymmetric stretching vibrations ν_{as} (S-O) of the sulphate groups, at 1400 cm^{-1} and 1658 cm^{-1} bands assigned to the symmetric and asymmetric axial deformation of carboxylic group (CO) and at 3500cm^{-1} corresponding to the symmetric stretching vibration of O-H bonds.

4.4.3.1 Nanoparticle prepared by Polyelectrolyte complexation: bemiparin-chitosan NP

Chitosan/bemiparin nanoparticles were produced by the spontaneous interpolyelectrolyte complexation of polycationic chitosan and polyanionic bemiparin. The FTIR spectrum (Figure 60) of nanoparticles exhibited the characteristic absorption bands of chitosan at 1658 cm^{-1} (Amide I), 1595 cm^{-1} (-NH_2 bending) and 1314 cm^{-1} (Amide III). The presence of bemiparin was evidenced by a band at 1240 cm^{-1} corresponding to the asymmetric stretching vibrations ν_{as} (S-O) and the intensity increase in the carboxylic (CO) band at 1658 cm^{-1}.

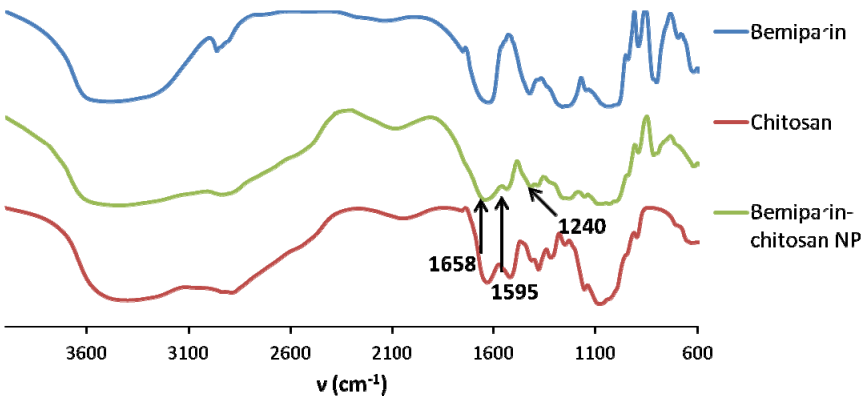

Figure 60. FTIR spectra of CHITOSAN (red), bemiparin (blue) and CHITOSAN-BEMIPARIN NP (green).

4.4.3.2 Nanoparticle prepared by Multiple emulsion

4.4.3.2.1 Bemiparin-RESOMER (PLGA) NP

The FTIR spectra (Figure 61), nanoparticle systems charged with bemiparin showed two different carbonyl group signs, the first one at 1650cm^{-1} assigned to bemiparin and the second one at 1750cm^{-1} assigned to PLGA. Furthermore, at 3500cm^{-1} the nanoparticle systems a wide band similar to bemiparin spectra was observed, assigned to the OH groups of bemiparin.

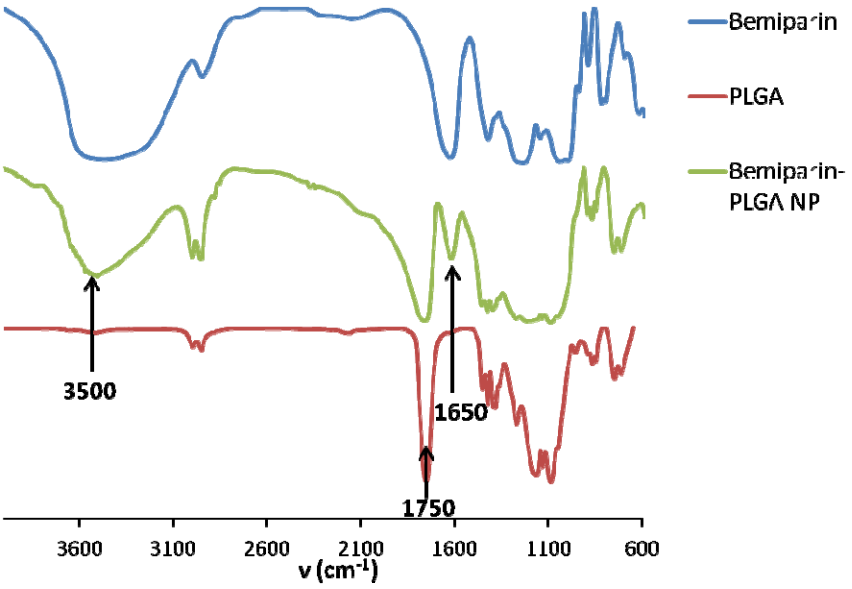

Figure 61. FTIR spectra of bemiparin (blue), PLGA (red) and nanoparticle system of PLGA loaded with bemiparin (green).

4.4.3.2.2 Bemiparin-Eudragit RS PO (poly(MMA-*co*-EA-*co*-MAETMA)) NP

Figure 62 shows the FTIR spectra of Bemiparin, Eudragit RS PO and Bemiparin-Eudragit RS PO NP. NP spectrum presents both characteristic peaks of the initial polymers: asymmetric stretching vibration of bemiparin carboxylic groups at 1650 cm^{-1}, and of Eudragit RS PO carboxylic groups at 1720 cm^{-1} and the asymmetric stretching vibration of O-H bonds corresponding to bemiparin, at 3500 cm^{-1}.

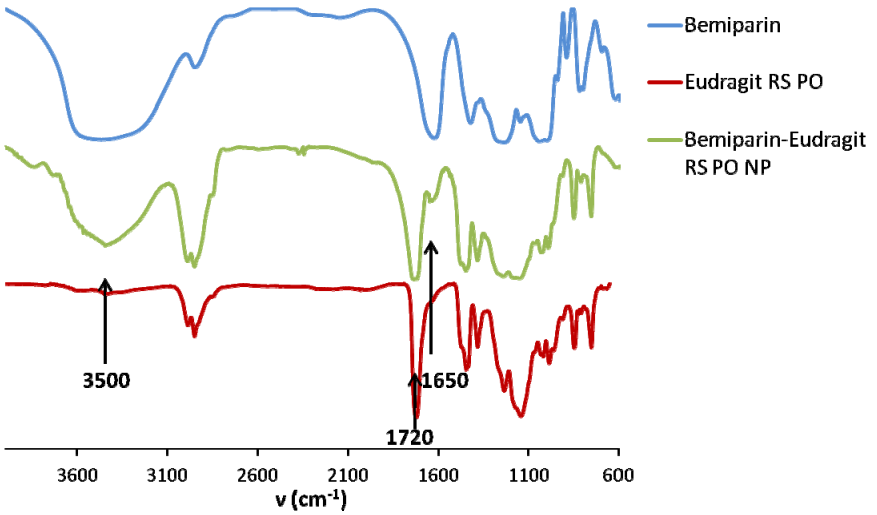

Figure 62. FTIR spectra of EUDRAGIT (red), bemiparin (blue) and EUDRAGIT NP loaded with bemiparin (green).

4.4.3.2.3 Bemiparin-RAFT block copolymers (PMMA-*b*-PMAETMA) NP

In the FTIR spectra of PMMA-*b*-PMAETMA NP system (Figure 63) both bands can be observed, the bemiparin carboxylic groups at 1650cm^{-1} and the block copolymer carboxylic groups at 1720cm^{-1}. The band at 2950cm^{-1} belongs to the C-H stretching vibrations of the alkane main chain of the polymer. Moreover, at 3500cm^{-1} the PMMA-*b*-PMAETMA NP system a wide band was observed, which corresponds to the stretching of the O-H bonds of bemiparin.

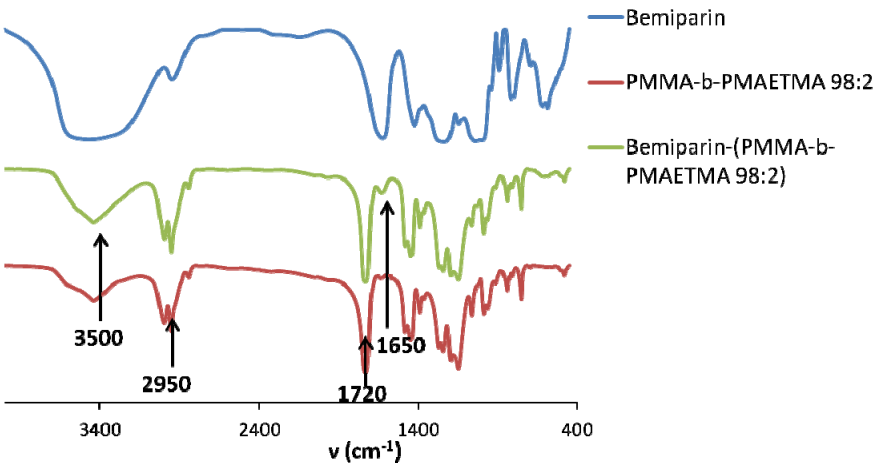

Figure 63. FTIR spectra of 94/6 p(MMA-*b*-MAETMA) block copolymer system (red), bemiparin (blue) and 94/6 p(MMA-*b*-MAETMA) NP LOADEd with bemiparin (green).

4.4.4 Thermogravimetrical Analysis

Table 7 shows the temperature at maximum degradation rate (T_{max}) of bemiparin, polymers and the nanoparticle systems. The thermal degradation of bemiparin took place in two phases: the first one (from 220 to 260 °C) is generally interpreted as the release of water retained into the bemiparin structure. The second region (from 270 to 320 °C) is attributed to the breakdown of the glycosidic rings of the bemiparin backbone. Bemiparin presents carboxylate ($-COO^-$) and sulphonate ($-OSO_3^-$) groups in its structure, which are highly hydrophilic and could strongly interact with water molecules through dipole-dipole or ion-dipole forces. For this reason, the retained water was not eliminated at around 100 °C, but at higher temperatures.

4.4.4.1 Nanoparticle prepared by Polyelectrolyte complexation: bemiparin-chitosan NP

Chitosan thermal degradation occured also in two weight loss stages. The first region (from 190 to 220 °C) belongs to the retained water. The second region (from 240 to 280 °C) is related to the breakdown of the glycosidic rings of the chitosan backbone.

Bemiparin-chitosan NP system showed a slightly increase in the degradation temperature maximum, due to the ionic complexation of bemiparin-chitosan, which result in an increase in the degradation temperature (Figure 64).

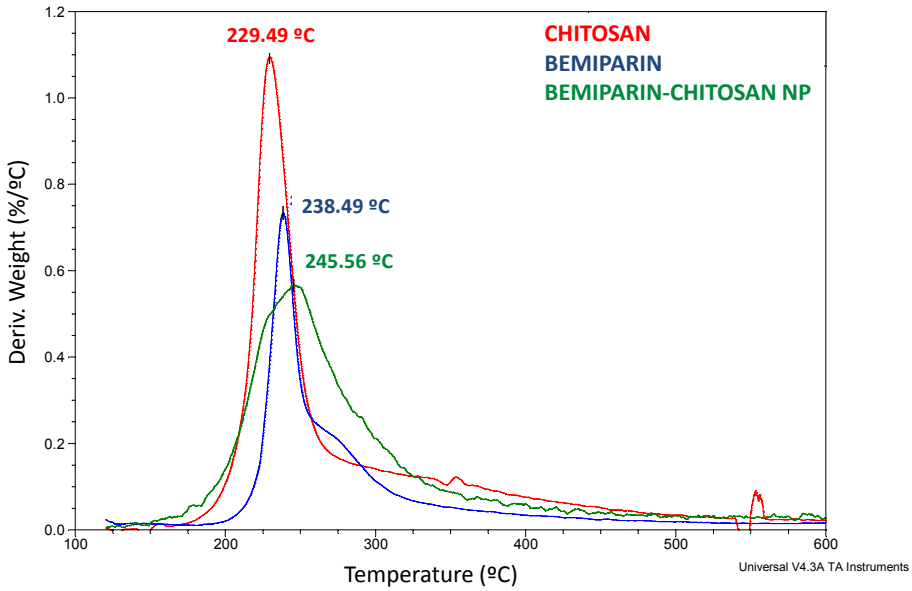

Figure 64. First derivate curve obtained from thermogravimetric degradation curve of chitosan (red), bemiparin (blue) and bemiparin-chitosan NP (green).

4.4.4.2 *Nanoparticle prepared by Multiple emulsion*

4.4.4.2.1 Bemiparin-RESOMER (PLGA)

PLGA degradation occurred in one stage between 250-325 °C with a temperature of maximum decomposition rate of 307 °C. This polymer degraded by the action of temperature by the random cleavage of the main chain to give oligomeric hydrocarbon compounds.

Bemiparin-PLGA NP thermal degradation occurred in one step and presented a T_{max} higher than the corresponding components, which indicated a thermal stabilization of both bemiparin and the polymer (Figure 65).

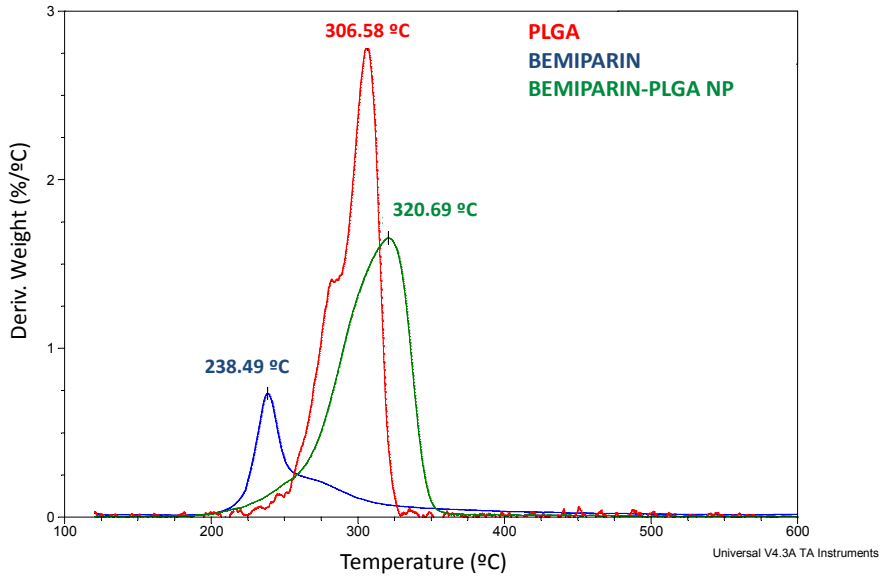

Figure 65. First derivate curve obtained from thermogravimetric degradation curve of PLGA (red), bemiparin (blue) and bemiparin-PLGA NP (green).

4.4.4.2.2 Bemiparin-Eudragit RS PO (poly(MMA-*co*-EA-*co*-MAETMA))

Eudragit RS PO degradation occurred in one only stage between 300-400 °C with a temperature of maximum decomposition rate T_{max} of 370 °C. Bemiparin-

Eudragit RS PO NP presented higher T_{max} (403 °C) than both polymers and this increase is more pronounced in this case than in the rest systems due to the presence of ionic interactions between both macromolecules (Figure 66).

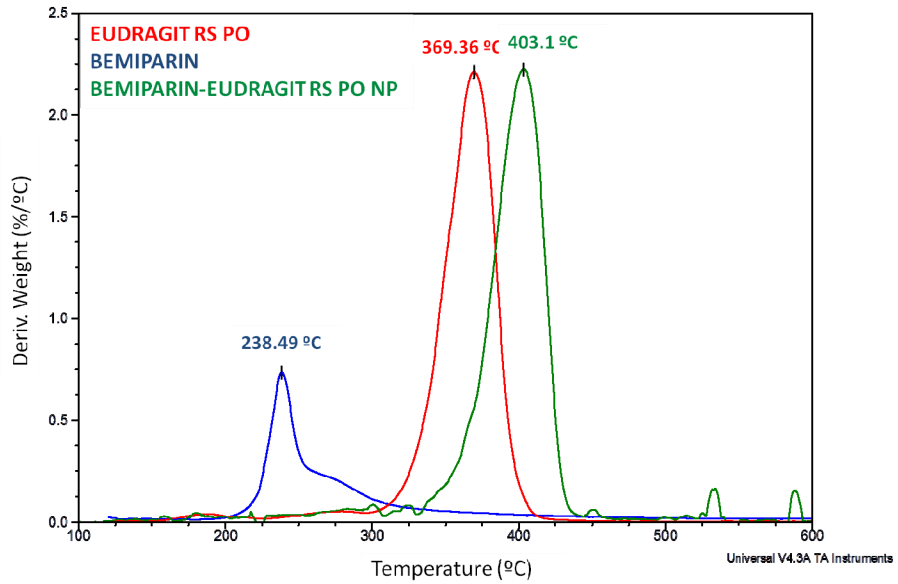

Figure 66. First derivate curve obtained from thermogravimetric degradation curve of EUDRAGIT RS PO (red), bemiparin (blue) and bemiparin-EUDRAGIT RS PO NP (green).

4.4.4.2.3 Bemiparin-RAFT block copolymers (PMMA-*b*-PMAETMA)

Thermal degradation of RAFT block copolymers took place in two different stages, the first region (from 250 to 320 °C) was attributed to the loss percentage of the corresponding MAETMA sequences in the copolymer, and it was corroborated with the observation of a higher weight loss percentage of the copolymer as a function of the MAETMA content in the copolymer. The second region (from 360 to 420 °C) was due to the weight loss percentage related to the MMA sequences, however this last degradation peak was affected by the MAETMA percentage into the block copolymer structure, T_{max} being higher with lower MAETMA content chain,

changing from 386 °C for PMMA-*b*-PMAETMA 86:14 to 394 °C for PMMA-*b*-PMAETMA 98:2 (Figure 67).

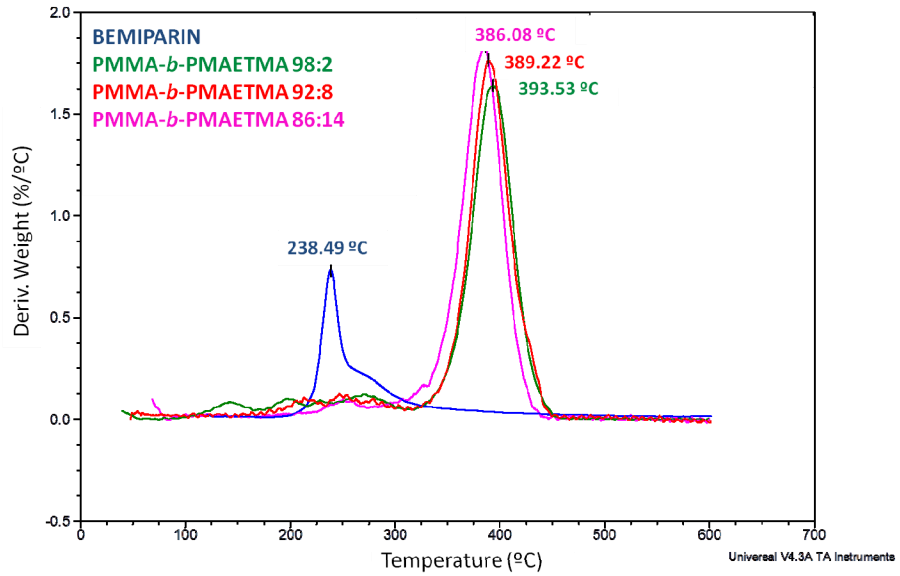

Figure 67. First derivate curve obtained from thermogravimetric degradation curve of RAFT block copolymers: PMMA-*b*-PMAETMA 98:2 (green), PMMA-*b*-PMAETMA 92:8 (red), PMMA-*b*-PMAETMA 86:14 (pink) and bemiparin (blue).

Bemiparin-RAFT block copolymer NP showed higher T_{max} than those obtained for block copolymers without bemiparin, however the tendency was similar: from 386 to 394 °C for block copolymers alone, and from 389 °C to 405 °C for NP systems prepared with these polymers. The increase in the T_{max} indicates thermal stabilization of both bemiparin and block copolymers (Figure 68).

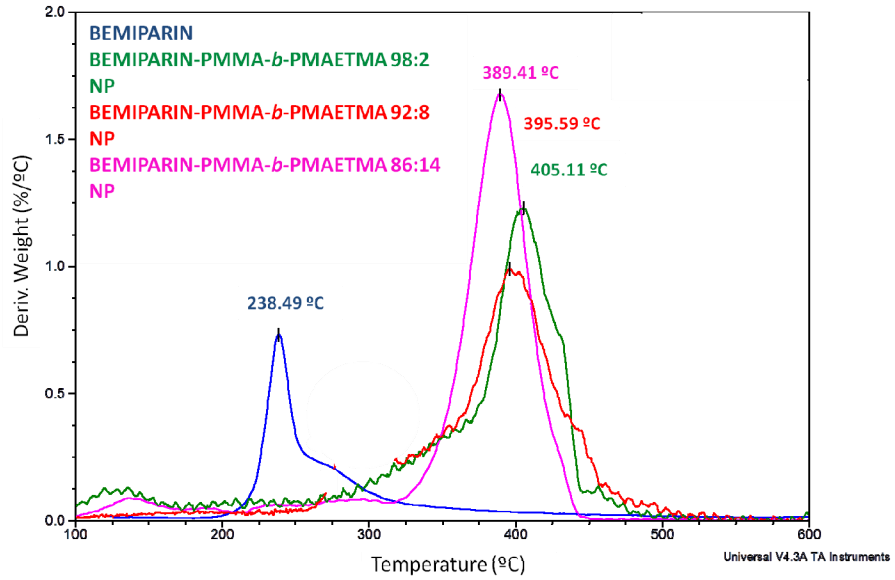

Figure 68. First derivate curve obtained from thermogravimetric degradation curve of RAFT block copolymers: Bemiparin-PMMA-*b*-PMAETMA 98:2 NP (green), Bemiparin-PMMA-*b*-PMAETMA 92:8 NP (red), Bemiparin-PMMA-*b*-PMAETMA 86:14 NP (pink) and bemiparin (blue).

Table 6. Maximum temperature degradation of the NP systems measured by TGA under nitrogen atmosphere at 10 °C/min.

SAMPLE	$T_{max\ degradation}$
BEMIPARIN	242 °C
PLGA	307 °C
PLGA NP loaded with BEMIPARIN	321 °C
EUDRAGIT	370 °C
EUDRAGIT NP loaded with BEMIPARIN	403 °C
86/14 BLOCK COPOLYMER	386 °C
86/14 NP loaded with BEMIPARIN	389 °C
92/8 BLOCK COPOLYMER	389 °C
92/8 NP loaded with BEMIPARIN	396 °C
98/2 BLOCK COPOLYMER	394 °C
98/2 NP loaded with BEMIPARIN	405 °C
CHITOSAN	229 °C
CHITOSAN NP loaded with BEMIPARIN	246 °C

4.4.5 Particle size and zeta potential (ZP) measurements by DLS

The Particle Size measured by DLS is the diameter of the sphere that diffuses at the same speed as the particle being measured. The size is determined by first measuring the Brownian motion of the particles, defined as 'the random movement of particles in a liquid due to the bombardment by the molecules that surround them'[157], and it is measured using dynamic light scattering (DLS).

When a charged particle is suspended in liquid ions of an opposite charge it will be attracted to the surface of the suspended particle. A negatively charged sample attracts positive ions from the liquid and conversely a positive charged sample attracts negative ions from the liquid. Ions close to the surface of the particle, will be strongly bound while ions that are further away will be loosely bound forming what is called a diffuse layer. Within the diffuse layer there is a notional boundary and any ions within this boundary will move with the particle when it moves in the liquid; but any ions outside the boundary will stay where they are (this boundary is called the slipping plane).

A potential exists between the particle surface and the dispersing liquid which varies according to the distance from the particle surface. This potential at the slipping plane is called the Zeta potential (Figure 69).

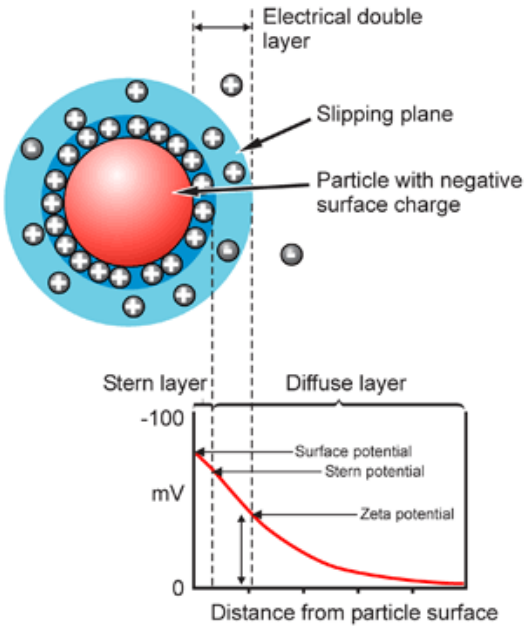

Figure 69. Zeta-potential measurements scheme. Supported by Malvern**.**

Zeta potential (ZP) is measured using a combination of the measurement techniques: electrophoresis and laser doppler velocimetry, sometimes called laser doppler electrophoresis. This method measures how fast a particle moves in a liquid when an electrical field is applied. Once velocity of the particle and the electrical field applied are known, it is possible, by using two other known constants of the sample, viscosity and dielectric constant, to work out the zeta potential.

The magnitude of the zeta potential gives an indication of the stability of the nanoparticles. Z-potentials higher than ±30 mV are considered stable. Those nanoparticles that present a positively charged surface will exhibit positive z-potential values while those negatively charged will be negative.

4.4.5.1 Nanoparticle prepared by Polyelectrolyte complexation: bemiparin-chitosan NP

Chitosan particles without bemiparin presented a mean size of 200 ± 55 nm, which is higher than bemiparin-chitosan particles (99 ± 12 nm). When chitosan is alone, electrostatic repulsion between positive charges of the amino groups are present, therefore polymer chains tend to be spread, forming bigger particle size. When bemiparin-chitosan complexes were formed, part of these positive charges were neutralized, decreasing the electrostatic repulsion, which resulted in a smaller particles. Chitosan nanoparticle suspension without bemiparin showed a positive zeta potential (42 ± 12 mV) due to the positive charge presents in the amino de-acetylated groups. When bemiparin-chitosan complexes were formed, zeta potential became negative (-22 ± 4 mV) due to the extra negative charges corresponding to the sulphate and carboxylic groups of bemiparin.

4.4.5.2 Nanoparticle prepared by Multiple emulsion

4.4.5.2.1 Bemiparin-RESOMER (PLGA) NP

PLGA NP showed a small negative ZP probably due to the carboxylic end groups of the copolymer chain. When bemiparin was encapsulated in the nanoparticle the zeta potential value became more negative, which can be attributed to the presence of bemiparin on the NP surface.

4.4.5.2.2 Bemiparin-Eudragit RS PO (poly(MMA-*co*-EA-*co*-MAETMA)) NP

Eudragit nanoparticles without bemiparin presented the highest mean size of 284 ± 42 nm with a positive zeta potential 20 ± 2 mV. However, when bemiparin was incorporated into the Eudragit matrix, smaller nanoparticles were obtained of approximately 142 ± 20 nm in size with a stable and negative zeta potential value of -32 ± 2 mV. The incorporation of bemiparin provided higher stability to the nanoparticle suspension.

4.4.5.2.3 Bemiparin-RAFT block copolymers (PMMA-*b*-PMAETMA) NP

Particles prepared with the cationic systems without bemiparin, exhibited strongly positive zeta potential values in water due to the presence of the ammonium charge group. Table 7 shows block copolymer composition influence in the ZP values obtained. The higher cationic segment length, the smaller ZP absolute value due to higher charge neutralization between bemiparin and the corresponding cationic block copolymers. It results in a higher D_h of the NP system. When all of the particles in suspension have a large negative or positive ZP then they will tend to repel each other and there will be no tendency for the particles to come together. However, if the particles have low ZP values then the aggregation is favoured and the D_h obtained is higher.

Encapsulated bemiparin not only neutralised the positive charges of Eudragit® RS PO, Chitosan and the RAFT made block copolymers, but also provided a negative ZP to the loaded NPs. The non-neutralised sulphate groups provided stability to the NP shell. Size distribution of all the systems revealed an almost monomodal particle size distribution with an average size shown in Table 7. The polydispersity Index (PDI) was lower than 1, indicating a good measurement quality and it was lower in the bemiparin loaded NP in all the cases, probably due to the higher stability of the system when bemiparin was incorporated.

Table 7. Mean hydrodynamic diameter (nm) and zeta potential value (mV) of the nanoparticle systems measured by DLS with a Zetasizer NanoZS (Malvern Instruments, UK) after precipitation from ethyl acetate solutions.

SAMPLE	D_h (nm) ± SD	ZP (mV) ± SD	PDI
98/2 NP	202 ± 25	14 ± 3	0.34
92/8 NP	165 ± 20	29 ± 4	0.48
86/14 NP	123 ± 14	39 ± 2	0.63
Eudragit® RS PO NP	284 ± 42	20 ± 2	0.53
PLGA NP	121 ± 5	-14 ± 1	0.34
Chitosan	200 ± 55	42 ± 12	0.57
Bemiparin loaded 98/2 NP	105 ± 12	-28 ± 1	0.28
Bemiparin loaded 92/8 NP	144 ± 21	-14 ± 1	0.31
Bemiparin loaded 86/14 NP	198 ± 17	-10 ± 3	0.30
Bemiparin loaded Eudragit® RS PO NP	142 ± 20	-32 ± 2	0.28
Bemiparin loaded PLGA NP	117 ± 13	-37 ± 2	0.27
Bemiparin loaded chitosan NP	99 ± 12	-22 ± 4	0.22

4.4.6 Size and morphology characterization of the NP systems by SEM

The morphology of the NP systems was analyzed by SEM and AFM (Figure 70 and Figure 71) revealing that the particles in the dry state have homogeneous size distribution and an almost spherical shape in all the cases. Evidence for the encapsulation of bemiparin was also provided by EDAX analysis, where the sulphur band of bemiparin was observed (Figure 72) and by FTIR spectroscopy, as previously described in this chapter. Non-loaded NPs did not give a detectable sulphur peak in the corresponding EDAX spectra, which would correspond to the sulphur contribution of the initiator linked at the end of the copolymer chains; however, due to the high molecular weight of these macromolecules, the contribution is not detected by this technique.

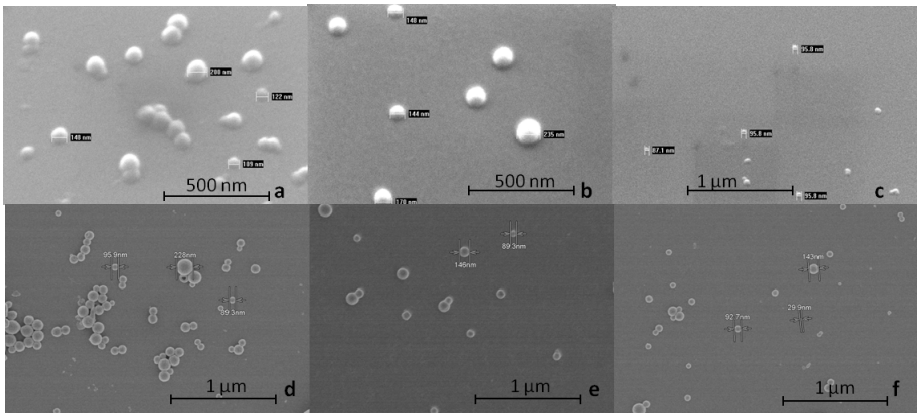

Figure 70. SEM images of bemiparin loaded NP systems: (a) Eudragit® RS PO, (b) PLGA, (c) Chitosan (d) 86/14 $PMMA_{970}$-*b*-$PMAETMA_{158}$, (e) 92/8 $PMMA_{970}$-*b*-$PMAETMA_{84}$, (f) 98/2 $PMMA_{970}$-*b*-$PMAETMA_{20}$.

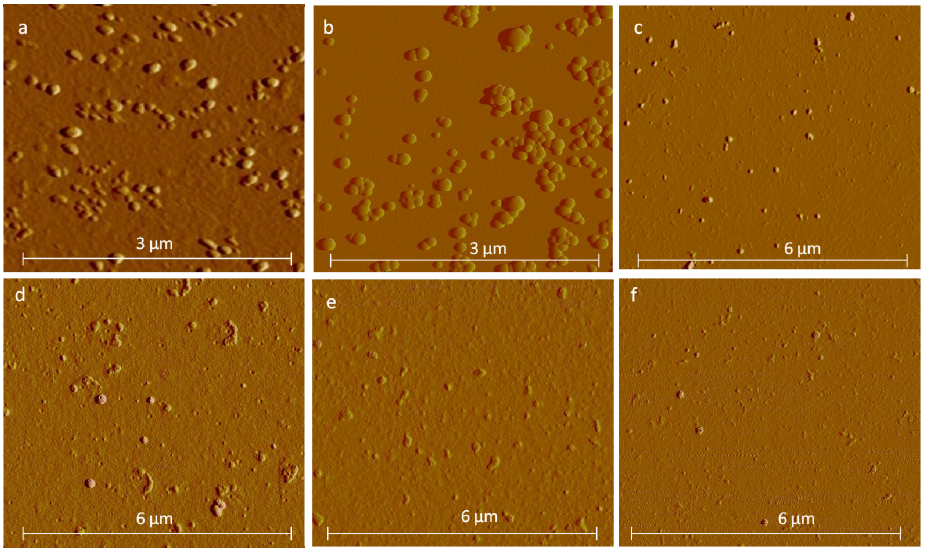

Figure 71. AFM amplitude images of bemiparin loaded NP systems: (a) Eudragit® RS PO, (b) PLGA, (c) Chitosan (d) 86/14 $PMMA_{970}$-*b*-$PMAETMA_{158}$, (e) 92/8 $PMMA_{970}$-*b*-$PMAETMA_{84}$, (f) 98/2 $PMMA_{970}$-*b*-$PMAETMA_{20}$.

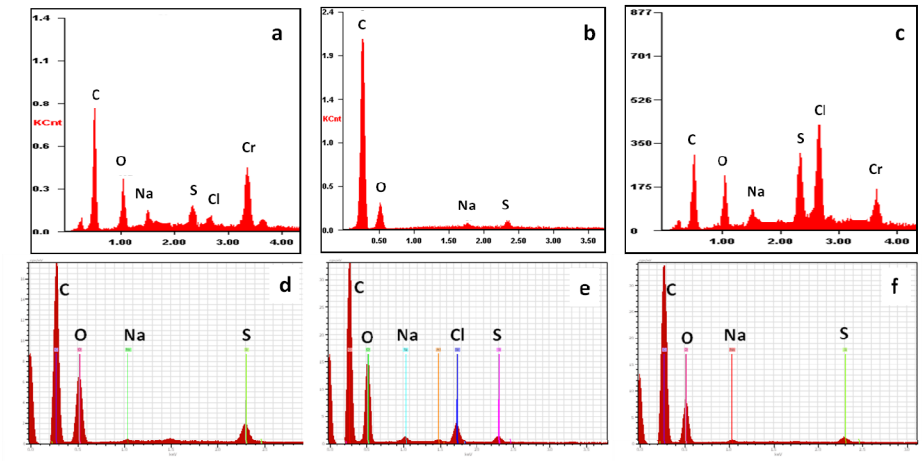

Figure 72. EDAX analysis at 15 KeV of bemiparin loaded NP systems: (a) Eudragit® RS PO, (b) PLGA, (c) Chitosan (d) 86/14 $PMMA_{970}$-*b*-$PMAETMA_{158}$, (e) 92/8 $PMMA_{970}$-*b*-$PMAETMA_{84}$, (f) 98/2 $PMMA_{970}$-*b*-$PMAETMA_{20}$

4.4.7 Encapsulation Efficiency (EE)

The amount of bemiparin entrapped within the polymeric nanoparticles was indirectly determined by measuring the amount of the drug released to the external aqueous solution recovered after the centrifugation and washing of the nanoparticles. The entrapment efficiency within polymeric nanoparticles was affected by the nature of the polymer (Table 8). When PMMA-*b*-PMAETMA, Eudragit® RS PO and chitosan polymers were used, the encapsulation efficiency of bemiparin was higher than that observed for the PLGA polymer. Owing to the polyanionic nature of bemiparin, ionic bonds between the drug and the quaternary ammonium groups of MAETMA or ionized amino groups of chitosan of the polymers led to an increase of bemiparin immobilization compared to the PLGA polymer. Considering the%EE, the mean charge density of bemiparin[21] and the corresponding charge density of the polymer systems, the bemiparin encapsulated percentage and the charge ratio of the NP systems was calculated. These results corroborated the

results obtained by ZP analysis, the higher cationic segment length (PMAETMA) the higher neutralization of the bemiparin charges (Table 8). It is noteworthly that the amount of loaded bemiparin is very similar for all the NP systems analyzed (Table 8).

Table 8.% Encapsulation Efficiency (EE) of bemiparin loaded NP systems measured by HPLC-UV. Charge densities, $^{+}\rho$ and $^{-}\rho$, are apparent relative densities.

NP SYSTEM	EE-% SD	mg bemiparin encapsulated (*)	wt-% bemiparin encapsulated into the NP (**)	$^{-}\rho$ (bemiparin density charge)x10^3 (***)	$^{+}\rho$ (polymer density charge)x10^3 (****)
PLGA NP	89 ± 3	178	15.1	1.53	-
86/14 NP	98 ± 2	196	16.4	1.68	2.39
92/8 NP	96 ± 3	192	16.1	1.65	1.31
98/2 NP	95 ± 4	190	16.0	1.63	0.36
Eudragit® RS PO NP	94 ± 2	188	15.8	1.61	0.33
Chitosan NP	90 ± 5	126	45.7	0.95	0.34

(*) Bemiparin encapsulated = ([mg bemiparin]$_0$ x%EE) /100

(**)%wt bemiparin encapsulated into NP = ([mg bemiparin encapsulated] x 100) / ([mg bemiparin encapsulated] + [mg polymer])

(***)$^{-}\rho$ = ([g bemiparin] / $M_{wbemiparin}$) x n° disaccharide units x 2.7 (negative density bemiparin / disaccharide).

(****)$^{+}\rho$ = ([g polymer]/$M_{w(polymer)}$) x n° [monomer units].

4.4.8 DSC measurements

PMMA-*b*-PMAETMA block copolymers showed a unique thermal transition (T_g) the value of which varied depended on the composition of between 86 and 110 °C, as was outline in chapter 2. However, when bemiparin-loaded NPs were analysed, two different glass transitions temperatures were observed, which belong to the MAETMA and MMA segments respectively. This is due to the interaction of the ionic drug bemiparin that increase the hydrophilic segment character and gives a

nano-domain segregation of both blocks. In that case, these T_g values approached values attained for the corresponding homopolymers (Table 9). The same behaviour was observed for the Eudragit system. However, for chitosan/bemiparin nanoparticles the glass transition temperature was not detected. Chitosan is not a completely amorphous polymer but a partially crystalline polymer, as some studies have demonstrated previously[158]. However, when the polyelectrolyte complex was formed with bemiparin, the system became more crystalline, decreasing the amorphous domain, therefore T_g was not detected.

Table 9. T_g values of the NP systems measured by DSC under nitrogen atmosphere at 10 °C/min.

	Non-loaded NP		Bemiparin-loaded NP	
SAMPLE	T_{g1} (°C)	T_{g2} (°C)	T_{g1} (°C)	T_{g2} (°C)
BEMIPARIN	-	-	-	-
Chitosan	-	195	-	-
PLGA	46.9	-	47.6	-
Eudragit® RS PO	68.0	-	44.9	89.2
86:14 PMMA-*b*-PMAETMA	-	86	39	112
92/8 PMMA-*b*-PMAETMA	-	93	36	114
98/2 PMMA-*b*-PMAETMA	-	110	38	118

4.4.9 Bemiparin release

Figure 73 illustrates the *in vitro* release profiles at pH 7.4 and 10 obtained for each formulation of encapsulated bemiparin, by presenting the percentage of bemiparin released. All the formulations showed an initial burst release; however a clear influence of the chemical structure of the polymers on the release profile obtained for the nanoparticles at pH 7.4 was observed. The most stable system was Eudragit® RS PO NP, probably due to ionic interactions between the quaternary ammonium groups of the polymers and the sulphate groups of bemiparin. Furthermore, due to the MAETMA random distribution along the polymer chain,

phase segregation did not occur and PMMA domains were the dominant within the copolymer, providing hydrophobic character to the whole polymer system which hinders water diffusion, and therefore limits the bemiparin release.

At pH 7.4 the highest bemiparin release (nearly 100%) occurred in PLGA NPs due to the amorphous structure and non-ionic character of PLGA polymer. Drug release from PLGA NPs was mainly controlled by the diffusion of bemiparin throughout the flexible chains, and/or erosion mechanisms of PLGA, as it is a biodegradable polymer[159]. In the first three weeks, the bemiparin release profile in PLGA NP system did not show a significant difference compared to the block copolymer systems, however after 25 days the bemiparin release increased, probably due to the higher erosion of PLGA by biodegradation. From this point on the rate of release was noticeably faster than in the other systems tested.

However, in the case of the cationic copolymers, bemiparin release was controlled by the three-dimensional network structure produced by ionic interactions following water diffusion into the nanoparticles. This explains the significant retardation of bemiparin release in the Eudragit® RS PO system.

The NPs prepared with PMMA-*b*-PMAETMA copolymers showed a higher bemiparin release compared to Eudragit® RS PO NP, due to the copolymers microstructure. These block copolymers forms a self-organized system with a core of PMMA blocks and a shell of the cationic PMAETMA complexed with bemiparin. The latter nano phase is very hydrophilic and might allow better water penetration compared to the Eudragit® RS PO.

The composition of the copolymer in the NP block copolymer systems slightly influenced the bemiparin release profile at pH 7.4, since NPs prepared from 86/14 copolymer presented a slower release than NP prepared using the copolymers with lower content on MAETMA blocks (92/8 and 98/2).

At pH 10 the bemiparin release is faster than at pH 7.4 in all of the NP systems, probably due to the hydrolisis of the carboxilic ester groups contained in the copolymer systems which is more favoured at pH 10 than at pH 7.4.

The comparison of the release profiles of the different NP systems at pH 10 shows that PLGA NPs and NPs prepared with PMMA-*b*-PMAETMA copolymers did not present a significatively different release profile. However, Eudragit® RS PO NPs

presented a slower release. This again can be attributed to the polymer microstructure, which makes the system more hydrophobic and therefore water diffusion was lower which impeded bemiparin release.

The release profile of bemiparin from chitosan/bemiparin nanoparticles is pH-dependent due to chitosan's weak polybasic nature which is related to its amino group. At pH 7.4 only 28% of the bemiparin was released during the first 72 hours, however at pH 10 the release reached the 70%. This is due to a pH-dependent polyelectrolyte complexation (Scheme 1). At pH 7.4 the pK_a of chitosan can be considered close to the intrinsic pK, $pK_a = 6.5$[160]. The classical Equation IX can used to calculate the degree of dissociation at physiological pH:

$$pK_a = pH + \log\frac{\alpha}{1-\alpha} = 6.5 \qquad \textbf{Equation IX}$$

where α is the degree of dissociation of chitosan, which at pH 7.4 is about 14%. [161] These cationic charges on the chitosan chain are sufficient to support the polyelectrolyte complex formed with bemiparin, whose sulphate groups can be considered as fully dissociated whatever the pH. However, at pH 10 almost all amino groups of chitosan are uncharged, and the complex breaks down releasing bemiparin. These results indicate the relatively high stability of the polyelectrolyte complex in physiological conditions. Not only ionic interactions but also weaken interactions (e.g. hydrogen bonds, macromolecular entanglements) are responsible for the high nanoparticle stability.

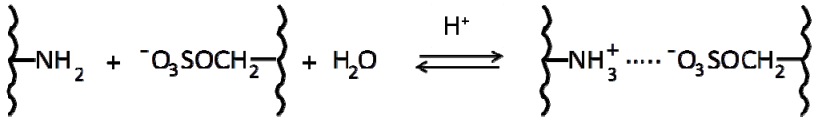

Scheme 1. Ionic interaction produced between the amino group of chitosan and the sulphate group of bemiparin.

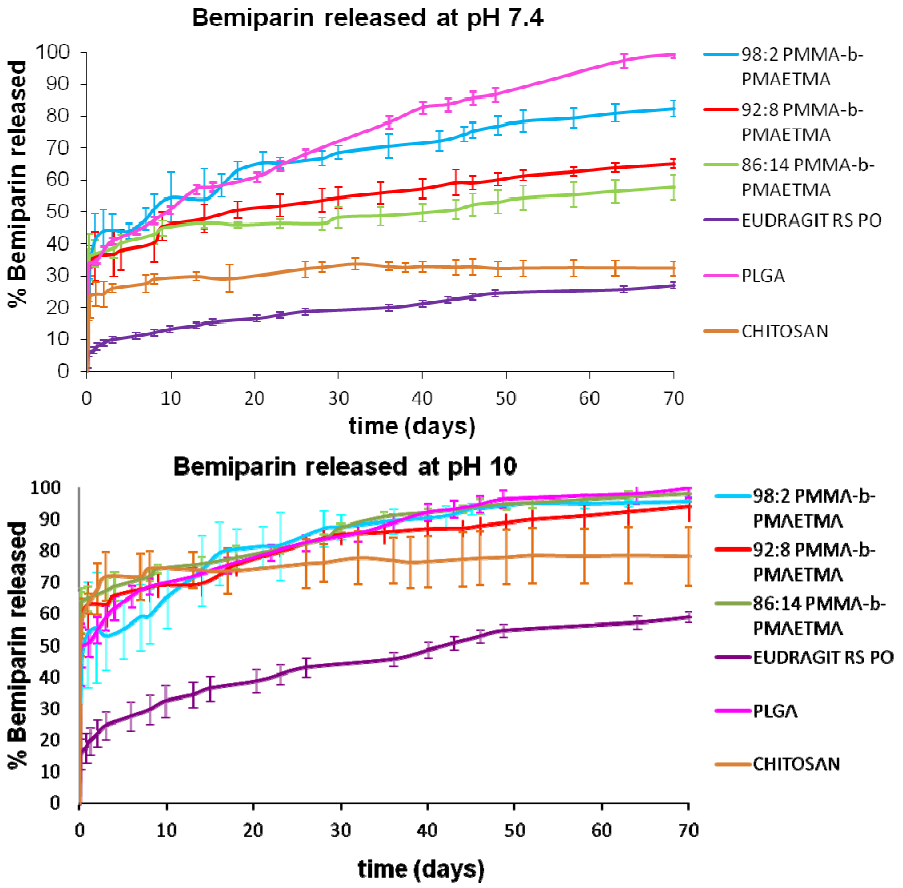

Figure 73. Bemiparin release profile in buffer at pH 7.4 and pH 10 using HPLC-UV detection at 242 nm.

4.4.10 BaF32 cell proliferation assay

The Baf32 cells provide a measure of the activity of the loaded bemiparin into the nanoparticle systems in comparison to the free bemiparin. This study measures the activity of the ternary complexes formed between bemiparin, FGF2 and FGF receptor 1c. The formation of these active ternary complexe induces cell proliferation which was measured by the MTS assay. The extent of proliferation is modulated by the concentration of FGF2 and bemiparin as well as the activity of the

bemiparin. As bemiparin was not chemically modified in each of the polymer systems, this assay provides a measure of the availability of bemiparin in the different polymer systems. FGF2 or bemiparin alone can induce the proliferation of the cells; however the presence of both in an active ternary complex enhances proliferation. This was observed when the Baf32 cells were exposed to free bemiparin in the concentration range of 5 – 60 nM in the presence or absence of FGF2 (Figure 74). There was, however, no dose-dependent increase in the proliferation of the cells in the presence of increasing concentrations of bemiparin. Bemiparin encapsulated in each of the polymer systems was also analysed in the Baf32 cell assay where cells were exposed to different concentrations of the polymer systems based on the amount of encapsulated bemiparin between 5 and 60 nM. Bemiparin encapsulated in PLGA NPs showed a dose-dependent increase in cell proliferation with increasing concentrations of encapsulated bemiparin. The highest dose of bemiparin encapsulated in PLGA NP was equally as active as free bemiparin ($p<0.05$). This may be due to the 40% release of bemiparin from PLGA within 72 h (Figure 73). Bemiparin encapsulated in Eudragit® RS PO was significantly less active than free bemiparin ($p<0.05$) except at the highest concentration used and this can likely to be attributed to the low release of bemiparin at 72 h of approximately 10%. When PMMA-*b*-PMAETMA block copolymers were used to encapsulate bemiparin, the systems were significantly less active than free bemiparin ($p<0.05$) probably due to the ionic retention of bemiparin with the cationic group of the polymer carrier. The 98/2 PMMA-*b*-PMAETMA system became dose-dependent similar to PLGA system because at pH 7.4 the bemiparin release in that system was close to 40% at 72h (Figure 73). The bemiparin-chitosan NPs also showed the formation of the active ternary complex which presents similar biological activity as free bemiparin, but without the dose-dependent behavior observed for the PLGA or the 98:2 PMMA-*b*-PMAETMA NP systems.

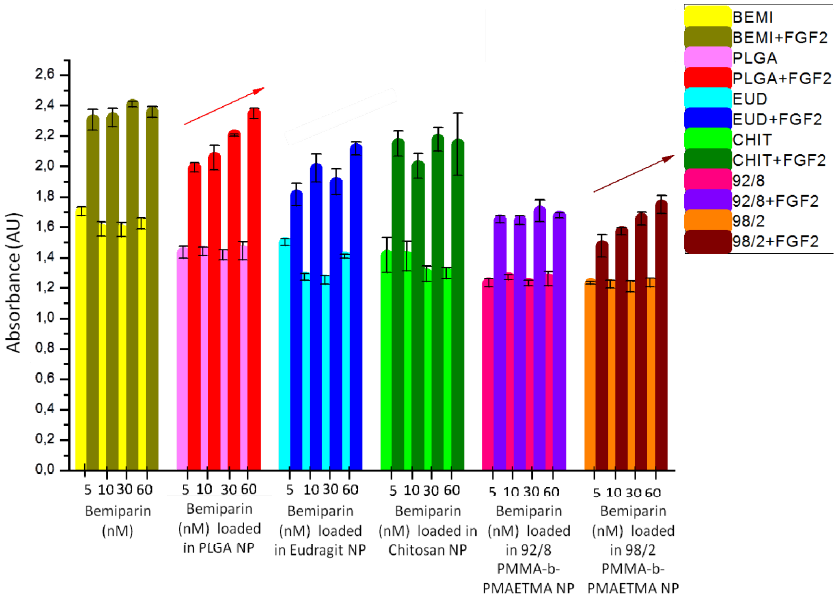

Figure 74. Proliferation of BaF32 cells expressing FGFR 1c in the presence of bemiparin, PLGA containing bemiparin, Eudragit® RS PO containing bemiparin, Chitosan-bemiparin complexes, 92/8 PMMA-*b*-PMAETMA containing bemiparin, 98/2 PMMA-*b*-PMAETMA containing bemiparin either in the presence or absence of FGF2. Polymer systems were analyzed at a range of concentrations based on the amount of encapsulated bemiparin at the start of the assay. Data presented as mean ± SD and corrected for the proliferation of cells in the presence of medium only (n=3). Statistical analysis was performed using a One-way ANOVA, using a $p<0.05$. (*) indicates a significant statistical difference ($p<0.05$).

4.5 CONCLUSIONS

Chitosan-bemiparin nanoparticles were prepared using the complex coacervation method, obtaining particles with an average size of 99 ± 12.5 nm which were morphologicaly spherical. At pH= 7.4 nanoparticles released up to 28% of bemiparin in 72 hours whereas at pH=10, 70% bemiparin was released during the first 72 hours, proving that this behavior is pH dependent. Bemiparin-chitosan nanoparticles displayed a similar biological activity to free bemiparin to form a ternary complex with FGF2 and its membrane receptor FGF 1c.

Amphiphilic block copolymers of PMMA-*b*-PMAETMA were used as carriers for the controlled delivery of bemiparin due to their tendency to form micellar self-assembled nanoparticle structures which could be loaded with bemiparin. Loaded NPs of predominantly spherical morphology were prepared by the multiple emulsion technique and were approximately 100-200 nm in size, depending on the block copolymer composition. Eudragit® RS PO was used as a structural and chemical model with positively charged functions but a different microstructure. PLGA was taken as a biodegradable and biocompatible model (common used in drug delivery). RAFT block copolymers yielded similar release profile plots to the PLGA system and higher drug release than Eudragit® RS PO. The encapsulated-bemiparin in the PLGA and 98/2 block copolymer systems showed a dose dependent behavior in temrs of cell proliferation, which was not observed in the Eudragit® RS PO NP or non-encapsulated bemiparin systems. The encapsulation with the block copolymer system offers a modulate release way for the protection and application of bemiparin as an activating agent of the function of growth factors.

This block copolymer encapsulation systems could be a promising candidate for the modulate release of bemiparin, since the bemiparin is protected and can be applied to the area of interest to activate cell growth factors.

4.6 REFERENCES

132. S. Flor, V. T., M. Contin1, C. Dobrecky and S. Lucangioli, Spectroscopic approach of the association of heparin and its contaminant and related polysaccharides with polymers used in electrokinetic chromatography. *Journal of Chemical and Pharmaceutical Research* 2012, *4* (2), 972-979.

133. David GRANT, W. F. L., Frank B. WILLIAMSON, Infrared spectroscopy of heparin-cation complexes. *Biochemistry Journal* **1987,** *244*, 143-149.

134. Hans, M. L.; Lowman, A. M., Biodegradable nanoparticles for drug delivery and targeting. *Current Opinion in Solid State and Materials Science* **2002,** *6* (4), 319-327.

135. (a) Fuster, M. M.; Wang, L.; Lijuan, Z., Endothelial Heparan Sulfate in Angiogenesis. In *Progress in Molecular Biology and Translational Science*, Academic Press: Vol. Volume 93, pp 179-212; (b) Johnson, Z.; Proudfoot, A. E.; Handel, T. M., Interaction of chemokines and glycosaminoglycans: A new twist in the regulation of chemokine function with opportunities for therapeutic intervention. *Cytokine & Growth Factor Reviews* **2005,** *16* (6), 625-636; (c) Liu, D.; Sasisekharan, R.; Hari, G. G.; Robert, J. L.; Charles A. HalesA2 - Hari G. Garg, R. J. L.; Charles, A. H., Chapter 25 - Role of Heparan Sulfate in Cancer. In *Chemistry and Biology of Heparin and Heparan Sulfate*, Elsevier Science: Amsterdam, 2005; pp 699-725; (d) Tumova, S.; Woods, A.; Couchman, J. R., Heparan sulfate proteoglycans on the cell surface: versatile coordinators of cellular functions. *The International Journal of Biochemistry & Cell Biology* **2000,** *32* (3), 269-288.

136. Lee, G. Y.; Kim, S. K.; Byun, Y., Glucosylated heparin derivatives as non-toxic anti-cancer drugs. *Journal of Controlled Release* **2007,** *123* (1), 46-55.
137. Lee, D. Y.; Kim, S. K.; Kim, Y. S.; Son, D. H.; Nam, J. H.; Kim, I. S.; Park, R. W.; Kim, S. Y.; Byun, Y., Suppression of angiogenesis and tumor growth by orally active deoxycholic acid-heparin conjugate. *Journal of Controlled Release* **2007,** *118* (3), 310-317.
138. Rajangam, K.; Behanna, H. A.; Hui, M. J.; Han, X.; Hulvat, J. F.; Lomasney, J. W.; Stupp, S. I., Heparin Binding Nanostructures to Promote Growth of Blood Vessels. *Nano Letters* **2006,** *6* (9), 2086-2090.
139. (a) Fux, L.; Ilan, N.; Sanderson, R. D.; Vlodavsky, I., Heparanase: busy at the cell surface. *Trends in Biochemical Sciences* **2009,** *34* (10), 511-519; (b) Sun, L. M. H. Q. C. H. Q. Y. C. H. A. C. J. R. K. X., Modulating the interaction of CXCR4 and CXCL12 by low-molecular-weight heparin inhibits hepatic metastasis of colon cancer. *Invest New Drugs* **2012,** *30* (2), 508-517.
140. Liu, Z.; Jiao, Y.; Wang, Y.; Zhou, C.; Zhang, Z., Polysaccharides-based nanoparticles as drug delivery systems. *Advanced Drug Delivery Reviews* **2008,** *60* (15), 1650-1662.
141. (a) Bertrand, N.; Gauthier, M. A.; Bouvet, C.; Moreau, P.; Petitjean, A.; Leroux, J.-C.; Leblond, J., New pharmaceutical applications for macromolecular binders. *Journal of Controlled Release* **2011,** *155* (2), 200-210; (b) Canali, M. M.; Pedrotti, L. P.; Balsinde, J.; Ibarra, C.; Correa, S. G., Chitosan enhances transcellular permeability in human and rat intestine epithelium. *European Journal of Pharmaceutics and Biopharmaceutics* **2012,** *80* (2), 418-425.
142. (a) Jiao, Y.; Ubrich, N.; Marchand-Arvier, M.; Vigneron, C.; Hoffman, M.; Lecompte, T.; Maincent, P., In vitro and in vivo evaluation of oral heparin-loaded polymeric nanoparticles in rabbits. *Circulation* **2002,** *105* (2), 230-235; (b) Hoffart, V.; Ubrich, N.; Lamprecht, A.; Bachelier, K.; Vigneron, C.; Lecompte, T.; Hoffman, M.; Maincent, P., Microencapsulation of low molecular weight heparin into polymeric particles designed with biodegradable and nonbiodegradable polycationic polymers. *Drug Delivery: Journal of Delivery and Targeting of Therapeutic Agents* **2003,** *10* (1), 1-7.
143. Lamprecht, A.; Ubrich, N.; Maincent, P., Oral low molecular weight heparin delivery by microparticles from complex coacervation. *European Journal of Pharmaceutics and Biopharmaceutics* **2007,** *67* (3), 632-638.
144. Mundargi, R. C.; Babu, V. R.; Rangaswamy, V.; Patel, P.; Aminabhavi, T. M., Nano/micro technologies for delivering macromolecular therapeutics using poly(d,l-lactide-co-glycolide) and its derivatives. *Journal of Controlled Release* **2008,** *125* (3), 193-209.
145. Jiao, Y. Y.; Ubrich, N.; Hoffart, V.; Marchand-Arvier, M.; Vigneron, C.; Hoffman, M.; Maincent, P., Preparation and Characterization of Heparin-Loaded Polymeric Microparticles. *Drug Development and Industrial Pharmacy* **2002,** *28* (8), 1033-1041.
146. Ceballos, A.; Cirri, M.; Maestrelli, F.; Corti, G.; Mura, P., Influence of formulation and process variables on in vitro release of theophylline from directly-compressed Eudragit matrix tablets. *Il Farmaco* **2005,** *60* (11-12), 913-918.
147. Trapani, A.; Di Gioia, S.; Ditaranto, N.; Cioffi, N.; Goycoolea, F. M.; Carbone, A.; Garcia-Fuentes, M.; Conese, M.; Alonso, M. J., Systemic heparin delivery by the pulmonary route using chitosan and glycol chitosan nanoparticles. *International Journal of Pharmaceutics* **2013,** *447* (1–2), 115-123.
148. Tang, D.-W.; Yu, S.-H.; Ho, Y.-C.; Mi, F.-L.; Kuo, P.-L.; Sung, H.-W., Heparinized chitosan/poly(γ-glutamic acid) nanoparticles for multi-functional delivery of fibroblast growth factor and heparin. *Biomaterials* **2010,** *31* (35), 9320-9332.
149. Johnson, Z.; Proudfoot, A. E.; Handel, T. M., Interaction of chemokines and glycosaminoglycans: A new twist in the regulation of chemokine function with opportunities for therapeutic intervention. *Cytokine & Growth Factor Reviews* **2005,** *16* (6), 625-636.
150. Nilasaroya, A.; Poole-Warren, L. A.; Whitelock, J. M.; Jo Martens, P., Structural and functional characterisation of poly(vinyl alcohol) and heparin hydrogels. *Biomaterials* **2008,** *29* (35), 4658-4664.
151. Sasisekharan, R.; Shriver, Z.; Venkataraman, G.; Narayanasami, U., Roles of heparan-sulphate glycosaminoglycans in cancer. *Nat Rev Cancer* **2002,** *2* (7), 521-528.
152. Freitas, S.; Merkle, H. P.; Gander, B., Microencapsulation by solvent extraction/evaporation: reviewing the state of the art of microsphere preparation process technology. *Journal of Controlled Release* **2005,** *102* (2), 313-332.
153. Delgado, A. V.; González-Caballero, F.; Hunter, R. J.; Koopal, L. K.; Lyklema, J., Measurement and interpretation of electrokinetic phenomena. *Journal of Colloid and Interface Science* **2007,** *309* (2), 194-224.
154. (a) Peniche, C.; Argüelles-Monal, W.; Davidenko, N.; Sastre, R.; Gallardo, A.; San Román, J., Self-curing membranes of chitosan/PAA IPNs obtained by radical polymerization: preparation, characterization and interpolymer complexation. *Biomaterials* **1999,** *20* (20), 1869-1878; (b) Tang, E. S. K.; Huang, M.; Lim,

L. Y., Ultrasonication of chitosan and chitosan nanoparticles. *International Journal of Pharmaceutics* **2003,** *265* (1–2), 103-114.
155. M A Krayukhina, N. A. S. a. I. A. Y., ChemInform Abstract: Polyelectrolyte Complexes of Chitosan: Formation, Properties and Applications. *ChemInform* **2009,** *40* (18).
156. Ma, O.; Lavertu, M.; Sun, J.; Nguyen, S.; Buschmann, M. D.; Winnik, F. M.; Hoemann, C. D., Precise derivatization of structurally distinct chitosans with rhodamine B isothiocyanate. *Carbohydrate Polymers* **2008,** *72* (4), 616-624.
157. Tscharnuter, W., Photon Correlation Spectroscopy in Particle Sizing. In *Encyclopedia of Analytical Chemistry*, John Wiley & Sons, Ltd: 2006.
158. Rinaudo, M., Chitin and chitosan: Properties and applications. *Progress in Polymer Science* **2006,** *31* (7), 603-632.
159. Anderson, J. M.; Shive, M. S., Biodegradation and biocompatibility of PLA and PLGA microspheres. *Advanced Drug Delivery Reviews* **1997,** *28* (1), 5-24.
160. Domard, A., pH and c.d. measurements on fully deacetylated chitosan: application to CuII polymers interactions. *Int J Biol Macromol* **1987,** *9*, 98-104.
161. Denuziere, A.; Ferrier, D.; Damour, O.; Domard, A., Chitosan-chondroitin sulfate and chitosan-hyaluronate polyelectrolyte complexes: biological properties. *Biomaterials* **1998,** *19*, 1275-1285.

Synthesis of a Biocompatible, Biodegradable and Bioactive Bilayer Dressing for Wound Healing

CHAPTER 5

5.1 INTRODUCTION

Acute wounds in normal, healthy individuals heal through an orderly sequence of physiological events that include hemostasis, inflammation, epithelialization, fibroplasia, and maturation. When this process is altered or stalled, a chronic wound may develop and is more likely to occur in patients with underlying disorders such as peripheral artery disease, diabetes, venous insufficiency, nutritional deficiencies, and other disease states. Chronic wounds are defined as lesions that do not heal in normal conditions, in an orderly set of stages and in a predictable amount of time the way most wounds do. Chronic wounds often remain in inflammatory stage for too long and the precise balance between production and degradation of collagen is lost, and degradation plays too large a role[162]. Chronic ulceration commonly affects the lower extremities with a prevalence that ranges between 0.18 and 1.3 percent in the adult population.

Vascular diseases in combination with concomitant pathologies such as diabetes and/or cardiovascular or cerebrovascular disorders are frequent problems commonly treated in clinic. Vascular pathologies lead to cutaneous lesions in the lower limbs which are often complicated by ischemia. Actual treatments for venous and diabetic ulcers include the application of hydrogels in combination with cells or biological skin substitutes[163]. However, these topical treatments for skin wounds have not shown consistent results in terms of promoting healing[164]. Actually, new combined tissue engineering products consisting on 3D degradable hydrogels bioactivated with growth factors, and low molecular weight molecules that facilitate wound closure by directing keratinocyte/fibroblast migration and promoting vascular network formation (angiogenesis) are fast being developed for the treatment of this kind of skin lesions[165].

Wound healing will be favored if re-epithelization, connective tissue fiber regeneration, and angiogenesis are stimulated in the damaged tissue. However,

chronic non-healing wounds appear when these natural phenomena are impaired by tissue ischemia, bacterial infections, and/or chronic inflammation.[166] Therefore, natural or artificial compounds based on biodegradable and biocompatible polymeric HG loaded with bioactive drugs, that promote the former processes and/or prevent the latter may represent good candidates for the treatment of chronic wounds.

An ideal dressing for skin wound regeneration must fulfill the following requirements:

-Keeps a moist environment, which allows cells colonization and proliferation in the wound.

-Releases bioactive molecules that promote regeneration. These bioactive molecules should ideally have pro-angiogenic, anti-microbial and re-epithelialization properties, and modulate the activity of growth factors involved in regeneration process, such as fibroblast growth factor (FGF) or vascular endothelial growth factor (VEGF).

-Protect the wound from possible pathogens and maintain a hydrated environment.

-Biodegradates during the regeneration process.

Hydrogels (HGs) based on natural or synthetic polymers have become especially attractive as matrices for regenerating and repairing a wide variety of tissues and organs[167]. HGs can be classified as 'physical' or 'chemical' depending on the nature of the crosslinking bonds. Physical HGs are reversible polymeric networks due to the stabilization of the structure is based on weak interactions, i.e. hydrogen bonds, dipole-dipole interactions or ionic interactions. In contrast to chemical HGs, which are irreversible networks, due to the fact that the structure stabilization is based on covalent crosslinks.

The use of HGs or membranes as biomaterials requires the study of their structure and mechanical properties[168]. The basic requirements of a biomaterial to be suitable for tissue engineering are the following: biocompatibility, biodegradability, good mechanical properties and resistance, but at the same time

high elasticity to allow an easy manipulation, optimal size and if it is possible, be inexpensive for high scale production in the industry[169].

Among the natural polymers forming HG, an important role is played by polysaccharides because they are either components of, or have macromolecular properties similar to, the natural extracellular matrix (ECM). Hyaluronic acid (HA) is a mucopolysaccharide found in various tissues in the organism. It presents high hydrophilicity, biocompatibility, biodegradability and non immunogenicity which makes it very interesting for tissue engineering and drug delivery applications[170]. Moreover, being applid externally to a skin wound, HA promotes epithelial migration and differentiation, improves angiogenesism and enhances collagen production. Its industrial production is based on microbial fermentation, enabling the scaling up of derived products and avoiding the risk of animal-derived pathogens. However, polymers based only on HA undergo a fast degradation by hyaluronidase *in vivo*[171]. Several attempts were made to counteract these degradative processes, and new materials with similar compatibility and bioactivity to HA, but more stable against enzymatic attach were prepared for their application in new biomaterials formulations, mainly for soft tissue regeneration or delivery of biologically active substances.

Gelatin is obtained by thermal denaturation or physical and chemical degradation of collagen, the most widespread protein in the body occurring in most connective tissues as skin, tendon and bone. The present wide interest in gelatin is mainly due to its biodegradability and non-immunogenecity. Most frequent uses in the biomedical field include hard and soft capsules, microspheres, sealants for vascular prostheses, wound dressing and adsorbent pad for surgical use, as well as membranes for tissue regeneration applications[172]. Gelatin undergo a sol-gel transition in aqueous media at remperatures around 40 ºC due to a conformational disorder–order transition of the gelatin chains which form thermoreversible networks by the association of gelatin helices in junction zones stabilized by hydrogen bonds. The mechanism of gelation and the properties of gelatin gels have been extensively investigated.[173,174] The main disadvantage of gelatin as a biomaterial is its poor mechanical properties[175]. Therefore, thermal and mechanical

stability of gelatin in aqueous media should be improved by crosslinking in order to be used in long-term biomedical applications.[176]

In this work, HA was combined with gelatin and the mixture was crosslinked with different crosslinking agents in order to improve its mechanical properties and enzyme degradability. Glutaraldehyde (GTA) is the most common chemical crosslinking agent used to get gelatin networks, however, it presents a high toxicity and secondary calcification problems[177]. For this reason, genipin and other biocompatible physical crosslinking agents were studied in this work as an alternative to GTA. Genipin is an aglycone derivative from an iridoid glycoside called geniposide, obtained via enzymatic hydrolysis with β-glucosidase[178]. Typically, genipin has been used in Chinese medicine for its antiphlogistic, antiinflammatory, diuretic, choleretic and haemostatic properties for many years, but is now being introduced as a crosslinking agent for pharmaceutical applications. Genipin has been approved for food use in Japan, Korea, Taiwan and in southeastern Asia.

Semi-interpenetrating Polymer Networks (SIPNs) are composed of one linear polymer entrapped within the network of another polymer. The IUPAC definition is: 'A polymer comprising one or more networks and one or more linear or branched polymer(s) characterized by the penetration on a molecular scale of at least one of the networks by at least some of the linear or branched macromolecules'[179]. The use of SIPN formed by biodegradable polymers as gelatin and sodium hyaluronate is very common in tissue engineering applications, such as the replacement or repair of a wide range of diseased tissues and organs[180].

Gelatin-HA crosslinked hydrogel was loaded with proadrenomedulina (PAMP), a peptide that behaves as a potent pro-angiogenic factor. Angiogenesis process is the formation of new blood vessels from preexisting ones and it is a physiological process that takes part in embryogenesis, growth, wound healing, and the endometrial cycle[181]. PAMP is an amidated, regulatory peptide which is known as a potent hypotensive and vasodilatory agent[182]. PAMP exhibits a potent angiogenic potential at femtomolar concentrations, whereas classic angiogenic factors such as VEGF and adrenomedullin mediate a comparable effect at nanomolar concentrations[183]. Exposure of endothelial cells to PAMP increases gene expression

of other angiogenic factors such as adrenomedullin, VEGF, bFGF, and platelet-derived growth factor (PDGF)[8].The ability of PAMP to promote angiogenesis can be used as a means to increase vascularization in specific tissue areas or to treat patients with ischemic diseases[184]. PAMP also possesses antimicrobial activity against Gram-negative microorganisms[185] and it is expressed at high levels in the integument, especially by the keratinocytes and all the secretory cells of the skin glands, suggesting that PAMP may be exerting a protective role at this location and might constitute a natural mechanism of response when skin wounding occurs.

Segmented polyurethanes (SPUs) have been widely used in biomaterials field for various commercial and experimental blood-contacting and tissue-contacting applications such as vascular prostheses, blood pumps, endotracheal tubes, mammary prostheses, heart valves, etc[186]. SPUs are polyurethanes composed by a hard segment which confer the mechanical properties and a soft segment that gives the elasticity, forming in combination an elastomeric physical structure[187]. Soft segment is formed by a flexible macrodiol, which is able to form an urethane bond with a diisocyanate[188]. The hard segment can be composed by two diisocyanate molecules interconnected through the urethane bond with a short diol, which is generally known as the 'chain extender', thus a macromolecular segment rich in diisocyanate groups may be developed with its length being easily adjusted on demand. One of the main problems remained for the conventional PUs as biodegradable materials is their diisocyanate raw materials, especially those aromatic diisocyanates such as 4,4-di-phenylmethane or toluene diisocyanate. The carcinogenic and mutagenic aromatic diamines have been described to be the potential degradation products, thereby making them undesirable for *in vivo* use[189]. Diisocyanates derived from amino acids constitute an alternative to aromatic isocyanates as they provide biodegradable PUs that are expected to yield only non-toxic degradations products. L-lysine methyl ester diisocyanate (LDI) is a very attractive amino acid derived diisocyanate because it is a hydrolytic product, non-toxic and lysine is vital to the living system.

Polycaprolactone (PCL), an ideal scaffolding material owing to its biodegradability and biocompatibility, is a semicrystalline polymer with a relatively

low melting temperature (T_m = 64 °C). It is approved by the U.S. Food and Drug Administration, and it has good mechanical properties when it is biaxially stretched[190]. Because of its inherent biodegradability and biocompatibility, PCL has been widely explored for its potential use in medicine, such as membranes for supporting the growth of fibroblasts and osteoblasts to improve the tissue regeneration of articular cartilage defects[191]. The reason lies on the fact that the ester group is more susceptible to chemical and enzymatic hydrolysis, a condition that is easily achieved *in vivo*.

Triblock copolymers of poly(ethylene oxide)-poly(propylene oxide)-poly(ethylene oxide) (PEO-PPO-PEO), commercially known as Pluronic®, are surface active molecules with amphiphilic characteristics which have been applied in drug delivery systems, in gene delivery, as biological adjuvants and so on due to their drug loading capacity and acceptable biocompatibility[192]. The use of Pluronic® in combination with PCL to form SPU segments is very interesting because they are capable of sensitizing multidrug-resistant cells and increasing drug transport across cellular barriers[193]. Besides, the combination of both polymers overcomes the undesirable gel properties associated with Pluronic®, such as weak mechanical strength and rapid erosion. In this work, copolymers made of Pluronic L61 and PCL were synthesized giving the soft segment of the SPU.

Poly(tetramethylene ether) glycol or poly(tetramethylene oxide) (PTMG), is a very common and suitable polymer to obtain elastic fibers such as Spandex (elastan) for stretchable fabrics and for polyurethane resins. They are used in the manufacture of artificial skin. In this work, the PTMG was combined with LDI to obtain the hard segment of the SPU with flexible mechanical properties[194]. In this way, segmented polyurethanes (SPUs) containing polycaprolactone (PCL) and pluronic (PL61) as components of the soft segment of SPU, and PTMG with the amino acid derived diisocyanate LDI as the hard segment have been prepared. This SPU can be applied as scaffold in the biomaterials field due to their good physicochemical and mechanical properties while exhibiting an acceptable biological performance.

Bemiparin is a modulator of thrombotic and restenotic processes[195] and also is able to form active complexes with growth factors (FGF and VEGF etc.), modulating the biological activity of these factors in tissue repairing[196], and specifically in wound healing.

5.2 AIMS OF THE WORK

This chapter is devoted to the preparation and characterization of a bilayer wound dressing based on a first layer, of a hydrophilic hydrogel, and a second layer of segmented polyurethane, both layers being biocompatible, biodegradable and biore-absorbable (Figure 75). Therefore, this chapter describes, on the one hand, the preparation of hydrogels (HG) formed by gelatin and sodium hyaluronate crosslinked with different crosslinking agents, getting a SIPN, where both polymers provide a synergic effect in the mechanical properties and thermal stability. The swelling and rheological properties of the obtained physical and chemical hydrogels were compared depending on the nature of the crosslinking agent. The optimal HG in terms of mechanical and rheological properties was loaded with a bioactive peptide, the proadrenomedullin (PAMP)[197], with pro-angiogenic, anti-microbial and re-epithelialization properties. On the other hand, it is described the synthesis and characterization of a biodegradable and biocompatible segmented polyurethane (SPU) based on *L*-lysine methyl ester diisocyanate (LDI), poly(tetramethylene glycol ether) (PTMG), polycaprolactone diol (PCL), and pluronic L-61 (PL61), to be used as a protective layer, avoiding pathogens colonization in the wound. Besides, this protective layer acts as a drug carrier of bemiparin loaded nanoparticles, which allow the modulation of growth factors, such as FGF and VEGF[198]. The combination of both layers, the HG with PAMP and the polyurethane with bemiparin-based NPs, constitutes a sophisticated and promising bioactive, biodegradable and biocompatible bilayer dressing for wound healing, that release in a time-dependent fashion, different signaling molecules that facilitate skin regeneration processes[199]. *In vivo* experiments were carried out using rat and rabbit model to test the bioactivity of this system.

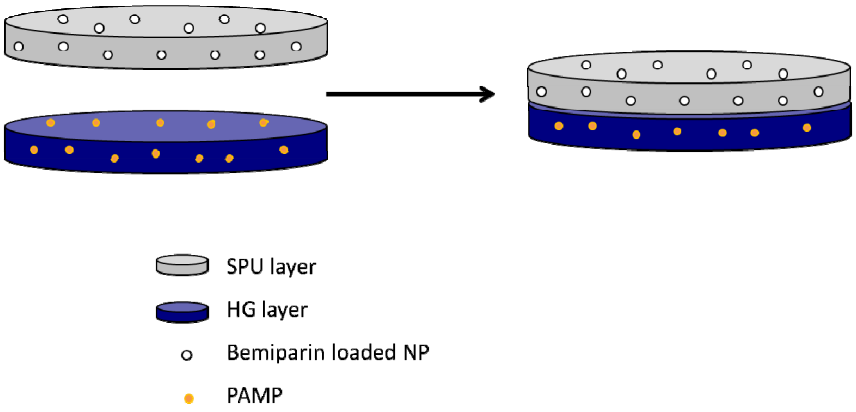

Figure 75. Scheme of the bilayer system prepared.

5.3 Materials and Methods

5.3.1 Materials

Gelatin A type from porcin skin, 240-260 bloom, was purchased from Sigma-Aldrich, sodium hyaluronate oral grade with a M_w = 100 kDa was obtained from Bioiberica, genipin was purchased from Challenge Bioproducts Co. Sodium tripolyphosphate (TPP, 85%), D-(-)-salicin (99%), glycerol phosphate disodium salt (GP, 98%), poly(ethylene glycol) diglycidyl ether (PTMG), with a hydroxyl average number 55.1 (M_w = 2000, Terathane®2000), poli(caprolactone diol) (PCL) with 2000 molecular weight, L-lysine methyl ester diisocyanate (LDI), Pluronic-L61 (PL61) with 2,000 molecular weight , tetrahydrofuran (THF), dimethyl formamide anhydrous (DMF) and stannous 2-ethyl-hexanoate were purchased from Aldrich. All these reagents were used without further purification. Proadrenomedullin (PAMP) was obtained from Phenix Pharmaceuticals (Mw = 2460.87 Da) and it was dissolved in phosphate buffer solution pH 7.4 (PBS). PBS buffer (140 mM NaCl, 10 mM phosphate

buffer, 3 mM KCl), pH= 2 buffer (citrate / hydrochloric acid) and pH= 10 buffer (boric acid / potassium chloride / sodium hydroxide) were purchased from Merck-Millipore in powder and they were disolved in 1 L, 0.5 L y 0.5 L of Milli-Q water, respectively.

5.3.2 Methods

5.3.2.1 Hydrogel preparation

Hydrogels (HGs) were prepared by casting method. 6 mL of an aqueous gelatin solution (100 mg/mL) and 8 mL of an aqueous hyaluronate solution (50 mg/mL) were placed in a flask at 40 °C. Different concentrations of the crosslinking agent were added to get 0.5, 1, 2 or 5%wt respect to the polymeric mixing. The solution (polymers and crosslinking agent) was stirred for 10 min at 200 rpm, sonicated for 5 min and finally it was poured in a teflon mold avoiding any air bubbles. The hydrogel was obtained by casting at room temperature during 48 h. The xerogel was washed several times (3-5) with distilled water and cut into 1 or 2 cm diameter spherical discs that were finally dried at room temperature.

5.3.2.2 Synthesis of SPU

5.3.2.2.1 Chain extender synthesis (Soft Segment)

The chain extenders were synthesized using PCL-diol and PL61 at a molar ratio of 1:1. A solution of PCL-diol (6.62 g, 3.3 mmol) in anhydrous DMF (50 mL) under nitrogen was heated at 135 °C during 20 min in a two-neck flask. Then stannous octoate (2-ethylhexanoate tin (II)) was added dropwise (30 µL, 0.093 mmol), and finally pluronic-L61 (7.04 g, 6.96 mL, 3.5 mmol) was added. The stirred solution was allowed to react for 24 h at 135 °C and then cooled down to room temperature. The chain extender obtained was designated as [50PCL-50PL61].

5.3.2.2.2 Polyurethane synthesis

The SPU was synthesized by the traditional two-step method; in the first one, a pre-polymer was obtained by reacting a slight excess of LDI with PTMG in the presence of stannous octoate at 60 °C for 2 h to form the hard-block segment. In the second step, this resultant prepolymer (hard segment) was reacted with the chain extender (soft segment) to form the SPU. Briefly, the diisocyanate methyl L-Lysine (2.38 g, 2.23 mL, 11.2 mmol) and the PTMG (7.62 g, 3.7 mmol) were mixed in anhydrous DMF (60 mL) and added stannous octoate (30 uL, 0.093 mmol). Secondly, the chain extender was added to the resulting pre-polymer to obtain the segmented polyurethane. The reaction was carried out under nitrogen at 75 °C for 24 h. The resulting polyurethane was precipitated in water and dried under vacuum at 50 °C for 48 h and was designated as SPU321-LDI-[50PCL-diol-50PL61].

5.3.2.2.3 Preparation of SPU membranes

3 mg of the previously prepared SPU were dissolved in 12 mL of THF and poured onto a Teflon mold avoiding bubbles generation. The formed film was allowed to dry overnight at room temperature and then placed under vacuum at 30 ^{o}C for 48 h.

5.3.2.3 Bilayer dressing preparation

5.3.2.3.1 Incorporation of Bemiparin-based NPs into SPU membranes

0.6 mL bemiparin-based NP aqueous dispersion (5 mg/mL) were loaded on 2 cm diameter discs of SPU321-LDI-[50PCL-50PL61] membranes and kept under saturated water vapor atmosphere for 24h. Membranes were dried at room temperature. The bemiparin-based NP formulations employed in the preparation of the loaded SPUs were Eudragit RS PO NP and PMMA-*b*-PMAETMA (98:2) NP,

previously described in chapter 4. Non-loaded NP were also prepared and used as control in the following experiments. In this case, only 0.6 mL distilled water was added on the SPU membranes. The membranes were immersed in liquid nitrogen and transversally cut in order to examine the distribution of the NP throughout the whole thickness of the sample by scanning electron microscope (SEM).

5.3.2.3.2 PAMP incorporation into genipin crosslinked HG

HGs based on 60% wt gelatin, 40% wt sodium hyaluronate and crosslinked with 1% wt genipin were selected to be loaded with PAMP. 0.5 mL or 1 mL of PAMP solution (2 mM in PBS buffer) was added onto xerogel discs of 1 cm or 2 cm diameter respectively. The PAMP loaded HG discs were kept under saturated water vapor atmosphere for 24 h to facilitate PAMP diffusion throughout the HG structure. Control samples were prepared without PAMP, under the same experimental conditions.

5.3.2.3.3 Bilayer dressing (HG and SPU) preparation

HG was placed onto SPU membrane previously loaded with the described NP. 0.5 mL of PAMP solution (2 mM PBS solution) was added on the HG and it was kept under saturated water vapor atmosphere for 24 h. The system was kept between two parafilm layers until used in order to avoid dehydration of the dressing. Control bilayer systems were prepared under the same experimental conditions without the bioactive molecules (bemiparin-loaded NP and/or PAMP).

5.3.2.4 Wound Healing Capacity Evaluation.

5.3.2.4.1 *In vivo* experiments of pro-angiogenic properties of the bilayer dressing in mouse model

The three types of bilayer dressings tested are described, an unloaded bilayer system (without bemiparin neither PAMP), a bemiparin loaded bilayer system (bemiparin NPs were charged on the SPU layer of the bilayer system), and both bioactive compounds loaded bilayer system (bemiparin NPs were charged on the SPU layer and PAMP was charged on the HG layer of the system). These bilayer dressings were placed in a pocket made in the dorsal dermis of genetically modified mice expressing green fluorescent protein (GFP) in the blood vessels. After 5 days, the membranes were removed and fixed in buffered formalin. Photographs were made with a magnifying glass membranes equipped with ultraviolet light and the following results were obtained. Images correspond to HG discs removed after 14 days of implantation and embedded in resin were obtained by an optical microscopy. Discs were previously stained with hematoxylin-eosin.

5.3.2.4.2 Wound healing capacity of the bilayer system: *in vivo* experiments on rabbit model

The animal used to test the bilayer systems was New Zealand white rabbits (male). Animals weighting 3.3 ± 0.2 Kg (n = 18), were caged under standard light and temperature conditions, with free access to food and water throughout the study. All the experimental procedures were approved by the local committee for animal welfare and were carried out in accordance with the European Community Council Directive (86/609/EEC). The induction of ischemia in the rabbit ear was carried out blocking its central blood vessels. The rabbit ear contains three main arteries, one running through the center and the others near the edges, which provide all the blood supply to this organ. In this study, it was ligated the central artery and vein were ligated at two points at the base of the ear using silk sutures (ASSUSILK 3/0,

Assut Europe, Rome, Italy) and the portion of the artery located between the sutures was excised to ensure complete blood flow interruption. The extent of the ischemic insult was assessed by measuring transcutaneous oxygen pressure in the ear before and after ligation and sectioning of the central artery using a TCM-4 (Radiometer Copenhagen, Madrid, Spain). With this inducted ischemia we simulated patients with a disruption of the normal structure and function of the skin and underlying soft tissue. The use of normoxic rabbits represents a normal patient model, without vascular disorders. Ischemic rabbits were used as model of patients with vascular disorders.

Rabbits with normoxic (n=9) or with ischemic ears (n=9) were anesthetized with a mixture of ketamine hydrochloride (Ketolar, Parke-Davis, 70 mg/Kg), diazepam (Valium, Roche, 1-5 mg/Kg) and chlorpromazine (Largactil, Rhone-Poulenc, 1.5 mg/Kg) administered intramuscularly. These rabbits were subjected to circular wounds in both ears, as described Bujan et al.[200] Briefly, a cylindrical cutting device was used to produce circular wounds, 2 cm in diameter, in the dorsal side of each ear. The wounds affected the perichondrium lining the ear cartilage (Figure 76). The bilayer dressings were incorporated to the wound, and immobilized using non-absorbable suture attached to the edges of the defect, following the diagonals of a regular pentagon (Figure 77). After surgery, each animal was fitted with a plastic neck collar (Bouvet, Madrid, Spain) to prevent them from scratching the wounds. All wounds were evaluated 14 days after surgery. Rabbit ear wounds were treated with 3 different kinds of samples: 1) untreated controls (n=3 normoxic + 3 hypoxic), 2) bemiparin NP (n=3 normoxic + 3 hypoxic), 3) a combination of both PAMP and bemiparin NP (n=3 normoxic + 3 hypoxic).

After 14 days treatment, at the macroscopic level, the extent of wound contraction and reepithelialization was measured. Photographs of the wounds were taken just after producing the defect and at the time of sacrifice. Computerized image analysis (ImageJ for Windows XP, NIH Image) was used to establish the overall surface area of each wound, as well as the non-epithelialized area at the end of the experiment. These measurements were carried out by two independent researchers blinded to the treatment and were expressed as mean ± standard deviation.

At the end of the experiment, tissue specimens were fixed in F-13 fixative aqueous solution (60% ethanol, 20% methanol and 7% poly(ethylenglycol) 300), dehydrated, and embedded in paraffin. Tissue sections (5 µm thick) were used to perform histological staining (Hematoxylin-eosin, Masson's Trichrome) and immunehistochemical procedures with antibodies against α-actin or myosin (both from Sigma Chemical Co., St Louis, MO) and against macrophages (RAM-11 clone, Dako, Denmark).

Areas of wound contraction and re-epithelialization, as well as microscopical parameters, were compared among treatments by ANOVA followed by the Mann-Whitney *U* test. Differences with $p<0.05$ were considered statistically significant.

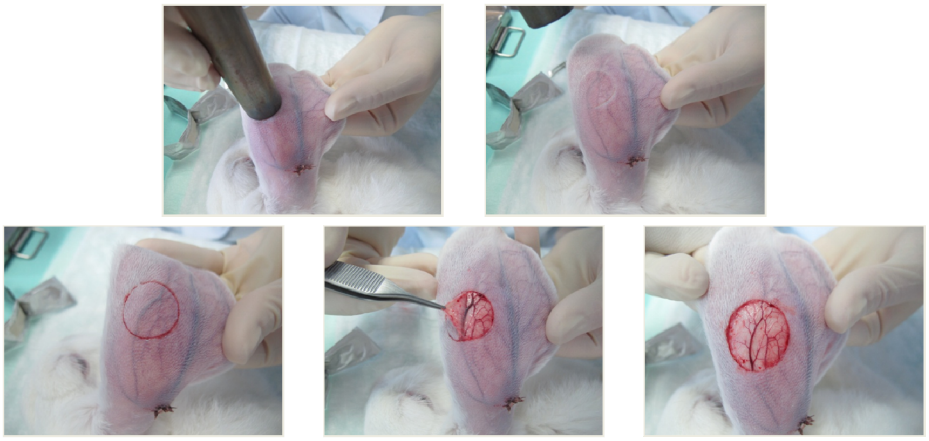

Figure 76. Pictures of wound production process in the ear rabbit.

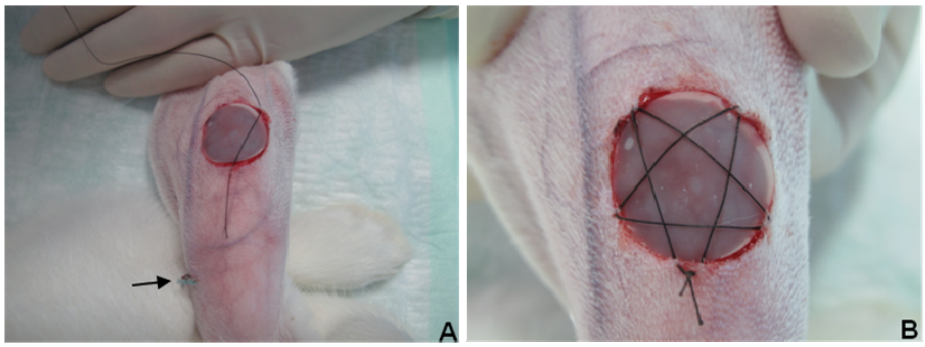

Figure 77. Bilayer dressing immobilization using a non-absorbable suture (A) suture followed the diagonals of a regular pentagon (B). The arrow indicates the place were blood circulation was blocked in order to obtain the ischemic model.

5.3.3 Characterization techniques

5.3.3.1 Swelling study

Dried HG discs (1 cm diameter and 2 mm height, 20-30 mg) were weighed accurately placed into flasks with 10 mL of buffered solutions (pH = 2, 7.4 and 10) and kept in a thermostated bath at 37 °C. The hydration degree,%H, was defined as:

$$\%H = \frac{W_t - W_o}{W_o} \times 100$$ **Equation X**

here W_t is the hydrogel weight in buffered medium at time *t* and W_o is the weight of dried hydrogel. Measurements were carried out in triplicate. The equilibrium hydration degree, W_e, was defined as the value at shich hydration degree was constant at least at three different times.

5.3.3.2 ATR-FTIR spectroscopy

The ATR-FTIR characterization was carried out by placing the xerogel between two CaF_2 crystals of 2 mm thick and 25 mm diameter. A Perkin-Elmer Spectrum One FTIR was used in the experiments. The spectral range was stablished from 4000 to 600 cm^{-1}. 32 scans were performed with a resolution of 4 cm^{-1}. Infrared spectra of the polyurethanes were obtained without CaF_2 crystals support, using the same experimental spectra range and resolution, with an average of 50 scans.

5.3.3.3 TGA analysis

Thermogravimetric Analysis (TGA) was performed on a TGA Q500 (TA Instruments), working from 25 to 500 °C at a heating rate of 10 °C/min, under 50 mL/min nitrogen flow.

5.3.3.4 Rheology Characterization

Rheology measurements were carried out using an ARG2 TA Instruments stress-controlled oscillatory rheometer using parallel plate geometry. Sol state samples were measured using a top plate of polymethylmethacrylate, 40 mm diameter, and for gel state samples it was used a steel 20 mm diameter plate. Dynamic mechanical analysis (stress-strain tests) was carried out to determine the viscoelastic properties of the HG, to obtain their storage (G') (elastic behavior) and loss (G'') (viscous behavior) moduli. Strain sweeps were performed between $1x10^{-3}$ and 10% strain, setting the normal force at 0.3 N with a frequency of 0.5 Hz. Frequency sweeps were done at 2% strain, 0.3 N normal force, from 0.1 to 100 Hz. On the one hand, strain and frequency sweeps were performed with samples swollen in PBS at equilibrium. On the other hand, time sweeps were carried out with

samples in the sol state at 2% strain, 0.3 N normal force and 0.5 Hz from 0 to 200 min. All the measurements were done at 25 °C. Different kind of crosslinking agents: genipin, glycerol phophate (GP), trypolyphophate (TPP) and salicin, at different concentrations (0, 1, 2 and 5%wt with respect to the polymeric blend) were tested. The sample with 0%wt of crosslinking agent was tested as a control.

5.3.3.5 Differential Scanning Calorimetry measurements

Differential Scanning Calorimetry (DSC) was used to determine the melting temperature (T_m) and the increase of enthalpy associated with the process. An enhaustively dried sample was placed in aluminum pans, which were sealed and heated at a constant rate of 5 °C / min, N_2 flow of 20 mL / min, in the range temperature between -20 to 100 °C. T_m were determined during the second scan of the sample. A DSC8500 Perkin Elmer calorimeter previously calibrated with Indium and Zinc was used in the experiments.

5.3.3.6 NMR characterization

SPUs were characterized by Proton Nuclear Magnetic Resonance spectroscopy (^{1}H-NMR) technique using a Varian Inova-400 MHz instrument. Samples were solved in deuterated chloroform ($CDCl_3$) and recorded at 25 ºC.

5.3.3.7 Molecular weight distributions: SEC characterization

Determination of molecular weight distribution (M_n, M_w) and poldispersity index (PDI) was carried out by size exclusion chromatography (SEC) in a Perkin-Elmer apparatus equipped with an isocratic LC pump 250 and a refractive index detector series 200. A set of 104 and 105 nm PL-gel columns conditioned at 70° C was used to

elute 3 mg/mL samples. The mobile phase was used *N*,*N*-dimethylformamide (DMF) with 0.1% of LiBr at a flow of 0.3 mL / min. Polystyrene standards with molecular weight between 10300 and 480000 Da were used for the calibration.

5.3.3.8 Mechanical properties determination: dynamic mechanical analysis

Dynamic Mechanical Analysis (DMA) was performed on a differential mechanical analyzer DMA METTLER 861e, performing scans temperature between 0 and 80 °C at different frequencies (0.5, 1, 3, 5 and 10 Hz).

5.4 RESULTS AND DISCUSSION

5.4.1 Preparation of the gelatin/hyaluronate HG

The effect of different crosslinking agents on the mechanical strength and swelling behavior of the HGs was investigated. Genipin was used as chemical crosslinker and GP, TPP and salicin as physical crosslinkers (Figure 78). The effects of the crosslinker concentration and pH on the functional properties (mechanical strength and swelling abilities) of the hydrogels were also evaluated.

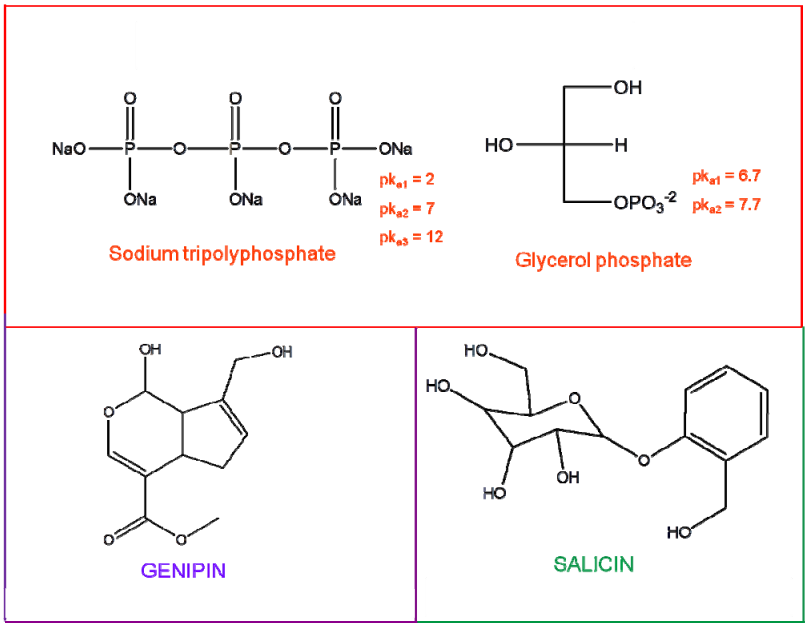

Figure 78. Chemical structures of the crosslinking agents used to get the gelatin-hyaluronate hydrogel.

5.4.2 *Physical Hydrogels*

Three different crosslinkers were used to stabilize and improve mechanical properties of the GE-HA gels.

Glycerolphosphate (GP) and sodium tripolyphosphate (TPP) are compounds naturally found in the body, which are usually used as a source of phosphate in the treatment of unbalance of phosphate metabolism. The addition of GP or TPP to the GE-HA solution promoted the formation of intramolecular interactions, which improved network strength. At basic pH, GP and TPP protect the hydration of the gelatin chains and kept the polymer chains stretched freely in solution. When HGs were crosslinked with GP or TPP in acid solution, the amino groups in gelatin were protonated and interacted with the free phosphate groups resulting in shrinkage of hydrogel. Therefore, HG crosslinked with GP or TPP showed more compact morphology at lower pH, enhancing functional properties.

Salicin, [2-(hydroxymethyl)phenyl-*b*-D-glucopyranoside], is a glycoside obtained from the fruit of the poplar plant (Populus) and willow (Salix) barks and it is the precursor of salicylic acid. It was used by ancient man as an anti-inflammatory, analgesic, and antipyretic prodrug. Salicin possesess an acidic hydroxyl group that can form hydrogen bonds with the amino and carboxylate groups of gelatin and hyaluronate.

In both physical crosslinking (ionic and hydrogen bond), hyaluronate chains are randomLy distributed along the crosslinked gelatin network, forming physical entanglements which strengthening the three dimensional network of the hydrogel.

5.4.3 Chemical Hydrogels

Genipin is a naturally occurring crosslinker extracted from either Gardenia jasmindides Ellis (Asia) or Genipin american (tropical America). In the presence of oxygen, genipin crosslinking leads to the formation of thermal, pH and light-stable blue pigments.[201] The biocompatibility of genipin in humans has not been assessed yet, but it is not cytotoxic in vitro and has been shown to be biocompatible after injection in rats. [202] The crosslinking of the HGs with a chemical crosslinker as genipin, involves the formation of covalent bonds between gelatin and genipin molecules, resulting in a chemically crosslinked matrix containing sodium hyaluronate chains randomLy distributed through Van der Waals interactions (hydrogen bonds, electrostatic interactions, hydrophobic forces, etc). This matrix results in a semi-interpenetrating network (SIPN) as shown in Figure 79.

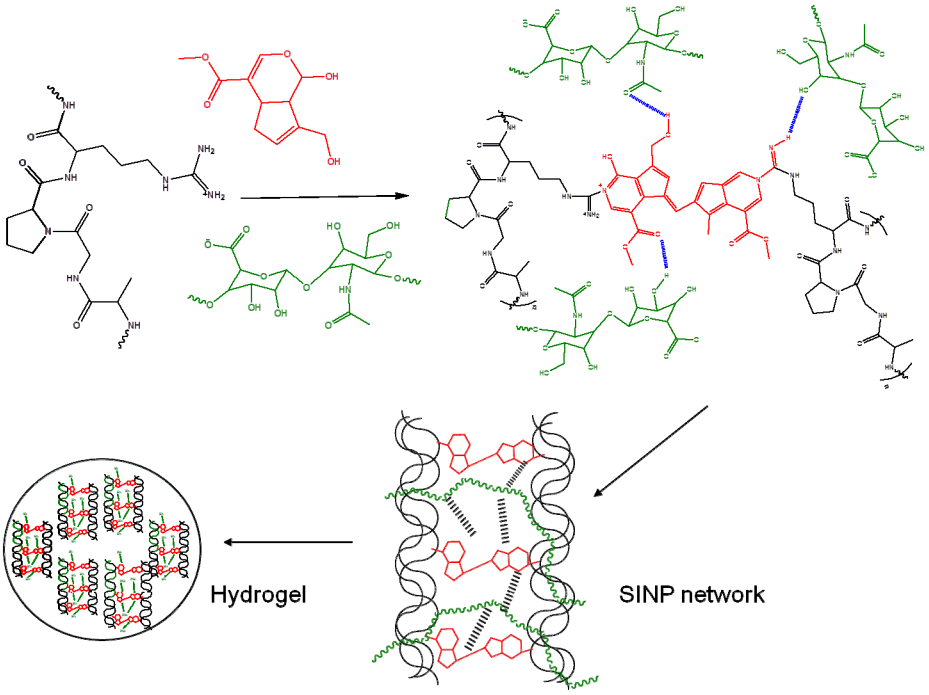

Figure 79. Scheme of the crosslinking of gelatin in the presence of hyaluronate to form the semi-interpenetrating network (SIPN).

5.4.4 ATR-FTIR study

Genipin crosslinking reaction was monitored by infrared spectroscopy technique (Figure 80) following the decrease of the band intensities of the characteristic functional groups (ν_{OH} = 3600 cm^{-1}, 3400 cm^{-1} ν_{NH2} = 1, ν_{CO} = 1660 cm^{-1}) of the hydrogel in the ATR-FTIR spectrum. When the crosslinking reaction occurs hydrogen bonds between the OH, COOH and NH_2 functional groups are produced, showing wider and less intense ATR-FTIR characteristic bands. In addition, it is observed a new carbonyl band at ν_{CO} = 1620 cm^{-1} due to the new covalent bond formed between the gelatin and the genipin, was a different chemical environment from the original carbonyl band (ν_{CO} = 1660 cm^{-1}).

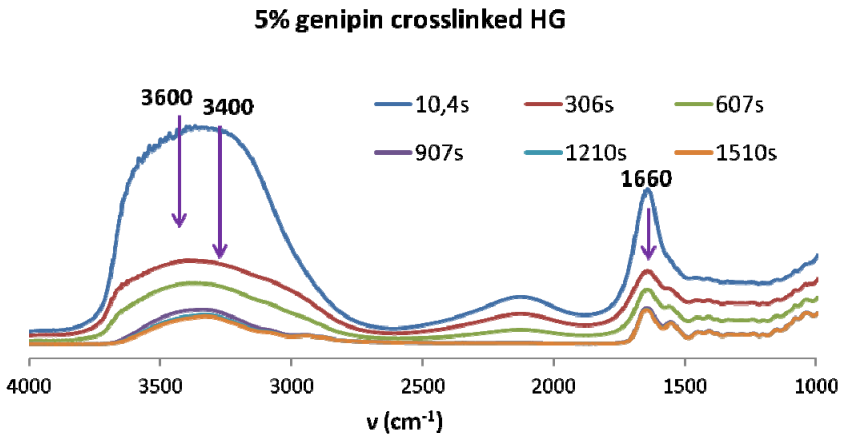

Figure 80. ATR-FTIR spectra of 5% genipin crosslinked HG at different reaction times.

5.4.5 Swelling study

Hydration degree of the hydrogels was measured at 37 °C using buffered solutions at different pH (2, 7.4 and 10). Figure 81 shows hydration degree of the hydrogels crosslinked with different concentrations of genipin at pH = 7.4. Initially the system is in a solid state (xerogel), forming a rigid network. When the system starts to hydrate the polymer chains swell and become more flexible, allowing the penetration of water molecules in the network. When the chain relaxation reaches a minimum energy state, equilibrium between chain relaxation and contraction of the polymeric network is reached, getting a stable level of hydration. The swelling degree of the hydrogels is affected noticeably by the content of the crosslinker, genipin because of the change of the crosslinking density. The level of equilibrium hydration degree in all the cases was very high but it changes from 3000% for the systems crosslinked with 0.5% of genipin, to 1000% for those systems prepared with 5% of genipin.

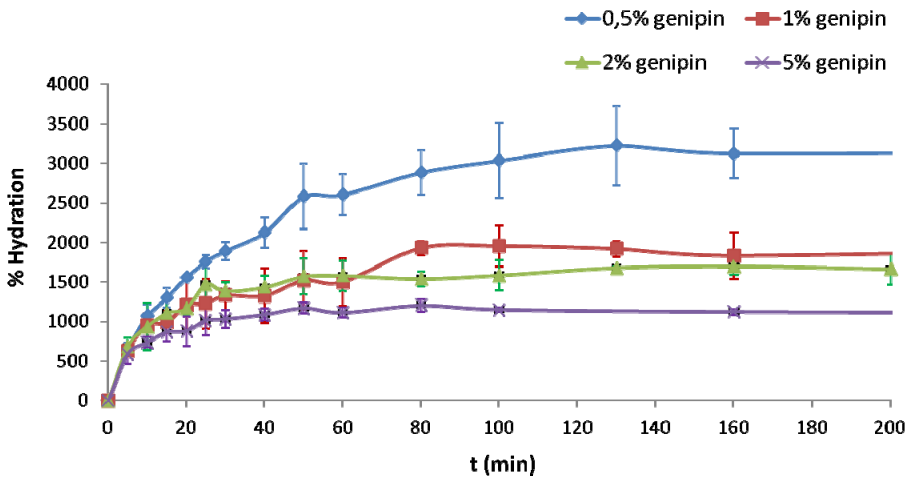

Figure 81.% hydration of genipin crosslinked hydrogels with the swelling time.

The equilibrium hydration degree (W_e) achieved by each of the hydrogel systems crosslinked with 5% of the corresponding crosslinking agent and swollen at different pH is shown in Figure 82. It is observed that the genipin crosslinked HG showed a higher swollen degree than the physical ones, due to the higher stability that confer the covalent bond domains of the HG network and therefore higher capacity to include water molecules into the HG without breaking its three dimensional network structure. A clear effect of the chemical structure of ionic crosslinkers (GP and TPP) in the swelling behavior of the HG was observed. TPP allowed higher swelling degrees than GP due to the presence of more phosphate ionic group that form more ionic crosslinking domains than GP. In the case of salicin, HGs showed a similar swollen degree at any of the pH medium and the equilibrium swelling W_e was similar to TPP crosslinked HG at physiological and basic pH, but not at acidic pH. This can be explained because of the non ionic nature of salicin. HGs crosslinked with salicin are stable due to hydrophobic-hydrophilic interactions and hydrogen bonds formation along the polymeric chains of gelatin and hyaluronate.

With GP or TPP crosslinkers HGs present pK_a values between pH 2 and pH 12 of pk_{a1}(TPP) = 2, pk_{a2}(TPP) = 7, pk_{a3}(TPP) = 12, pk_{a1}(GP) = 6.7, pk_{a2}(GP) = 7.7, and therefore the pH swelling medium greatly affects the swelling properties of the HG. The higher swelling degree was obtained at physiological pH (pH = 7.4). It is due to the ionization of the free amino groups of gelatin. At acid pH, amino groups of

gelatin (pk_a = 7-9) are protonated (NH_3^+) and they are able to form stronger ionic interaction with the free hydroxyl groups of the hyaluronate and/or salicin, and also with the phosphate groups of GP and TPP. This ionic interaction produces a more compact three dimensional network with lower swelling degree. At pH 7.4 the ionization of the amino groups is lower and therefore hydrogen or ionic bonds were formed and a higher swelling degree was obtained. At pH 10 the amino groups are not ionized anymore and only hydrophobic/hydrophilic interactions or hydrogen bonds are responsible of the hydration of the HG.

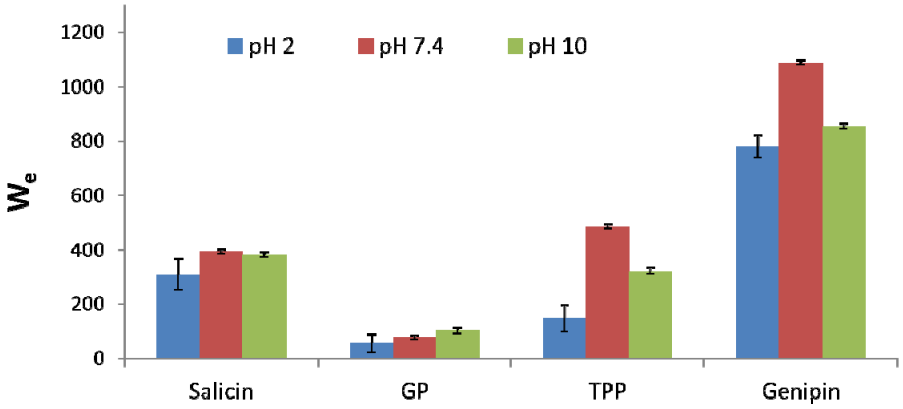

Figure 82. Swelling degree of different hydrogels in the equilibrium, at different pH.

The influence of the crosslinking agent concentration was also studied for each crosslinker at different pH. It was observed that the swelling degree decreased as the concentration of crosslinking agent increased, for all the HG systems as it is shown in Figure 82. Swelling degree of different hydrogels in the equilibrium, at different pH for genipin were represented in Figure 83, but there is not a noticeable influence of the pH.

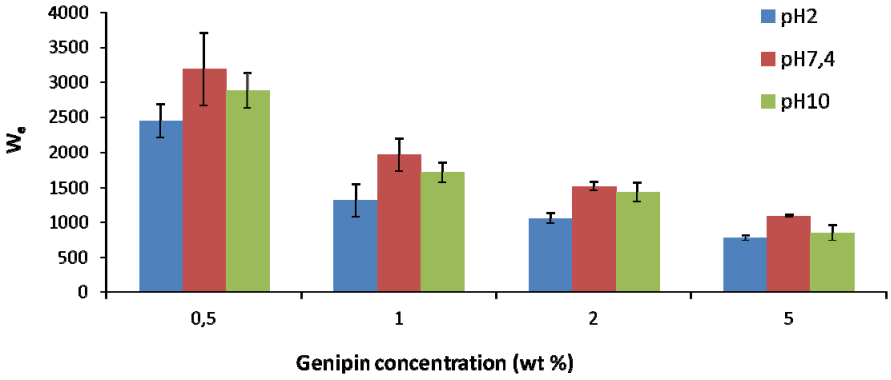

Figure 83. Swelling degree of genipin crosslinked hg in the equilibrium, at different concentration and different ph values.

It was also observed that at pH = 7.4 hydrogels exhibit a faster biodegradation than at pH = 2 and pH = 10. Thus, hydrogels crosslinked with 1% of genipin began to degrade at pH = 7.4 after 48 h whereas at pH = 2 and pH = 10 HG degradation began after the sixth and seventh day respectively. This corroborates that at acid pH, ionic interactions are higher and more compact crosslinked network is obtained. A pH = 10 carbonyl groups of hyaluronate (pK_a = 9.4) are negatively charged and can interact with the free amino groups present in the structure. However, at pH = 7.4 ionic groups are partially ionized and ionic interactions are less, allowing greater penetration of water molecules in the polymeric matrix, which produces a higher degree of hydration and faster degradation.

5.4.6 Degree of crosslinking for chemical HG

The hydration degree measurements allowed the determination of crosslinking density and the average molecular weight between nodes, parameters which define the three dimensional network structure of chemical HGs (irreversible HGs). These parameters determine the mechanical properties, stiffness and elastic behavior of the hydrogels. Considering the Flory-Rehner equation (Equation XI), the

average molecular weight between nodes (M_c) can be determined assuming that in the equilibrium state the sum of free energies is zero:

$$\frac{1}{\overline{Mc}} = \frac{2}{\overline{Mn}} - \frac{\bar{v}\left[\ln(1-v_{2,s}) + v_{2,s} + \chi v_{2,s}^2\right]}{V1} \Big/ \left(v_{2,s}^{1/3} - \frac{v_{2,s}}{2}\right)$$ **Equation XI**

Where M_n is the number average molecular weight of the linear polymer, v is the specific volume of the dry polymer, V_1 corresponds to the molar volume of the solvent, $v_{2,s}$ is the polymer volume fraction at equilibrium, and χ is the solvent-polymer interaction parameter. From the values of average molecular weight between nodes (M_c) the crosslinking density (ρ_x) can be calculated (Equation XII), which is defined as the average number of polymer units between two consecutive nodes. A low crosslinking density gives rise to a more open network, and a higher hydration degree. However, a high crosslinking density implies a lower hydration degree and less deformable hydrogel.

$$\boldsymbol{\rho_x} = \frac{1}{\bar{v}.\overline{M_c}}$$ **Equation XII**

The Flory-Rehner model was applied to hydrogels obtained with different genipin concentrations and M_c and ρ_x were determined for HGs swollen in PBS (pH = 7.4), considering the water molar volume V_1 = 18.1 (mL/mol), the average molecular weight of gelatin M_n = 50000 Da, gelatin density at 25 °C ρ_{GE} = 1.44 g/mL and the interaction parameter gelatin-water tabulated in literature χ_{GE} = 0.49 ± 0.05[203]. The M_c and crosslinking density (ρ_x) values are shown in Table 10. It is noted that increasing the concentration of crosslinking agent, M_c decreases, that is, the length of the polymer chains between two attached points is lower, while the crosslinking density increases.

Table 10. Average molecular weight between nodes and crosslinking density of SIPN crosslinked with different concentrations of genipin.

Genipin concentration (%-wt)	M_c	ρ_x
0.5% genipin	408 ± 48	0.17 ± 0.02
1% genipin	224 ± 15	0.30 ± 0.02
2% genipin	166 ± 31	0.41 ± 0.08
5% genipin	103 ± 10	0.65 ± 0.06

5.4.7 Rheological Characterization: mechanical stability measurements.

Rheological studies allow us to determine and quantify the mechanical properties of the HG when they undergo a certain deformation. Dynamomechanic assays were carried out in order to determine the viscoelastic properties of the prepared HGs. Storage modulus (G'), loss modules (G'') and sol-gel transition were determined.

5.4.7.1 Strain sweeps

Preliminary strain sweeps were conducted in order to determine the linear viscoelastic range (LVR) which is the range in which the HG fulfills the law of Hooke elasticity, $\sigma = G \bullet \gamma$, where σ is the applied stress, G is the relaxation modulus and γ is

the deformation of the material. For the determination of LVR, HGs with different gelatin/sodium hyaluronate weight ratio of 80:20, 60:40 and 50:50 without crosslinking agent were tested. For all the compositions, G' was always greater than G'' for strain values lower than 50%, however overcoming that value G' exceed G'', indicating that hydrogel structure is broken at that point (Figure 84). The composition of 60% gelatin and 40% sodium hyaluronate was selected for further studies, since it provided a high storage modulus value and a wide LVR.

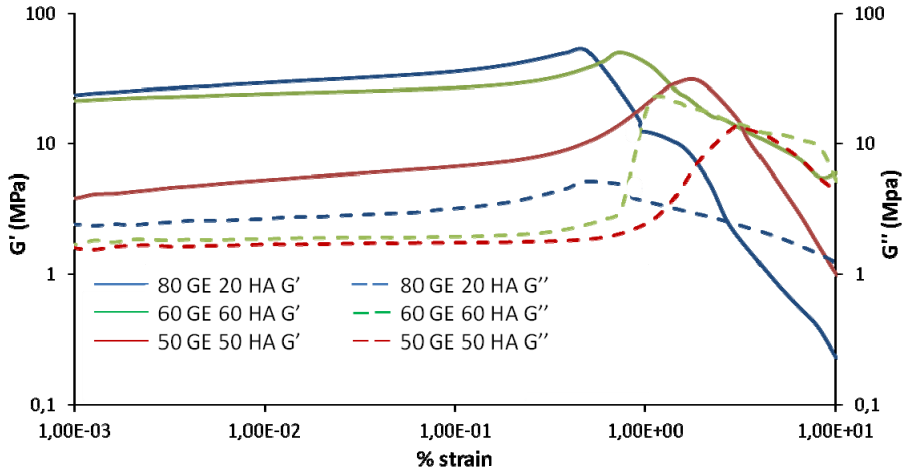

Figure 84.% strain sweep of the control hydrogel using different gelatin:hyaluronate ratios.

The addition of GP to the polymeric matrix aqueous solution forms electrostatic interactions and hydrogen bonds with gelatin and hyaluronate chains. The effective interactions responsible for the sol-gel transition could be multiple: the increase of gelatin chain hydrogen bonding as a consequence of the reduction of electrostatic repulsion due to the basic action of the GP salts, and electrostatic attractions between the ammonium and the phosphate groups of gelatin and GP respectively. This crosslinking increased the storage and loss modulus, but did not affect to the LVR compared with the control hydrogel (without crosslinking agent). GP concentration had an influence on both G' and G'': when increasing the GP

concentration higher G' and G'' were obtained, and more resistant and stable HGs were formed (Figure 85).

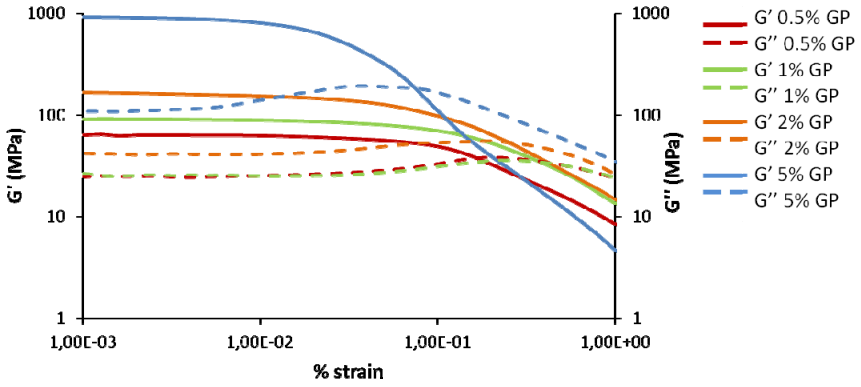

Figure 85.% Dynamic strain sweep of gelatin:sodium hyaluronate (60:40) HG with different concentrations of glycerol phosphate. Left Y axis shows the store modulus (G'), and the right Y axis shows the loss modulus (G'').

Higher G' and G'' values were obtained when TPP was used as crosslinker, if compared with GP-corsslinked HGs. Higher electrostatic interactions between amino groups of gelatin and phosphate groups of TPP are produced because it is a pentavalent electrolyte and therefore there are higher ionic interaction points to crosslink the polymeric matrix. Also the TPP concentration influence in the G' and G'' values (Figure 86) was observed. LVR obtained using TPP was a bit higher than using GP, but in both cases it was similar to control HG.

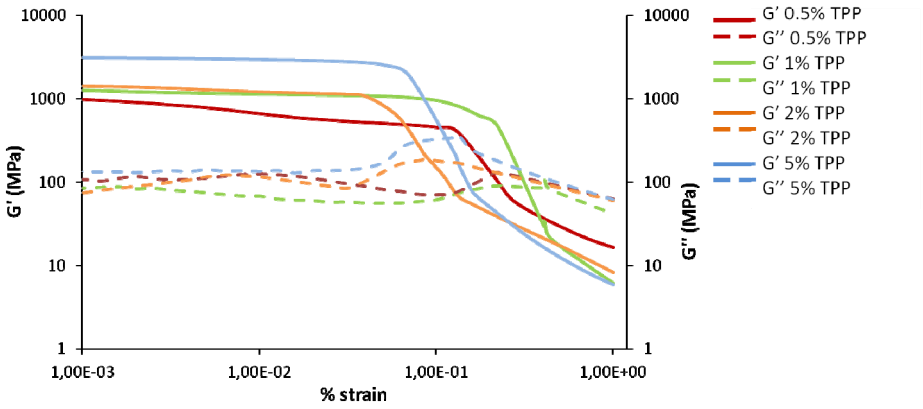

Figure 86. Dynamic strain sweep of gelatin:sodium hyaluronate (60:40) HG with different concentrations of TPP. Left Y axis shows the storage modulus (G'), and the right Y axis shows the loss modulus (G'').

Salicin crosslinking is due to the formation of hydrogen bonds between its oxygen groups and the carboxylic groups of the gelatin and sodium hyaluronate. The hydrogen bonds are formed when the carboxylic acid groups are protonated, which make the swelling of these hydrogels strongly dependent on the pH of the medium. However the influence of the concentration of salicin on the storage and loss modulus is lower than what observed for the rest of crosslinking agents, because it depends more on the amount of free carboxylate groups of the polymeric matrix than on the number of the crosslinking points. G' and G'' were higher than control HG, similar to GP crosslinked HG and lower than TPP crosslinked HG. No difference was shown in the LVR obtained for all the systems prepared (Figure 87).

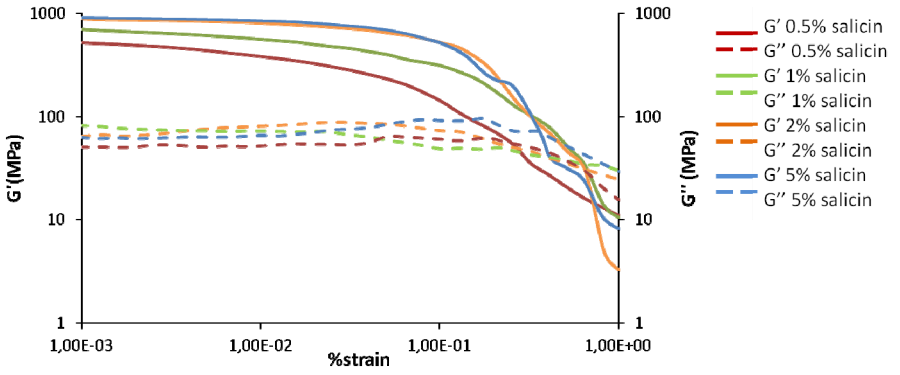

Figure 87.% Dynamic strain sweep of gelatin:sodium hyaluronate (60:40) HGs with different concentrations of salicin. Left Y axis shows the storage modulus (G'), and the right Y axis shows the loss modulus (G'').

Genipin crosslinked hydrogels are chemical, irreversible hydrogels and therefore their G' and G'' values were much higher than those obtained for physical crosslinked hydrogels. For this chemical HG, the strain sweep was performed between $1x10^{-3}$ and 10^{3} percentages, setting the normal force, frequency and temperature at 0.3 N, 0.5 Hz and 25 °C, respectively. HGs with different genipin concentrations were tested and the LVR obtained was higher than that obtained for the physical crosslinked HG (from $1x10^{-3}$ to 3% strain) for all the concentrations of genipin used (Figure 88). It was observed that the higher the concentration of the crosslinking agent, the higher G' and G'' moduli. Besides, the 1%wt genipin crosslinked hydrogel showed the wider LVR, from 0.01 to 5% strain.

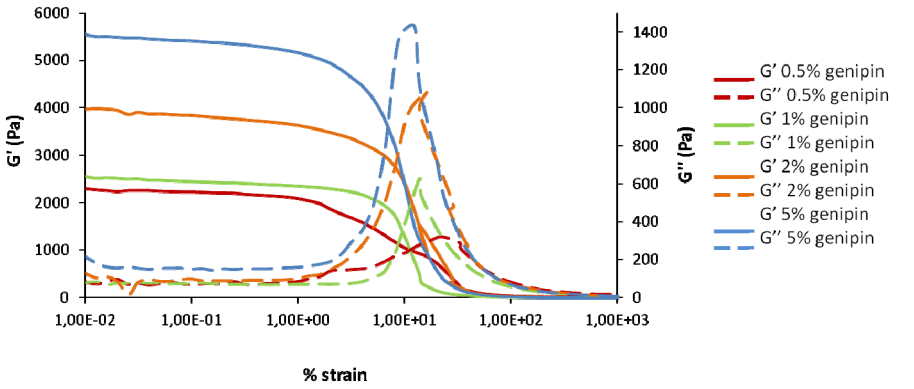

Figure 88. Dynamic strain sweep of gelatin:sodium hyaluronate (60:40) HGs with different concentrations of genipin. Left Y axis shows the storage modulus (G'), and the right Y axis shows the loss modulus (G'').

5.4.7.2 Time sweeps

Crosslinking reactions were monitored using viscoelastic dynamic time sweeps in order to determine the sol-gel transition time which is considered to be the intersecting point between G' and G'' (G' = G''). Normal force (0.3 N), strain (2%), temperature (25 ºC) and frequency (0.5 Hz) were set in advance. The results obtained are quoted in Table 11. At the beginning, when systems are in *sol* stage (solution), the viscous behavior of the material dominates in the initial part of the experiment. At this stage, the loss modulus, G'' is higher than the storage modulus, G'. As the molecular weight of the system increases due to the crosslinking process, the loss modulus decreases, while the storage modulus increases sharply until it exceeds the loss modulus. The crosslinking reaction finishes when both modulus are stabilized, reaching a plateau versus time.

Genipin chemical crosslinking reaction takes longer than physical crosslinking (Table 11), indicating different kinetics. All the systems showed longer crosslinking times when the crosslinking agent concentration decreased. Therefore, it can be concluded that the increasing of the crosslinker concentration leads to a faster

kinetic in the crosslinking reaction. Figure 89 shows the time sweeps of hydrogels prepared with different genipin concentration.

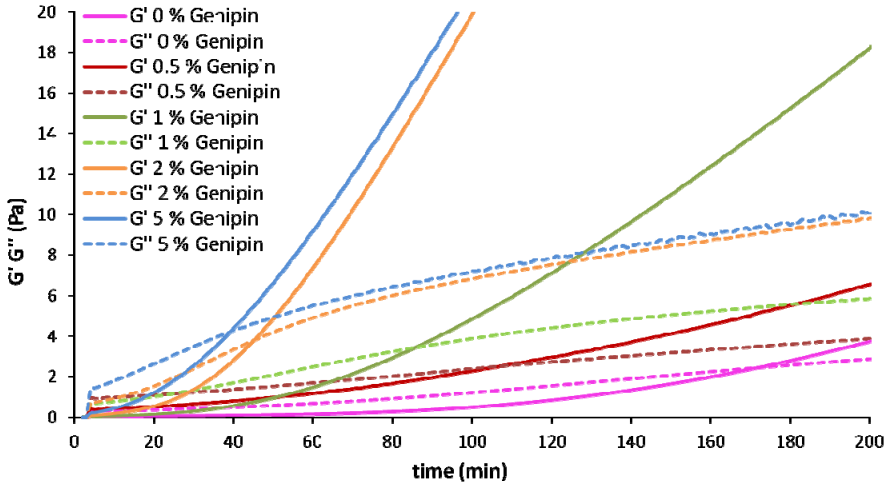

Figure 89. Dynamic time sweep of gelatin:sodium hyaluronate (60:40) HG with different concentrations of genipin. The intersecting point between both curves (G 'and G'') was considered the time at which the sol-gel transition occurs.

Table 11. Sol-gel transition time of hydrogels obtained with different crosslinking agents and different concentration of each one.

	TIME (min)				
	0%wt crosslinker	**0.5%wt crosslinker**	**1%wt crosslinker**	**2%wt crosslinker**	**5%wt crosslinker**
GENIPIN HG	177 ± 3	106 ± 5	88 ± 2	45 ± 2	39 ± 1
TPP HG	175 ± 4	7 ± 0.9	3.5 ± 0.8	3.1 ± 0.2	2.9 ± 0.4
SALICIN HG	182 ± 9	9.5 ± 1.1	8.1 ± 1.0	7.9 ± 0.8	5.8 ± 0.3
GP HG	170 ± 12	14.5 ± 1.9	13.6 ± 2.1	12.6 ± 2.1	11 ± 1.7

5.4.7.3 *Frequency sweeps*

The frequency sweep was conducted with 2% strain, 0.3 N, between 0.1 and 100 rad/s at 25 °C. The no dependency of G' with the frequency demonstrated the formation of the HG structure[204] (Figure 90). All the crosslinking agents at all the concentration tested produced a well defined HG structure; however the control HG showed a clear dependency with frequency at high angular frequency values, which means that the three dimensional network of this HG is not stable. An increasing in the G' with the concentration of crosslinker was observed (Figure 90), indicating higher stability of the HG structure.

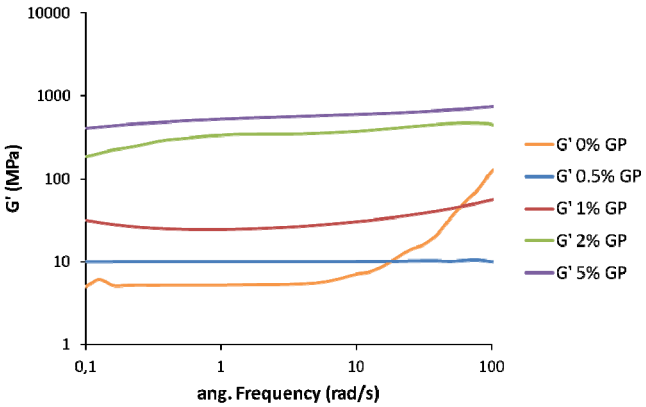

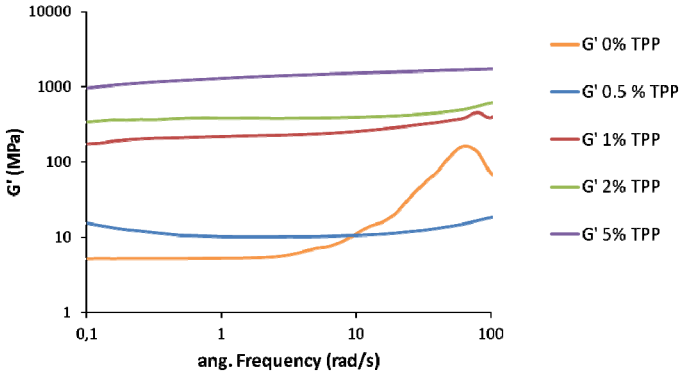

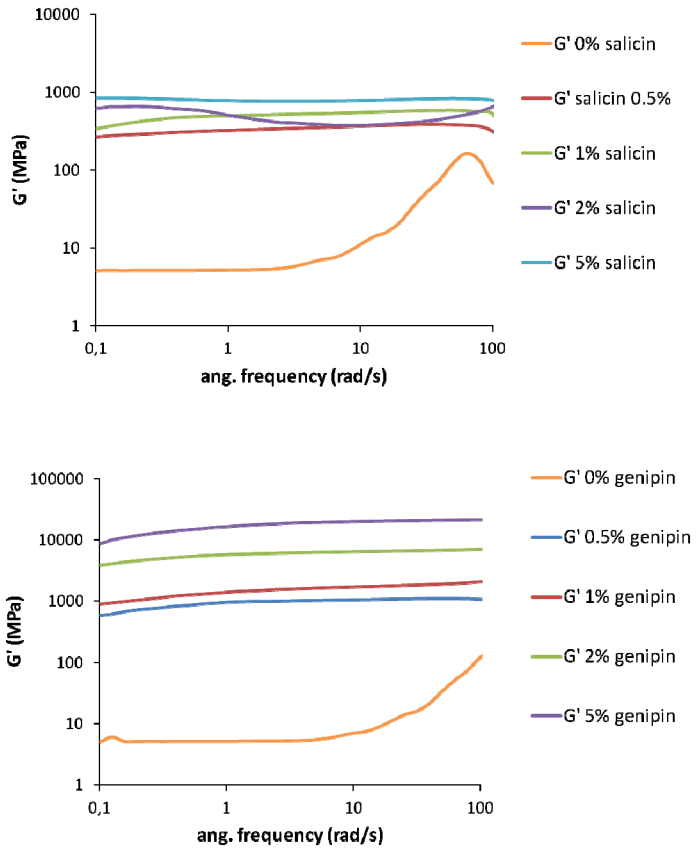

Figure 90. Dynamic frequency sweeps of gelatin:sodium hyaluronate (60:40) HGs with different crosslinking agents at different concentrations.

5.4.8 Thermal Stability

Thermal stability of the synthesized HGs was determined by thermogravimetric analysis (TGA). The%weight and derivative weight (%/°C) curves are shown in Figure 91. A 10% weight loss at temperatures around (100-120 ºC) was interpreted as the loss of adsorbed water due to the high hydrophilicity of both polymers, GE and HA. The HG thermal degradation occurs in two steps: between 200 and 270 °C a first drop of about 20% in sample weight occurs due to hyaluronate

thermal degradation, and in a second step between 270 and 400 °C, a weight drop around 50% occurs due to the gelatin thermal degradation. The weight residues left (around 20% weight) were due to the corresponding sodium salts of hyaluronate. Increasing the crosslinking agent concentration, a slightly increase of temperature values at which degradation rate is maximum for both stages of degradation was observed.

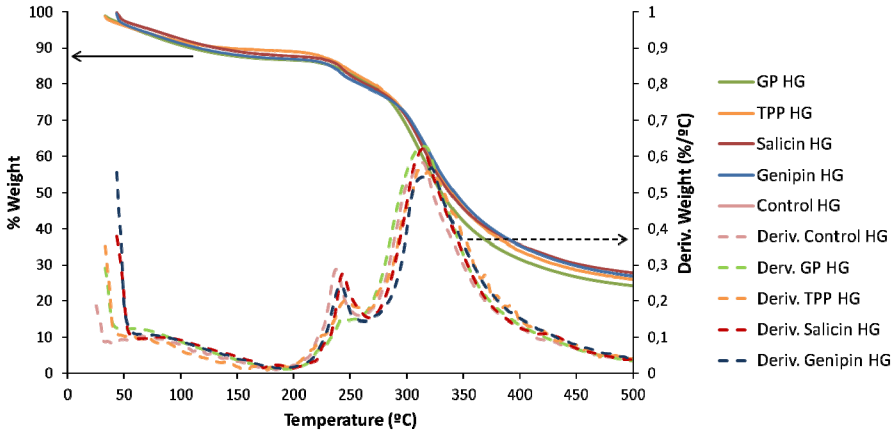

Figure 9891. Weight lost (%) and rate of weight loss (%/ºC) of GE/HA HGs obtained with 5%-wt of different corssliners.

5.4.9 Preparation of the segmented polyurethane

The synthesis of the segmented PU was carried out by the reaction of a pre-polymer obtained from LDI and a chain extender synthesized from PCL and PL61. As a natural amino acid derivative, LDI produces non toxic degradation products, e.g. L-lysine. Furthermore, it can react with quickly with the macrodiols to form urethane linkages. In addition, poly(tetramethylenglycol), PTMG, was used as a component to form the hard segment due to its flexibility. The stoichiometry of the reaction was approximately 3:2:1 (LDI:extender:PTMG) (Figure 92).

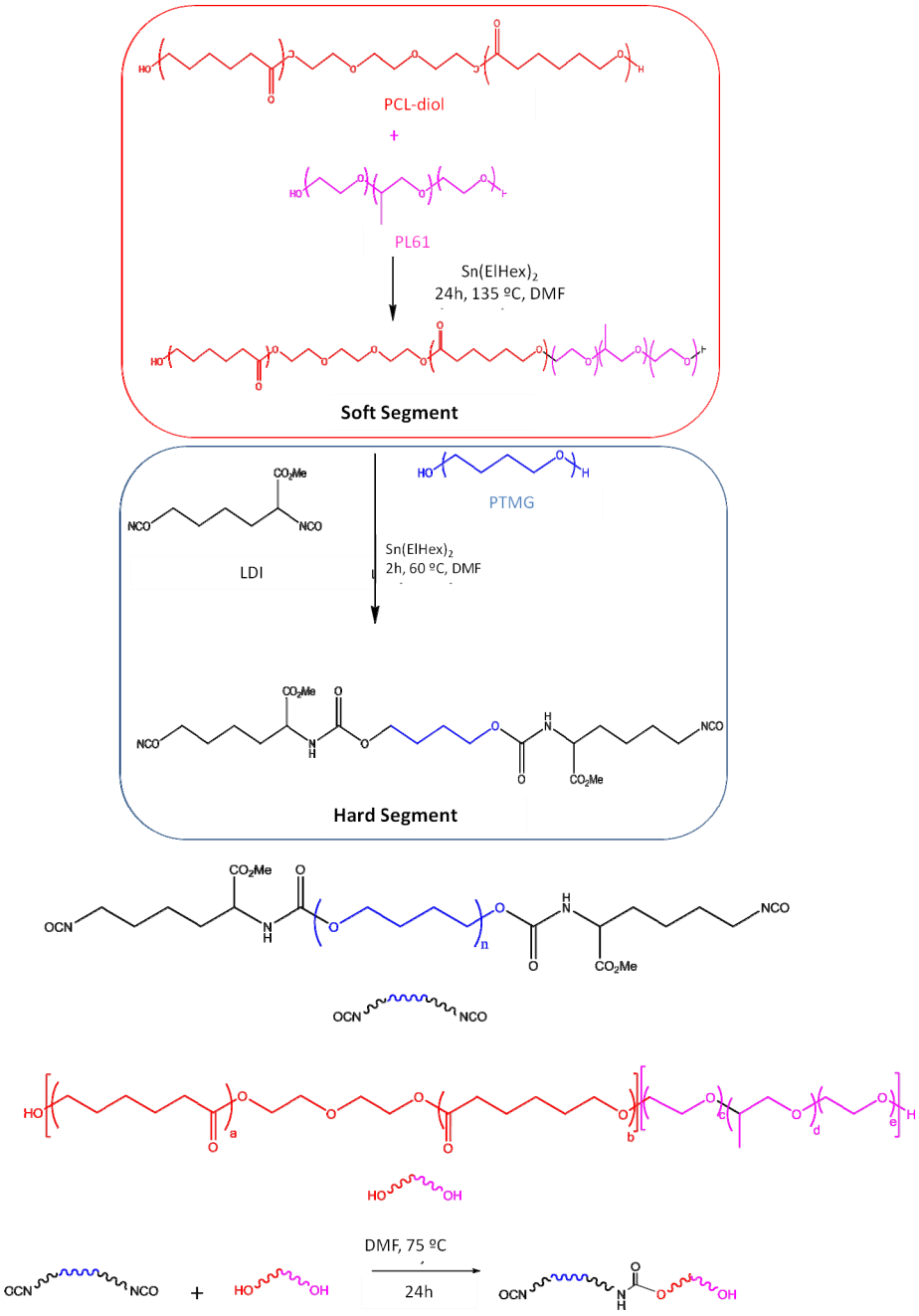

Figure 92. SPU synthesis scheme.

Figure 93 shows the infrared spectra for SPU321-[50PCL-50PL61]. The infrared absorption bands were assigned as follows: ν(cm^{-1}): 3346 [H bonded N-H stretching];

2935 [CH_2, asymmetric stretching (polyester and cyclohexane)]; 2858 [CH_2, symmetric stretching (polyester and cyclohexane)]; 2794 [Symetric CH_2 stretching in polyether]; 1723 [C=O stretching]; 1549 [C-N stretching and N-H bending]; 1449 [CH_2 bending]; 1369 [CH_2 wagging]; 1243 [C-N stretching; 1190 [C-O-C, asymmetric stretching (polyurethane and polyester)]; 1105 [symmetric C-O-C stretching in polyether]; 1046 [C-C, polyester; asymmetric ring stretching (cyclohexane)].

The absence of an absorption band at 2273 cm^{-1}, characteristic of isocyanate bonds (N=C=O stretching) indicates that the polymerization reaction was complete. The segmented nature of these PU was not difficult to demonstrated by FTIR as the hydrogen bonded (1703 cm^{-1}) and free (1733 cm^{-1}) carbonyl groups were not detected and only a single C=O absorption band was detected (1723 cm^{-1}). In the case of a higher hard segment content, the ratio (C=O bonded/C=O free) was expected to increase. Although infrared absorptions bands at 1703 cm^{-1} and 1733 cm^{-1} for hydrogen-bonded and free carbonyl groups have been reported for SPU based on LDI with different hard segment ratios.

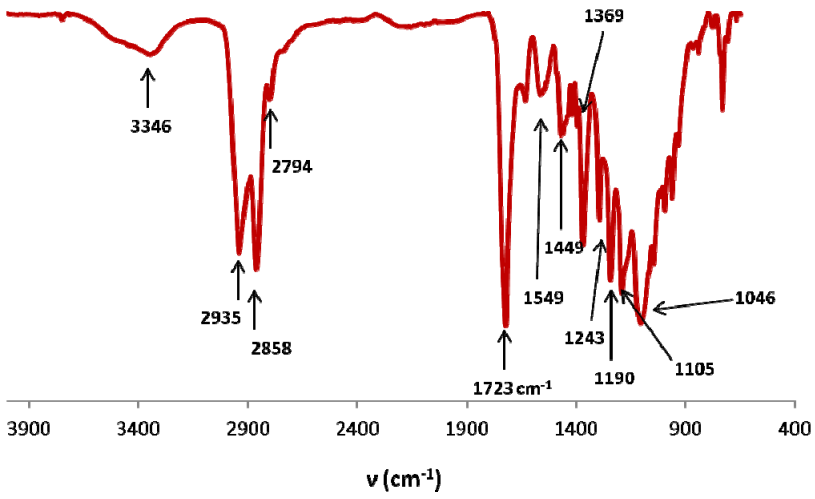

Figure 93. ATR-FTIR spectra of the SPU321-LDI-[50PCL-50PL61] synthesized.

^{1}H-NMR spectrum (Figure 94) showed characteristics signals of each component of the polyurethane. At 2.25 ppm appears the methylene group signal (-CH_2-) in α position to the carboxylate of PCL-diol, at 1.05 ppm appears the methyl group (-CH_3) of PL61, the corresponding signals to PTMG appear at 3.4 ppm (-CH_2-O-) and at 1.6 ppm (-CH_2-C-), overlapping with the other two components. And the LDI characteristics signals appear at 3.6 ppm and 4.1 ppm corresponding to the methyl (-CH_3) and the CH group in α position to the ester, respectively.

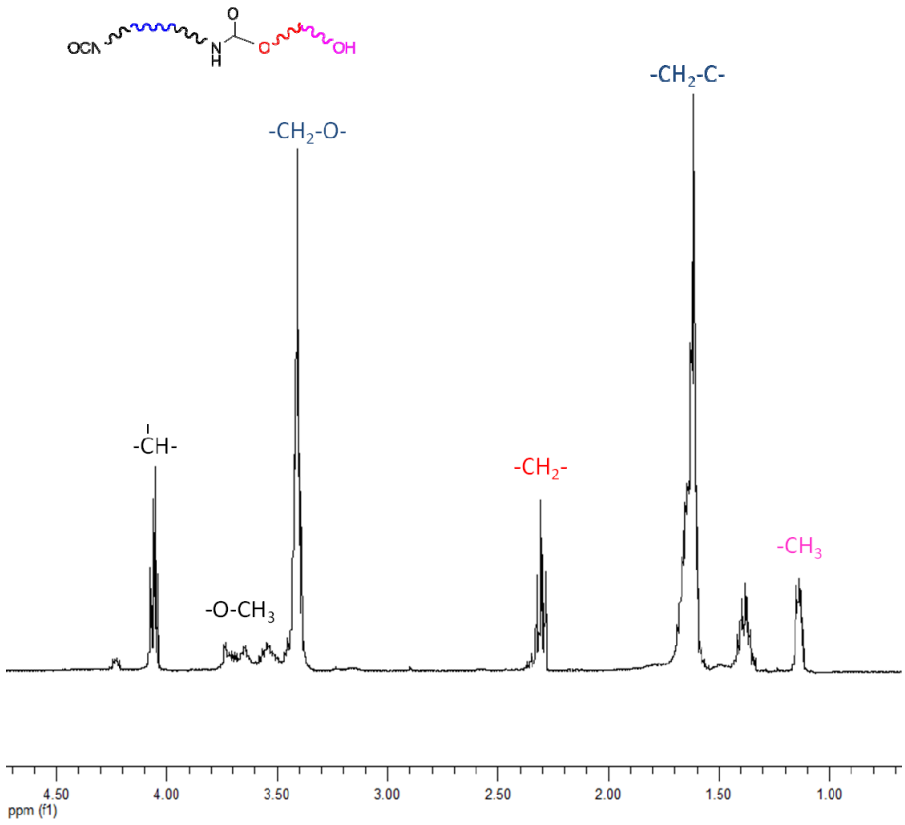

Figure 94. ^{1}H-NMR spectrum of SPU321-LDI-[50PCL-50PL61] registered in $CDCl_3$ at 25°C.

The DSC analysis showed three endothermic peaks at 29, 49 and 54 °C in the second heating cycle. These transitions were attributed to the melting of crystalline domains and reorganization of the polymeric chains. It is well known that the rigid

and soft segments of the SPU segregate in the solid state in their respective domains to produce a two-phase morphology[205]. During the heating process, the soft segments shrink or relax causing the monomer of some rigid segments from the rigid domains and a mixture of phases is developed. During cooling, the thermodynamic driving force leads to phase separation; however the high viscosity of the system induces a process of slow separation. The first endothermic transition (at 29.98 ºC) belongs to the melting of PTMG and the last two transitiojns correspond to the PCL-diol (at 48.98 ºC and at 53.97 ºC). These two transitions of the PCL-diol were due to the existence of two different crystalline domains[188], one with a higher degree of orientation in space (T_m = 54 °C) and another with a lower degree of orientation (T_m = 49 °C).

TGA analysis showed a two-step degradation process (Figure 95), which is in agreement with the presence of two phases. The first step is attributed to degradation of hard segments, while the second step is associated to degradation of soft segments[206].

Based on TGA measurements, SPU321-[50PCL-50PL61] contains approximately 42%-wt of rigid segment and 58%-wt of the soft segment.

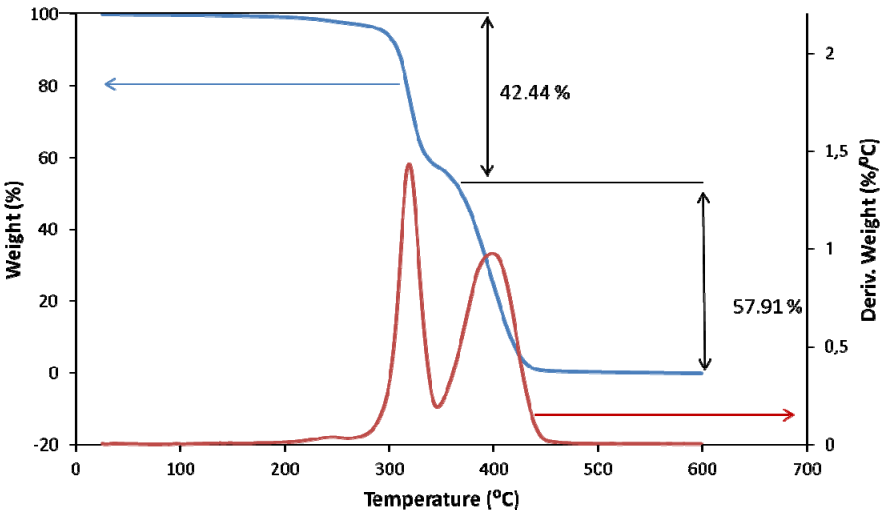

Figure 95. Weight loss (%) and rate of weight loss (%/ºC) of SPU321-LDI-[50PCL-50PL61].

The molecular weight distribution of the polyurethane was analyzed by SEC. The chromatogram showed a monomodal molecular weight distribution with an M_w = 19100 Da and M_n = 6983 Da. However, the molecular weight distribution showed high polidispersity (PDI = 2.73), which is indicative of the microphase segregation of both, the soft and hard segments. The mechanical properties, the storage (G') and loss (G'') moduli and T_g were evaluated by DMTA. SPU presented a T_g = 22 °C, lower than physiological temperature (37 °C). This means that this polymer will maintain its flexibility in physiological conditions. The high value of storage and loss moduli (G' = 2000 MPa, G'' = 500 MPa) makes this material suitable for the preparation of biomedical membranes[207].

For the hydration analysis of the polyurethane, films of 0.5-1 cm diameter were prepared. These films were used to calculate the hydration percentage of SPU321-LDI-[50PCL-diol-50PL61] at 37 °C in distilled water, performing each measurement in triplicate. The hydration profile showed a maximum around 10-15% after 15 days (Figure 96) and then the hydration degree decreased to a stable value of 9% from day 40. This behavior is attributed to the viscoelastic response of the polyurethane film. At the beginning, the system is in solid state, forming a rigid crystalline network (dry film). When polymer chains start to hydrate the amorphous domains swell and become more flexible, reaching the maximum degree of hydration. However, the system tends over time to a minimum energy state, so that the chains start to relax and contract, expelling water molecules that had penetrated into the polymer network to reach a stable level of hydration. This behavior is typical of viscoelastic gels.

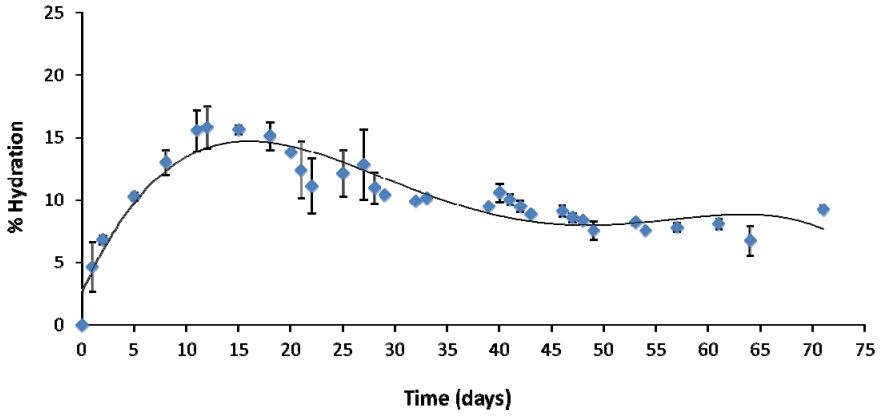

Figure 96. Hydration degree (%) of the SPU321-LDI-[50PCL-50PL61] in distilled water.

5.4.10 Preparation of the bilayer dressing

The regeneration bilayer system is formed by two polymeric layers of different structure and biodegradable nature: a gelatin/sodium hyaluronate SIPN HG and a SPU membrane. Both layers contain bioactive compounds, so that their release is controlled in a programmed manner. The bioactive components are PAMP for the HG and bemiparin loaded nanoparticles for the SPU membrane, both of them were added as aqueous solution onto the corresponding layer, so that they were physically incorporated in the biodegradable polymer matrix.

5.4.10.1 Preparation of the external layer (SPU charged with bemiparin loaded NP).

SPU321-LDI-[50PCL-diol-50PL61] was prepared and used as bemiparin-loaded NP delivery system. SPU layer was loaded bemiparin loaded NP. This block

copolymer was selected since it allowed faster and higher bemiparin release at pH 7.4 and a modulation of the biological bemiparin activity[208].

The nanoparticles loaded membranes were analyzed by SEM. Images were obtained from the upper and lower surface and the cross section of the polyurethane layer. The images obtained show that the nanoparticles diffused through the polyurethane membrane and they appeared randomly distributed, keeping their spherical morphology and its initial size (Figure 97).

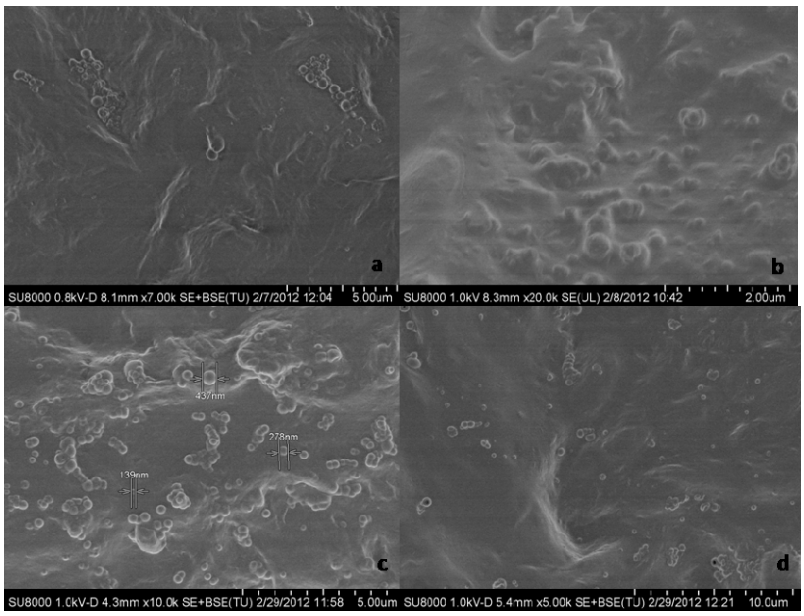

Figure 97. SEM images of the loaded SPU membranes containing bemiparin loaded nanoparticles. (a, b) Cross sections of the SPU membrane, (c) surface of SPU membrane, and (d) bottom of the SPU membrane.

5.4.10.2 Preparation of the internal layer (HG charged with PAMP)

Physical HGs showed lower hydration degree and poor mechanical properties compared to chemical HGs. Therefore, only genipin crosslinked HGs were used for

the preparation of the bilayer system for the bilayer dressing preparation. The crosslinker concentration strongly affected the gelation time. Higher crosslinker concentrations resulted in shorter gelation time as it was described in the 5.4.5.2 section of this chapter. However, when the crosslinker concentration is high (2 or 5%wt) a lower degradation rate than is desirable was observed. For that reason, 1%wt genipin was chosen as an optimum concentration of chemical crosslinker to do *in vivo* experimental tests. Therefore, the following bilayer systems were prepared for *in vivo* experiments (Table 12) as it was described in the materials and methods of this chapter (section 5.3.2.3.2).

Table 12. Polymers and bioactive molecules composition of the implanted bilayer dressings.

SAMPLE	SPU mass (mg)	NP mass (mg)	Bemiparin mass (mg)	UI bemiparin / disc	Moles (nmol) PAMP / disc
SPU+HG Control Sample	60	0	0	0	0
SPU + NP + BEMI + HG	60	3	0.3	33.4	0
SPU + NP + BEMI + HG + PAMP	60	3	0.3	33.4	1

5.4.11 In vivo mouse model test of the bilayer system

Finally, the activation of blood vessel formation by our bilayer system was studied in a mouse model. Mice were genetically modified to express green fluorescent protein (GFP) under a αSMA promoter which drives GFP expression in pericytes. These cells surround the blood vessels, including capillaries. Small disks (1 cm in diameter) of the bilayer system with the 3 compositions described above (-Bemi/-PAMP, +Bemi/-PAMP, and +Bemi/+PAMP) were inserted in a small skin pocket practiced in the back of the transgenic mice (n=5 animals per group) and the wound closed up with suture. After 5 or 14 days, mice were sacrificed, the membranes were removed and fixed in buffered formalin. Some disks were

observed directly with a confocal microscope (TCS SP5, Leica, Barcelona, Spain) (Figure 98a,b) whereas others were embedded in paraffin, sectioned, and stained with hematoxylin-eosin (Figure 98c,d). After 5 days of implantation, clear differences were appreciated between the un-loaded bilayer dressing (-Bemi/-PAMP) (Figure 98a), in which blood vessels were not observed, and the Bemiparin-based NPs and PAMP loaded bilayer dressing (+Bemi/+PAMP), that showed clear neo-vessel formation.

Fourteen days after implantation, clear differences were observed in the tissue directly in contact with the dressing. The connective tissue close to the unloaded disks (-Bemi/-PAMP) contained scarce blood vessel (Figure 98c) whereas tissue next to the 98:2 PMMA-*b*-PMAETMA-Bemiparin NP loaded SPU + PAMP loaded HG bilayer system presented numerous capillaries (Figure 98d).

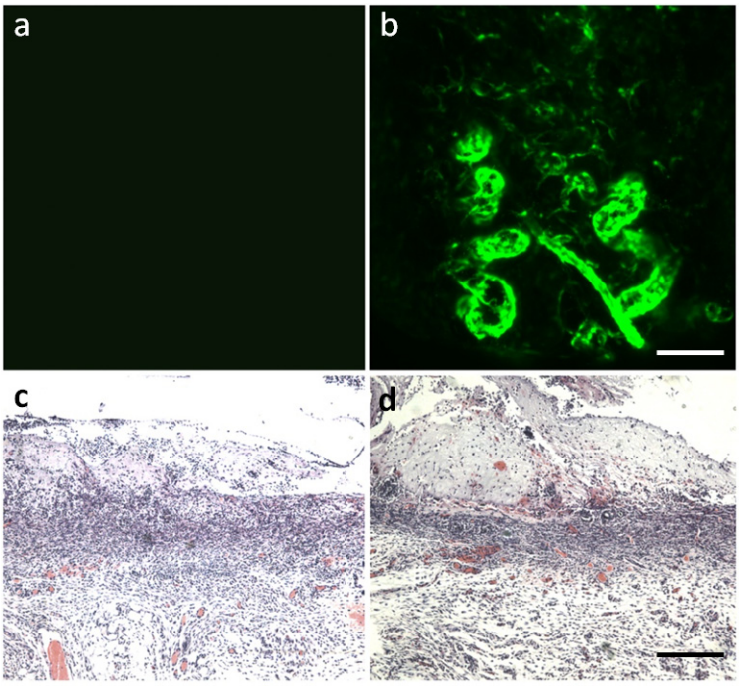

Figure 98. Images obtained with confocal (a,b) and brightfield (c,d) microscopy of disks implanted under the skin of transgenic mice. a) confocal image of control hydrogel (formed by the hydrogel without PAMP nor bemiparin); b) confocal micrograph of bilayer system containing 1nmol PAMP in the HG layer and 5% NP dispersion prepared with 98/2 p(MMA-*b*-MAETMA) system (0.3 mg encapsulated bemiparin) in the SPU layer, after being grafted for 5 days under the skin of a transgenic mouse; c) histological section stained with hematoxylin-eosin after 14 days of implantation of the control system; d) histological section of tissue next to a disk containing PAMP and bemiparin. Scale bar: a,b = 75 µm; c,d = 150 µm.

5.4.12 In Vivo evaluation of the bilayer system: comparison of normoxic and ischemia models

Discs of these bilayer systems were implanted in both normoxic and ischemic rabbits, as it is shown in the Figure 99. Once implanted, rabbits were sacrified after 14 days and the wounds were morphometricaly and histologicaly analyzed.

The macroscopic analysis of wounds (Figure 99) on both normoxic and ischemic rabbit ears demonstrated that lack of wound healing when no treatment was applied (Figure 99 a and f).

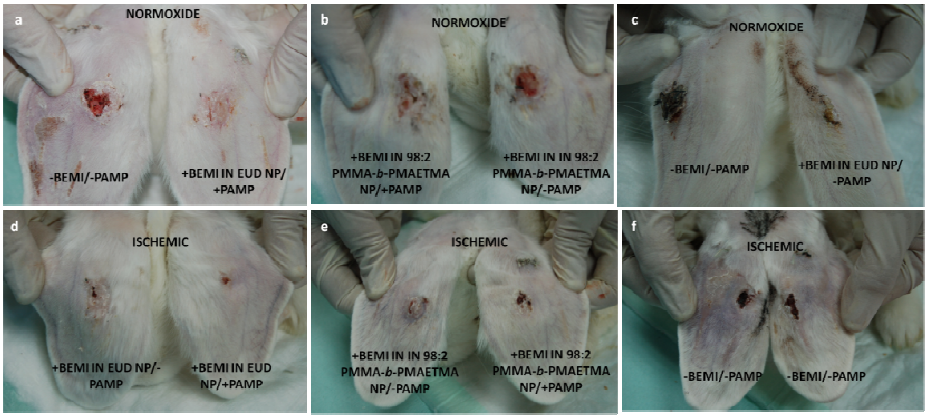

Figure 99. Normoxic and ischemic rabbit ears with different bilayer systems treatment after 14 days.

The morphometric analysis of the wounds allowed the quantification of wound healing by measuring the area of the wound after the rabbits were slaughtered (Figure 100a). Results showed that, although the percentage of healing was rather similar in all the groups, a different contribution of the contraction and epithelization to the process was shown. The wounds treated with PMMA-*b*-PMAETMA 98:2-bemiparin loaded NP and PAMP caused less wound contraction, which favoured the closure of wound by epithelialization, especially in the ischemic group (Figure 100b).

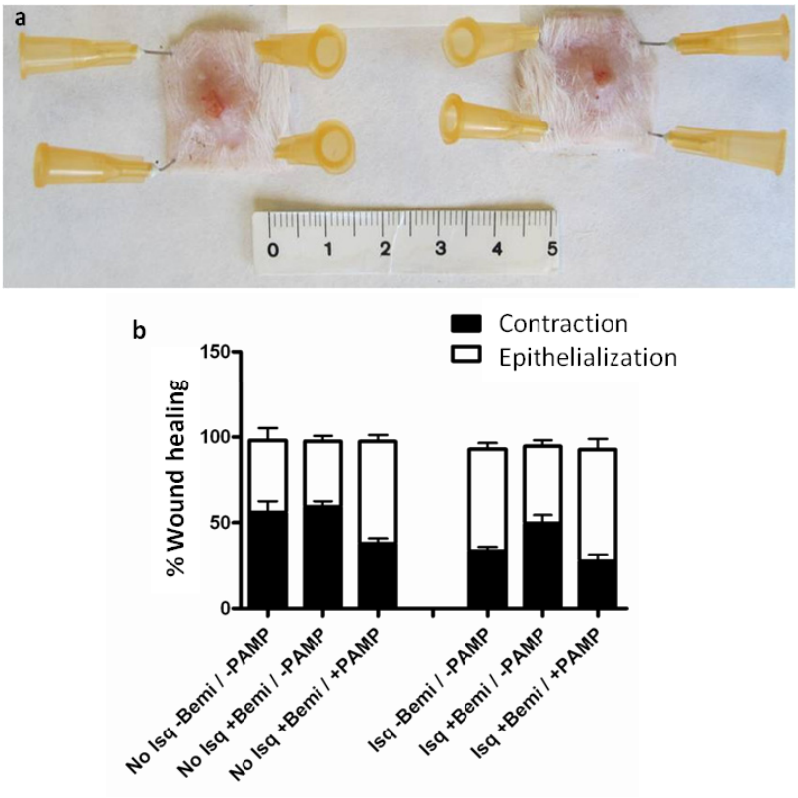

Figure 100. Morphometric analysis of the contraction and re-epithelialization process. Data were obtained from the measurements made on the rabbit wounds after they were slaughtered (a). There is a greater contribution of the re-epithelialization process versus contraction in the groups treated with PAMP and Bemiparin loaded systems. Data are expressed as percentage of the initial area covered by each process defect (b).

Histological analysis showed a higher level of angiogenesis in the wounds of ischemic rabbits treated with bemiparin NP and PAMP, as it was demonstrated by the inmunohistochemical analysis with antibodies agains α-actine from smooth muscle (αSMA). In the normoxide model, it was observed an increasing in blood vessel formation in wounds treated with bemiparin. In the ischemic model, the increasing in blood vessel formation in wounds treated was observed when bemiparin and PAMP were presented, as it is shown in the Figure 101.

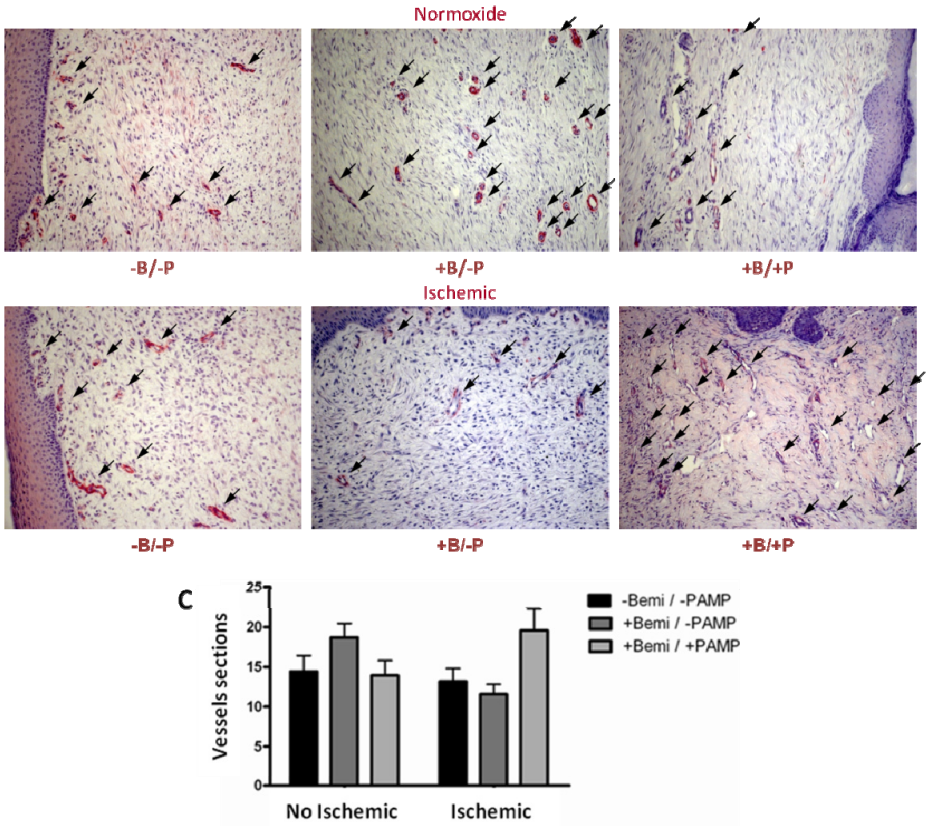

Figure 101. Immunohistochemistry against αSMA. There is a greater number of vessels sections (arrowheads) in the +Bemi/+PAMP group versus -Bemi/-PAMP in both groups, normoxides (NO ISCHEMIC) and ischemic rabbits. Images were taken at 200 magnifications. (C) Values were obtained by the counting of six rabbit groups, expressed as number of vascular sections for field observed at 200 magnifications.

The analysis of the macrographs obtained after staining with hematoxylin-eosin and the corresponding immunohistochemistry analysis against αSMA allows the quantification of the effect of the application of the bilayer system in the animal experimentation. The presence of both, PAMP protein and bemiparin have significant effects on the structure and morphology of the regenerated skin, with a clear uniform distribution and structure of the regenerated tissue (Figure 102).

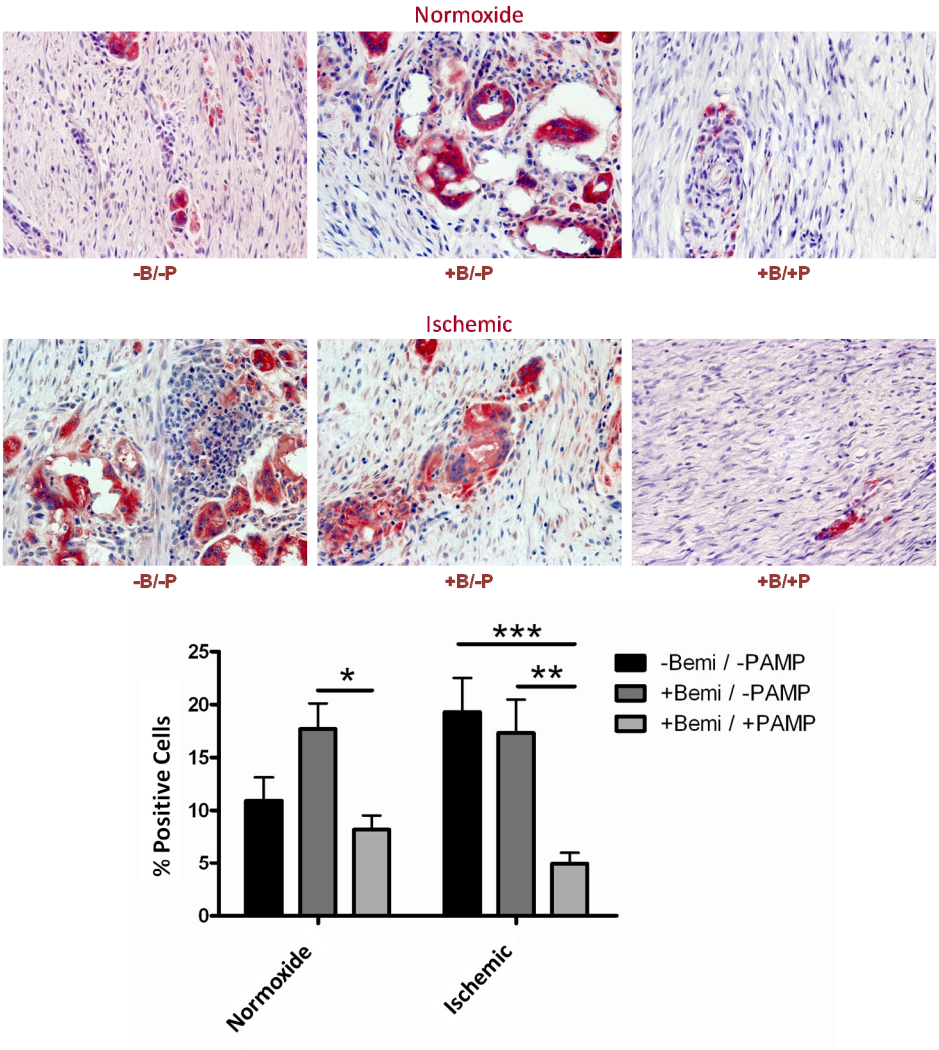

Figure 102. Hematoxylin-eosin staining of regenerated skin and immunohistochemistry against macrophages. There is a greater WOUND HEALING in the +Bemi/+PAMP group versus -Bemi/-PAMP in both groups, normoxides and ischemic rabbits. Images were taken at 200 magnifications. (C) Values were obtained by the counting of six rabbit groups, expressed as percentage of macrophages observed at 200 magnifications.

5.5 CONCLUSIONS

A bioactive and biodegradable bilayer dressing that improves wound healing and tissue regeneration has been prepared. The systems consists of an internal layer of a hydrogel based on gelatin and sodium hyaluronate crosslinked with genipin and charged with PAMP as bioactive compound, and an external layer composed of a segmented polyurethane charged with bemiparin loaded nanoparticles. The combination of both layers, hydrogel and segmented polyurethane, allowed a controlled dosing of both active components (PAMP and bemiparin), favoring revascularization of ischemic wounds.

Semi-interpenetrating polymer networks (hydrogels) were prepared to be in contact with the wound in order to maintain a hydrated environment that allows cell proliferation and migration and maintain moisture in the wound and to act as carrier of bemiparin-loaded NPs. These hydrogels were formed by gelatin and sodium hyaluronate crosslinked using different crosslinking agents at different concentrations. The rheology and swelling studies of these hydrogels (HGs) allowed determining their mechanical stability and viscoelastic properties of the crosslinked system. The crosslinking density of the HGs increases with the crosslinking agent concentration, and this can be used to modulate the degree of swelling reached at equilibrium. The swelling is pH dependent, being greater at physiological pH which makes these HGs very useful as drug carrier systems and tissue engineering. PAMP was incorporated in the HG and its appropriate controlled release to the wound favored the formation of new blood vessels (angiogenesis) in the superficial skin layers.

Biodegradable and re-absorbable SPU based on LDI were successfully synthesized to be used as the external layer of the wound dressing in order to improve the mechanical properties of the supported HG.

It has been demonstrated that PAMP and bemiparin combination improves wound repair in a rabbit ear model under both normoxic and ischemic conditions.

Topical treatments with PAMP and bemiparin resulted in significant improvements of healing, when compared to untreated wounds. The combination of both bioactive compounds was very effective in promoting re-epithelialization and angiogenesis, with less wound contraction. This dressing comprised of two bio-functionalized layers may be used to improve the healing of wounds and ulcers, especially in cases where the process is hindered as in diabetic patients with reduced blood flow and elderly people.

5.6 REFERENCES

162. Schönfelder, U.; Abel, M.; Wiegand, C.; Klemm, D.; Elsner, P.; Hipler, U.-C., Influence of selected wound dressings on PMN elastase in chronic wound fluid and their antioxidative potential in vitro. *Biomaterials* **2005,** *26* (33), 6664-6673.

163. Mat Saad, A. Z.; Khoo, T. L.; Halim, A. S., Wound Bed Preparation for Chronic Diabetic Foot Ulcers. *ISRN Endocrinology* **2013,** *2013*, 9.

164. Martin, T. A. H., J.; Jiang, W. G.; Harding, K., Effect of human fibroblast-derived dermis on expansion of tissue from venous leg ulcers. *Wound Repair Regen* **2010,** *11* (4), 292-6.

165. Barbucci, R., Hydrogels, biological properties and applications. Barbucci, R., Ed. Springer: Milan, 2009.

166. Guo, S.; DiPietro, L. A., Factors Affecting Wound Healing. *Journal of Dental Research* **2010,** *89* (3), 219-229.

167. Hoffman, A. S., Hydrogels for biomedical applications. *Advanced Drug Delivery Reviews* **2012,** *64, Supplement* (0), 18-23.

168. (a) Buenger, D.; Topuz, F.; Groll, J., Hydrogels in sensing applications. *Progress in Polymer Science* **2012,** *37* (12), 1678-1719; (b) Klouda, L.; Mikos, A. G., Thermoresponsive hydrogels in biomedical applications. *European Journal of Pharmaceutics and Biopharmaceutics* **2008,** *68* (1), 34-45; (c) Lee, S. C.; Kwon, I. K.; Park, K., Hydrogels for delivery of bioactive agents: A historical perspective. *Advanced Drug Delivery Reviews* **2013,** *65* (1), 17-20; (d) Omidian, H.; Rocca, J. G.; Park, K., Advances in superporous hydrogels. *Journal of Controlled Release* **2005,** *102* (1), 3-12.

169. Vroman, I.; Tighzert, L., Biodegradable Polymers. *Materials* **2009,** *2* (2), 307-344.

170. Collins, M. N.; Birkinshaw, C., Hyaluronic acid based scaffolds for tissue engineering—A review. *Carbohydrate Polymers* **2013,** *92* (2), 1262-1279.

171. (a) Jeon, O.; Song, S. J.; Lee, K.-J.; Park, M. H.; Lee, S.-H.; Hahn, S. K.; Kim, S.; Kim, B.-S., Mechanical properties and degradation behaviors of hyaluronic acid hydrogels cross-linked at various cross-linking densities. *Carbohydrate Polymers* **2007,** *70* (3), 251-257; (b) Yang, Y.-l.; Sun, C.; Wilhelm, M. E.; Fox, L. J.; Zhu, J.; Kaufman, L. J., Influence of chondroitin sulfate and hyaluronic acid on structure, mechanical properties, and glioma invasion of collagen I gels. *Biomaterials* **2011,** *32* (31), 7932-7940.

172. (a) An, J.; Gou, Y.; Yang, C.; Hu, F.; Wang, C., Synthesis of a biocompatible gelatin functionalized graphene nanosheets and its application for drug delivery. *Materials Science and Engineering: C* **2013,** *33* (5), 2827-2837; (b) Balaji, S.; Kumar, R.; Sripriya, R.; Kakkar, P.; Ramesh, D. V.; Reddy, P. N. K.; Sehgal, P. K., Preparation and comparative characterization of keratin–chitosan and keratin–gelatin composite scaffolds for tissue engineering applications. *Materials Science and Engineering: C* **2012,** *32* (4), 975-982; (c) Landi, E.; Valentini, F.; Tampieri, A., Porous hydroxyapatite/gelatine scaffolds with ice-designed channel-like porosity for biomedical applications. *Acta Biomaterialia* **2008,** *4* (6), 1620-1626.

173. Ai, H.; Mills, D.; Jonathan, A.; Jones, S., Gelatin-glutaraldehyde cross-linking on silicone rubber to increase endothelial cell adhesion and growth. *In Vitro Cell.Dev.Biol.-Animal* **2002,** *38* (9), 487-492.

174. Kosaraju, S. L.; Puvanenthiran, A.; Lillford, P., Naturally crosslinked gelatin gels with modified material properties. *Food Research International* **2010,** *43* (10), 2385-2389.

175. Pavlov, G.; Grishchenko, A.; Puaud, M.; Hill, S.; Mitchell, J., Orientational order in surface layers of gelatin films. *European Polymer Journal* **2001,** *37* (1), 179-182.

176. Bigi, A.; Cojazzi, G.; Panzavolta, S.; Roveri, N.; Rubini, K., Stabilization of gelatin films by crosslinking with genipin. *Biomaterials* **2002,** *23* (24), 4827-4832.
177. Gough, J. E.; Scotchford, C. A.; Downes, S., Cytotoxicity of glutaraldehyde crosslinked collagen/poly(vinyl alcohol) films is by the mechanism of apoptosis. *Journal of Biomedical Materials Research* **2002,** *61* (1), 121-130.
178. Butler, M. F.; Ng, Y.-F.; Pudney, P. D. A., Mechanism and kinetics of the crosslinking reaction between biopolymers containing primary amine groups and genipin. *Journal of Polymer Science Part A: Polymer Chemistry* **2003,** *41* (24), 3941-3953.
179. J. Alemán, A. V. C., J. He, M. Hess, K. Horie, R. G. Jones, P. Kratochvíl, I. Meisel, I. Mita, G. Moad, S. Penczek and R. F. T. Stepto, Definitions of terms relating to the structure and processing of sols, gels, networks, and inorganic-organic hybrid materials (IUPAC Recommendations 2007). *Pure Appl. Chem.*

2007, *79* (10), 1801-1829.
180. (a) Yu, F.; Cao, X.; Zeng, L.; Zhang, Q.; Chen, X., An Interpenetrating HA/G/CS BiomimicHydrogel via Diels-Alder Click Chemistry for Cartilage Tissue Engineering. *Carbohydrate Polymers* **2013,** (0); (b) Lee, F.; Kurisawa, M., Formation and stability of interpenetrating polymer network hydrogels consisting of fibrin and hyaluronic acid for tissue engineering. *Acta Biomaterialia* **2013,** *9* (2), 5143-5152; (c) Liu, Y.; Chan-Park, M. B., Hydrogel based on interpenetrating polymer networks of dextran and gelatin for vascular tissue engineering. *Biomaterials* **2009,** *30* (2), 196-207.
181. (a) Contois, L.; Akalu, A.; Brooks, P. C., Integrins as "functional hubs" in the regulation of pathological angiogenesis. *Seminars in Cancer Biology* **2009,** *19* (5), 318-328; (b) Zygmunt, M.; Herr, F.; Münstedt, K.; Lang, U.; Liang, O. D., Angiogenesis and vasculogenesis in pregnancy. *European Journal of Obstetrics & Gynecology and Reproductive Biology* **2003,** *110, Supplement* (0), S10-S18.
182. Martínez, A., A new family of angiogenic factors. *Cancer Letters* **2006,** *236* (2), 157-163.
183. Eklund, L.; Bry, M.; Alitalo, K., Mouse models for studying angiogenesis and lymphangiogenesis in cancer. *Molecular Oncology* **2013,** *7* (2), 259-282.
184. (a) Bunton, D. C.; Petrie, M. C.; Hillier, C.; Johnston, F.; McMurray, J. J. V., The clinical relevance of adrenomedullin: a promising profile. *Pharmacology & Therapeutics* **2004,** *103* (3), 179-201; (b) López, J.; Martínez, A., Cell and molecular biology of the multifunctional peptide, adrenomedullin. In *International Review of Cytology*, Kwang, W. J., Ed. Academic Press: 2002; Vol. Volume 221, pp 1-92.
185. Allaker, R. P.; Kapas, S., Adrenomedullin and mucosal defence: interaction between host and microorganism. *Regulatory Peptides* **2003,** *112* (1–3), 147-152.
186. Santerre, J. P.; Woodhouse, K.; Laroche, G.; Labow, R. S., Understanding the biodegradation of polyurethanes: From classical implants to tissue engineering materials. *Biomaterials* **2005,** *26* (35), 7457-7470.
187. (a) Dulińska-Molak, I.; Lekka, M.; Kurzydłowski, K. J., Surface properties of polyurethane composites for biomedical applications. *Applied Surface Science* **2013,** *270* (0), 553-560; (b) Mondal, S.; Martin, D., Hydrolytic degradation of segmented polyurethane copolymers for biomedical applications. *Polymer Degradation and Stability* **2012,** *97* (8), 1553-1561.
188. Rueda-Larraz, L.; d'Arlas, B. F.; Tercjak, A.; Ribes, A.; Mondragon, I.; Eceiza, A., Synthesis and microstructure–mechanical property relationships of segmented polyurethanes based on a PCL–PTHF–PCL block copolymer as soft segment. *European Polymer Journal* **2009,** *45* (7), 2096-2109.
189. Pinchuk, L., A review of the biostability and carcinogenicity of polyurethanes in medicine and the new generation of 'biostable' polyurethanes. *Journal of Biomaterials Science, Polymer Edition* **1995,** *6* (3), 225-267.
190. Eshraghi, S.; Das, S., Mechanical and microstructural properties of polycaprolactone scaffolds with one-dimensional, two-dimensional, and three-dimensional orthogonally oriented porous architectures produced by selective laser sintering. *Acta Biomaterialia* **2010,** *6* (7), 2467-2476.
191. Kweon, H.; Yoo, M. K.; Park, I. K.; Kim, T. H.; Lee, H. C.; Lee, H.-S.; Oh, J.-S.; Akaike, T.; Cho, C.-S., A novel degradable polycaprolactone networks for tissue engineering. *Biomaterials* **2003,** *24* (5), 801-808.
192. Kabanov, A. V.; Batrakova, E. V.; Alakhov, V. Y., Pluronic® block copolymers as novel polymer therapeutics for drug and gene delivery. *Journal of Controlled Release* **2002,** *82* (2–3), 189-212.
193. Park, E. K.; Kim, S. Y.; Lee, S. B.; Lee, Y. M., Folate-conjugated methoxy poly(ethylene glycol)/poly(ε-caprolactone) amphiphilic block copolymeric micelles for tumor-targeted drug delivery. *Journal of Controlled Release* **2005,** *109* (1–3), 158-168.
194. (a) Hu, J.; Zhu, Y.; Huang, H.; Lu, J., Recent advances in shape–memory polymers: Structure, mechanism, functionality, modeling and applications. *Progress in Polymer Science* **2012,** *37* (12), 1720-1763; (b) Szymczyk, A.; Senderek, E.; Nastalczyk, J.; Roslaniec, Z., New multiblock poly(ether-ester)s based on poly(trimethylene terephthalate) as rigid segments. *European Polymer Journal* **2008,** *44* (2), 436-443.

195. Yang, Z.; Tu, Q.; Wang, J.; Huang, N., The role of heparin binding surfaces in the direction of endothelial and smooth muscle cell fate and re-endothelialization. *Biomaterials* **2012,** *33* (28), 6615-6625.
196. Martino, M. M.; Briquez, P. S.; Ranga, A.; Lutolf, M. P.; Hubbell, J. A., Heparin-binding domain of fibrin(ogen) binds growth factors and promotes tissue repair when incorporated within a synthetic matrix. *Proceedings of the National Academy of Sciences* **2013,** *110* (12), 4563-4568.
197. Martínez, A.; Bengoechea, J. A.; Cuttitta, F., Molecular Evolution of Proadrenomedullin N-Terminal 20 Peptide (PAMP): Evidence for Gene Co-Option. *Endocrinology* **2006,** *147* (7), 3457-3461.
198. Ravikumar T., S. N., Jayaraman V., Ramakrishnan K.M., Babu M., LOW MOLECULAR WEIGHT HEPARIN-INDUCED PHARMACOLOGICAL MODULATION OF BURN WOUND HEALING. *Annals of Burns and Fire Disasters* **2006,** *XIX* (3).
199. Ezzat, A. A. H. H. S. E. A. A., Prognostic value of plasma pro-adrenomedullin and antithrombin levels in neonatal sepsis. *Indian Pediatrics* **2011,** *48* (6), 471-473.
200. Bellón, J. M.; López-Hervás, P.; Rodríguez, M.; García-Honduvilla, N.; Pascual, G.; Buján, J., Midline Abdominal Wall Closure: A New Prophylactic Mesh Concept. *Journal of the American College of Surgeons* **2006,** *203* (4), 490-497.
201. Yang, Y.; Zhao, W.; He, J.; Zhao, Y.; Ding, F.; Gu, X., Nerve conduits based on immobilization of nerve growth factor onto modified chitosan by using genipin as a crosslinking agent. *European Journal of Pharmaceutics and Biopharmaceutics* **2011,** *79* (3), 519-525.
202. Alfredo Uquillas, J.; Kishore, V.; Akkus, O., Genipin crosslinking elevates the strength of electrochemically aligned collagen to the level of tendons. *Journal of the Mechanical Behavior of Biomedical Materials* **2012,** *15* (0), 176-189.
203. Bohidar, H. B.; Jena, S. S., Kinetics of sol--gel transition in thermoreversible gelation of gelatin. *The Journal of Chemical Physics* **1993,** *98* (11), 8970-8977.
204. (a) Lee, K. Y.; Kong, H. J.; Larson, R. G.; Mooney, D. J., Hydrogel Formation via Cell Crosslinking. *Advanced Materials* **2003,** *15* (21), 1828-1832; (b) Yamaguchi, N.; Chae, B.-S.; Zhang, L.; Kiick, K. L.; Furst, E. M., Rheological Characterization of Polysaccharide−Poly(ethylene glycol) Star Copolymer Hydrogels. *Biomacromolecules* **2005,** *6* (4), 1931-1940.
205. Prisacariu, C., Structural studies on polyurethane elastomers. In *Polyurethane Elastomers*, Springer Vienna: 2011; pp 23-60.
206. Juan V. Cauich-Rodríguez, L. H. C.-C., Fernando Hernandez-Sánchez, José M. Cervantes-Uc, Degradation of Polyurethanesbfor Cardiovascular Applications. 2013.
207. Carlos A. Martínez-Pérez, I. O.-A., Javier S. Castro-Carmona, Perla E. García-Casillas *Scaffolds for Tissue Engineering Via Thermally Induced Phase Separation* Sabine Wislet-Gendebien: 2011.
208. Reyes-Ortega, F.; Rodriguez, G.; Aguilar, M. R.; Lord, M.; Whitelock, J.; Stenzel, M. H.; San Roman, J., Encapsulation of low molecular weight heparin (bemiparin) into polymeric nanoparticles obtained from cationic block copolymers: properties and cell activity. *Journal of Materials Chemistry B* **2013**.

Conclusiones Finales

CAPÍTULO 6

Se han preparado novedosos sistemas poliméricos con una distribución de peso molecular definidos, sensibles a la temperatura y al pH utilizando la polimerización radical controlada por transferencia de átomo (ATRP).

Estos polímeros 'inteligentes' se han combinado con bemiparina funcionalizada utilizando 'química click', obteniendo sistemas bioactivos con propiedades muy interesantes desde el punto de vista biomédico, como la presencia de una temperatura de solución crítica (LCST) cercana a la temperatura fisiológica o el cambio de solubilidad por modificación en el pH del medio.

Se han sintetizado nuevos copolímeros de bloque anfifílicos en base a polimetacrilato de metilo (PMMA) y poli (cloruro de metacriloiloxi-trimetil amonio) (PMAETMA) mediante polimerización radical controlada por adición, fragmentación y transferencia reversible de cadena (RAFT), obteniendo sistemas con distintas longitudes de cadena del componente PMAETMA. Esta familia de copolímeros de bloque ($PMMA_n$-*b*-$PMAETMA_m$) tienen la capacidad de formar estructuras micelares que permiten la encapsulación de fármacos hidrosolubles como la bemiparina.

Se han preparado sistema biocompatibles nanoparticulados portadores de bemiparina utilizando dos métodos distintos: formación de complejos polielectrolíticos, que ha dado lugar a la obtención de nanopartículas de bemiparina-quitosano, y el método de la emulsión múltiple, que ha permitido la obtención de nanopartículas de bemiparina-Resomer, bemiparina-Eudragit RS PO y bemiparina-$PMMA_n$-*b*-$PMAETMA_m$. Los sistemas preparados proporcionan una liberación controlada de la bemiparina, manteniendo y modulando su capacidad de interacción con el factor de crecimiento de fibroblastos básico (FGF-2).

Se han obtenido hidrogeles de gelatina e hialuronato sódico entrecruzados por vía física o química, siendo estos últimos los que presentan mejores propiedades mecánicas y por tanto, son los que se han utilizado como soporte para la liberación controlada del componente bioactivo proadrenomedulina (PAMP). Esta secuencia

peptídica de 20 aminoácidos presenta propiedades pro-angiogénicas, anti-microbianas y re-epitelizantes, favoreciendo procesos de cicatrización de heridas, en concreto de heridas comprometidas.

Se han sintetizado poliuretanos segmentados biocompatibles y bioabsorbibles en base al diisocianato de L-lisina (LDI) y poli(éter de terametilenglicol) (PTMG), que forman el segmento rígido, y un segmento blando formado a partir de policaprolactona diol (PLC) y plurónico 61 (PL61). Este poliuretano segmentado se ha utilizado para preparar películas cargadas con nanopartículas de bemiparina.

Finalmente se ha diseñado y patentado un apósito de aplicación epidérmica constituido por una capa de hidrogel cargado con PAMP y otra de poliuretano bioreabsorbible cargado con nanopartículas de bemiparina, para su aplicación en procesos de regeneración y cicatrización epidérmica. Este sistema bicapa bi-funcionalizado mejora la cicatricación de heridas y úlceras, especialmente en los casos en que el proceso está dificultado como sucede en pacientes diabéticos, con reducido riego sanguíneo y personas edad avanzada.

Final Conclusions

CHAPTER 6

Novel polymeric systems, sensitive to pH and temperature, have been prepared with a defined molecular weight distribution, by atom transfer radical polymerization (ATRP).

These 'smart' polymers have been combined with functionalized bemiparina using 'click chemistry,' obtaining bioactive systems with interesting properties to be used in biomedical applications due to the presence of a lower critical solution temperature (LCST) that is similar to the physiological temperature or their ability to modulate solubility by pH changes of the medium.

New amphiphilic block copolymers based on poly(methyl methacrylate) (PMMA) and [2-(methacryloyloxy)ethyl] trimethylammonium chloride (PMAETMA) have been synthesized by controlled radical polymerization by reversible addition-fragmentation chain transfer (RAFT), obtaining different chain lengths of the PMAETMA block. This family of block copolymers ($PMMA_n$-*b*-$PMAETMA_m$) is able to form micellar structures, allowing the encapsulation of water-soluble drugs such as bemiparin.

Bemiparina biocompatible nanoparticle systems were prepared using two different methods: the polyelectrolyte complexes formation, which resulted in obtaining bemiparin-chitosan nanoparticles, and the multiple emulsion method, which allowed the preparation of bemiparina-nanoparticles with the following polymers: Resomer (PLGA), Eudragit RS PO and $PMMA_n$-*b*-$PMAETMA_m$. The nanoparticle systems prepared provided bemiparin controlled release, modulating its ability to interact with the basic fibroblast growth factor (FGF-2).

Hydrogels of gelatin and sodium hyaluronate were obtained via physical or chemical crosslinking. Chemical hydrogels showed better mechanical properties and, therefore, they were used as carriers for the controlled release of the bioactive component proadrenomedullin (PAMP). This 20 amino acid peptide sequence presented pro-angiogenic, anti-microbial, and re-resurfacing properties, promoting wound healing processes in particular critical wounds.

Biocompatible and bioabsorbable segmented polyurethanes (SPU) based on L-lysine diisocyanate (LDI) and polytetramethylene ether glycol (PTMG), which form

the hard segment and polycaprolactone diol (PLC) and Pluronic 61 (PL61), that form the soft segment. This SPU was loaded with bemiparina nanoparticles.

Finally, an epidermal application dressing has been designed and patented, comprising a hydrogel layer loaded with PAMP and a bioresorbable polyurethane layer charged with bemiparin loaded nanoparticles, for regenerative processes and epidermal healing applications. This functionalized bi-layer system improves wound and ulcer healing, especially in cases where the process is hindered as in diabetic patients with reduced blood flow and elderly people.